ANALYSIS AND DESIGN OF SMART ANTENNA ARRAYS (SAAs) FOR IMPROVED DIRECTIVITY AT GHz RANGE FOR WIRELESS COMMUNICATION SYSTEMS

Thesis submitted for the fulfilment of requirements for the degree of

DOCTOR OF PHILOSOPHY

in

Electronic Engineering

by

AYODELE SUNDAY OLUWOLE

HOWARD COLLEGE, UNIVERSITY OF KWAZULU-NATAL,

DURBAN – 4041, SOUTH AFRICA

STUDENT NO.: 215000088

JANUARY 2018

ANALYSIS AND DESIGN OF SMART ANTENNA ARRAYS (SAAs) FOR IMPROVED DIRECTIVITY AT GHz RANGE FOR WIRELESS COMMUNICATION SYSTEMS

Student:

Mr. Ayodele Sunday Oluwole

Supervisor:

Prof. (Dr.) Viranjay M. Srivastava

This thesis submitted in fulfilment of the requirements

for the degree of Doctor of Philosophy: Electronic Engineering

in the

Howard College of Agriculture, Engineering & Science

University of KwaZulu-Natal, Durban - 4041

South Africa.

As the candidate's supervisor I have approved this thesis for submission.

Signed……... Date: 22 Jan. 2018

Name: Prof. (Dr.) Viranjay M. Srivastava

DECLARATION 1

PLAGIARISM

I, **AYODELE SUNDAY OLUWOLE** with student number 215000088, declare this thesis titled ***"ANALYSIS AND DESIGN OF SMART ANTENNA ARRAYS (SAAs) FOR IMPROVED DIRECTIVITY AT GHz RANGE FOR WIRELESS COMMUNICATION SYSTEMS"*** and the work presented in it are my own. I confirm that:

i. The research reported in this thesis, except where otherwise indicated is my original work.

ii. This thesis has not been submitted for any degree or examination at any other university.

iii. This thesis does not contain any other persons' data, pictures, graphs or other information, unless specifically acknowledged as being sourced from other persons.

iv. This thesis does not contain other persons' writing, unless specifically acknowledged as being sourced from other researchers. Where other written sources have been quoted, then:

a) their words have been re-written, but the general information attributed to them has been referenced;

b) where their exact words have been used, their writing has been placed inside quotation marks, and referenced.

v. Where I have reproduced a publication of which I am author, co-author or editor, I have indicated in detail which part of the publication was actually written by myself alone and have fully referenced such publications.

vi. This thesis does not contain text, graphics or tables copied and pasted from the Internet, unless specifically acknowledged, and the source being detailed in the thesis and in the references sections.

Signed…….. Date: 22 / Jan. / 2018

DECLARATION 2

LIST OF PUBLICATIONS

Journal Publications

1. **Ayodele S. Oluwole** and Viranjay M. Srivastava, "Features and futures of smart antennas for wireless communications: A technical review," *Journal of Engineering Science and Technology Review*, under review, Jan. 2018, (Chapter 2).
2. **Ayodele S. Oluwole** and Viranjay M. Srivastava, "Analysis and synthetic model of adaptive beamforming for smart antenna systems in wireless communication," *Journal of Communications*, Accepted for publication, Jan. 2018.
3. **Ayodele S. Oluwole** and Viranjay M. Srivastava, "Determination of directivity and Gain for improved performance of smart antenna," *International Journal on Communications Antenna and Propagation*, vol. 7,no. 4, pp. 298-305, Sept. 2017.
4. **Ayodele S. Oluwole** and Viranjay M. Srivastava, "Smart antenna for wireless communication systems using spatial signal processing," *Journal of Communications*, vol. 12, no. 6, pp. 328-339, June 2017.
5. **Ayodele S. Oluwole** and Viranjay M. Srivastava, "Design of smart antenna by circular pin-fed linearly polarized patch antenna," *International Journal of Wireless and Microwave Technologies*, vol. 6, no. 3, pp. 40-49, May 2016.
6. **Ayodele S. Oluwole** and Viranjay M. Srivastava, "Smart antenna at 300MHz for wireless communications," *IEEE African Journal of Computing & ICT*, vol. 8, no. 3, pp. 193-201, Oct. 2015.

Conference Publications

7. **Ayodele S. Oluwole** and Viranjay M. Srivastava, "Designing of smart antenna for improved directivity and gain at terahertz frequency range," *Progress In Electromagnetics Research Symposium (PIERS)*, Shanghai, China, pp. 473, Aug. 2016.
8. **Ayodele S. Oluwole** and Viranjay M. Srivastava, "Analysis of smart antenna with improved signal quality and spatial processing," *Progress In Electromagnetics Research Symposium (PIERS)*, Shanghai, China, pp. 474, Aug. 2016.

9. **Ayodele S. Oluwole** and Viranjay M. Srivastava, "Performance analysis of smart antenna bandwidth at terahertz frequency range," *Progress In Electromagnetics Research Symposium (PIERS)*, Shanghai, China, pp. 475-476, Aug. 2016.
10. **Ayodele S. Oluwole** and Viranjay M. Srivastava, "Modeling of RF security system using smart antennas," *IEEE International Conference on Cyberspace (CYBER-Abuja 2015)*, Abuja, Nigeria, pp. 118-122, Nov. 2015.
11. **Ayodele S. Oluwole** and Viranjay M. Srivastava, "Design of smart antennas using waveguide-fed pyramidal horn antenna for wireless communication systems," *12th IEEE Annual India International Conference (INDICON 2015)*, New Delhi, India, pp. 1-5, Dec. 2015.
12. **Ayodele S. Oluwole** and Viranjay M. Srivastava, "Design of smart antenna using planar phased-array antenna for wireless communication systems," *IEEE International Conference on Trends in Automation, Communications and Computing Technologies (ITACT-2015)*, Bangalore, India, pp. 1-5, Dec. 2015.

DEDICATION

This thesis is dedicated to

The Only wise God.

With Him all things are possible.

ACKNOWLEDGEMENTS

Glory and honour to God Almighty who made this thesis possible. Appreciation to my Supervisor and mentor Prof. (Dr.) Viranjay M. Srivastava for his professional and excellent supervision, and counselling throughout the research study. I am greatly indebted to him for his unconditional help, invaluable advice and for propelling me further in every aspect of my academic life. His presence and optimism have provided an invaluable influence on my career and outlook for the future. I consider it my good fortune to have got an opportunity to work with such a wonderful person. My gratitude goes to Professor Thomas J. O. Afullo for his financial contribution in the course of this programme.

The pursuit of a Ph.D can be a long, arduous and largely solitary process, especially when it comes to writing the thesis. In my experience, there were two key factors which kept me going. The first was the time expended during the process of research and the desire to complete the degree. The second and by far the most important was the support, compassion, understanding, faith and gentle prodding of those around me towards submission.

I want to appreciate friends and colleagues in the Deeper Life Campus Fellowship (DLCF), Bro. Oyedeji Okiki, Bro. Luke and his family, Bro. Emmanuel Onuh and his family, Bro. Gbenga Imole and his family, and father in the Lord Bro. Lanre and his family. Thanks for your prayer and support. I would also acknowledge my colleagues and workmates, Odeyemi Kehinde, Dhawan Singh, Adejumobi Babatunde, and ever dependent Gbenga Afolayan, for their advice and their willingness to share their bright thoughts with me.

Finally, I recognize my wife for her prayers and children, for enduring lonesomeness during the programme.

ABSTRACT

Theoretical advancement in antennas has introduced various new techniques that depend on smart antennas and have objectives of increasing the data rate, beamforming, target surveillance features, diversity gain, or to provide multi-user capabilities. Though smart antenna arrays techniques have attracted a lot of attention, some aspects such as directivity and transmissions of datas at a higher frequency range from gigahertz (GHz) to terahertz (THz) technology have to be examined. Hence, the motivation for this research that emphasizes the analysis and design of Smart Antenna Arrays (SAAs) for improved directivity from (GHz) to (THz) range for wireless communication systems traversing from theoretical analysis to simulation on the effect of the antennas and their performances.

Smart antenna arrays are designed to improve radiation in one direction and null out interference in other direction. This has been realized as a result of increasing the directivity of each antenna elements which lead to gain in a specific direction. At high frequency, transmission of signals is characterized by impairments. Mitigation of these signal impairments can be accomplished through the improvement of directivity and gain of the smart antenna systems at higher frequency range. Smart antenna arrays examined in this thesis can be applied to far distance communications and has been operational at high-frequency (HF) radio waves. Its efficiency has been optimized and simulated with the aid of commercially available full-wave, Finite Element Method (FEM) based electromagnetic simulator Agilent's Advanced Design Software (ADS). The designed and the simulated prototype is suitably operating at 300 GHz to 3 THz for wireless local area network applications that uses high-frequency radio waves. The antenna has been put together on a Rogers_DT_Duroid dielectric substrate of Svensson/Djordjevic loss type with the dielectric permittivity of $\varepsilon r = 2.33$, loss factor/tangent ($tan\ \delta$) of $1.2*10^{-3}$, relative permeability (μr) = *1* and the thickness of $h = 0.80\ mm$. Rogers RT Duroid dielectric substrate has been taken as our substrate due to the low dielectric loss which makes it suitable for high-frequency laminate over the FR-4 substrate. The antenna receives input power and radiated power at 15.55Watts in a specific direction, focusing the desired signals from where they come forth allowing for increased radiation efficiency of *100%* and mitigate interfering signals from unwanted sources. The antenna has a peak directivity of 17.6 dB, this made it possible for the maximum power transfer.

The smart antenna arrays analysed in this research work mitigates interference of signals transmission by adaptive beamforming technique known as spatial signal processing. This technique creates radiation pattern on the array of antennas by means of signals weights addition in a constructive manner. Uniform array of isotropic elements *M (10, 15, and 20)* has been considered having their coordinate system in the direction of *y*. The spacing of the antenna elements is varied at *d (0.5λ, 0.6λ and 2λ)*. The angles at which the grating lobe appears, steering angle, and the antenna element's effect spacing on beamforming has been examined. The following are the observation as the antenna element spacing are increasing; narrower main lobe, grating lobes, reduction in beamwidth thus making the array more directional, and reduction in sidelobe level, thus improving beamforming. It is also observed that there is no grating lobe when $d/\lambda = 0.5$, which has been considered as the optimal design spacing for the array antenna elements. The centrality of smart antenna arrays is controlled by the signal processing of the arrays and algorithm for effective delivery of quality signals. The proposed algorithms are 'Spatial Reference' algorithms. MATLAB software has been used for the performance and comparison of algorithms used.

In this thesis, an emphasis is laid on linear arrays, array synthesis, and array signal processing. At the output of antenna receiver, Signal-to-Interference-plus-Noise-Ratio (SINR) expression is derived from the analytical model which allows the Bit Error Ratio (BER) to be evaluated. The automatic extraction of the desired signal from noise and interferer has made smart antenna different from other antennas. The number of antenna elements, geometrical arrangement, relative amplitude and phases determines its angular pattern. This work has compared antenna geometries and their array weights are optimized by different techniques. Dolph-Chebyshev and Taylor array synthesis weighting methods have been used for the antenna arrays synthesis and analysis.

Throughout this research, results from numerical simulations have been presented, often in association with analytical calculations to explore the accuracy of approximate derived formulas for the design. The approach adopted in the analysis and design in this thesis can be used in the treatment of several antenna types. After a general discussion of the principles, design formulas are derived and explained. These derived formulas are used for easy evaluation of performance parameters for the antenna type. The operating range of antenna elements analysis in this thesis varies from MHz to THz. This research is based on theoretical analysis and design which are of practical benefits in implementation.

TABLE OF CONTENTS

LIST OF FIGURES

LIST OF TABLES

ACRONYMS

3-D	Three-dimensional
AOA	Angle of arrival
AF_{array}	Array factor
AR	Axial ratio
BS	Base station
CA	Circular array
CP	Circular polarization
D_{array}	Array directivity
DBF	Digital beamforming
DOA	Direction of arrival
DSP	Digital signal processor
ERP	Effective radiated power
G	Gain
Gbps	Gigabit per second
HPBW	Half power beamwidth
ISI	Intersymbol interference
LMS	Least mean square
MMSE	Minimum mean square error
MSE	Mean square error
MS	Mobile station
QoS	Quality of Service
RF	Radio frequency
RLS	Recursive least squares
Rx	Receiver
SDMA	Space division multiple access
SNR	Signal-to-noise-ratio
SINR	Signal to interference plus noise ratio
SLL	Side lobe level
SNOI	Signals not of Interest

SOI	Signals of interest
Tbps	Terahertz bit per seconds
THz	Terahertz
Tx	Transmitter
ULA	Uniform linear array
WLAN	Wireless local area network

LIST OF SYMBOLS

θ	angle of elevation
φ	directivity angle (phase angle)
ϕ	spherical coordinate angle (path difference)
$\mathbf{R}$	array correlation matrix
y	array output
α	array steering vector
ε_{eff}	effective relative permittivity
e	error signal
d	inter element spacing
L	length of radiating patch
$\mathbf{n}$	noise vector
N	number of array elements
τ_j, τ_i	path delay
P	output power of the array
U	radiation intensity (isotropic source)
p	total radiated power
$\mathbf{r}$	received signal vector
λ	RF waveform length
μ	step size
s	the steering vector
$\mathbf{a_1 \ldots a_m}$	weighting coefficients of the constant-vector beams
W	weight vector
w	width of radiating patch
w_{rad}	radiated power

CHAPTER 1

Introduction

The challenge to transmit high data rates in wireless communication systems in the present scenario precisely gigabit-per-second (Gbps) as the contemporary communication devices necessitate larger Band Width (BW). Coupled smart antenna arrays with sufficient directivity, high gain, and power (that provides real-time adaptive nulling and beamforming) are required for the effective transmission of signals. Smart antenna arrays is a necessity in this contemporary wireless communication systems [1-4]. Antenna arrays are spatial distribution antenna elements, arranged on a collective structure in accordance with geometric forms (e.g. linear, circular, rectangular, planar, etc.) [5, 6]. These are cooperated together for improved higher data transmission rate, better quality of signals in wireless communication, and demonstrate additional tasks such as target surveillance which has need of direction finding Direction of Arrival (DOA) and requires the realization of antenna arrays that maintain a high radiation efficiency [7]. The directional reception and transmission (beamforming) achieved using antenna arrays has made it suitable for its rare position in wireless communications. Antenna arrays have various antenna element and when it is used for reception of signals, the received signals of the individual elements are weighted and then combined [8]. If the antenna array is used for transmission, the transmit signals of the individual antenna elements can be weighted prior to transmission. Again, the weights can be chosen so that the individual signals combined coherently in the preferred direction where signals will be concentrated at the receiver end. In both cases, the antenna array can create a beam towards the desired user direction [9-14].

Beamforming also directly improves received signal quality by the continuous utilization of adaptive adjustment of the antenna arrays parameter in a specific direction to attain optimum efficiency while concurrently removing interferer's effects. It has been found that narrow azimuthal beamwidth in an elevated Base Station (BS) transmit antenna arrays, reduces the multipath fading at mobile station, while narrow beamwidth on the vertical plane increases the received power at the mobile station [15-19]. Another direct benefit of beamforming is interference suppression. When an antenna array forms a beam as described above, the signals received from or transmitted in the direction of non-desired users have a small amplitude. This effectively suppresses interference from/to other Co-channel users, improving the overall system performance [20-23]. This basic concept is known as Spatial Division Multiple Access

(SDMA) [24-26] and is one of the best and effective utilization of smart antenna arrays technology [27-30]. Advancement of spatial signal processing of Spatial Division Multiple Access capacity aids in targeting many users, forming diverse beams for each user.

Another reason for using antenna array is their steering and spatial diversity support beyond simple beam steering [31] which also results in multipath fading reduction [30]. Typically, the individual elements of an antenna array are spatially separated, so they sample or probe in different locations of the three-dimensional space. When the distance between these elements are sufficiently large, there is a small correlation among their signals, providing spatial diversity [32-34]. The immediate benefit is a reduction in probability of deep multipath fading of the received signal amplitude, and Signal to Noise Ratio (SNR) enhancement which is normally traded off in various ways [21, 25]. For instance, it can be used in cell size increment, reduction in a number of base stations required to serve a particular location, and ultimately the total cost of the system (especially desired at the initial stages of a mobile communication system deployment where cost minimization is of paramount importance). At later stages where the initial cost is no longer a major issue and the user demand for mobile communication is greater, antenna arrays gain can also be used for system capacity improvement by serving more users. Likewise, this gain can be used for better quality of service, by improving the quality of the already existing services and offering the possibility for new ones. Furthermore, the spatial processing gain from antenna arrays can be used to reduce the performance overhead of power control, since interference from high power users can be spatially suppressed [26, 33]. Antenna array's formation increases the range of communications and likewise supports the use of smart antennas with directive characteristics and applications [9, 10].

Smart antenna arrays are array of antennas with sophisticated Digital Signal Processing (DSP) capacity having algorithms that can dynamically calculates the amplitudes and phase parameters of the driven Radio Frequency (RF) signal attached to specific radiative elements. These arrays are placed in a particular configuration which can be in either linear, circular or matrix form so as to emphasize the signals of interest and place a null in the level of interfering signals, for efficient performances of wireless communication system [30, 34-52]. The aims of digital signal processing are to evaluate the Direction of Arrival (DOA) of any interrupting signal from the phase delays for every antenna elements, the suitable weight for scanning radiation pattern of antenna towards the desired signal, and put nulls in the interference signals direction [53, 54]. Null steering is usually achieved by controlling the complex weights of all or most of the array elements [55]. Smart antenna arrays are studied and considered useful in a

various signal environment for the purposes of enhancing the base station performance in multipath fading conditions and increasing SNR of the receiver [56-59]. The effort by researchers on smart antenna systems has encouraged research in adaptive array signal processing algorithms, for instance, the direction of arrival and adaptive beamforming [53, 60].

In wireless communication system, smart antennas are also known as adaptive beamforming system. By using its spatial domain channel, maximum beamforming gain increases. In accordance with the signal received, beamformer weights can be determined by an adaptive process using temporal information (reference signal) or spatial information (direction of the user). The central beam focuses the main user, whereas its nulls are in sync to the interferers [60, 61].

Through adaptive updating of weights connected to the individual antenna element, smart antennas place nulls towards interferers and deliver maximum main lobe in the direction of the preferred signal simultaneously, with the aim of using signal to interference ratio [52, 62]. The main lobe beampattern could be tracked so as to get the desired signal and thus null out most of the co-channel interferences. Thus, determining suitable attenuation values along the jammers directions, and consequential in a better signal quality reception. Through the DOA algorithms, smart antenna arrays have the capacity to track user within a cell. The beam formation in the direction of the desired signals and formation of null towards the interferers could be achieved by adjusting the excitation distribution of the arrays [56].

1.1. Research Motivation

The extensive use of wireless communication technologies application in the society has increased the necessity for efficient and reliable signal transmission. One way of achieving these requirements is by using smart antenna system. Conventional antenna systems use the standard omnidirectional antenna that transfers signal in every direction as well as directions where the signal is not required. However, in real situations, the required signal is not necessarily coming from all directions. This results in inefficient signal transmission and power wastage. Hence, the idea of smart antennas is introduced.

The development of smart antenna arrays has triggered enormous interest in the past decades for its potential to provide better services and an increasing number of users. Smart antennas consist of an array of antenna that has the intelligence to adjust its radiating beam depending on the operational environment. In smart antennas, it is desirable to achieve a radiation pattern as narrow as possible and the directivity as high as possible. A smart antenna

system is desirable and it has demonstrated a number of benefits in ongoing research [52, 62-64]. A smart antenna produces a highly directive radiation pattern that can be electronically controlled. This means the radiation of a smart antenna can be steered over the best signal path, and consequently reduce the power consumption of the wireless devices.

1.2. Research Objectives

This thesis analyses various approaches for the smart antenna elements and performs various signal processing algorithms on the antenna arrays in an attempt to enhance smart antenna arrays capabilities. This has been achieved by proposing strategies to improve the effectiveness of these algorithms when tackling smart antenna array problems. The main objectives of this research work are to:

- Understand the geometrical characteristics of antenna arrays and how they determine the shape of their radiation pattern. This is carried out by analysing antenna configurations at various frequencies range of transmission.
- Study how various antenna configurations generated different results with some arrays performing better in scenarios than others.
- Examine antenna array synthesis pattern using different methods such as Taylor and Dolph-Chebychev.
- Analysis for optimal beamformer with its weight unconstrained, and to determine its directivity and gain.
- Propose strategies to enhance the effectiveness of algorithms for the smart antenna arrays (SAAs).

1.3. Smart Antenna Technologies

The technology of smart antenna has a major impact in wireless communication systems due to its ability of improved the directivity for antenna's beam which improves the desired signals at the reception devoid of impedance to any radio users [60]. Smart antenna technologies enable advanced system capacity in communication networks, reduction in multipath signal, and Cochannel interference [47, 50]. This can be achieved through sampling of its existing environment when a beam-steering command is supplied by a particular algorithm from the adaptive processor. This dynamically regulate antenna's element weights and focus beam radiation pattern only in the desired direction and place nulls in the direction

of the other unconnected user equipment to reduce the effect of Co-channel interference [40, 50]. The signal processing algorithms functioning at the baseband (that forms the array's signals elements) is known as *smart antennas* [9]. A smart antenna system makes use of the spatial antenna arrays and processes the received signals through digital signal processor once the conversion from analog to digital, hence it is called an *adaptive filter signal processing*. Due to the digital signal processing capabilities embedded in this antenna, it is tagged "smart antenna/software antenna/digital beamforming antenna". It means the smart antenna is intelligent which is different from the conventional antenna that only receives/transmit signals devoid of reflections. The digital beamforming antenna provides optimal gain, while concurrently classifying, tracking, and reducing reception of interfering signals. The concepts adaptive antenna and smart antenna are substitutable in this thesis [10, 50].

1.3.1 Smart antenna arrays processing procedures

Smart antenna systems comprise of an array of antenna, in conjunction with signal processing algorithm both in space and time domain. It uses the spatial signal processing technique to obtain an optimum combination of excitation sources, called weights, to form maximum radiation directions (beams) towards desirable signals while also to form minimum radiation directions (nulls) towards undesirable interference sources. The processing of arrays leads to enhancement of reception/detection of the desired signal that may be either random or deterministic in a signal environment [46]. The desired signal may also contain one or several uncertain parameters (e.g. spatial location, signal energy, phase) that may be advantageous to estimate. Fully adaptive smart antennas [27] can steer nulls and beam independently using phase and amplitude control.

Smart antenna array adaptation processing algorithms are established on spatial correlation matrix configuration of the antenna array. Diverse types of smart antennas have been designed to accomplish several needs, for instance, it is normally used in military, base-station tracking, downlink diversity transmission, fibre wireless networks, etc. Electrically Steerable Passive Array Radiator (ESPAR) antennas have acknowledged consideration smart antennas recently. In an ESPAR antenna, only one feed is coupled to the active antenna element, and beam steering can be recognized by a number of reactance loads associated with the passive antenna elements [56].

1.3.2 Benefits of smart antenna arrays

In a nutshell, the following listed below enumerates some of their benefits and contributions to the wireless communication systems:

a) **Increased Security in wireless networks –** Most of the security problems in network physical layer are related to the fact that in wireless communication, information is exchanged over the air and may be captured or interfered by adversaries. The aim of physical layer security is to ensure reliable delivery of information to the intended receiver and, at the same time, prevent malicious access and interferences. Both these two aspects are highly influenced by the status of the wireless communication channel. While the channel variation due to the natural environment is beyond our control, the powerful smart antenna technology makes signal tuning at the transmitters (TX) and receivers a possible solution to get control over the wireless communication links. In [64] the authors introduced artificial noise produced by the smart antennas to confuse the eavesdroppers with carefully designed noise signals, which can be cancelled at the intended receiver. One straightforward security benefit of using smart antennas in communication is that the wireless signal will be more concentrated to the intended receiver. The reduced signal radiation to other directions results in lower chances of eavesdropping attacks. The connection of tapping at the base station is also problematic to hackers/intruders when smart antennas are in operation. This scenario was demonstrated by *Oluwole and Srivastava* [65]. For effective communication tap connection, the intruder/hacker must be aligned as the user. Hence, this makes smart antennas to cut-off information away from the base station.

b) **Reconfigurability and compatibility –** Smart antenna technology has found a wide application in different multiple access techniques. Nearly all modulation methods are compatible with smart antennas due to its reconfigurability to changing channel propagation in addition to network conditions [66]. For example, MIMO compatibility in both communications and radar [30].

c) **Co-channel interference reduction –** The capacity of wireless communication systems are impaired with co-channel interference as a result of the reuse of existing system resources by network consumers. Co-channel interference is often insignificant and there is a reduction in sidelobe levels by placing nulls in the direction of the radiation pattern.

d) **Higher coverage range area expansion –** Smart antennas can increase the network throughput so as that the spatial reuse could be allowed for the wireless channel and can also increase the coverage range of cell significantly through its individual antenna elements gain and interference rejection. Hence, fewer sites are needed when smart antennas are employed in base stations to cover a specified area. Larger coverage areas are covered if the antenna is at a greater height above average terrain. The gain of the antenna arrays increases the link budget, this leads to range expansion [63, 67].

e) **Increase in system capacity –** Smart antennas enables the possibility of having multiple cells on a particular RF channel with different spatial channels at a specific cell site. A reuse unity factor is allowed, i.e. using a single frequency spectrum simultaneously in all cells. Through directional communication links, the number of available voice channels can be increased subject to propagation environment, and the amount of dynamic channel assignment allowed. To meet the requirements of user-selectable data transfer rates, smart antennas allow the adjustment of RF channels through link power control.

f) **Signal quality improvement –** There is an increase in signal quality when smart antennas are in usage because of its beamforming gain, and signal fading effects are reduced to the barest minimum.

g) **Efficient higher power control –** Effective power control is realized by the use of diversity gain existing through an antenna array (fading reduction). Whenever signal transmission is towards the desired user, there will be low power consumption and the amplifier cost will be reduced unlike omnidirectional antenna [66].

h) **Handoffs reduction –** Cellular network are always overcrowded, hence it is necessary to break down the congested cell into smaller cells to allow increment in the frequency reuse factor. As the cell size is becoming smaller, this results in handoffs.

i) **Improved data throughput** - A quick measure of the value of smart antennas is required to see their effect on the network. A useful measure is a number of datas that are normally transmitted through the network per unit time. It can be expressed in kilobits per second over the cell (kbit/s/cell). At random half (50%) of the sites are installed with smart antennas. In a second case, these smart antennas are deployed in an optimal way. It follows just using smart antennas results in a 75% increase in network throughput. With the optimization, this can be increased by a further 36%.

1.4. Research Contributions

The research makes the following contributions to the field of antenna and smart antenna systems.

Firstly, to understand the analytical study of smart antenna arrays as one of the prominent techniques that proffer solution for the mitigation of mobile impairments such as multipath fading, and co-channel interference, polarization mismatch, etc. in wireless communication systems, and to improve on the performance smart antenna arrays in terms of directivity and gain.

Secondly, the study examines how smart antennas can be used for security purpose. This has been established in chapter two of this work.

The research work has been able to identify various antenna elements that can be used effectively for the implementation of smart antennas. Smart antenna directivity and gain has been identified and the closed form expression has been derived. Using a planar phased array antenna yields various, concurrent readily obtainable beams. These beams can have high gain directivity, optimum sidelobe suppression, and beam width controlled. Planar phased array antenna can automatically adjust the array pattern to optimize some typical features of the received signal i.e. phases and amplitudes. These multiple beams formed by planar array antenna are steered by means of electronic control. The consideration of smart antenna system using an *8x8* planar phased-array antenna offers the synthesis of a needed beam pattern which is not obtainable with a single patch antenna element. In this research work, a high-performance planar phased-array antenna has been designed using an 8x8 square grid of *z*-controlled antenna monopoles with a length of 0.482λ. The considered element spacing is 0.315λ and average directivity of *22.0 dBi*. The uniform current distributions and binomial current distribution have been used for the design. To minimize the side lobe level characteristic to a lower one of *-20 dB* with reference to the main beam, the binomial current distribution is preferred for the work. This approach for the synthesis of antenna's beam pattern reduces multiple interferences by installing nulls in the course of signals interference and putting the central beam pattern in the track of the targeted signals in phase and amplitude regulation.

This study examines the design of smart antenna to improve radiation in one direction and null out interference in other direction. It has been realized by directivity of antenna's element which leads to gain in a specific direction. At high frequency, transmission of signals is characterized by impairments. Mitigation of these signal impairments can be accomplished through the improvement of directivity and gain of the smart antenna system at terahertz

frequency range. This research work proposed and examined smart/ adaptive antennas array at terahertz (THz) frequency range, which can be applied for far distance communications and can be extended to the far-field region of an antenna. The smart antenna arrays has been appropriately operational at *0.3 THz* to *3 THz* for Wireless Local Area Network (WLAN) applications that use High-Frequency (HF) radio waves. The efficiency of this adaptive array antennas system has been optimized and simulated with the aid of commercially available full-wave, Finite Element Method (FEM) based electromagnetic simulator Agilent's Advanced Design Software (ADS).

Finally, different algorithms for the performance of smart antennas are established in the study. To realize smart antennas necessity with wideband in wireless communication systems, three main fundamental approaches are (i) space-time signal processing, (ii) spatial-frequency signal processing (filtering of signals that overlay with noise in space and frequency), and (iii) spatial signal processing (beamforming). This research work deals with the spatial signal processing (beamforming) due to its spatial access to the radio channel through diverse approaches. This is based on directional specifications of the second order spatial analysis of communication radio channel. Space-time processing decreases the interference and improves the desired signal. Delay-and-sum beamformer response tuned to for monochromatic plane has been established in this work. The results of the analysis and simulations shown validate the benefits of the proposed technique.

1.5. Thesis Organization

The organization of the thesis are as follows:

Chapter one provides an overall overview to the work, research motivation and objectives directing the research. Smart antenna arrays and technologies are briefly explained with the benefits of using the technologies in wireless communications system.

Chapter two presents a comprehensive evaluation of the significant information in the area of smart antennas array and their relevance in wireless communication systems. Some of the fundamental principles of antennas and array are highlighted including the definition of the Figure of merits. Several techniques that can be employed to enhance system performance by means of smart antenna systems are re-examined. This is followed by considering the trade-offs between the performance and complexity of the several combining algorithms used in smart antennas.

In **chapter three** of the thesis, various methods, and approaches by which smart antenna arrays could be analyzed and design are highlighted. Circular pin-fed linearly polarized patch antenna and waveguide-fed pyramidal horn antenna are used as an antenna element. The design of smart antenna using waveguide-fed pyramidal horn antenna gives a better system performance of directional radiation beam pattern with a high gain and wide impedance bandwidth. The work in this chapter presents an innovative approach to designing smart antenna using a waveguide-fed pyramidal horn antenna for wireless communication systems. Also, the mathematical model for uniform and circular array radiation synthesis has been established.

Chapter four deals with the analysis and design of smart antenna system that operates at Terahertz (THz) frequency ranging from *0.3 THz* to *3THz*. An array with high directivity focus with a frequency range from *0.3-3THz*. In this chapter, Dolph-Chebyshev and Taylor methods are applied for the synthesis of an antenna array radiation pattern.

In **chapter five**, the consideration of smart antenna system using an *8 x 8* planar phased-array antenna offers the synthesis of a needed beam pattern which is not obtainable with a single patch antenna element. In this chapter, a high-performance planar phased-array antenna has been designed using an *8x8* square grid of z-controlled antenna monopoles with a length of *0.482λ*. The considered element spacing is *0.315λ* and the average directivity of *22.0 dBi*. Using a planar phased array antenna yields various, concurrent readily obtainable beams. These beams can have high gain directivity, optimum sidelobe suppression, and beam width controlled. Planar phased array antenna can automatically adjust the array pattern to optimize some typical features of the received signal i.e. phases and amplitudes. These multiple beams formed by planar array antenna are steered by means of electronic control.

In **chapter six**, a closed-form expression for the smart antennas adaptive beamforming algorithm has been derived. The adaptive beamforming is used as a technique to create radiation beam pattern on antenna arrays by means of addition of signals weights constructively in the preferred direction of the signal and nulling pattern in the interference direction. The following are the observation as the antenna element spacing are increasing; narrower main lobe, grating lobes, reduction in beamwidth thus making the array more directional, and reduction in sidelobe level, thus improving beamforming. It is also observed that there is no grating lobe when $d/\lambda = 0.5$, which we considered as the optimal design spacing for the array antenna elements in the smart antenna. The LMS and RLS algorithms results are evaluated for their convergence rate and beamforming.

Chapter seven presents a succinct and the conclusions of the work including the main contributions and possible future research works in the thesis are suggested.

1.6. Scholarly Publications

The contributions of my thesis have resulted in journals and conferences paper from my time as the Ph.D. student has been published and submitted for publication in the course of this research, and parts of their materials are included in the dissertation. The related published and under-review articles for this thesis are as follows:

1. **Ayodele S. Oluwole** and Viranjay M. Srivastava, "Features and futures of smart antennas for wireless communications: A technical review," *Journal of Engineering Science and Technology Review*, under review, Jan. 2018, (Chapter 2).
2. **Ayodele S. Oluwole** and Viranjay M. Srivastava, "Analysis and synthetic model of adaptive beamforming for smart antenna systems in wireless communication," *Journal of Communications*, Accepted for publication, Jan., 2018, (Chapter 6).
3. **Ayodele S. Oluwole** and Viranjay M. Srivastava, "Determination of directivity and Gain for improved performance of smart antenna," *International Journal on Communications Antenna and Propagation*, vol. 7, no. 4, pp. 298-305, Sept. 2017, (Chapter 4).
4. **Ayodele S. Oluwole** and Viranjay M. Srivastava, "Smart antenna for wireless communication systems using spatial signal processing," *Journal of Communications*, vol. 12, no. 6, pp. 328-339, June 2017, (Chapter 6).
5. **Ayodele S. Oluwole** and Viranjay M. Srivastava, "Design of smart antenna by circular pin-fed linearly polarized patch antenna," *International Journal of Wireless and Microwave Technologies*, vol. 6, no. 3, pp. 40-49, May 2016, (Chapter 3).
6. **Ayodele S. Oluwole** and Viranjay M. Srivastava, "Smart antenna at 300MHz for wireless communications," *IEEE African Journal of Computing & ICT*, vol. 8, no. 3, pp. 193-201, Oct. 2015, (Chapter 3).
7. **Ayodele S. Oluwole** and Viranjay M. Srivastava, "Designing of smart antenna for improved directivity and gain at terahertz frequency range," *Progress In Electromagnetics Research Symposium (PIERS)*, Shanghai, China, pp. 473, Aug. 2016, (Chapter 4).

8. **Ayodele S. Oluwole** and Viranjay M. Srivastava, "Analysis of smart antenna with improved signal quality and spatial processing," *Progress In Electromagnetics Research Symposium (PIERS)*, Shanghai, China, pp. 474, Aug. 2016, (Chapter 6).
9. **Ayodele S. Oluwole** and Viranjay M. Srivastava, "Performance analysis of smart antenna bandwidth at terahertz frequency range," *Progress In Electromagnetics Research Symposium (PIERS)*, Shanghai, China, pp. 475-476, Aug. 2016. (Chapter 4)
10. **Ayodele S. Oluwole** and Viranjay M. Srivastava, "Modeling of RF security system using smart antennas," *IEEE International Conference on Cyberspace (CYBER-Abuja 2015)*, Abuja, Nigeria, pp. 118-122, Nov. 2015, (Chapter 2).
11. **Ayodele S. Oluwole** and Viranjay M. Srivastava, "Design of smart antennas using waveguide-fed pyramidal horn antenna for wireless communication systems," *12th IEEE Annual India International Conference (INDICON 2015)*, New Delhi, India, pp. 1-5, Dec. 2015, (Chapter 3).
12. **Ayodele S. Oluwole** and Viranjay M. Srivastava, "Design of smart antenna using planar phased-array antenna for wireless communication systems," *IEEE International Conference on Trends in Automation, Communications and Computing Technologies (ITACT-2015)*, Bangalore, India, pp. 1-5, Dec. 2015, (Chapter 5).

CHAPTER 2

Research Background

This chapter provides a general idea and detail background of the theoretical principles for antennas, antenna arrays, smart antenna systems, and their functions in wireless communication systems is the basis of this thesis. It also examines the basis of smart antenna arrays and with emphasis on the signal processing algorithms that make the antenna to be smart.

2.1. Introduction

With the exponentially increasing demand for increased performance of wireless communication systems and networks, the capability of contemporary cellular systems cannot handle the increasing network traffic. Smart antennas is mostly preferable when considering the kind of antennas to break this barrier of network capacity increase. This has motivated recent research towards various factors, especially on various antennas used for transmission and reception of signals [50]. Antennas with various efficiencies are needed for the propagations of signal, which is the crucial sandwiched between the controlled signal and the atmosphere [68-72].

Smart antenna arrays system play a prominent role in space diversity to increase channel capacity, reliability, higher throughput and enhanced the Quality of Service (QoS) [50, 73]. The signal processing aspect of smart antenna i.e. the algorithms is most important area that researchers lay much emphasis. The functions of algorithms in smart antennas has given it the edge over all other antennas. The algorithms process the incoming signals and focus the beam radiation in a specified direction, these aids the overall improvement of system performance.

2.2. Fundamental Principles of Antenna Theory and Antenna Arrays

In communication systems, the role of an antenna is a crucial, without which transformation of RF signal into electromagnetic wave vis-a-vis in mobile communications is not easy [74]. This can be defined as the portion of an antenna for transmitting/receiving system designed for radiation/reception of electromagnetic waves [75]. Proper antenna selection is essential for the transmitting/receiving of signals in the communication system. The antenna selected must have enough capacity to radiate or receive energy efficiently so that the supplied power is not wasted. Antennas need to be designed with special parameters such as directivity

and gain so as to be used for long-distance transmission/reception, hence the need for arrays which is another approach to high-gain and directivity antennas [76]. Generally, increment in electrical size of antenna would make this to be realizable. Apart from this, we can achieve this when we have assemblage of antennas that are radiating in nature and with electrical configuration. With this, we might not need to increase the size of the antenna elements due to their assemblage and their electrical configuration [6, 77]. The mechanism by which multi-element complex radiation from a group of identical antennas can be realized without altering the antenna impedance is through antenna arrays. Antenna arrays increase the gain and directivity of a single antenna, thereby improves the transmission and reception patterns of antennas used in communications systems [78]. The vector summation of each antenna element, when combined in space and amplitude gives the total electromagnetic field of the array. In space-time field, the array can be used to filter signals by means of exploiting their spatial characteristics [6, 77, 79]. The synthesis and analysis of arrays radiation characteristics can be simplified by using basic array geometries.

2.3. Parameters of Antenna

Some features of an antenna are important in characterizing the performance of antenna. Most of these parameters have correlation with one another. Specification for most of these parameters are not needed for complete description of performance of an antenna.

2.3.1 Radiation Intensity

Consider an isotropic radiator with equal radiation in all directions and with a symmetric radiation. The spherical coordinate angles (θ *and* ϕ) are function of that angles and a radial component of that angles. Total radiated power is expressed in mathematical form as [54]:

$$p_{rad} = 4\pi r^2 w_{rad} \tag{2.1}$$

Therefore, the radiation intensity (isotropic source) denoted by:

$$U = \frac{p_{rad}}{4\pi} = \frac{4\pi r^2 w_{rad}}{4\pi} = r^2 w_{rad} \tag{2.2}$$

In terms of antenna's radiated power and unit solid angle, in a specific direction of (θ, ϕ), the radiation intensity is:

$$U(\theta,\phi) = r^2 p_d(\theta,\phi) \tag{2.3}$$

Then, the total radiated power is expressed as:

$$p_{rad} = \int_{\phi=0}^{2\pi} \int_{\theta=0}^{\pi} U(\theta,\phi) \sin\theta d\theta d\phi \tag{2.4}$$

while its average value is:

$$U_{avg} = \frac{P_{rad}}{4\pi} \tag{2.5}$$

Detailed information for this analysis has been given by *Balanis* [54]. This parameter has been utilized for this present research work of antenna element in chapter 4, section 4.2.3. Radiation intensity parameter has also been used for the determination of maximum directivity of broadside antenna array in section 5.4.1 of this thesis.

2.3.2 Antenna's Gain

Antenna gain and directivity are closely related to each other. For ideal antennas, the gain is just the maximum directivity expressed in dB. Specific antenna type directional is determined by gain. Through gain, we know how directional the type of antenna we have. Highly directional antennas normally characterize higher gain. Sometimes, if the observation direction is not specified, directivity could be used in such a situation. Hence, gain and directivity are the same. The strength of transmitting/receiving can be improved through gain. The capability of an antenna to focus its input power into radiation in a specific direction is called gain. Gain measurement takes place at the peak of radiation intensity. Antenna gain takes directional capabilities of an antenna into account as well as its efficiency [54].

Assuming we want to feed a signal into an antenna having 3 dB of gain, the signal transmitted at the receiving end will be two times strong as if there is no gain for the transmitting antenna. Gain offers a good compromise. For instance, feeding an antenna with 4 dBi of gain with a transmitter power output of *15 Watts* signal will give an Effective Radiated Power (ERP) of *30 Watts* or *13.6 dBW* and Effective Isotropic Radiated Power of (EIRP) of *37.7 Watts* or *15.8 dBW*. Gain and radiation patterns are closely related to each other. Mathematically, an antenna gain can be expressed as [54, 80]:

$$G = 10\log_{10}\frac{\max(U)}{U_o} \tag{2.6}$$

where the maximum (U) is calculated over all possible directions. For our research work, this antenna parameter has been useful for the derivation of the proposed gain model of this work in chapter 4, section 4.2.

2.3.3 Antenna's Directivity

Directivity is one of the most important performance measures in antenna. The ratio of the radiation intensity in a given direction from the antenna to the radiation intensity averaged over all directions is referred to as antenna's directivity [54, 79, 81]. For a better antenna reception, directivity is the maximum goal. Antenna directivity is the normalized radiation intensity (in dB):

$$D = 10\log_{10}\frac{U}{U_o} \tag{2.7}$$

The normalization factor U_o is the total radiated power divided by 4π (power per unit solid angle) [80]:

$$U_o = \frac{p_{rad}}{4\pi} \tag{2.8}$$

Antenna's directivity towards a single direction (θ, φ) can be expressed as [75]:

$$D(\theta,\varphi) = \frac{U(\theta,\varphi)}{U_o} = 4\pi\frac{U(\theta,\varphi)}{w_{rad}} \tag{2.9}$$

where w_{rad} is the radiation power. Mathematically, directivity can be expressed as Equation (2.10), when it is defined as the frequency range over which a particular antenna can properly radiates and receive energy, and this equation can be used to find the directivity for array [42, 46, 82]:

$$D = \frac{\left|AF_{\max}\right|^2}{\frac{1}{4\pi}} \times \left[\int_0^{2\pi}\int_0^{\pi}\left|F(\theta,\phi)\right|^2 \sin\theta d\theta d\phi\right]^{-1} \tag{2.10}$$

Directivity is always in favour of one direction at the expense of another direction. Hence, there will be a better SNR, reduction in interference reception from sides and back, and higher concentration on receiving/transmitting target direction. Directivity has been derived for the pyramidal horn in section 3.2.2 for our research work. The directivity control has also been derived in section 5.4.2.

2.3.4 Radiation pattern

Antenna radiation pattern can be defined as the spatial distribution of power radiated variation of a specific antenna which acts as a directional function away from that antenna. The power variation depends on the direction of arrival of the antenna and is observed in the far field region of that antenna. Radiation pattern provides details like the values of field quantity

and the range of angles over which data is plotted [54]. Some of the radiation properties of the antenna are directivity, gain, radiation intensity, etc.

Antenna radiation pattern can also be described as a plot/chart which can be depicted in 2-D, and as well as 3-D cross section which illustrates the value of antenna's directivity towards all directions in space. To achieve a 2-D plane, the vertical plane and horizontal plane must correspond to the two planes used in as a reference. Radiation pattern in 3-D plot can be developed through the combination of two graphs. The equation for this parameter has been derived and identified with beamwidths and sidelobe levels in section 3.2.3 for our research work, while the isotropic radiator for a far-field radiation pattern has been represented in section 3.3.1.

2.3.5 Null

The zone at which the effective radiated power of an antenna's radiation power is minimum is called a null. The directivity's angle of an antenna's null is always narrower than the main beam. Nulls are normally use to: suppress signals interference in a specified direction, protect interferences from other transmitters when in the horizontal plane. However, null prevents signals reception from another direction not of interest accidentally if not carefully planned. To prevent this, we place null in the vertical plane. Smart antennas is one of the antennas that normally use null to prevent signal interference because it has sharp and narrow null. Antennas void of null when used for direction finding are directed away from the desired signal [54]. The equation that gives the direction of null has been derived in chapter five, section 5.4.1, while the equation for the beamwidth between the first null has also been derived in the same section of chapter for the proposed design.

2.3.6 Polarization

Electric field orientation of an electromagnetic field is used to define the polarization of an antenna. For an antenna to have a good reception of the signal, the polarization of the signal and that of the antenna must match. If there is a mismatch between that of the signal and antenna, there will be poor reception even if, we have the best antenna. Classification of polarization is linear, circular and elliptical. Antenna normally launches electromagnetic waves into space, this determines the initial polarization of the radio wave.

Electric field vector determines the polarization categories. There exist linear polarization, circular polarization and elliptical polarization. If the electric field vector is in the same plane in the direction of propagation, then we have a linear polarization. In Circular

Polarization (CP), the electric field vector rotates round the direction of propagation with a circular motion, achieving one full turn for each Radio Frequency (RF) cycle. There are two types of rotation, (a) Left rotation, and (b) Right rotation. Their rotation can be either of the two [54]. Some of the advantages of circular polarization are: it minimizes the "clutter" echoes received from raindrops in microwave radar application, it is also used to reduce multipath, etc. For elliptical polarization, the electric field remains constant along the length but traces an ellipse as it moves forward.

2.4. Types of Antenna and Their Applications

The three main types of antennas are (a) isotropic, (b) omnidirectional, and (c) directional antennas.

(a) *Isotropic (hypothetical lossless) antenna* emits electromagnetic power in equal amount in all directions. That is equal radiation in all directions. It is an antenna whose response does not depend on the signal's direction of arrival (DOA). It has neither spatial selectivity nor nulls. The isotropic antenna is a theoretical reference point for stating the directive properties of the real antenna. This is a type of antenna that usually uses a mathematical model when developing signal processing algorithms for smart antenna systems. Sensor is an example of isotropic antenna [79].

(b) *Omnidirectional antenna* emits and receive same electromagnetic power/signal in equal amount in all directions on a single two-dimensional (2D) plane in space [83]. In any orthogonal plane, an omnidirectional antenna has a directional pattern, but it has a non-directional pattern in a given plane. It has low gain. One way of increasing omnidirectional antenna gain is to narrow the beamwidth along the vertical or elevation plane. Hence, the antenna's energy will be focussed towards the horizon. Some of the antennas that exhibit omnidirectional patterns are dipoles, loops, and broadside arrays [54]. During its power transmission, energy is wasted because transmission is directed in all directions. Hence, co-channel and adjacent channel interference is increased without need in the system.

(c) *Directional antennas* focus the radiated electromagnetic power to a particular direction in space. Its radiating and receiving electromagnetic waves property in specific directions has made it reduce power loss to the barest minimum. We can also determine antenna's group by the amount of measured power by which a particular antenna radiates in all directions in space. These antennas have a well-defined main beam in the desired directions. They have high gain and shows a high spatial selectivity, highly directive in a specific direction,

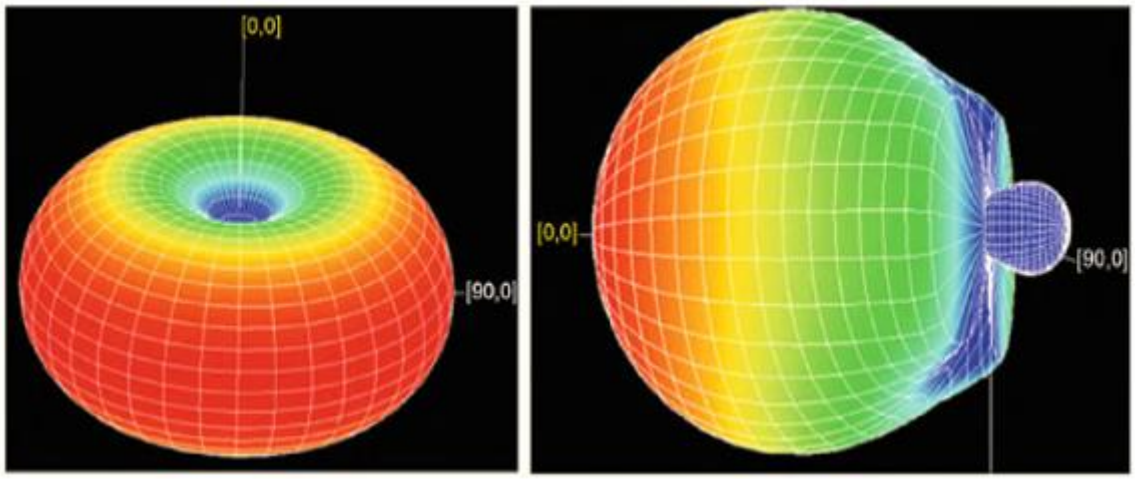

Omnidirectional Directional

Figure 2.1. Omni-directional Radiation Pattern and Directional [9].

and narrow bandwidth [9, 54, 83]. Examples of antenna with omnidirectional and directional radiation patterns are shown in Figure 2.1.

The three fundamental types of antenna that exist are (a) wire-type antenna, (b) aperture type antenna, and (c) antenna arrays. Antenna arrays is a combination of individual antenna elements of either wire antenna or aperture antenna.

2.5. Antenna Arrays

In wireless and mobile communications systems, antenna arrays play a vital role due to its directional reception and transmission (beamforming) [84]. Antenna arrays with signal processing capability have been extensively utilized to improve signal quality, by this means, system capacity, range coverage and link quality are increased [50, 85]. The systems performance depend largely on the design of the antenna arrays. Antenna arrays are applied in radar, sonar, wireless communications, direction-finding, seismology, medical diagnosis and treatment, and has been used to achieve resolution goals in radio astronomy [8, 46, 78, 79, 86]. The field radiated by a small linear antenna is not distributed uniformly in the direction perpendicular to the axis of the antenna. As in the case of a short dipole, the maximum radiation takes place in the direction perpendicular to the axis of the dipole. But radiation decreases to minimum when the polar angle decreases. So this non-uniform radiation characteristics may be used for many broadcast services. But such a characteristics are not preferred in point to point communication. In this type of communication, nearly all the energy are radiated in a specific direction. That means it is desired to have greater directivity in a desired direction

particularly which is not possible with single dipole antenna. Hence the need to increase the field strength in the desired direction by using group of antennas excited simultaneously. Such a group of antennas is called array of antennas or simply antenna arrays.

Higher directivity involving wave interference phenomenon cannot be achieved with conventional antennas, but with antenna arrays, it can be achieved with sidelobe suppression and beamwidth reduction. Grating lobes which are sidelobes can be avoided if random arrays are used wherever the antenna elements are distributed above the geometry structure with unequal spacing. Array randomness elements produce sidelobes levels that are lower than the main lobe level. The unequal spacing technique can also be used to reduce the side-lobe level. The existence of sidelobes indicates that the array is radiating energy in unwanted directions [8]. Antenna elements that are equally spaced have periodic radiation pattern with deterministic side lobes.

2.5.1 Adaptive antenna arrays beamforming and beam steering

One of the utmost significant techniques in smart antennas and centrality to all antenna arrays is beamforming. For a specified angle of an antenna, beamforming has the capacity to change the radiation pattern at that angle [87, 88]. For an antenna to remain in a constant position for a specified angle, then the signal loss will be very high [60, 89]. Spatial selectivity is an important factor that must be accomplished either at the transmitting or receiving ends of an antenna. This is possible when beamforming are present. Spatial selectivity is also known as spatial filtering, and can be referred to as a suitable feeding which enables steering and nulling of an arrays of antenna beam to their various directions of interest/not of interest [90]. In the transmission mode, most of the signal energy transmitted from sensors array can be directed in a chosen angular direction. In the reception mode, you can calibrate your group of sensors when receiving signals such that you predominantly receive from a chosen angular direction. The systems that make the beamforming is called beamformer. Beamformer has two major capacity; steering capability and cancellation of interference [91].

Adaptive beamforming is a method which has the capacity to regulate the array pattern in a dynamic way in order to optimize the parameters of the signals received by the antenna elements. Antenna arrays using adaptive beamforming methods can be referred to as a filter because it has the capacity to reject any unwanted signals that its direction of their arrivals are not the same with the wanted signals, due to the spatial properties of the beamforming [91, 92]. This capability can be exploited to increase the spectral efficiency, reduction in multipath fading, etc., and thereby improve the capacity of wireless communication systems. With

adaptive beamforming technique, bit-error rates are reduced and also the co-channel interferences. Adaptive beamforming capability are realized through the use of algorithms.

The simplest adaptive array beamforming algorithm is the Least Mean Square (LMS) algorithm and its modifications. This is method depends on the stochastic approximation of steepest descent method [93, 94]. The second class called the Recursive Least Square (RLS) algorithm. The RLS algorithm has matrix inversion algorithms. The array processor in which the RLS algorithm depends on has an inversion correlation matrix which is used for the processing. One of the popular beamforming algorithm is called the cooperative algorithm. This algorithm can also be referred to as Particle Swarm Optimization (PSO). The function of this algorithm is to overwhelmed series of jammers positions in the field regions from the antenna position.

2.5.2 Antenna arrays factor and pattern multiplication theorem

The basis of the array theory is the pattern multiplication theorem. This theorem states that the combined pattern of *N* identical array elements can be expressed as the element pattern times an array factor [80],

$$\Lambda(\theta, \phi) \tag{2.11}$$

where θ and ϕ are the polar (elevation) and azimuthal (spherical coordinate angle) angles respectively as shown in Figure 2.2. We will derive the pattern multiplication theorem in the azimuthal plane namely $\theta = 90^0$, keeping in mind that the same derivation holds in the elevation plane. Let us assume that a signal from the first array element has phase zero at an observation point located very far from the array. The corresponding phase factor will be e^{j0}. The signal from the second element will have the relative phase at the observation point [80].

$$\varphi = kd\cos\phi + \delta \tag{2.12}$$

Equation (2.12) gives the sum of two components. One of them is the incremental phase shift δ, in the array element feed. The other is the phase shift arising from the different propagation distances to the observation point. The propagation distance for the second element is smaller by $d\cos\phi$ (Figure 2.2).

The corresponding phase shift is that difference multiplied by the wavenumber, *k*. Therefore the phase factor of the second element will be $e^{j\varphi}$. Analogous the phase factor of the third element is $e^{j2\varphi}$, and so on. The field at the observation point is the sum of all element contributions, which yields [42, 80]:

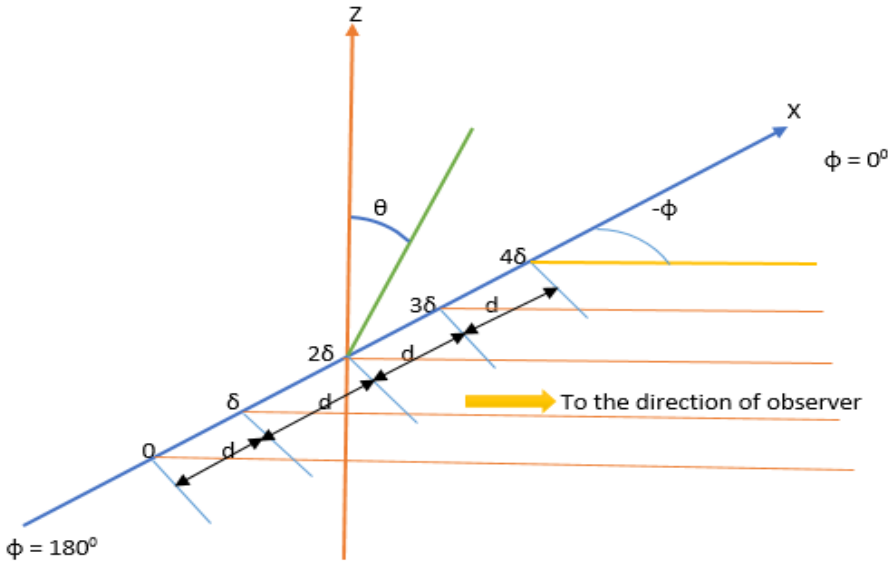

Figure 2.2. A linear five-element array of dipoles.

$$\Lambda(\varphi) = e^{j0} + e^{j\varphi} + e^{j2\varphi} + \mathrm{L} + e^{j(N-1)\varphi} \tag{2.13}$$

To simplify the preceding expression for $\Lambda(\varphi)$, let us multiply both sides by $e^{j\varphi}$, obtaining

$$e^{j\varphi}\Lambda(\varphi) = e^{j\varphi} + e^{j2\varphi} + \mathrm{L} + e^{j(N-1)\varphi} \tag{2.14}$$

Subtracting Equation (2.14) from (2.13) yields:

$$(1-e^{j\varphi})\Lambda(\varphi) = 1-e^{jN\varphi} \tag{2.15}$$

Solving for the array factor, we obtain:

$$\Lambda(\varphi) = \frac{1-e^{jN\varphi}}{1-e^{j\varphi}} = \frac{e^{jN\varphi/2}}{e^{j\varphi/2}} \times \frac{e^{-jN\varphi/2} - e^{jN\varphi/2}}{e^{-j\varphi/2} - e^{j\varphi/2}} = e^{j\varphi\left[(N-1)/2\right]} \frac{\sin\left(\frac{N\varphi}{2}\right)}{\sin\left(\frac{N\varphi}{2}\right)} \tag{2.16}$$

Since we are usually concerned only with the magnitude of the far-zone radiation pattern, we can drop the exponential phase term called the array factor as:

$$\Lambda(\varphi) = \left| \frac{\sin\left(\frac{N\varphi}{2}\right)}{\sin\left(\frac{N\varphi}{2}\right)} \right| \tag{2.17}$$

Note that $\Lambda_{max}(\varphi)$ attains a maximum value of $\Lambda_{max} = N$ when $\varphi = 0$. If the number of elements are fixed, there are a great variety of different array factors that can be obtained, depending on the element spacing d and differential phase shift δ. Once the array factor is calculated using Equation (2.17), the beam pattern is obtained as a product of $\Lambda(\varphi)$ and the beam pattern of the individual array element [80].

The array response is also known as array factor. The array response depends on the antenna element parameters and its geometries [9, 54]. The combination of radiating elements effect without specification to the element radiation pattern being taken into account are measured by array factor. The normalized array pattern $\Lambda_n(\theta,\phi)$, for each element can be expressed as

$$NF(\theta,\phi) = \sum_{N=1}^{N} T_n \Lambda_n(\theta,\phi) e^{j(\xi_n+\delta_n)} \times \left[\max \left\{ \left[\sum_{n=1}^{N} T_n \Lambda_n(\theta,\phi) e^{j(\xi_n+\delta_n)} \right] \right\} \right]^{-1} \tag{2.18}$$

2.6. Effects of Mutual Coupling in Antenna Arrays

Theoretical array does not gives optimum array pattern synthesis performance. Practically, emphasis must be laid on: the effects of system errors on antenna performance, for instance mutual coupling (which is an important electromagnetic characteristics between the antenna elements) [95], cross correlation of the complex patterns, and signal's distortion on the circuitry of transceivers, affects the array gain, beamwidth, etc.

In a real antenna array, the antenna elements interact with one another electromagnetically and alter the currents and impedances from what would exist if the elements were isolated.

Mutual coupling effects between antenna elements in an array must be reduced because the existence of mutual coupling affects the performance of a smart antenna arrays when the inter-element spacing is greater than or lower than the half-wavelength, and also reduces the speed of its response [96, 97]. *Babur et. al.* [98] have analysed mutual coupling effects and proposed adequate calibration on the beamforming transmit for the ideally orthogonal signals as well as for three typical space-time codes. *Abdala* and *Abdelraheem* [99] investigated mutual coupling reduction between array elements by applying UC-EBG structure in between the antenna elements. The characterisation of the EBG is prioritized, while the transmission coefficient from one element to another while feeding the array elements individually was examined separately. *Bernety and Yakovlev* used a confocal elliptical metasurface cloaks for the reduction of mutual coupling between neighboring strips of the dipole antennas located in close proximity to each other. The author used a mantle cloaking method realized by conformal and confocal elliptical printed subwavelength structures in order to make resonating elements invisible [100]. In [101], a new fundamental technique that was suitable for the analysis of

near-field different from the previous perspective of far-field and circuit parameters was examined.

Mutual coupling are normally characterized by using the parameters such as mutual impedance, s-parameters, a coupling matrix, or an embedded element. Strong mutual coupling are experienced strongly whenever the arrays are able to scan its beam closely towards the end-fire direction [102]. With this, the steering vectors are bound to change. The change will cause inaccuracies in steering vectors of the antenna arrays. The performances of some adaptive nulling algorithms will be affected and also the estimation of the direction of arrival [103]. It has a tremendous influence on the BER for the switched beam approach, hence reducing the system performance [29, 104].

2.7. Brief History of Smart Antennas

Historically, the word ‘‘Smart Antenna’’ came from the adaptive antenna. Smart antennas is the vital component of the wireless communications system that transmits/receive Radio Frequency (RF) signals for advance processing to realize an array gain that improves the spectral efficiency. In the early 1990s, smart antenna systems were born into the family of adaptive antenna arrays for military use so as to suppress interfering signals from their enemy during the World War II. This application was brought into mobile communications by various scientists and researchers. Due to the characteristics of smart antennas, its technology found a wide application in military communication systems such as radar system [105-109].

The adaptive antennas usage technique in communication systems originally attracted attention in military utilizations; as the systems were designed for use in military earlier, especially in electronic warfare so as to oppose electronic jamming from the enemy [10, 104, 110]. The application uses a radio frequency receiver. The function of this radio receiver is to sample incoming signals from various directions in space. The radio receiver are embedded with multiple antennas and signal processing algorithm that aid the signal processing for the exact location of their enemy radio transmission. This concept uses the propagation delay of that particular transmission if the signal is propagated as a plane wave. Such a receivers are called “smart antennas”. Its application in the military is easy communication in the battlefield, no spoofing, low power consumption on high-speed multimedia battlefield networks, and lightweight video displays with in-built smart antenna usage for the interchange of time maps and pictures.

Smart antennas are sometimes describe as smart/intelligent antennas. In a real scenario, antennas cannot make themselves smart but the systems that comprises the antennas are smart. It is the automatic change in radiation pattern and its response to the available environmental signals with the aid of the associated Digital Signal Processor (DSP) and the array of antennas that makes the system to be called smart antennas. This aids in increasing the system performance characteristics of wireless communication systems [18]. To process any information that are sensitive directionally, array of antennas is needed, with the conglomerate of inputs to control the transmitted signal adaptively which our main research work is based on the structure.

2.8. Types of Smart Antennas

There are mainly three techniques to realize special antennas which has the ability to change their antenna radiation patterns dynamically to lessen signal impairments effects and simultaneously reduce multipath fading and increase range coverage [50]. They are [31, 37, 67, 111]:

2.8.1 Switched beam approach

The switched beam system comprises simply RF switch between discrete directional antennas pattern of an array which can be formed by beamforming network, while aiding high gain and controlled beamwidth [47, 92, 112]. This approach can be considered as an extension of cellular sectrorization scheme [50, 56, 67]. It has a number of fixed antenna beams covering a specific sector. The system will turn on a beam towards a desired signal at a time in order to increase the received signal strength. If the received signal is changing direction or multiple desired signals exist, the system will turn on the appropriate beam so that all the desired signals can be covered.

This system consist of basic switching task between distinct directive antennas/array of antennas. It has a higher network capacity due to its exploitation of antenna arrays and signal processing techniques to centre its energy in a specific beam-width when compared to omnidirectional antenna. Due to its high directive beams, it chooses the beam which gives the best signal-to-noise-ratio. In some recent researches, it has been shown that in WLAN access points can use switched beam for the extension of their network capacity [56, 113].

This approach is usually realized using a passive feeding networks, such as Butler matrices. Several techniques have been proposed through research so as to reduce the sidelobe level in switched beam antennas as follows:

i. *Chou and Yu* [114], examined a switch beam in which the transmitting antenna switches beams to search for the RX antennas from a spot to another as those conceptually introduced in the conventional far-field smart antennas. The author used a one-dimensional (1D) beam-switching device in the antenna design with the other dimension to ensure that focused fields are radiated in the designated near zone.
ii. The technique of increasing the number of radiating elements and using power dividers to obtain amplitude taper across the antenna array. This require an increase of antenna aperture, and consequently, narrower beams are accomplished and there is a reduction in beam crossover.
iii. The technique in which two separate feeding networks are used for generating all beams, which results in the need of switching between feeding networks or doubling the aperture size [115].

Switched beam antenna systems employ array of antenna which radiates some coinciding fixed beams that cover a selected angular space. Figure 2.3 shows shows a beamforming network comprising of a phase shifting network, which forms various beams looking in a specific direction. RF switch function as an actuator that activates the exact beam in the desired direction, while the control logic as a selector that picks the right beam. The control logic is controlled by means of an algorithm that scans all the beams and chooses the one that receives the strongest signal centred on a measurement through the detector.

Switched beam approach is easy in operation nevertheless is not appropriate for high interference zones, but best suitable for zero-interference environment. With the aid of multibeam feed networks (Butler matrix), we can have a beam-switching antennas, but such a Butler matrix are large in size and lossy, hence we have more than a portable smart antennas [116]. Some of the approaches that utilize fixed phase shifting networks (Butler matrix arrays and Blass matrix arrays) are discusses below:

(a) Butler matrix arrays

A Butler matrix consists of *N* multiple inputs and *N* multiple outputs. Each of the input port will produce linear phase distribution at each output. In comparison to other networks, Butler matrix has a lot of advantages such as easier in implementation using its hybrids and phase shifters than others switched beam networks, the beam generated by Butler matrix is narrow and has high directivity, beam scanning continuity is realizable using Butler matrix, its

amplitude/phase is accurate and high in operational, the matrix generated by Butler matrix can decouple orthogonal modes in a natural form, it has low insertion loss. Butler matrix techniques is used to provide the necessary phase shift for a linear antenna array. It is used to control the beamforming and beam steering process through an antenna array. The advantage of using the Butler Matrix include frequency reuse and an improved signal to clutter/noise ratio [117]. It is a beamforming network that uses a combination of 90^0 hybrids and phase shifters [10, 42, 92].

N x N Butler matrix is a passive microwave network consisting of *N* inputs, *N* outputs, *N* hybrids, *N* crossover to isolate the cross-lines in the planar layout and some phase shifters [118, 119]. To form multibeam radiation, the phase difference between antenna elements for a *d*-spaced *N*-element array for the *pth* beam radiation direction of θ is given by [40, 120]

$$\mu_n = kd \sin\theta = \pm \frac{2p-1}{2N} \times \pi \tag{2.19}$$

Consider the complete *8 x 8* Butler matrix array as shown in Figure 2.4. Exciting one of the input ports by RF signal, the output ports feeding the array elements are excited correspondingly although in a progressive phase between them. This gives the beam radiation at a particular angle. If there is a need for multiple beams, two or more input ports needed to be excited instantaneously.

Earlier researchers proposed a beam-steering antenna array using a Butler matrix, which has an irreducible complexity [121], while others have used Electromagnetic Band-Gap

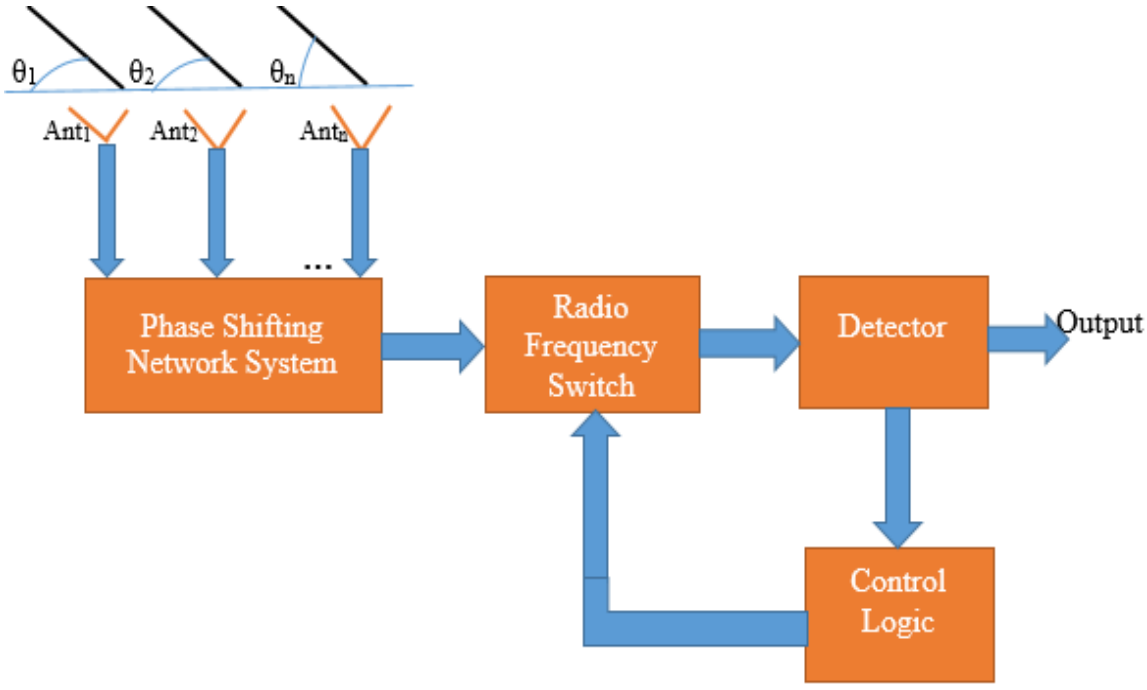

Figure 2.3. Block diagram of a switched-beam antenna structures.

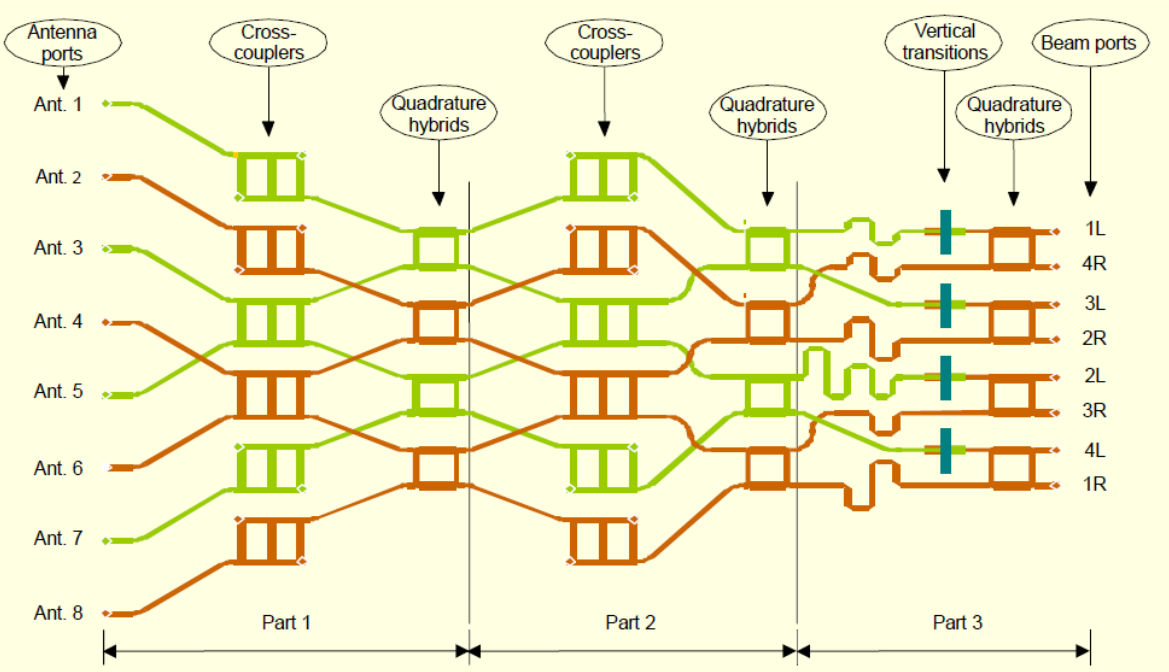

Figure 2.4. Butler Matrix array [120].

(EBG) structures to produce reconfigurable agile antennas. However, reconfigurable EBG structures contain a lot of active elements, which leads to more complexity, more power supply, and high cost.

Obviously, the major challenge of reconfigurable antennas resides in the number of active elements used in the design [122, 123]. The multiport network of Butler matrix is relatively bulky and intricate. [124]. It presents a multilayer *N x N* Butler matrix based on corrugated slot-coupled structures, which operates over the complete UWB band (*3.1 to 10.6 GHz*) with excellent phase and amplitude performance, it makes use of highly optimized building elements (i.e., phase shifters and quadrature hybrids) with excellent broadband performance.

(b) Blass matrix arrays

A Bass matrix [42, 92, 125, 126] consist of a microwave feeding network for antenna arrays comprising of a number of rows that are equivalent to the number of beams to be instantaneously created and a number columns joined to the radiating elements as shown in Figure 2.5. The Blass matrix is a very flexible beamformer that is suitable for broadband operation. It has the capacity to generate random beams at random positions and in spite of random shapes. It is cheaper and has a low profile.

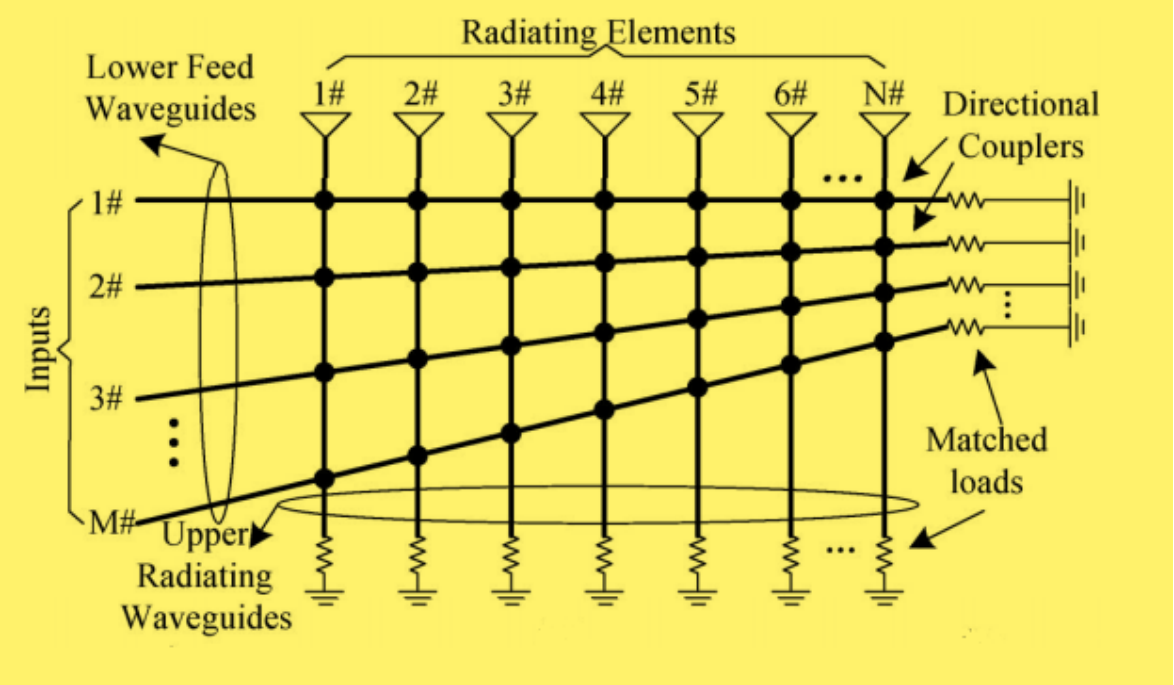

Figure 2.5. Schematic of a Blass matrix [125].

The Blass matrix has two sets of transmission lines. The transmission lines are normally referred to as (rows and columns) matrix. The rows and columns matrix are traversed as each row and column crossover through a directional cross coupler. The corresponding feed lines must be ended on a matched load in order to avoid signals reflection due to the application of signals at each input port. The signals are propagated through the feed lines. The radiating elements are excited because at each crossover, a slight percentage of the signal is coupled into each column. *Chen et. al*. [125], demonstrated the principle of Blass matrix arrays using a double layer planar SIW. With SIW, a slot array antennas were installed at the output ports of the upper radiating SIWs. In ref. [126], a novel Lossy Blass Matrix Beam-Forming Network (LBMBFN) design method was proposed.

2.8.2 Adaptive Array (or Optimum combining) Approach:

The adaptive antenna has become a core system component in future-generation mobile networks due to its operational benefits by exploiting the spatial domain via adaptive beamformer [40], and can also be referred to as digitally adaptive beamformers or adaptive antenna [50]. In adaptive array systems, signal-processing methods are used to increase the capacity and the coverage, to improve the link quality and last but not the least to improve the spatial reuse. The beamforming and the Direction-Of-Arrival (DOA) algorithms represent some examples in this area. In this approach, the beam-pattern is adapted to the received signal

using a reference signal. The Direction-Of-Arrival (DOA) estimation algorithms for determining the direction of interferers can be added. The beam pattern can then be adjusted to null the interferers. The adaptive antenna is capable of increasing the reception of intended signals and suppressing the interference signals. This capability is achieved through algorithms that are able to locate the direction of both desired and interference signals. This information is then used to steer the main beam towards the desired signals and place nulls on the interference signals by an adjustable weighting set [112].

Adaptive antennas have the capacity to separate the desired signals from interferer signals and external noise, and sometimes called filter antennas [127]. This can be realized by radiation power in a precise direction and rejecting undesired signals from another incidence angles [30].

It has been presented in [92] that adaptive arrays provide a better range increase and the received signal quality than switched-beam (multi-beam) antennas. Since switched-beam antennas require less complexity, particularly with respect to weight/beam tracking, they appear to be preferable for Code Division Multiple Access (CDMA) [67, 10]. In contrast, adaptive arrays are more suitable for Time Division Multiple Access (TDMA) applications, especially in environments with the large angular spread. The adaptive array system is the "Smarter" of the three techniques and characterizes the utmost advanced smart antennas method up to the present time. Using a diversity of state-of-the-art signal-processing algorithms, the system tracks down the mobile user signals dynamically by steering the main beam radiated towards the user and simultaneously forming spatial nulls in the directions of the radiation pattern of the unwanted interference signal. This Technology is used to detect and monitor signals in heavy interference environments as shown in Figure 2.6 [50].

Arrays are incorporated in the system like switched beam systems. Normally, the received signals from the individual spatially scattered antenna elements are multiplied by weights. These weights are complex in nature and have the capacity to change the amplitude and phase. A weight is normally assigned to each antenna array element amplitudes and phases; these are constantly updated/adjusted electronically to reflect/generate desired radiation pattern in response to the changing signal environment. This is done in order to increase the antenna gain in the desired direction while attenuating in the direction of the unwanted signals.

Both systems try to increase gain in accordance with the user's location; however, only the adaptive system provides optimal gain while simultaneously identifying, tracking, and minimizing interfering signals. Switched beam and adaptive array systems, have several hardware characteristics in common and are well-known mostly by their adaptive/smart signal processing algorithms capabilities called intelligence. The algorithm constantly differentiates

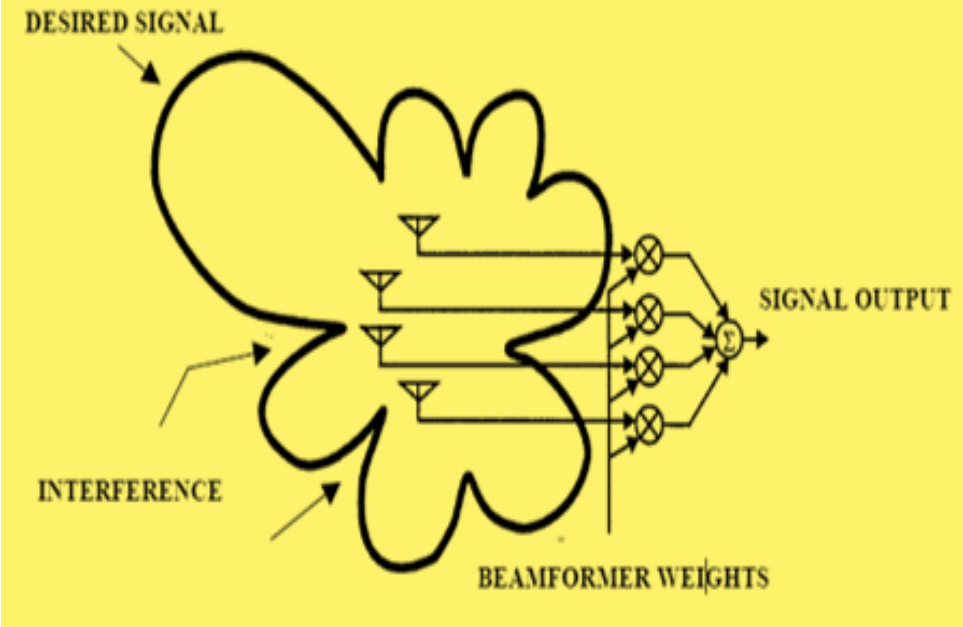

Figure 2.6. Adaptive array [128].

between desired signals, multipath, and interfering signals in addition to the directions of arrival calculations. Adaptive arrays consist of adjusting beam pattern in multipath environments to use the Signal to Noise Ratio (SNR) on the antenna array gain and nulling out interference in the direction of the signal [30]. Due to the ability of adaptive array system to adjust the radiation pattern to the RF signal environment in real time, hence it provides more degree of freedom [47, 67, 92, 128]. Figure 2.7 shows the basic layout of an adaptive antenna array that has numbers of antenna array. The array of antenna elements are connected together through the controller so as to form a *Beamforming network* output.

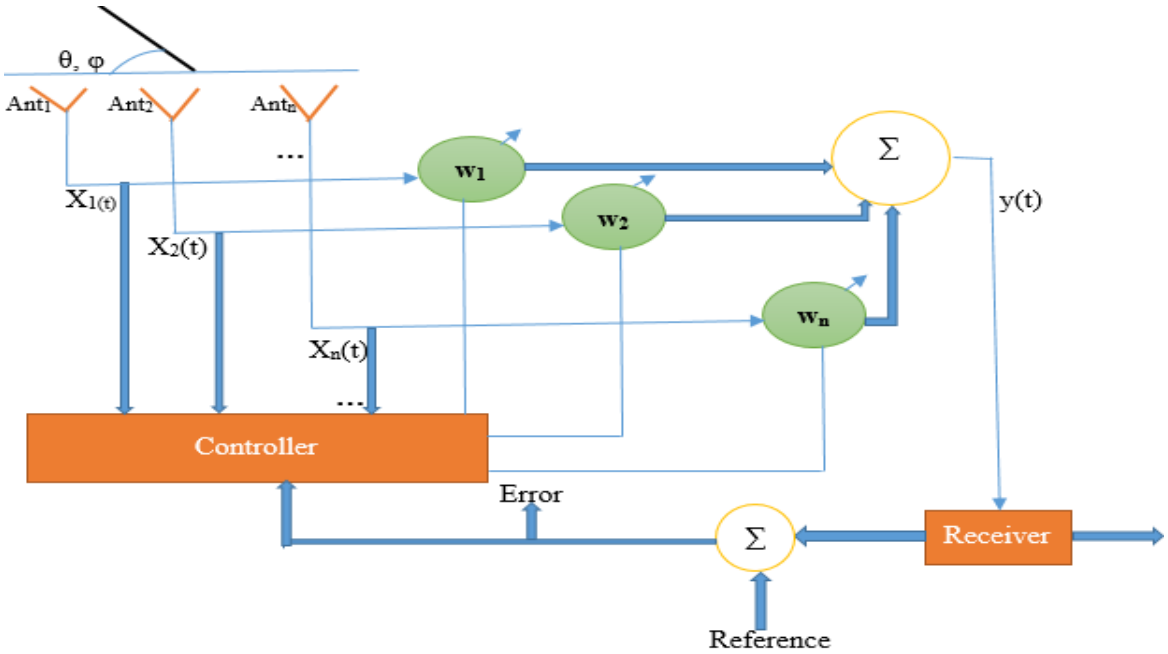

Figure 2.7. Basic layout for adaptive antenna array.

For a signal s of wavelength λ (plane wave) incident on an N element array with spacing d from direction (θ, φ), the phase shift due to propagation delay from the origin to element (x_i, y_i, z_i) can be expressed generally as

$$\delta\varphi = \frac{2\pi}{\lambda}\left(x_i \cos\varphi \sin\theta + y_i \sin\varphi \sin\theta + z_i \cos\theta\right) \tag{2.20}$$

For the case of a linear array with elements equally spaced along the x-axis ($\delta_x = d$), the received signal at antenna element n can be expressed as Equation (2.21)

$$x_n(t) = s(t)e^{-j\frac{2\pi}{\lambda}nd\cos\varphi\sin\theta} \tag{2.21}$$

and the signal at the antenna array output is

$$y(t) = \sum_{n=0}^{N-1} w_n x_n(t) = s(t)\sum_{n=0}^{N-1} w_n e^{-j\frac{2\pi}{\lambda}nd\cos\varphi\sin\theta} = s(t)\, f(\theta,\varphi) \tag{2.22}$$

where the term $f(\theta,\phi)$ is the array factor. Note that in the general case the array factor should include another (multiplicative) term, the field pattern of each array element (i. e. the above assumes that each array element pattern is isotropic). For a signal incident from direction (θ,ϕ), the phase of the signal available at each antenna element represents the *steering vector*, (viewed in another way can be considered as the impulse response of the array). The set of steering vectors for all values of (θ,ϕ) is called the *array manifold*.

2.8.3 Dynamically phased array (or direction findings) approach:

In a phased array the phases of the exciting currents in control of the beam steering in each of the antenna element of the array are adjusted to change the pattern of the array, typically to scan a pattern maximum or null to a desired direction.

Phased array antennas (Figure 2.8) make use of the angle-of-arrival information from the desired user to steer the main beams towards the desired user [56]. In this case, directions of arrival from the users are first estimated, then the weights of the beamformer are calculated in accordance with the specified directions. By the application of direction of arrival algorithm for the signal received signal from the mobile subscriber, this will enable continuous tracking of the user and it can be viewed as a generation of the switched beam concept [50]. The receiver power is maximized and it does not null the interference. Phased array using active array configurations can adapt the antenna pattern according to the change of mobile communication environment.

An array of antenna elements can be pointed in a direction by changing the phase of the signals emitted from each element so that they arrive on the wavefront in the preferred direction

at the same time, thus constructively interfering in the pointing direction and destructively interfering in most if not all other directions. The power pattern of an array antenna is the product of the power pattern of the individual elements, assuming the same pattern for each element, and the power pattern of the array factor which accounts for the constructive and destructive interference [31].

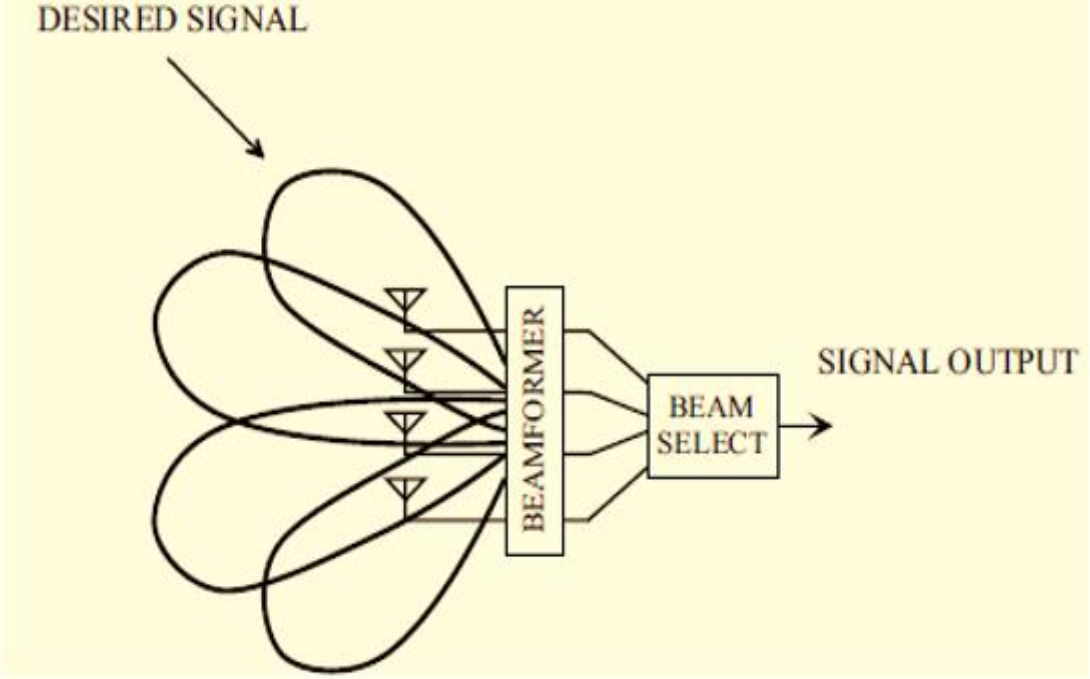

Figure 2.8. Phased array [128].

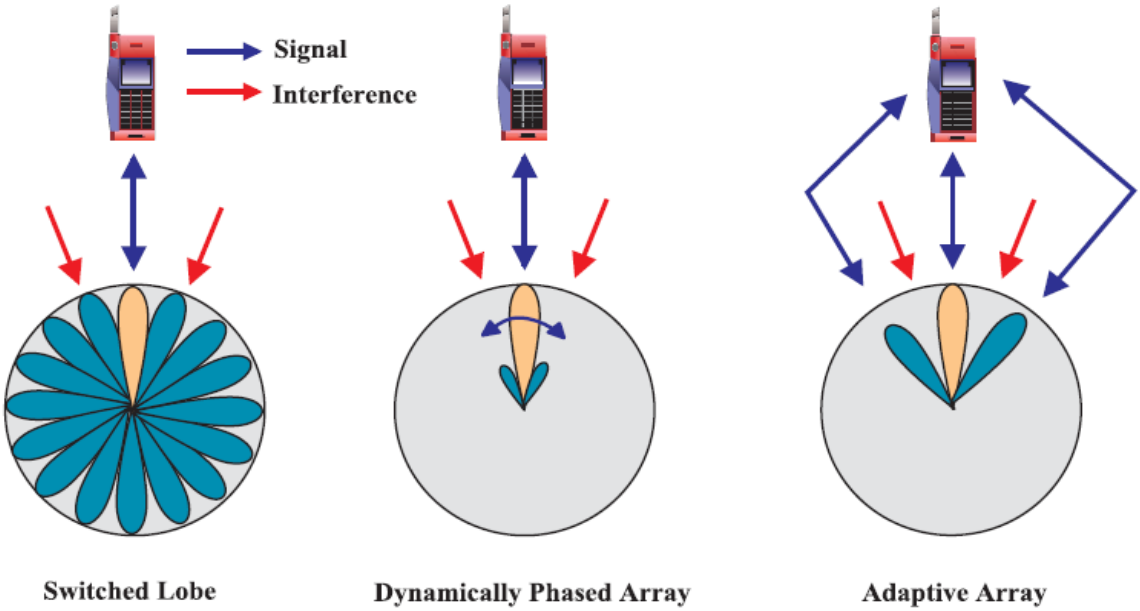

Figure 2.9. Different smart antenna concepts [10].

Table 2.1. Features of three main techniques of smart antennas

Switched Beam Technique	**Dynamically Phased Arrays Technique**	**Adaptive Arrays Technique (used in our proposed research model)**
Fixed multiple directional beams and narrow beamwidths are used.	It can be used to steer arrays so as to increase its sensitivity in a specified direction.	It steers beam towards SoI and places null in the interference directions.
It needed a phase shifts in comparison to Butler matrix which are supplied by means of simple fixed phase shifting.	It is normally used so as to deliver diversity reception.	It requires implementation of DSP technology
Simple algorithms are selected for beam selection.	Its capacity to allow beam jumping within the juxtapose target happens in few microseconds.	Beam and null steering require complex adaptive algorithms.
In comparison with adaptive array, reasonable interaction is required the base station and mobile unit.	It has enough capacity to make available agile beam even under computer control.	It has a better advantage of increased capacity and coverage over switch beam systems because of improved interference rejection.
It is cheap and has low complexity in structure due to its low technology	Indiscriminately methods of surveillance and tracking.	It is difficult and expensive to integrate into existing cellular systems.
Simple and cheap to Integration into existing cellular system.	Its dwell time are free and eligible.	As the mobile moves, continuous steering of the beam is vital, as the mobile unit and base station needs constant contact.
Significant increase in coverage and capacity is provided in comparison with conventional antenna based systems.	It has multiple mode of function during its operation through the simultaneous emission of various beams.	Continuously adapting the pattern towards the optimal characteristic
Due to multiple narrow beams usage, frequent intra-cell hand-offs between beams have to be handled as mobile changes position from one beam to another.	Dynamically Phased Arrays systems have a constant operation despite even if there is fault in one of the components which reduces its beam sharpness.	Frequent intra-cell hand-offs are less due to continuous following of the mobile user.
It can neither distinguish between direct signals nor interfering/multipath signals, hence the interfering signal increases more than the desired signal.	It has a limited coverage area of 120^0 in azimuth and elevation angle, which is a disadvantage.	Multipath components can either be added or rejected through the delays correction so as to improve signal quality.

Electronically-steered phased arrays are well known for their ability to generate a directive beam according to a given control signal and may be a possible multipath mitigation solution [120]. Phased arrays are being developed for land mobile stations for the satellite communication system [74]. Figure 2.9 shows the three techniques used in smart antenna systems. Some of the features of these techniques are highlighted in Table 2.1.

2.9. Basic Operation of Smart Antenna Systems

Smart antennas performs two major functions [18]: (i) DOA estimation and (ii) beamforming. In order for the smart antenna to be able provide the required functionality and optimisation of the transmission and reception, they need to be able to measures the Direction of Arrival (DOA) of the signals [18]. The information received by the antenna array is passed to the signal processor within the antenna and this provides the required analysis. This is achieved through the direction of arrival algorithms. After the analysis of DOA and interfering signals, the control circuitry within the antenna is able to optimise the directional beam pattern of the adaptive antenna array to provide the required performance.

From the phased arrays, it is obvious that the direction of radiation of the main beam in an array is subjected to the phase difference between the antenna elements of the array. Hence it is possible to continuously steer the main beam in any direction by adjusting the progressive phase difference between the elements. The power of smart antenna comes from the fact that it can steer and reshape its radiation pattern to maximize Signal to Noise Ratio (SNR) or interference alleviation [18]. This is done electronically using beamforming algorithms without the involvement of the mechanical parts to steer the array [4].

The most imperative process in smart antenna system is beam forming, which changes the beam pattern of an antenna for a particular angle. If the antenna does not change the position for the specified angle, then the signal loss will be very high [60]. For beamforming, the signals that are incident on each antenna elements are combined dynamically to form the desired beamformed output. Before the incoming signals are weighted they are brought down to baseband or Intermediate Frequencies (IF). The receivers provided at the output of each element perform the necessary frequency down conversion. The digital signal processors (DSP) in the system is used to weigh the incoming signal. Hence it is essential that the down-converted signal be converted into digital format before they are processed by the DSP. Analog to digital converters (ADC's) are provided for this purpose. For accurate performance, they are required to provide accurate translation of the RF signal from the analogue to the digital

domain. The digital signal processor accepts the intermediate frequencies signal in digital format and the processing of the digital data is driven by software. The processor interprets the incoming data information, determines the complex weights (amplification and phase information) and multiplies the weights to each element output to optimize the array pattern. The optimization is based on a particular criterion, which minimizes the contribution from noise and interference while producing maximum beam gain at the desired direction. There are several algorithms based on different criteria for updating and computing the optimum weights, this is the main novelty in smart antenna systems.

2.10. Novelty and Performance Improvements on Smart Antennas

The simple architecture of smart antennas design has led to the wide-spread research in antenna and signal processing. We refer to it as a *smart antenna divide* because is a combination of antenna arrays and signal processing algorithms. To design a suitable smart antennas, an antenna arrays is needed that can provide signals from each antenna element. The signals are transmitted for processing in Digital Signal Processing (DSP). The digital processing of the signal has nothing to do with the design of a particular antenna, but it models the antennas as sampling point in the spatial domain. This method of smart antennas design is known as analytical approach of smart antennas. This has been effective for years supported by researchers, and has produced an amazing smart antenna systems. Researches in smart antennas has made antenna arrays processing [15] and digital signal processing to be areas where a researcher can have a place of haven to develop their talents. Most of the signal processing algorithms in smart antennas are used in the area of estimation of direction of arrival and beamforming processing algorithms.

The performance of smart antennas depend on the proper implementation of Direction-Of-Arrival (DOA) algorithms estimation [14] and Beam-forming [11]. Various algorithms are used for the calculation of the optimum weights. Multiple Signal Classification (MUSIC) [7, 10, 18, 30], Root MUSIC [16], and ESPRIT [10, 30] algorithms, blind source separation algorithms, and SDMA [10, 30] algorithms have improved the capacity of cellular systems. To improve the performance of smart antennas, it is necessary to bridge the gap between the antenna design domain and the digital signal processing domain. Hence, the journey of smart antenna techniques began and a large amount of scientific contributions have been published on numerous conferences and in scientific journals.

A lot of research had been done by various researchers on how to improve the performance of smart antenna systems using various techniques [15, 29, 40, 45, 57, 60, 61]. The performance improvements is majorly based on the digital signal processing algorithms. Various algorithms have been used such as Least Mean Square (LMS) algorithm [94], Recursive Least Square (RLS) algorithm, Normalized Least Mean Square (NLMS), Fractional Least Mean Square (FLMS), and Constant Modulus Algorithm (CMA), etc. [106]. LMS algorithm is a popular algorithm in smart antenna, hence researchers are continuously improving on it. *Godara* [129] describe the application of LMS algorithm, while *Ali et. al*. [93] described the Robust Least Mean Square (R-LMS) algorithm with ratio parameters so as to regulate product vectors contribution. The applications of these algorithms has been applied in chapter six of this thesis.

2.11. Modelling of RF Security Systems using Smart Antennas.

Smart antennas are applied in various areas of communications. One of its application is in RF security systems reported by *Oluwole* and *Srivastava* [65].

The work introduced an analysis about how a radio frequency can be secured using smart antenna arrays. To receive radio signals, an antenna is required for signal propagation. Nevertheless, as the antenna will take up thousands of radio signals simultaneously, a radio tuner is indispensable to tune into a precise frequency. In the research analysis, three antenna elements array were used: (a) the first antenna elements was used for the transmission/reception (transceiver) of RF signal. The transceiver was purposely used for transmitting virtual information signal far away from the mobile station. (b) The two antenna elements at the mobile station is being used as descrambler against any illegitimate activities.

Wireless networks transmit their data at any layer of the open systems interconnection protocols stack using Radio Frequency (RF) or optical wavelengths. Signal transmission through free space offers opportunities for interlopers and hackers that come from any direction. A foremost problem to secure communication systems is the probability of unlicensed penetration. The unlicensed penetration of this kind is popularly known as hacking. Numerous techniques have been employed to overcome the problem of hacking. Firmly speaking, is commonly refers to a person/software that breaks into or interrupts computer systems or networks to manoeuvre data or generate havoc by uploading malicious code. HackRF provides an assessment equipment module for RF associated research and measurements which apply to a frequency range from *1 MHz* to *6 GHz*, and spread over many

registered and unregistered as well as ham radio bands. Hacker may possibly target the RF modulation plane with customary electronic warfare, the objective could be congested with adequate RF power or echo attacks could possibly be used. Hacks could be away from modulation in binary level. This conveys that any signal received by the radio is sufficient to hack the system.

2.11.1 Smart antennas as a transceiver

Antenna arrays can be adopted in any wireless communication transceiver (receiver/transmitter) at communication base station that transmits/receives radio frequency signals by means of a single or multiple antennas. The advantage of antenna arrays in such a communication station is responsible for the performance enhancements above the use of only one antenna element. These antenna enhancements comprise directionality, Signal to Noise Ratio (SNR), interference elimination for received signals, security, and decreased power transmitted signals requirement for the transmit power. Hence, antenna arrays could be adopted for signal transmission/reception.

The transceiver comprises an array of transmit antenna elements. The array transmits antenna elements and the two other antennas connected to the main transceiver is used for the mode of the operation. Here in this research work (*Oluwole* and *Srivastava* [65]), smart antenna is used for security purpose against any hackers on the RF transmission signals. The wireless transceiver antenna arrays is used for remotely transmitting information signal virtual to mobile station, while the two antennas at the mobile station is being used as descrambler against any criminal activities. The proposed block diagram for smart antenna RF security is shown in Figure 2.10. Transceiver uses antenna array for communicating in a cellular communication system with a polarity of mobile stations. Therefore, the antenna array of the transceiver is used in this research work to design and communicate with antennas at the mobile stations. When there is an attack on the RF, there will be signal alarm in the transceiver for remotely transmitting alarm information relative to mobile station.

2.11.2 RF Security Antenna Design

Nearly all radio transceiver systems will have to a certain degree of related architectures and part common characteristics and difficulties. They all need some form of antennas, RF transmit and receive amplifiers, RF/baseband transmit and receive filters, transmitter and receiver modulation circuits and Digital Signal Processing (DSP), descrambler, frequency synthesizers and clock generators (often shared by both receive and transmit circuits), and DC

power supplies. All these are coupled together in Figure 2.11. The hacking prevention system works through a descrambler in the RF board level in Figure 2.11. This is an electronic device that decodes a scrambled transmission, typically a radio signal, into a signal that is intelligible to the receiving device. This will make the radio or telephonic message impenetrable to hackers by analytically varying the transmission frequencies. A random number is generated in the descrambler. Using this random number, a key is calculated, which corresponds to the authorization packet corresponding to the generated random number.

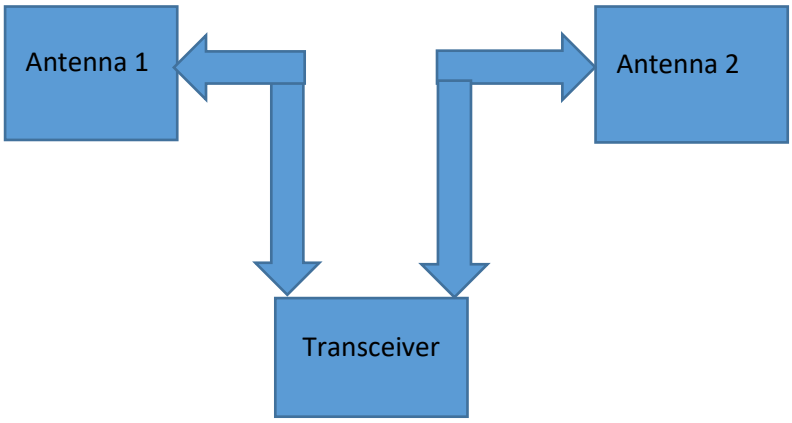

Figure 2.10. Block diagram for RF smart antenna security system.

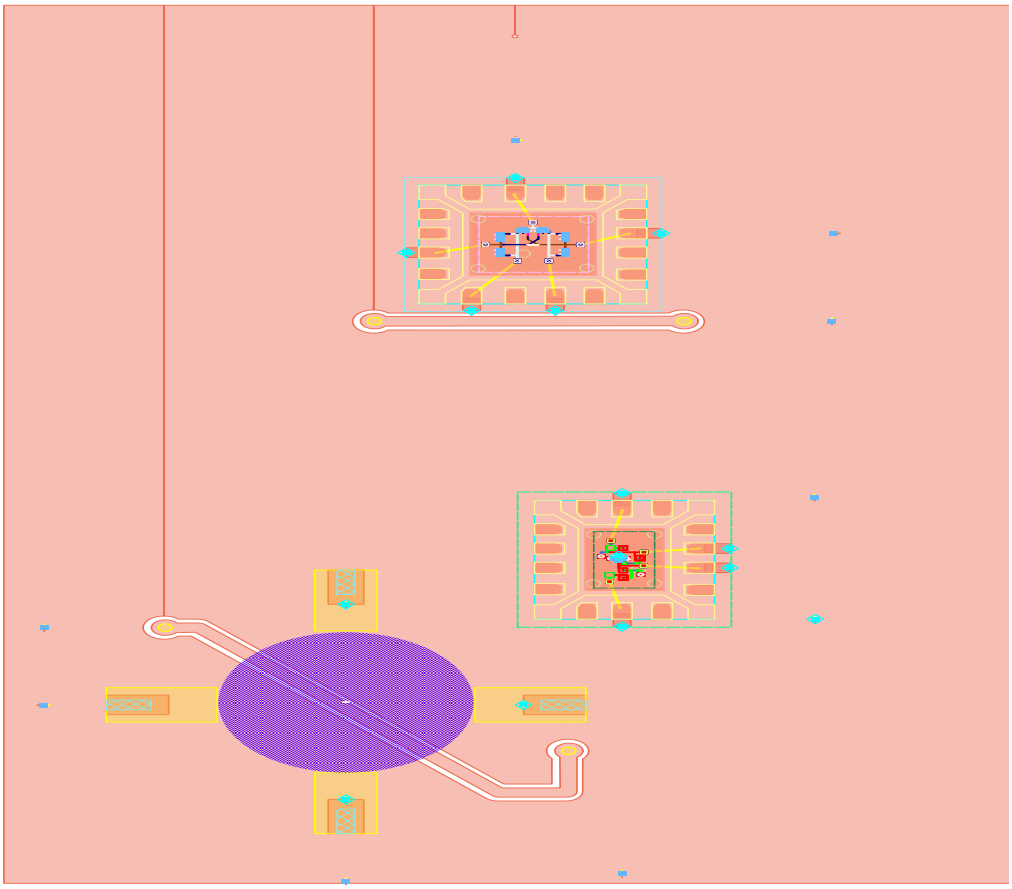

Figure 2.11. RF board level smart antenna transceiver system layout.

This generated key and the offset value, which corresponds to the generated random number, are used for descrambling key analysis. The two antenna elements shown in Figure 2.10 perform the function of sensor networks between the transceiver and the outside world. Whenever there is an attack on the RF, an alarm switch included in the transceiver will indicate the presence of intruder/hacker on the system.

The transceiver comprises of an array of transmit antenna elements. The technique adopts the distant transceiver for signals reception when the central transceiver transmits downlink setting signals. When the focal transceiver likewise has a receive antenna array, the distant transceiver can transmit uplink setting signals to the central transceiver for decisive uplink identity/signature. The downlink and uplink identities/signatures are used to control a calibration task as a description for intruders/hackers in the successions that comprise the antenna arrays, and that facilitate downlink smart antenna processing identities to be driven from uplink smart antenna processing identities when the central transceiver includes channels for smart antenna processing according to identities.

Hence, hackers can steal data/information on the transmitted signal. At frequencies outside the working frequency, tracks and antenna elements do not behave as ideal elements. Figure 2.11 shows the RF layout system for the work. The electronic antenna switch in the transceiver that links the antenna to the transmitter or receiver cantered on the logic state of one or else two control levels. This switch was used to switch ON alarm system in the case of hackers/intruders. Immediately the alarm is on, the transmitting signal will be blocked. This is similar to the case of loading a credit card on the telephone system. Whenever a wrong code is being sent twice, that line will be blocked. This will prevent theft/hacking on the system. Figure 2.12 shows the 3D EM preview of the designed Figure 2.11 before simulating using the EMDS simulator. This validated that the three dimensional design has been properly constructed.

Smart antennas combines the antenna arrays elements of the transceiver and that of the antennas at the mobile station for the optimization of radiation beam pattern. The algorithm needed to recognize the identity of the hacker is known as signal processing algorithm. This algorithm aid in the identification of hacker that wants to intrude on the transmitted signal. As the antennas at the mobile stations communicate with each other using RFs between *1 GHz* and *7 GHz*, neighbouring channels can only receive signal at frequency below *1 GHz* but not secured. If the neighbouring channels receive signal at the specified/ designed frequency and hacking is ON, there will be no alarm in the system as illustrated in Figure 2.13.

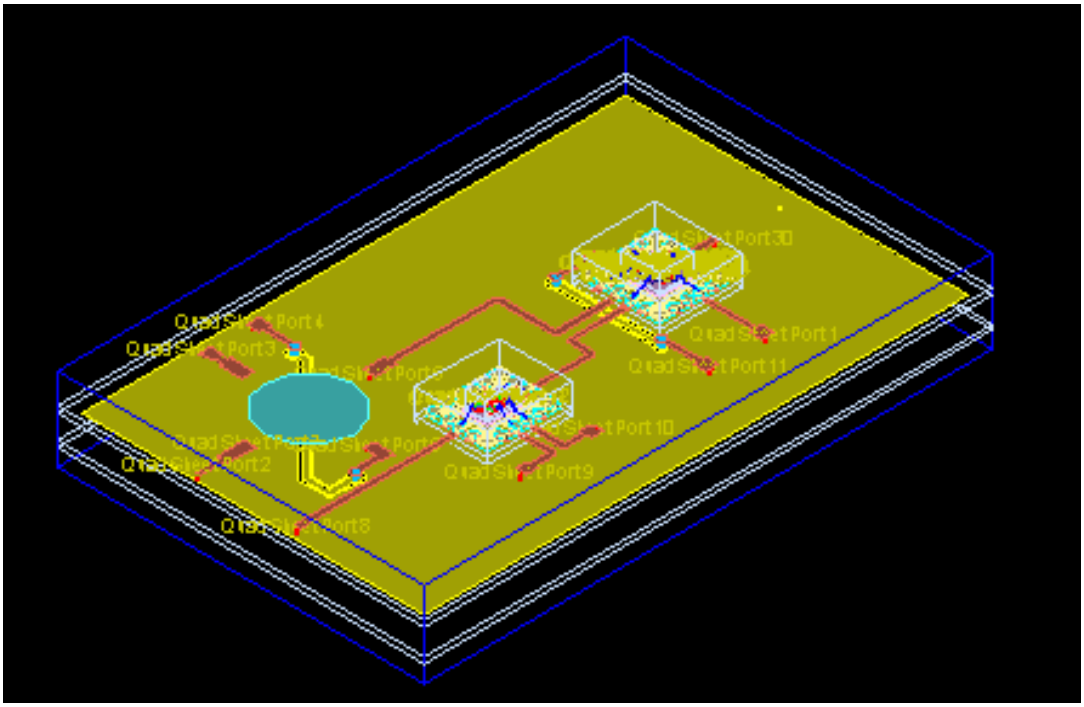

Figure 2.12. Isometric 3 D EM Preview of the designed Antenna.

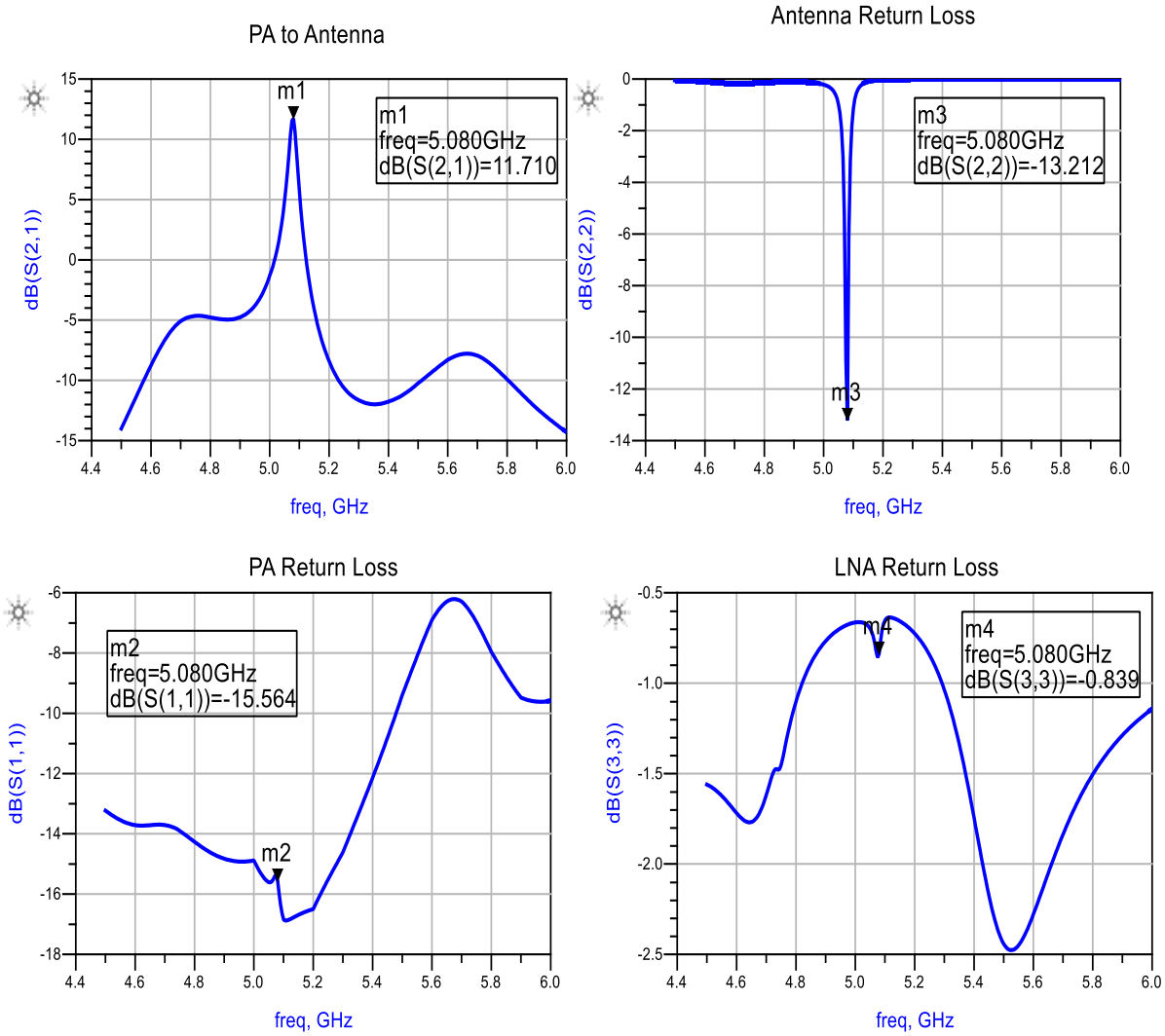

Figure 2.13. Graph of RF transceiver antenna.

2.12. Open Problems in Smart Antenna Arrays

(a) *Research gap in adaptive array antenna*: There are drawbacks in smart/adaptive array antenna. Implementation is one of the major issue in relation to higher complexity relating to design in smart antenna array. Research work in this area depends on specific estimation of channel besides speed of convergence in correlation to its beamforming technique. Therefore, implementation in MAC layer is difficult. The unsolved problem is its application towards cross layer.

(b) *Insufficient techniques in multicarrier systems*: Multicarrier techniques is a promising area for researchers with respect to smart antenna. Number of published works towards multiplexing techniques over wireless network are few.

This research work has analysed and design smart antenna arrays for improved directivity in wireless communication system. Different elemental antenna response parameters has been analysed for the performance of smart antenna in this research work. The performance analysis of the antenna parameters has been examined for the proposed model using *Dolph-Chebyshev*. Phased-Tapered weights for the proposed model has been considered. The signal processing has been solved using the spatial signal processing, and the adaptive algorithms equation for the model has been derived.

2.13. Conclusions

In this chapter, a vital and theoretical background of our research work has been presented. Several areas of research on smart antenna arrays design specifically study on antenna design that focusses on the selection of special radiating antenna elements have been reviewed, which we considered necessary and attractive for various high gain and directivity applications, such as DOA algorithms as it depends on antenna gain. The three basic types of smart antennas have been analysed and their features are highlighted in this chapter. Beamforming which is an integral part of smart antenna array has been examined. Beamforming has the capacity to change the radiation pattern at a specified angle. Finally, signal processing algorithms (LMS and RLS) that makes the antennas to be smart have been studied.

CHAPTER 3

Smart Antenna Arrays Performance

This chapter deals with the different antenna elements used in analysis of smart antenna arrays. Smart antenna using circular pin-fed linearly patch antenna and waveguide-fed pyramidal antenna has been analysed in this chapter.

3.1. Introduction

Active or parasitic radiators are actively used in smart antenna arrays by distributing its signal into every antenna element with correct phase and amplitude. This is done in order to achieve a spatial electromagnetic power combining.

In this chapter, some of the antenna elements used in the analysis has been discussed in subsections below

3.2. Circular Pin-Fed Linearly Patch Antenna

Various antenna element can be used for the performance analysis and design of smart antenna arrays in wireless communication systems using different methods and approaches. One of these methods is circular pin-fed linearly polarized patch antenna (used as antenna element). It has a characteristics of transmitting signals at various angles.

When the antenna is stationary at an azimuth angle of φ of 90^0, at the elevation angle θ of 0^0, 30^0, 60^0, and 90^0, there is decent prospective in the transmitting ultra-wide band signals with slightest alteration. However, when the antenna is not fixed at the azimuth angle, the transmitting signals at angles ($\theta = 0^0$, 30^0, 60^0, and 90^0) will be highly distorted. Hence, there will be signals fading.

A circular pin-fed linearly polarized patch antenna is a directional antenna adapted for determining and transmitting of signals in a specified direction, especially for radio broadcast and wireless communication systems due to the unique property of its radiation. To overcome these challenges, smart antenna is a favourable technique. The consideration of smart antenna system using a uniform circular pin-fed linearly polarized patch antenna offers the advantages of light weight, low cost, planar or conformal, and ability of integration with the circuitry of signal processing and electronic system [27, 54, 69].

Patch antenna is a very prominent antenna in the microwave frequency spectrum due to its simplicity and compatibility with the Printed Circuit Board (PCB) technology. A patch antenna is simply a rectangular piece of conducting material placed above a ground, similar to a microstrip [69]. The wavelength of radiation is determined by the length of the patch as the design antenna demonstrates a precise radiation array. The general radiation array switches when numerous antenna elements are joined in an array. This effect is due to the array factor [54]. Circularity can be achieved in various ways. One of these ways, for example, is to feed the antenna with two different lines, one phase shifted by 90^0 from the other. The following equations have been used to describe the geometry of the proposed antenna and to determine the various parameters [54, 69]:

$$f = \frac{\gamma_{xy} s}{6.284 d_k \left[\varepsilon_k\right]^{\frac{1}{2}}} \tag{3.1}$$

For the circular patch in this research work, equation (3.1) is used for our design work. where

$$d_k = \sqrt{d\left\{1+\frac{2h}{3.142 d\varepsilon_k}\left[\ln\left(\frac{\pi}{2h}\right)\right]+1.8\right\}} \tag{3.2}$$

Hence, Equation (3.1) can be written as:

$$f = \frac{\gamma_{xy} s}{6.284\sqrt{d\left\{1+\frac{2h}{3.142 d\varepsilon_k}\left[\ln\left(\frac{\pi}{2h}\right)\right]+1.8\right\}}\left[\varepsilon_k\right]^{\frac{1}{2}}} \tag{3.3}$$

$$= \frac{\gamma_{xy} s}{6.284\sqrt{d\left\{1+\frac{2h}{3.142 d\varepsilon_k}\left[\ln\left(\frac{\pi}{2h}\right)\right]+1.8\right\}}\sqrt{\varepsilon_k}} \tag{3.4}$$

$$= \frac{\gamma_{xy} s}{6.284\sqrt{d\left\{1+\frac{2h}{3.142 d\varepsilon_k}\left[\ln\left(\frac{\pi}{2h}\right)\right]+1.8\right\}}\sqrt{\varepsilon_k}} \tag{3.5}$$

$$= \frac{\gamma_{xy} s}{6.284 d\left\{1+\frac{2h}{3.142 d\varepsilon_k}\left[\ln\left(\frac{\pi}{2h}\right)\right]+1.8\right\}\left(\varepsilon_k\right)} \tag{3.6}$$

$$= \frac{\gamma_{xy} s}{6.284d\left\{\frac{3.142d\varepsilon_k + 2h}{3.142d\varepsilon_k}\left[\ln\left(\frac{\pi}{2h}\right)\right] + 1.8\right\}(\varepsilon_k)} \tag{3.7}$$

where *s* is the speed of light, *f* is the resonant frequency for the radiating patch. γ_{xy} is the x^{th} zero of the Bessel's role derived equation in the order of y. d signifies the patch's bodily radius. *y* in equation above signifies the angular process number, and x is the radial mode number [54, 69, 80]. The effective relative permittivity ε_k of the substrate regulates the fringing field. To obtain a better antenna radiation, the permittivity must be low so that a wider fringes can be achieved. If the permittivity is decreased, the antenna's bandwidth and efficiency will be increased. Hence, antenna's impedance is directly proportional to permittivity. For a linear array with a uniform excitation, the beamwidth is given as [69]:

$$\theta_{3db} = \cos^{-1}\left[\sin(\theta_o) - 0.443\frac{\lambda_o}{l}\right] - \cos^{-1}\left[\sin(\theta_o) + 0.443\frac{\lambda_o}{l}\right] \tag{3.8}$$

where θ_0, λ_o and *l* are the mean beam pointing angle, the free space wavelength and the total array length, respectively.

3.2.1 Design parameters for circular pin-fed linearly patch antenna

The design and performance of the proposed antenna were strictly based on Equation (3.1) to Equation (3.8). The dimension of the model preview square patch is *550 x 550 mm*^{2}. The horizontal and vertical distance among the patches have the same dimension. In order to support transmission of data at gigabits per second, Equation (3.5) has been used to calculate the frequencies at *1 GHz* and *10 GHz*. Using Equation (3.5), the effective relative permittivity ε_{eff} is *0.2*. The electrical height of the substrate in the medium is 3λ. The height (h) is *5 mm*, the substrate height as a percentage of wavelength in the medium is *60%*. Increasing the substrate height will upsurge the bandwidth as the height *h* of the substrate also controls the bandwidth, but will the resonant frequency will be decreased. From Equation (3.7), the value of *W* is calculated for *1 GHz* and *10 GHz*. It has been discovered that the value of *w* reduces with increase in frequency. The fringe factor can be determined using Equation (3.4), the value remains the same for all operating frequency.

The pin-fed patch can be fed by using a circular hole in the substrate and ground plane, and bringing the center conductor of a coaxial connector or cable into ohmic contact with the patch at an appropriate point.

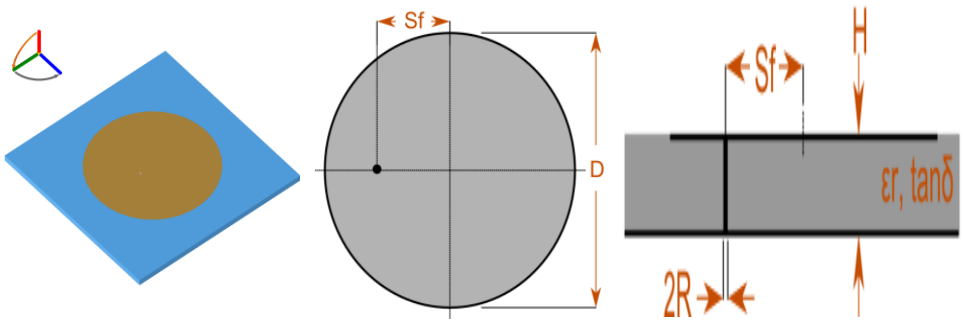

(a) (b) (c)

Figure 3.1. Model of antenna design (a) Model preview, (b) Top view, and (c) Side view.

3.2.2 Simulation results for circular pin-fed linearly patch antenna

The simulated results for the antenna at *1 GHz* and *100 GHz* are shown in Figure 3.2 and Figure 3.3. The polar radiation pattern shown in Figure 3.2 is really moderately easy to create using antenna arrays. The radiation pattern of the array depends on the individual patch element, feed network layout and spacing arrangement of the array. The feed network fed the individual antenna element in the array. Feed network complexity can be determined by its ability to perform beam steering. The region about the direction of extreme radiation is the main beam. This is the area that is contained by *3 dB* of the peak of the main beam in Figure 3.2 (a). This region is concentrated at 90^0. The smaller beam that is away from the main beam is the sidelobe.

The sidelobe is radiated in undesired direction and occur at 0^0. The angular separation in which the magnitude of the radiation pattern decreases from the peak of the main beam that is the half power beamwidth is 0^0. Null-null beamwidth which is the angle that separated the magnitude of beam radiation pattern decreases to zero away from the main beam. Here, null-null beamwidth is $(315^0 - 45^0)$ which equals 270^0. The sidelobe level (S_{ll}) which is the maximum level of the sidelobes away from the main radiation beam pattern is *7.1 dBi*. In Figure 3.2 (b), main beam occurs at 0^0, main *3 dB* beamwidth (frequency) $(\varphi = 0^0) = 78^0$, *-7.1 dBi* at $\theta = 90^0$.

In Figure 3.2 (c), Peak gain at angle (frequency) $[\varphi = 90^0]$, main *3 dB* beamwidth (frequency) $[\varphi = 90^0] = 147^0$, *-2.7 dBi* at $\theta = 120^0$. Figure 3.3 shows the plane cut in polar form. The normalized radiation pattern in dB was computed against the H-plane E_θ, degrees. The measured – *3 dB* beamwidth in Figure 3.3 (a) are 0^0, 45^0, 320^0 *and* 355^0. In Figure 3.3 (b), it occurs at 50^0 and 125^0. Figure 3.3 (c) has *-3 dB* beamwidth as -162.5^0, -12.5^0, 23^0 and 162.5^0 respectively.

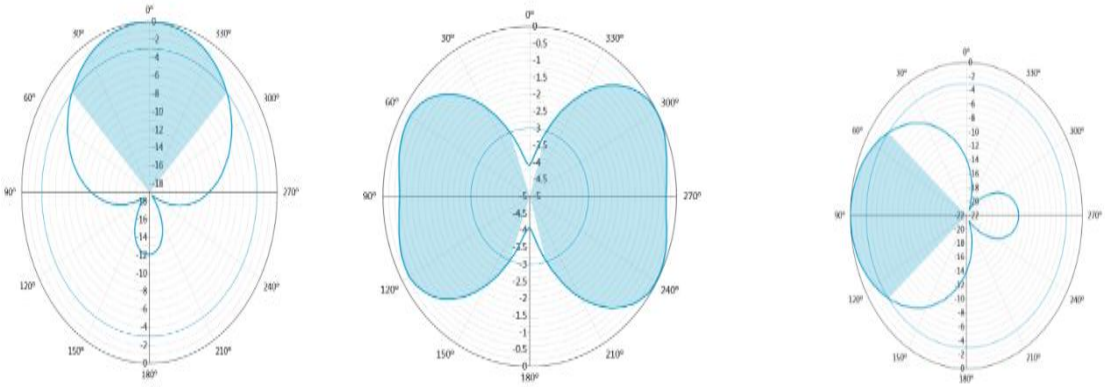

(a) (b) (c)

Figure 3.2. The polar radiation pattern measured along for (a) XY-Plane cut polar, (b) YZ-Plane cut polar, and (c) XZ-Plane cut at 1 GHz.

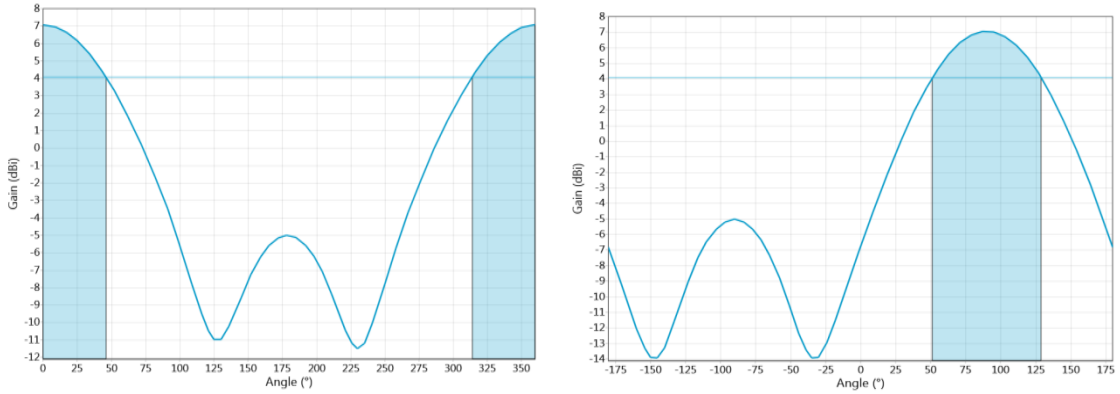

(a) (b)

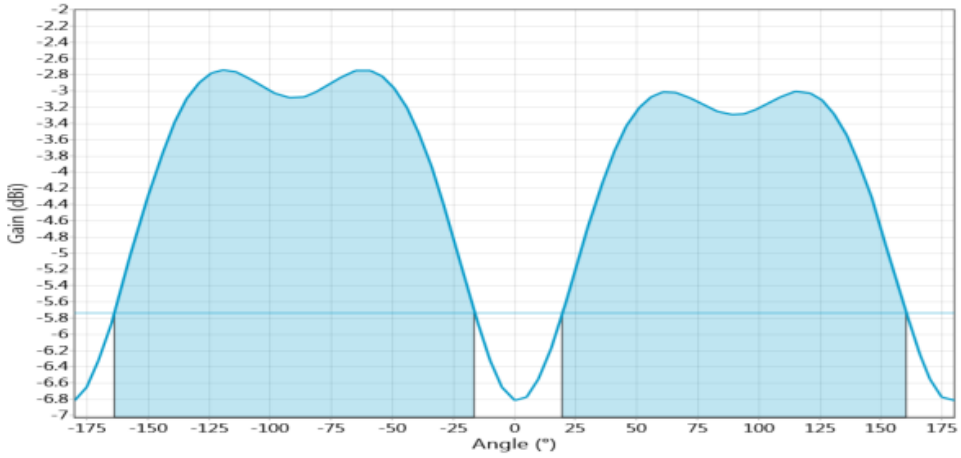

(c)

Figure 3.3. Polar plane cut at 1 GHz for (a) XY-Plane cut, (b) XZ-polar plane cut, and (c) YZ-polar plane cut.

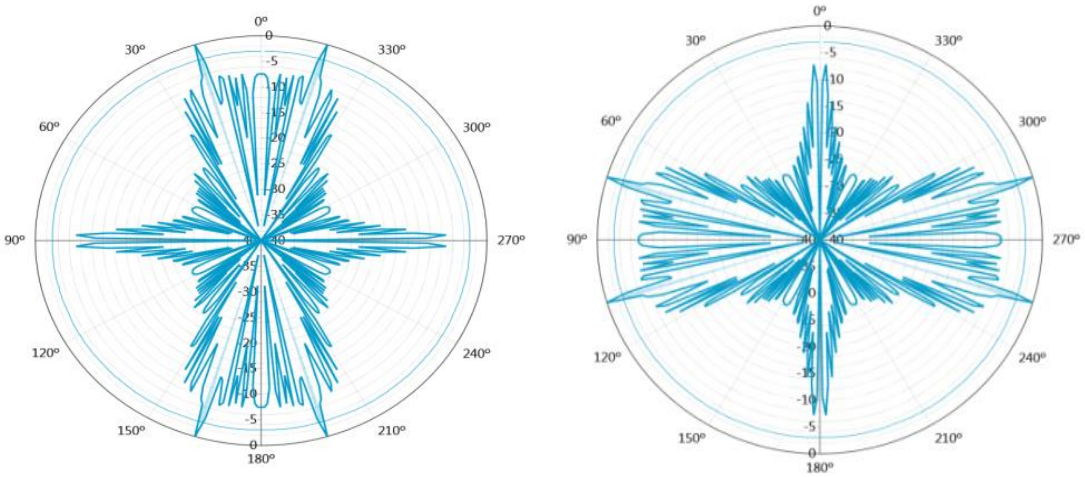

(a) (b)

Figure 3.4. Cartesian plane cut at 10 GHz for (a) XY-polar plane cut, and (b) XZ-polar plane cut.

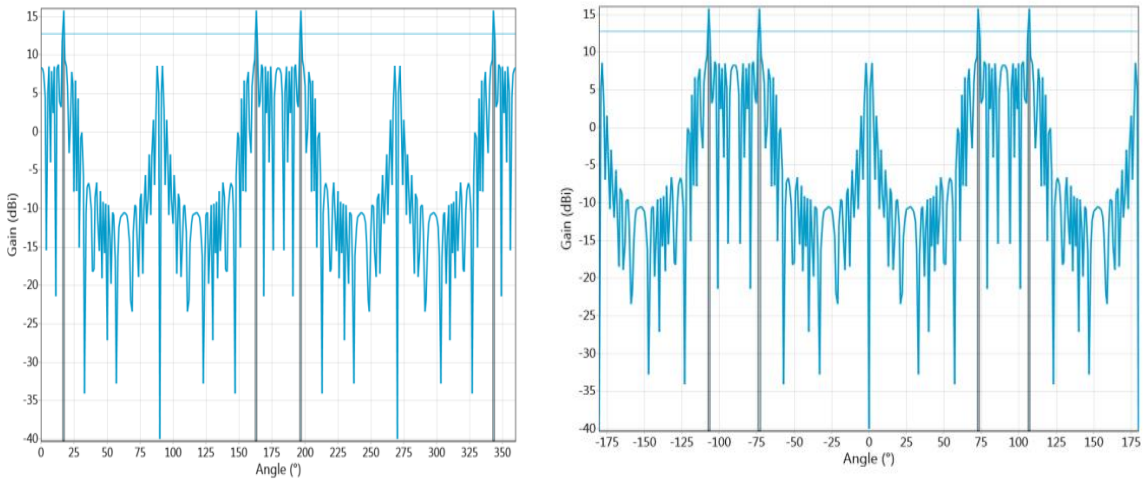

(a) (b)

Figure 3.5. Polar plane cut at 10 GHz.

Figure 3.4 (a), the main 3dB beamwidth (frequency) *[θ =90^0] = 1.2^0, 16 dBi* at *φ =163^0*. In Figure 3.4 (b), Peak gain at angle (frequency) *[φ =0^0]*, main *3 dB* beamwidth (frequency) *[φ =0^0] = 1.2^0, 16 dBi* at *θ =-107^0*. Figure 3.5 shows the beamwidth waveform. In (a), the highest gain occurs at *20^0*, *160^0*, *200^0* and *345^0*. In (b) it occurs at *-75^0*, *-90^0*, *75^0* and *110^0*.

The significant differences in radiation pattern at 1GHz and 10GHz are mostly due to slight differences which are probably due to errors in entering the antenna geometry into simulator, and in simulating the antenna with a gap feed across the slot. The differences are highlighted as follows:

At 1 GHz, there is a phase difference for the far field at any point in the boresight direction, and it is very linear where the antenna is not launching a pencil beam. The radiation pattern is stable at 1GHz, but at 10GHz, the radiation pattern is unstable. The polar radiation pattern is really moderately easy to create. The sidelobe is radiated in undesired direction and occur at 0^0. The main beam occurs at 0^0, main *3 dB* beamwidth at 1GHz $(\varphi = 0^0) = 78^0$, *-7.1 dBi* at $\theta = 90^0$. Peak gain at angle at 1GHz $[\varphi = 0^0]$, main *3 dB* beamwidth (frequency) $[\varphi = 0^0] = 1.2^0$, *16 dBi* at $\theta = -107^0$.

At 10GHz, the reflection coefficient converges to a high frequency limit. The radiation pattern at this frequency has become a pencil beam, and it stays this way right through to with fairly constant gain, and just changes to the beamwidth and sidelobes. At this frequency, the beamwidth waveform is uniform. The highest gain occurs at 20^0, 160^0, 200^0 and 345^0. At 10GHz, there is reduction in beamwidth and gain, the difference is as large as 10dB.

From the results we inferred that, this antenna is best suited for huge bandwidth.

3.3. Waveguide-Fed Pyramidal Horn Antenna

Antennas with various efficiencies are needed in the various propagations of signal systems. Waveguide-fed Pyramidal horn antenna plays a vital role in navigation and surveillance applications. It varies widely in size, gain and have the capability of being designed and developed within wide range of frequencies ranging from *MHz* to *THz* [130]. Pyramidal horns work by selecting the polarity of the received waves, this is an advantage for it to attenuate interfering signals from the neighbouring channels and transponders. Due to these, it is very useful as element in smart antenna arrays.

The design of smart antenna using waveguide-fed pyramidal horn antenna gives a better system performance of directional radiation beam pattern with a high gain and wide impedance bandwidth. As suggested by *Oluwole* and *Srivastava* [68], this section presents an innovative approach of designing smart antenna using a waveguide-fed pyramidal horn antenna as an element for wireless communication systems. Smart antennas using waveguide-fed pyramidal horn antenna with a requisite radiation beam pattern which is capable of segregating against any interfering signal of interest is needed for the transmission of signals. Due to its better electrical distinctive feature, the horn can be used as feed for antenna reflectors [130, 131].

Figure 3.6 shows the designed physical antenna element for the system that is the waveguide-fed pyramidal horn antenna of side-lobe level *14 dBi, 3 dB* specify beamwidth of 32^0, operating frequency *10 GHz*, *E_3 dB_bw* is 30^0 and *H_3 dB_bw* is 24.4^0. With these

parameters, the inter component configuration was 0.5λ when the design algorithm was used, while the acquaintance radiators have a space of $\lambda/2$. The pattern array radiation in the X-Z plane can be given as [68]:

$$F(\phi) = \sum_{i=1}^{N} w_1 p_1(\phi) e^{-j\frac{2\pi}{\lambda}\tau l.c} \tag{3.9}$$

where w, c and $p_1(\phi)$ denote the weight of the vector, speed of light, and radiation pattern of the l^{th} antenna element respectively.

3.3.1 Modelling of the antenna element

The parameters used to design this antenna have been detailed in Table 3.1. The selected frequency of operation is *10 GHz*. To obtain maximum gain and minimum reflection, the flare angle between 0^0 and 90^0 must be maintained, where W_g is the larger dimension of rectangular waveguide, H_g is the smaller dimension of rectangular waveguide, H_a is the dimension of rectangular aperture parallel to H_g, and W_a is the dimension of rectangular aperture parallel to W_g. H_a and W_a are the aperture dimensions. L_f is the distance from apex to aperture of horn in E-plane and L_g is the distance from apex to aperture of horn in H-plane. R_e is the slant edge from apex to aperture in E-plane:

$$R_e = \sqrt{L_f^2 + \left(\frac{H_a}{2}\right)^2} \tag{3.10}$$

R_h is the slant edge from apex to aperture in H-plane:

$$R_h = \sqrt{L_f^2 + \left(\frac{W_a}{2}\right)^2} \tag{3.11}$$

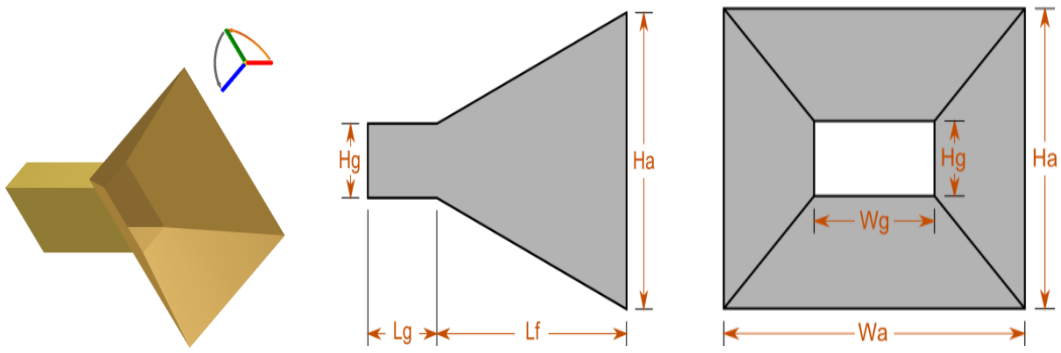

(a) (b) (c)

Figure 3.6. Geometry of waveguide-fed pyramidal horn antenna (a) Model preview, (b) Side view, and (c) End view.

$$\text{Flare angle} = \tan^{-1}\frac{\frac{H_a}{2}}{L_f} = 24.88^0$$

The pyramidal horn structures can be used as a feed horns for antenna reflector. The horn-shaped shown in Figure 3.6 are normally used to control radio waves in a beam.

3.3.2 Design equations of horn antenna

Consider E-plane sectoral horn as shown in Figure 3.7, the electromagnetic horn produces uniform phase front using a larger aperture as compared with waveguide, hence there is increase in directivity. Let us assume that a line source is radiating a cylindrical waves and the apex horn is imaginary, the constant wavefronts are cylindrical as the waves propagate radially in the outwards direction. There is a phase difference in the direction of the aperture due to the fact that the wave traces different distances from apex to the aperture. From Figure 3.7, δ is the phase difference in the direction of the aperture. Geometrically,

$$\cos\theta = \frac{p}{p+\delta} \text{ and } \tan\theta = \frac{\frac{h}{2}}{p} = \frac{h}{2p} \text{ Hence we can write,}$$

$$\theta = \cos^{-1}\left[\frac{p}{p+\delta}\right] = \tan^{-1}\left[\frac{h}{2p}\right] \tag{3.12}$$

where θ is the optimum aperture (elevation). From right angle triangle OBA, using a Pythagoras theorem:

$$(p+\delta) = \sqrt{p^2 + \left(\frac{h}{2}\right)^2}$$

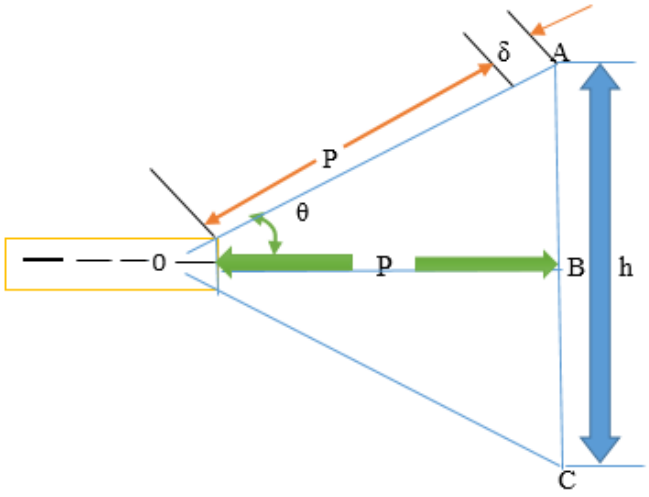

Figure 3.7. E-plane view.

Therefore,

$$(p+\delta)^2 = p^2 + \left(\frac{h}{2}\right)^2$$

$$(p^2 + 2p\delta + \delta^2)^2 = p^2 + \frac{h^2}{4}$$

As δ is fractional, δ^2 will be smaller than δ hence neglecting:

$$2p\delta = \frac{h^2}{4}$$

$$\therefore p = \frac{h^2}{8\delta} \text{ when } \delta \ll p \tag{3.13}$$

where p is the distance and equations (3.12) and (3.13) are called design equations of horn antenna.

The smaller the flare angle θ, the smaller the aperture area for the specified length p. Thus, uniform phase front is at the mouth of the horn, which increases directivity with decrease in the beam width. The directivity of the pyramidal horn is highest as compared to other types of the horns because they have more than one flare angle. One more advantage of the horn antenna is that it can be operated over a wide range of high frequency as there is no resonant element in the antenna. The directivity can be written as Equation (3.14) in terms of effective aperture of the horn provided there is no loss:

$$D = \frac{4\pi A_e}{\lambda^2} = \frac{4\pi \in_p A_p}{\lambda^2} \tag{3.14}$$

where A_e and A_p are the Effective aperture (m^2) and Physical aperture (m^2) respectively.

$$\in_p = \frac{A_e}{A_p}$$

where ϵ_p is the aperture efficiency. The length (p) of the horn, H-plane aperture and flare angles θ_E and θ_H (E and H-planes respectively) of a pyramidal horn for which E-plane aperture is 10λ can be determined from the equation above. The horn is fed with a rectangular waveguide with TE_{10} mode. For the E-plane, $\delta = 0.2\lambda$, and 0.375λ in H-plane. Then the required length of the horn is given by:

$$p = \frac{h^2}{8\delta} = \frac{a_E}{8\delta}$$

Substituting values,

$$p = \frac{(10\lambda)^2}{8 \times 0.2\lambda} = 62.5\lambda$$

Now the flare angle in E-plane is given by:

$$\theta_E = 2\tan^{-1}\left(\frac{h}{2p}\right) = 2\tan^{-1}\left(\frac{a_E}{2p}\right)$$

$$\theta_E = 2\tan^{-1}\left(\frac{10\lambda}{262.5\lambda}\right) = 9.14^0$$

In H-plane, $\delta = 0.375\lambda$, then the flare angle in H-plane is given by,

$$\theta_H = 2\cos^{-1}\left(\frac{p}{p+\delta}\right) = 2\cos^{-1}\left(\frac{62.5\lambda}{62.5\lambda + 0.375\lambda}\right) = 12.521^0$$

Now the H-plane aperture is given by,

$$a_H = 2p\tan\frac{\theta_H}{2} = 2(62.5\lambda)\tan\left[\frac{12.521}{2}\right] = 13.7129\lambda$$

Half Power Beamwidth (HPBW) in E-plane is given by,

$$\text{HPBW (E-Plane)} = \frac{56^0\lambda}{a_E} = \frac{56^0\lambda}{10\lambda} = 5.6^0$$

Similarly the half power beamwidth in H-plane is given by,

$$\text{HPBW (H-Plane)} = \frac{67^0\lambda}{a_H} = \frac{67^0\lambda}{13.7129\lambda} = 4.8859^0$$

The directivity is given by,

$$\text{D (in dB)} = 10\log_{10}\left(\frac{7.5A_p}{\lambda^2}\right) = 10\log_{10}\left(\frac{7.5A_p \times a_H}{\lambda^2}\right)$$

$$= 10\log_{10}\left(\frac{7.5 \times 10\lambda \times 13.7129\lambda}{\lambda^2}\right) = 30.1219 \text{ dB}$$

Table 3.1. Parameters for the design of waveguide-fed pyramidal horn antenna.

Parameters	Waveguide width	Waveguide height	Waveguide length	Aperture width	Aperture height	Flare of length
Symbol	W_g	H_g	L_g	W_a	H_a	L_f
Values (mm)	23.53	11.77	44.97	69.24	50.71	26.66

Table 3.2. Simulated results for the design of waveguide-fed pyramidal horn antenna.

Frequency (GHz)	7	8	9	10	11	12	13
Directivity (dBi)	14.07	15.18	16.14	16.90	17.79	18.55	18.89
Beamwidth	37.5^0	30.0^0	29.0^0	25.8^0	21.8^0	20.9^0	20.0^0

From these tables, we can conclude that the directivity of the waveguide pyramidal horn antenna is increasing and bandwidth is decreasing with increase infrequency. Antenna arrays chosen for this work is waveguide-fed pyramidal horn antenna. This antenna has no resonant element, but wide frequency of operation, wide bandwidth, and slow varying input impedance over this wide frequency range. It allows low voltage standing wave ratio over its bandwidth, and has a high gain ranging up to *25 dBi.*

3.3.3 Estimated performance of the smart antenna element

The designed antenna has been simulated in antenna magus software using the specifications stated in table 3-1 and its performances have been discussed as in following sections. Figure 3.8 implies that the antenna radiates optimally at *-16.5 dB*. At *-27.55 dB* with frequency *8 GHz*, it will radiate practically nothing. As s-parameter (S_{11}) is approaching *0 dB*, all the power is reflected. The antenna bandwidth also has been determined which is refer to as VSWR.

Bandwidth characterizes the frequency range between *154 MHz* to *1848 MHz* at which the antenna will settle to perfectly radiate or receive energy. For the modelled antenna design *VSWR* is *1.198*. It means the reflection coefficient (*M*) is less than *0.1597*. The return loss has been calculated by $20*log_{10}(M)$. Hence the return loss for the designed structure will be *-15.93*. The various radiation patterns in 3-D at *10 GHz* with its divers gain are shown in Figure 3-9. This can vary with frequency but the shape of the radiation doesn't change entirely. The variation of the power radiated is a function of the angle of arrival (AOA) and this is observed

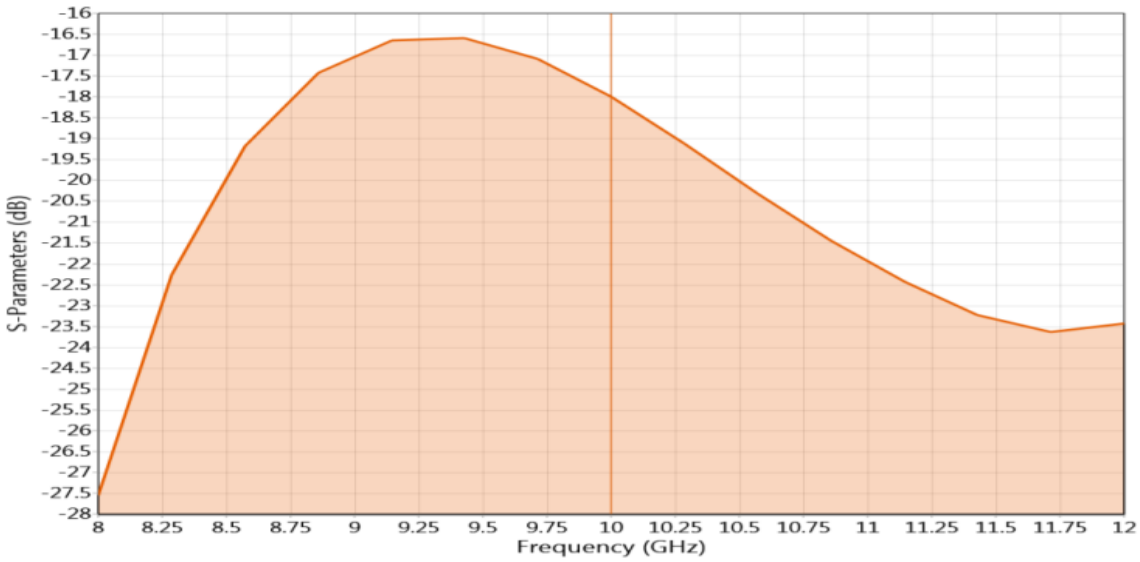

Figure 3.8. Graph of S_{11} (reflection) versus frequency.

in the far field region of the antenna. Right-hand circular gain is not included in the diagram because the left-hand circular gain and right-hand circular gain are the same. Antenna radiation pattern are identified by the beamwidths and sidelobe levels. This approach can be represented by [68]:

$$R(\theta) = \sin\theta \frac{\sin\left\{4\left(\theta - \frac{\pi}{2}\right)\right\}}{4\left(\theta - \frac{\pi}{2}\right)} \tag{3.15}$$

Using Equation (3.15), Figure 3.9 (a) has been generated. Figure 3.9 (b) shows the H-plane and E-plane for right-hand circular (RHC), linear and left-hand circular (LHC) having plane zero for all maximum and minimum axial ratio (AR) at angle $\varphi = 0^0$ and 90^0 when $\theta = -180^0$. In Figure 3.9 (c), *80 dB* was obtained for all maximum and minimum axial ratio at angle $\varphi = 0^0$ and 90^0 when $\theta = -180^0$. In Figure 3.9 (d), the peak gain at angle $\varphi = 90^0$ is *1.391 dBi* when $\theta = -52^0$. Peak gain at angle $\varphi = 0^0$ is *13.59 dBi* when $\theta = 0^0$. Main *3 dB* beamwidth at $\varphi = 90^0$ is 64.03^0, while the main *3 dB* beamwidth at $\varphi = 32.92^0$. Figure 3.9 (e) shows the total gain for both Hand E-plane having a peak gain of *13.59 dBi* and *0.5371 dB* at $\varphi = 0^0$ and 90^0 for $\theta = 0^0$ and -22^0. Its main *3 dB* beamwidth is 31.49^0 and 34.03^0 when $\varphi = 90^0$ and 0^0.

Figure 3.9 (f) is the LHC gain that has the same structure but different values of peak gain with RHC gain. For LHC, peak gain value is *13.59 dBi* when $\varphi = 0^0$ and 90^0 at $\theta = 0^0$. Its main *3 dB* beamwidth is 33.47^0 and 35.24^0 when $\varphi = 90^0$ and 0^0. For RHC, peak gain value is *10.58 dB* when $\varphi = 0^0$ and 90^0 at $\theta = 0^0$. Its main *3dB* beamwidth is 33.47^0 and 35.24^0 when $\varphi = 90^0$ and 0^0. The horizontal gain for H and E-plane is depicted in Figure 3.9 (g). This has the same values with the RHC gain. Figure 3.9 (h) shows the vertical gain in H-plane. The peak gain and main 3 dB beamwidth is indeterminate at $\varphi = 90^0$. The peak gain and main 3dB beamwidth is *13.59 dBi* ($\theta = 0^0$) and 35.24^0. Figure 3.9 (i) shows the axial ratio (handed) in E-plane. The peak gain and main *3 dB* beamwidth is indeterminate at $\varphi = 0^0$. The peak gain and main *3 dBi* beamwidth is *13.59 dBi* ($\theta = 90^0$) and 33.47^0.

Figure 3.10 (a) has a peak gain of *14.71 dBi* at *12 GHz* for ($\theta = 0^0$; $\varphi = 0^0$). At *-3dB* bandwidth is indeterminate for ($\theta = 0^0$; $\varphi = 0^0$). In Figure 3.10 (b), peak gain of *11.70 dBi* at *12 GHz* for ($\theta = 0^0$; $\varphi = 0^0$). At *-3 dB* bandwidth is indeterminate for ($\theta = 0^0$; $\varphi = 0^0$). Figure 3.10 (c) has the same value when simulated. Figure 3-10 (d), has the same value with the left-hand circular gain.

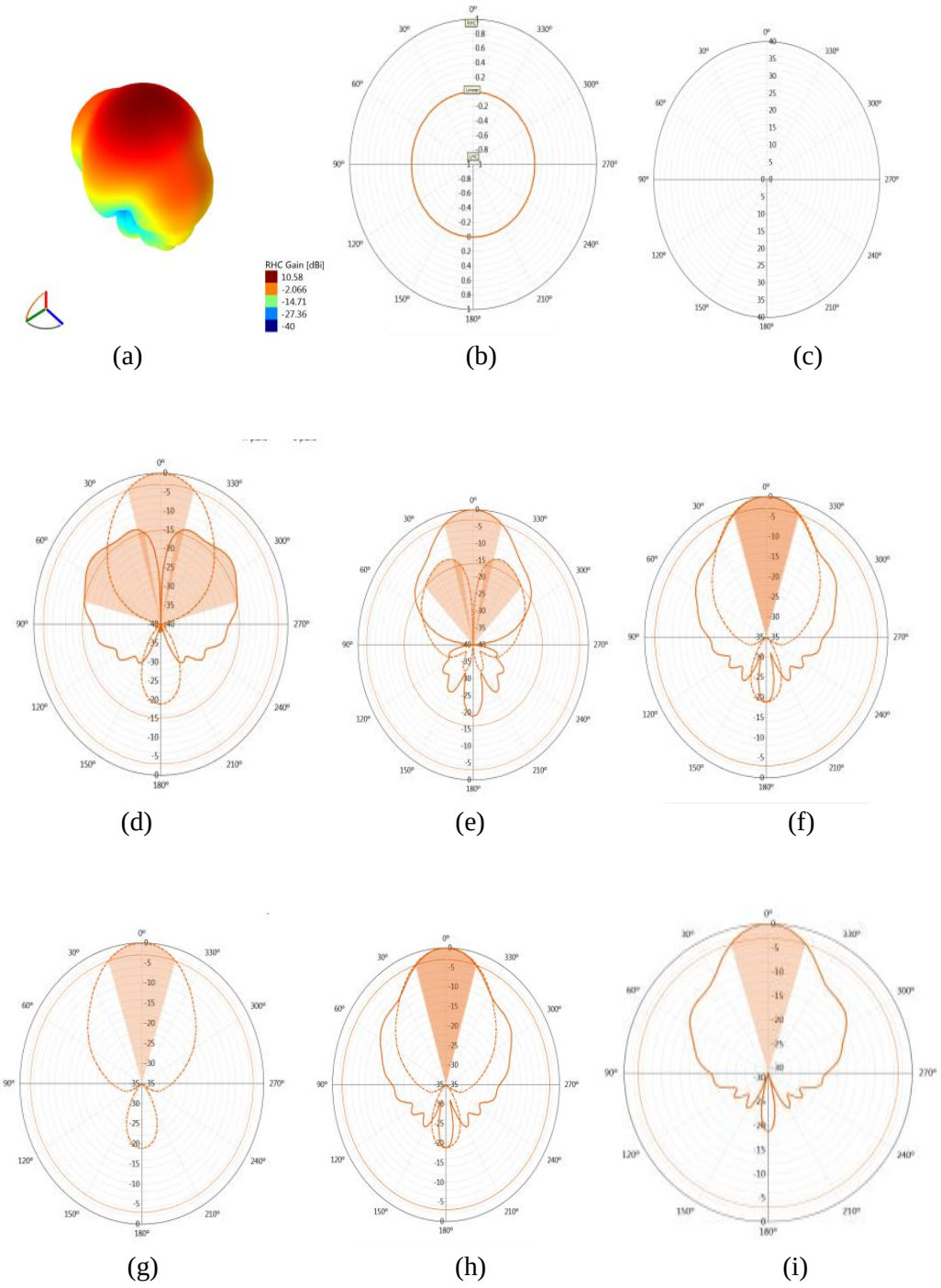

Figure 3.9. Radiation pattern at 10 GHz (a) 3-D, (b) Axial ratio, (c) Ludwig III (co), (d) Ludwig III (cross), (e) Total gain, (f) Left-hand circular gain, (g) Vertical gain, (h) Horizontal gain, and (i) Axial ratio (handed).

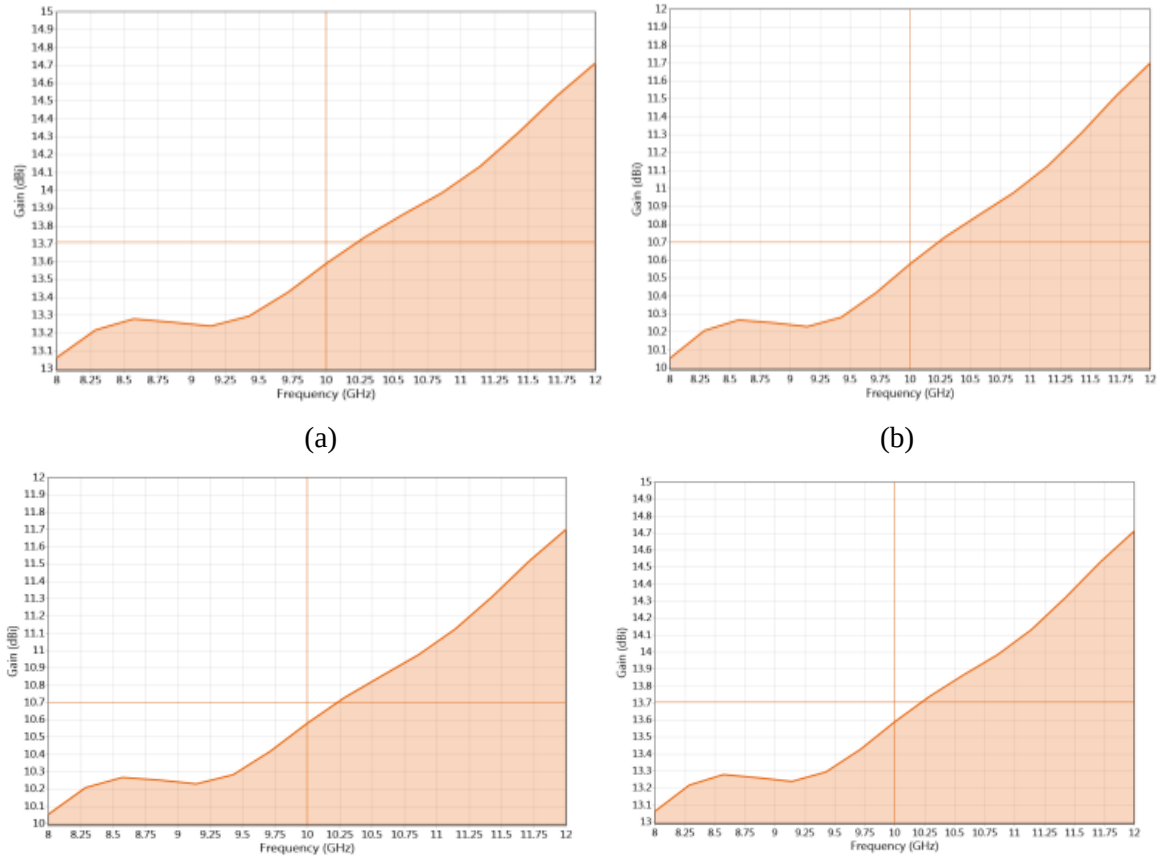

(a) (b)

(c) (d)

Figure 3.10. Gain versus frequency (bore sight) (a) Left-hand circular gain, (b) Right hand circular gain, (c) Horizontal gain, and (d) vertical gain.

The main reason for the calculation/simulation of Right Hand Circular (RHC) or Left Hand Circular (LHC) for the linearly polarized antennas is to have a more directive and high radiation gain. The RHC/LHC for the intended circular polarization depends on the excitation of the antenna. If the axial ratio is one (1), half of the real gain will be realized. Calculation/simulation of Right Hand Circular (RHC) or Left Hand Circular (LHC) for the linearly polarized antennas work better in some antennas receiver such as planar antenna. For example, if a particular antenna is perfectly circularly polarized in all directions, then a linearly polarized antenna will measure 3dB less gain in all direction but with the correct pattern shape.

3.4. Antenna Arrays Analysis and Synthesis

Antenna arrays are categorized into two: array analysis and array synthesis. In array analysis, radiation patterns are examine for a specific configurations of antenna array, while in array synthesis, antenna array configurations are designed to achieve a desired radiation. Array

analysis is purely academic work and its applications, while array synthesis is a design engineering work problem. Nitty-gritties understanding of array analysis is imperative to the design of array analysis. An array consists of two or more antenna elements that are spatially arranged and electrically interconnected to produce a directional radiation pattern. Electrically dipole antenna particularly those near resonant size are used mainly as elements in directional arrays [54].

Pattern synthesis is to determine the excitation function for the desired beam pattern. For a linear array, the antennas are positioned along a line called the axis of the array. The antenna elements in general could have arbitrary spacing between them and could be excited with different complex currents. The analysis is as follows.

3.4.1. Mathematical model of uniform linear array synthesis

Uniform antenna array has a peculiar characteristics of its antenna elements being uniformly spaced in a linear progressive phase manner and equal spacing/amplitude. In a uniform antenna array, the antenna are equi-spaced and are excited with unvarying current and constant progressive phase shift between adjacent antenna elements as shown in Figure 3.11.

We assume that the arrays have an N elements and the antennas are isotropic. All the antennas are excited with equal amplitude currents. Let us define the following for the array. The *d* is the inter-element spacing between the neighbouring elements of the array and properly fed with equal magnitude. δ is the equal progressive phase-shift between currents on any neighbouring antenna elements. The field due to an antenna is proportional to its current. Also for a faraway point, the fields due to individual antennas have equal amplitude but different phases. The isotropic radiator has a far-field radiation pattern of:

$$E(u) = \sum_{n=1}^{N} A(X_n) e^{j\frac{2\pi l}{\lambda}[ux_n + \phi(x_n)]} \tag{3.16}$$

where E(u) is electric field intensity, U is sinθ, θ is the angle of observation. Also, $A(X_n)$ is Amplitude distortion for $2l/\lambda$ (array length) and X_n is spacing function and $\phi(x_n)$ is phase function as $\varphi = \beta d\cos\phi + \delta$. Assuming the electric field due to a specific antenna has a unit amplitude at the point observation *P*. We use the first element as our reference point. Hence, the phase of the field due to the first antenna element is zero. The total field at the observation point is:

$$E = e^{j0} + e^{j\varphi} + e^{2j\varphi} + \mathrm{L} + e^{j(N-1)\varphi}$$

$$E = \left\{1 + e^{j\varphi} + e^{2j\varphi} + \mathrm{L} + e^{j(N-1)\varphi}\right\} \tag{3.17}$$

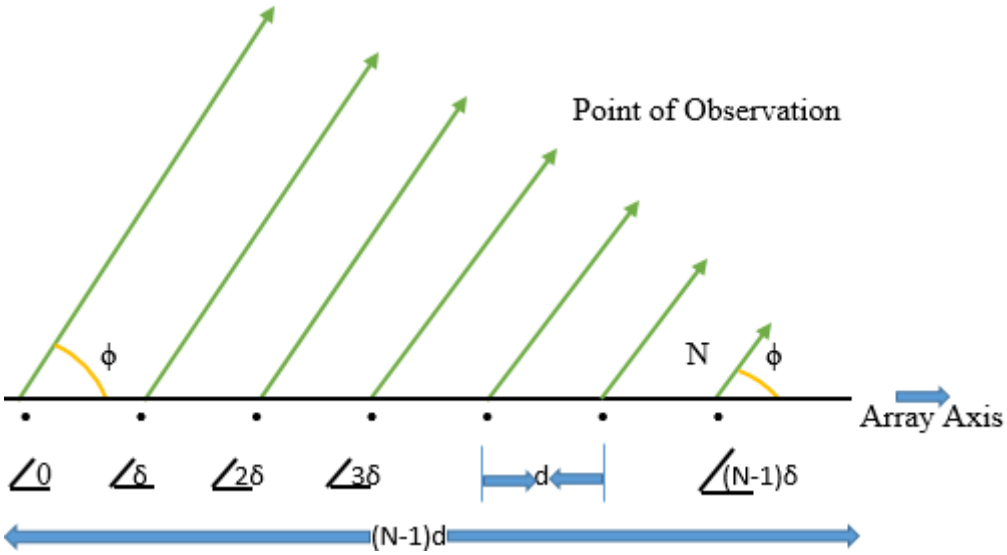

Figure 3.11. Uniform linear array with phase shift.

Sum of *n* terms for Geometric Series (GS):

$$s_n = \frac{a\left(r^n - 1\right)}{r-1}, |r| > 1$$

$$= \frac{a\left(1 - r^n\right)}{1-r}, |r| < 1$$

where first term, $r = \frac{u_n}{u_{n-1}}$ is the common ratio and u_n is the n^{th} term and a=1, $|r| = |e^{j\varphi}| > 1$.

Therefore, the right hand side of Equation (3.17) is a geometric series with summation given by:

$$E = \frac{e^{jN\varphi} - 1}{e^{j\varphi} - 1}$$

To get the electric field at the observation point, we need algebraic manipulation. Recall:

i. $e^{jx} = \cos x + j\sin x$,
ii. $|\sin x| = |\cos x| = 1$
iii. $\cos x = 1 - 2\sin^2(x/2)$
iv. $\sin x = 2\sin x/2 \cos x/2$

Thus,

$$E = \frac{e^{jN\varphi} - 1}{e^{j\varphi} - 1} = \frac{\cos(N\varphi) + j\sin(N\varphi) - 1}{\cos\varphi + j\sin\varphi - 1} = \frac{1 - 2\sin^2\left(\frac{N\varphi}{2}\right) + j\sin(N\varphi) - 1}{1 - 2\sin^2\left(\frac{\varphi}{2}\right) + j\sin(\varphi) - 1}$$

$$= \frac{-2\sin^2\left(\frac{N\varphi}{2}\right) + j\sin(N\varphi)}{-2\sin^2\left(\frac{\varphi}{2}\right) + j\sin(\varphi)} = \frac{-2\sin^2\left(\frac{N\varphi}{2}\right) + 2j\sin\left(\frac{N\varphi}{2}\right)\cos\left(\frac{N\varphi}{2}\right)}{-2\sin^2\left(\frac{\varphi}{2}\right) + 2j\sin\left(\frac{\varphi}{2}\right)\cos\left(\frac{N\varphi}{2}\right)}$$

$$= \frac{-2\sin\left(\frac{N\varphi}{2}\right)\left(\sin\left(\frac{N\varphi}{2}\right) - j\cos\left(\frac{N\varphi}{2}\right)\right)}{-2\sin\left(\frac{\varphi}{2}\right)\left(\sin\left(\frac{\varphi}{2}\right) - j\cos\left(\frac{\varphi}{2}\right)\right)}$$

Hence,

$$|E| = \frac{\left|\sin\left(\frac{N\varphi}{2}\right)\right|\left|\sin\left(\frac{N\varphi}{2}\right) - j\cos\left(\frac{N\varphi}{2}\right)\right|}{\left|\sin\left(\frac{\varphi}{2}\right)\right|\left|\sin\left(\frac{\varphi}{2}\right) - j\cos\left(\frac{\varphi}{2}\right)\right|} = \frac{\left|\sin\left(\frac{N\varphi}{2}\right)\right|(1+1)}{\left|\sin\left(\frac{\varphi}{2}\right)\right|(1+1)}$$

$$= \frac{2\left|\sin\left(\frac{N\varphi}{2}\right)\right|}{2\left|\sin\left(\frac{\varphi}{2}\right)\right|} = \frac{\left|\sin\left(\frac{N\varphi}{2}\right)\right|}{\left|\sin\left(\frac{\varphi}{2}\right)\right|} = \left|\frac{\sin\left(\frac{N\varphi}{2}\right)}{\sin\left(\frac{\varphi}{2}\right)}\right|$$

Hence,

$$|E| = \left|\frac{\sin\left(\frac{N\varphi}{2}\right)}{\sin\left(\frac{\varphi}{2}\right)}\right|$$

The maximum electric field is obtained when all the terms in the series add in phase (i.e. for $\varphi = 0$). The maximum field therefore is N. The expression gives the radiation of field as a function of the direction, φ, and hence is the radiation pattern of the antenna array. The radiation pattern is usually normalized in regard to the highest value of N so as to obtain the Array Factor as [42, 46, 55]:

$$AF = \frac{1}{N}\frac{\sin\left(\frac{N\varphi}{2}\right)}{\sin\left(\frac{\varphi}{2}\right)} \tag{3.18}$$

For a linear antenna array, the radiation patterns F_{array} elements can be estimated by multiplying the array factor *(AF)* with the element radiation pattern $(F_{element})$ if all elements are considered for a vast array, then $F(\theta, \varphi) = F_{element}(\theta, \varphi) \times AF_{array}(\theta, \varphi)$.

There is no equal radiations between the antenna elements if the number of antenna elements used in the array are small. Effects of increasing the number of antenna elements are

improved in directivity and larger number of side lobes with total reduction in level, hence a narrower main lobe [132]. The linear array factor depends on the wavelength *(λ)*, the direction of angle *(θ)*, the distance *(d)* between the spacing and the number of antenna elements *(N)*.

$$AF_{array}(\theta,\varphi) = \sum_{n=1}^{N} a_n e^{jkd\sin\theta\sin\varphi} e^{j\Delta\phi} \tag{3.19}$$

$$k = \frac{2\pi}{\lambda}$$

$$\Delta\varphi = \frac{2\pi d\sin\theta}{\lambda}$$

From Equation (3.19), it can be simplified by introducing $\Psi = kdsin\theta + \Delta\varphi$ and Substituting (ψ) and $\Delta\varphi$ into Equation (3.19) results in:

$$AF_{array}(\theta,\varphi) = \sum_{n=1}^{N} a_n e^{j\psi} \tag{3.20}$$

The series in Equation (3.20) can be further simplified and normalized. This leads to the normalized array factor in Equation (3.18). For the uniform linear array with phase shift shown in Figure 3.11, the pattern formula can be expressed as [133]:

$$F(\theta) = \sum_{n=1}^{N} I_n \exp\left[j(n-1)kd\cos\theta + \varphi_n \right] \tag{3.21}$$

where I_n is the n^{th} element's amplitude, φ_n is the phase difference between adjacent elements; θ is the angle between the array axis and the ray, d is the space between the elements, $k = 2\pi/\lambda$ is the wave number.

Let the antenna array's main-lobe point at θ_o, then $\varphi_n = -(n-1)kd\cos\theta_o$, Equation (3.21) can be expressed as [133]:

$$F(\theta) = \sum_{n=1}^{N} I_n \exp\left[j(n-1)kd(\cos\theta - \cos\theta_o) \right] \tag{3.22}$$

Let the pattern's imaginary part be zero, Equation (3.22) cab be written as following:

$$F(\theta) = \sum_{n=1}^{N} I_n \cos\left[(n-1)kd(\cos\theta - \cos\theta_o) \right] \tag{3.23}$$

If N is even and the current's amplitudes is symmetrical, then the equation is:

$$F(\theta) = \sum_{n=1}^{\frac{N}{2}} 2I_n \cos\left[\frac{n-1}{2} kd(\cos\theta - \cos\theta_o) \right] \tag{3.24}$$

In antenna array, the symmetric array is usually used to cut down the parameters' number, then reducing the computing amount [133, 134].

3.4.2. Uniform circular array radiation pattern Synthesis

In uniform circular arrays, radiation pattern are normally varied in both azimuth and elevation planes due to the advantage of its azimuthal symmetry. A complete coverage is provided in circular array geometry from the base station as the beam can be steered through 360^0. Circular array has different patterns [79]. *Taylor and Bayliss* are the popular method use in the synthesis of circular and planar array radiation pattern. *Taylor* is used in beam efficiency while *Bayliss* is used in aperture distribution. The key to Taylor synthesis procedure is the equal-sidelobe pattern function which is the continuous-aperture analogue to the *Chebyshev* polynomial pattern for arrays:

$$E(U) = \cos \pi \sqrt{u^2 - A^2} \tag{3.25}$$

where $U = \pi A \sin\theta/\lambda$, A is the length of the aperture and θ is the measured angle relative normal to the array. This function has the highest value of $\cosh \pi A$ when $U = 0$ and unit sidelobes extending to $U = \pm\infty$. Taylor showed that the pattern of Equation (3.25) is not physically realizable from a continuous aperture distribution, just as the *Dolph* array excitation becomes increasingly impractical in the limit of large arrays. His brilliant solution to this problem was:

(a) For all zeros of the synthesized pattern functions, which we will call $E_s(u)$, from the nth from the origin to ∞ ∞, the locations will be the same as those from a uniformly illuminated aperture of the same size. That is,

$$E_s(u) = 0 \text{ for } u = n \text{ for } n \geq \bar{n}.$$

(b) For the first $\bar{n} - 1$ zeros, their locations will be determined by the zeros of $E(u)$, scaled so that the nth zero is located at $u = \bar{n}$. The aperture distribution is determined by performing a Woodward synthesis of $E_s(u)$. That is, we define a set of functions of the form

$$F_n = \sin(u - n) \frac{\pi}{(u - n)\pi},$$

and then construct $E_s(u)$ from the $F_n(u)$

$$E_s(u) = \sum_{n=-\infty}^{\infty} E_s(n) F_n(u) \tag{3.26}$$

Since we have defined $E_s(n) = 0$ for $n \geq \bar{n}$, Equation (3.26) becomes:

$$E_s(u) = \sum_{n=-\bar{n}-1}^{\bar{n}-1} E_s(n) F_n(u) \tag{3.27}$$

Fourier transformation of Equation (3.27) yields the aperture distribution:

$$A(x) = \int_{-\infty}^{\infty} E_s(u) e^{j2xu\frac{\pi}{a}} du$$

$$= \int_{-\infty}^{\infty} \sum_{n=-\bar{n}-1}^{\bar{n}-1} E_s(u) e^{j2xu\frac{\pi}{a}} du \qquad (3.28)$$

That is, *A(x)* is a weighted sum of integrals of the form,

$$\int_{-\infty}^{\infty} \frac{\sin(u-n)\pi}{(u-n)\pi} e^{j2xu\frac{\pi}{a}} du$$

Let $u^{!} = u\text{-}n$ results in

$$e^{j2n\frac{\pi}{a}} \int_{-\infty}^{\infty} \frac{\sin u^{!}\pi}{u^{!}\pi} e^{j2xu^{!}\frac{\pi}{a}} du^{!}$$

Since the imaginary part of the integrand is odd, this becomes

$$e^{j2n\frac{\pi x}{a}} \int_{-\infty}^{\infty} \frac{\sin u^{!}\pi \cos 2xu^{!}\dfrac{\pi}{a}}{u^{!}\pi} du^{!}$$

$$e^{j2n\frac{\pi x}{a}} \int_{-\infty}^{\infty} \frac{1}{2} \left[\frac{\sin u^{!}\pi\left(1-\dfrac{2x}{2}\right) \sin u^{!}\pi\left(1+\dfrac{2x}{2}\right)}{u^{!}\pi} \right] du^{!} \qquad (3.29)$$

A standard definite integral is

$$\int_{-\infty}^{\infty} \frac{\sin bz dz}{z} \qquad \begin{aligned} &= \pi \ for \quad b > 0 \\ &= 0 \ for \quad b = 0 \\ &= -\pi \ for \quad b < 0 \end{aligned}$$

Application of this integral to Equation (3.29) and hence to Equation (3.28) yields

$$A(x) = \sum_{n=-\bar{n}+1}^{\bar{n}-1} E_s(n) e^{j\frac{2\pi nx}{a}}$$

$$= E_s(0) + \sum_{n=-\bar{n}+1}^{\bar{n}-1} E_s(n) \cos\frac{2\pi nx}{a} \ for \quad |x| \ll \tfrac{a}{2} \qquad (3.30)$$

$$= 0 \qquad \text{for } |x| > a/2$$

The continuous aperture distribution given by Equation (3.30) is sampled to give the element excitation values for a discrete array. This last step is approximate, and the pattern function of the array is obviously different from $E_s(u)$. This approximation is acceptable provided that the number of elements in the array is much greater than $\bar{n}$ and the sidelobe level is not extremely low.

Those equations will determine the aperture illumination coefficients for a linear array of *N* elements to produce a Taylor-type pattern function with $\bar{n}$ sidelobes on each side of the main beam at a level *(L)* dB. The procedure involves three steps. The first $\bar{n}$ -1 zeros of the pattern are determined. Then the appropriate pattern function samples are determined. Finally, the array element illumination coefficients are determined by a harmonic analysis of the pattern function samples.

A particular advantage of this synthesis is that the knowledge of all of the pattern function zeros allows the computation of the pattern function as a product rather than as a polynomial. The product computation involves only one trigonometric function evaluation for each pattern function value. All other constants need to be evaluated only once for each array. The pattern function zeros are given by:

$$z_n = \frac{2\pi\sqrt{A^2+\left(n-\frac{1}{2}\right)^2}}{N\sqrt{A^2+\left(n-\frac{1}{2}\right)^2}} \; for \quad n=1 \quad to \quad \bar{n}-1 \tag{3.31}$$

$$= \frac{2\pi n}{N} \; for \quad n=\bar{n} \quad to \quad M,$$

where

$$M = \text{int}\left(\frac{N-1}{2}\right)$$

and A is given by:

$$A = \frac{1}{\pi}\cosh^{-1}\left[10^{\left(\frac{L}{20}\right)}\right]$$

$$\approx \frac{(L+6.02)}{27.29} \tag{3.32}$$

where *L* is the sidelobe level (positive) in dB. Equation (3.32) is an excellent approximation, especially for large *L*. The pattern function is given by

$$E(z) = \cos\frac{z}{2}\prod_{n=1}^{M}\left(\frac{\cos z-\cos z_n}{1-\cos z_n}\right) \quad \text{N even}$$

$$= \prod_{n=1}^{M}\left(\frac{\cos z-\cos z_n}{1-\cos z_n}\right) \quad \text{N odd} \tag{3.33}$$

The pattern samples to be used to find the array element illumination coefficients are given by:

$$a_m = E\left(\frac{2\pi m}{N}\right) for \quad m = 1 \quad to \quad \bar{n} - 1.$$

The element excitation coefficients are given by

$$e_p = 1 + 2\sum_{m=1}^{\bar{n}-1} a_m \cos\frac{m(2p-1)\pi}{N} \qquad \text{N even, p = 1 to M + 1}$$

$$= 1 + 2\sum_{m=1}^{\bar{n}-1} a_m \cos\frac{2mp\pi}{N} \qquad \text{N odd, p = 0 to M} \qquad (3.34)$$

where *p* is an index or element number staring at the center and moving to either end of the array.

3.5. Conclusions

Smart antenna systems consist of four assemblages: the physical antenna, radio unit, beamforming, and the Digital Signal Processor (DSP). In this chapter, circular pin-fed linearly patch antenna and waveguide-fed pyramidal horn as antenna elements have been considered. A circular pin-fed linearly polarized patch antenna is a directional antenna adapted for determining and transmitting signals in a specified direction, especially for radio broadcast and wireless communication systems due to the unique property of its radiation.

Wave-guide pyramidal horn antenna is a microwave horn antenna that has a flickering metal waveguide conFigured to optimize radio waves in a beam. The waves then radiate out the horn end in a narrow beam. Wave-guide pyramidal horn antenna has been considered because its popularity at UHF (*300 MHz – 3 GHz*) and higher frequencies it is somewhat intuitive and relatively simple to manufacture. The design of smart antenna using waveguide-fed pyramidal horn antenna gives a better system performance of directional radiation beam pattern with a high gain and wide impedance bandwidth.

CHAPTER 4

Performance Analysis of Smart Antenna Arrays

Array of antenna consist of number of antenna elements. The antenna element has spacing between them, and the phase and excitation parameters of these array of antenna determines its characteristics which will subsequently determines the directivity factor, main lobe, and sidelobe levels. Due to changes in characteristic of an array antenna by controlling its parameters give rise to synthesis problem [135].

4.1. Introduction

In antenna design, pattern synthesis is one of the most important analysis that must be put into consideration [77]. Antenna arrays can be synthesized with a few number of antenna elements. There are a lot of benefits attach to the synthesis of antenna arrays. The benefits varies from weight reduction to simplification in feeding network [136].

Until now, we have a lot of approaches to synthesize antenna arrays so as to get the radiation pattern. For a linear array to be synthesized, *Woodward–Lawson and Dolph–Chebyshev* techniques are normally applied for the synthesis. Each of these techniques creates their own special radiation pattern. The radiation pattern created by Dolph-Chebyshev is different from the one created by *Woodward-Lawson* technique. With *Woodward-Lawson* technique, it has a favourite radiation pattern in its sampling point position. Its disadvantage is that it cannot control its radiation ripples generated at a specified direction and the sidelobes level. *Chebyshev* technique is normally use to realize the narrowest main lobe for a specified sidelobe level. Taylor method current distribution technique more gradual in comparison to Chebyshev approach. Hence, it is extensively applied in aperture antennas and array antennas [135].

4.2. Analysis of the Proposed Model's Weighting Methods and Optimization of Radiation Pattern

Antenna array distribution and their associated patterns are now designed on physical principles, based on placement of zeros of the array polynomial. Distribution discussed in this

section are *Dolph-Chebyshev*, phase-tapered weights, and those that allow side lobe envelope shaping. All distributions have constant phase [137].

4.2.1 Phase-tapered weights

To determine the phase-tapered weight for antenna array, we consider a standard hexagonal array with N_x elements along the x-axis. The nm^{th} term in the array multiple vector can be written as:

$$[vec_H(u_x,u_y)]_{nm} = \exp\left\{ j\pi \left[m\frac{\sqrt{3}}{2}u_y + nu_x - \frac{N_x - |m| - 1}{2}u_x \right] \right\}$$

The beam pattern is:

$$B_u(u_x,u_y) = \sum_{m=-\frac{N_x-1}{2}}^{m=\frac{N_x-1}{2}} w_{nm}^* \exp\left\{ j\pi \left[m\frac{\sqrt{3}}{2}u_y + \frac{N_x - |m| - 1}{2}u_x \right] \right\} \cdot \sum_{n=0}^{N_x-|m|-1} \exp\{ j\pi n u_x \}$$

For uniform weighting, $w_{nm} = \frac{1}{N_H}$,

and $$B_u(u_x,u_y) = \frac{1}{N_H} \sum_{m=-\frac{N_x}{2}}^{m=\frac{N_x}{2}} \exp\left\{ j\pi \left[m\frac{\sqrt{3}}{2}u_y - \frac{N_x - |m| - 1}{2}u_x \right] \right\} \cdot \sum_{n=0}^{N_x-|m|-1} \exp\{ j\pi n u_x \}$$

If $N_x = 11$, we can have a typical corresponding hexagonal array with *91* elements. The MATLAB simulation is shown in Figure 4.1.

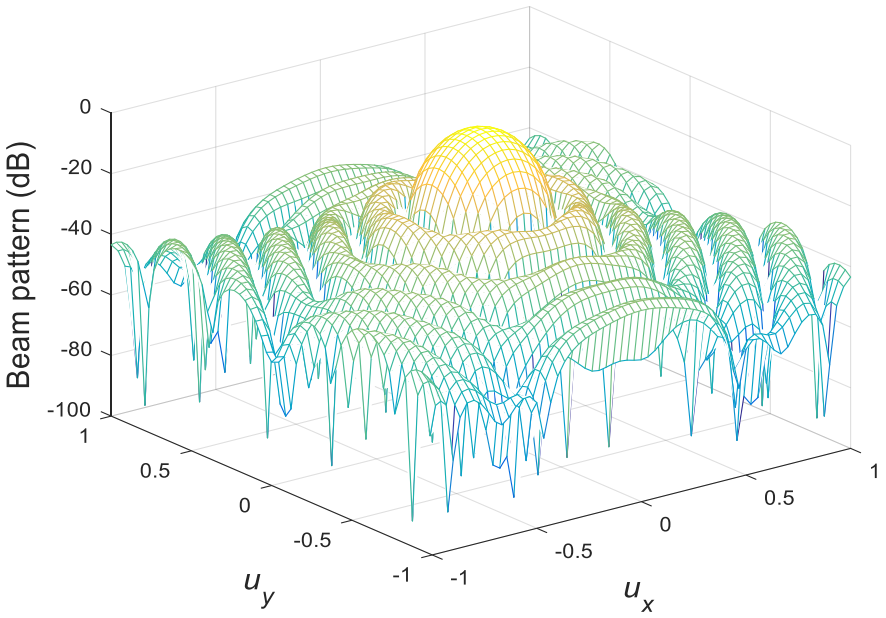

Figure 4.1. Uniform hexagonal array beam pattern weighting.

4.2.2 Dolph-Chebyshev arrays method for the proposed model

Chebyshev array is one of the uniform space linear arrays that has correlation with the conventional antenna arrays with respect to directivity and half-power beam width in an innovative manner [138]. Chebyshev is used to obtain sidelobe level. For the analysis of Chebyshev arrays, assuming we have an array factor of $f(\theta)$, N antenna element, where θ is the angle of elevation. For p basis *Chebyshev arrays*, and $f(\theta)$ as the array factor of the *nth* basis *Chebyshev array* ($1 \leq n \leq p$), then:

$$f(\theta) = \prod_{n=1}^{p} f_n(\theta) \tag{4.1}$$

If $f_1(\theta) = \ldots = f_p(\theta)$, hence $f(\theta) = f_o^{\,p}(\theta)$, this represent the modified Chebyshev array. For series of $f_n(\theta)$, we can write $f(\theta)$ as [138]:

$$f(\theta) = f\left(u = 2\pi\left(\frac{d}{\lambda}\right)(\cos\theta - \cos\theta_o)\right) = \prod_{n=1}^{p}\left(\sum_{k=0}^{N_n-1} I_{n,k}\exp(ju)^k\right) = \sum_{q=0}^{N-1} I_q z^q \tag{4.2}$$

where d is the inter-element spacing, λ is the wavelength, θ_o is the angle of elevation of the maximum radiation, N_n is the number of elements of the n^{th} basis array, $I_{n,k}$ is the excitation of the k^{th} element of the nth basis array, and I_q is the excitation of the q^{th} element of the generalized *Chebyshev array*. From Equation (4.2), it can be deduced that:

$$N - 1 = \sum_{n=1}^{p}(N_n - 1) \Rightarrow N = \left(\sum_{n}^{p} N_n\right) - p + 1 \tag{4.3}$$

So, to design an N element generalized Chebyshev array, the basis Chebyshev arrays should be selected such that the sum of their number of element is:

$$\sum_{n=1}^{p} N_n = N + p - 1 \tag{4.4}$$

and their sidelobe levels should be such that:

$$\prod_{n=1}^{p} R_n = R \tag{4.5}$$

where R is the desired upper bound on the sidelobe level, and R_n is the sidelobe level ratio of the nth basis Chebyshev array.

Dolph-Chebyshev distribution of series of excitation coefficients for an equi-spaced linear array antenna such that the array factor can be stated as a *Chebyshev polynomial*. The *Dolph-Chebyshev* pattern is conceptually simple, as it consists of a main pencil beam, plus side lobes of equal level [137, 138]. *Dolph-Chebychev* linear arrays have ideal radiation properties in that all side lobes in their radiation pattern are of equal magnitude, they provide the narrowest

first null beamwidth possible for a given sidelobe ratio [75, 139]. In addition, the connection between the directivity and sidelobe level for these arrays is optimal because for a given sidelobe level the beam width is the lowest, and, otherwise for a specified beam width the sidelobe level is the lowest. These acceptable radiation characteristics, conversely, put a constraint on the flexibility of putting nulls in the sense that once the sidelobe level or directivity is fixed, the nulls have directions dictated by the *Dolph-Chebychev* excitations [140]. The *Dolph-Chebyshev* pattern is given by [141]:

$$F(u) = T_{N-1}\left(x_o \cos \pi \frac{u}{2} \right) \tag{4.6}$$

The excitation A_n of the n^{th} element is obtained by writing the pattern with the array center as phase reference:

$$F(u) = \sum_{1}^{N} A_n \exp\left[j\left(2n - N - 1\right)\pi \frac{u}{2} \right] \tag{4.7}$$

This is a finite *Fourier series* and the inverse gives the coefficients. The *Dolph-Chebyshev* polynomial of order *m*, is defined by Equation (4.8), where m is an integer. The array polynomial method is used to synthesize the equispaced linear array pattern with null steering [76, 141, 142]:

$$T_m(x) = \begin{cases} \cos(m\cos^{-1} x) & -1 < x < 1 (a) \\ \cosh(m\cosh^{-1} x) & |x| > 1 \quad (b) \\ (-1)^m \cosh\left(m\cosh^{-1}|x|\right) & x < -1 \quad (c) \end{cases} \tag{4.8}$$

It can be confirmed by means of simple trigonometry that $T_m(x)$ is a polynomial of x of order m and the subsequent iteration holds:

$$T_{m+1}(x) = 2xT_m(x) - T_{m-1}(x) \tag{4.9}$$

Here *m* is integer constant with range from *0 to* ∞, let us now obtain *Tchebyscheff polynomials* for different values of *m*. The *Tchebyscheff* polynomials are summarized in Table 4.1 using Equation (4.8).

Now the polynomials with higher values of *m* (5-7) can be obtained by using recursive formula given by:

$$T_m(x) = 2xT_m(x) - T_{m-1}(x) \tag{4.10}$$

From (4.8) we see that the magnitude of a Chebyshev polynomial lies between zero and unity if $|x| < 1$ and exceeds unity if $|x| > 1$. This property of the polynomial is utilized to construct the array factor.

Table 4.1. *Tchebyscheff* Polynomials for the proposed model.

S/N	m	$T_m(x)$
0	0	1
1	1	x
2	2	$2x^2-1$
3	3	$4x^3-3x$
4	4	$8x^4-8x^2+1$
5	5	$16x^5-20x^3+5x$
6	6	$32x^6-48x^4+18x^2-1$
7	7	$64x^7-112x^5+56x^3-7$

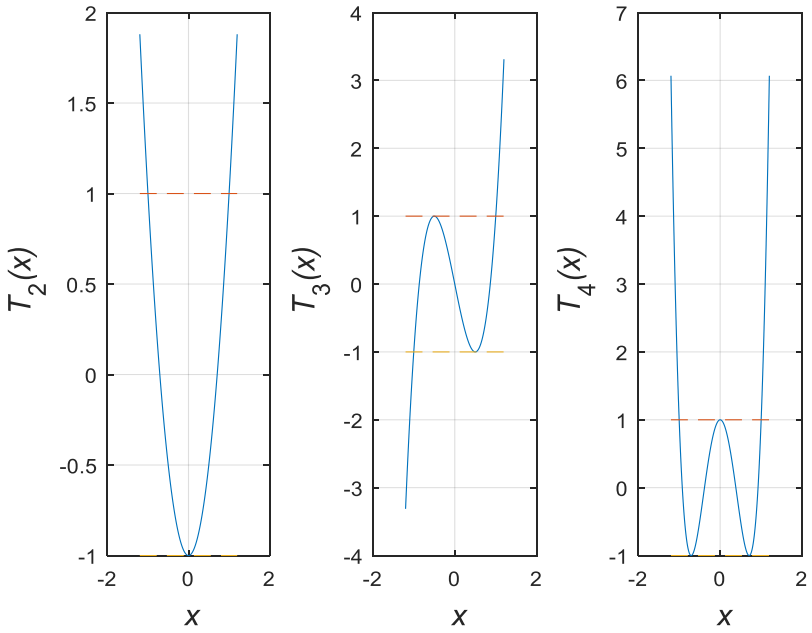

Figure 4.2. Dolph-Chebyshev polynomials for m = 2, 3, and 4.

Figure 4.2 to 4.4 shows the graph of the first *six* Chebyshev polynomials for $0 \le m \le 6$. Chebyshev polynomial can be used to obtain sidelobes level. The array of Chebyshev are non-unform amplitude, when fed with optimum source of amplitude distribution for a specified side lobe level, it will produce same level for all side lobes [143]. Given a side lobe level for Chebyshev polynomial method, it is certain to have the narrowest main-lobe; if the width of the main lobe is given, we can gain the lowest side-lobe on the same level, as it shown in Figure 4.5.

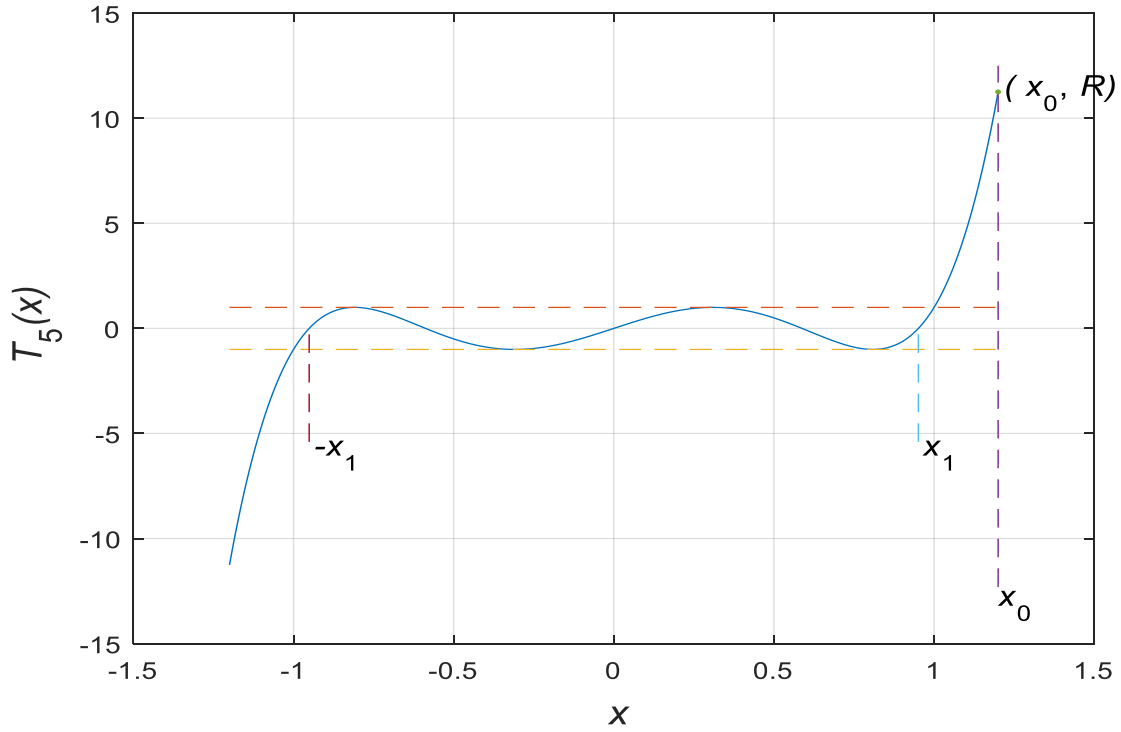

Figure 4.3. *Dolph-Chebychev* polynomial for *m = 5*.

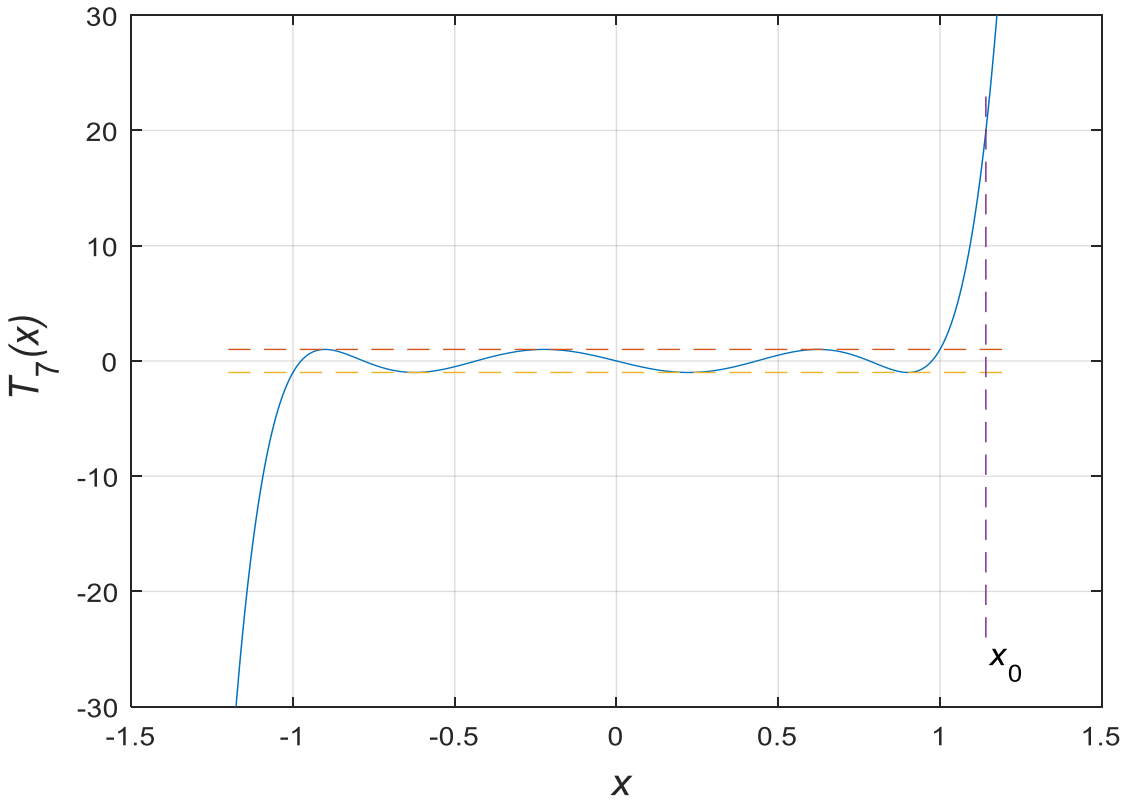

Figure 4.4. *Chebyshev polynomial* of the seventh degree for *m = 6*.

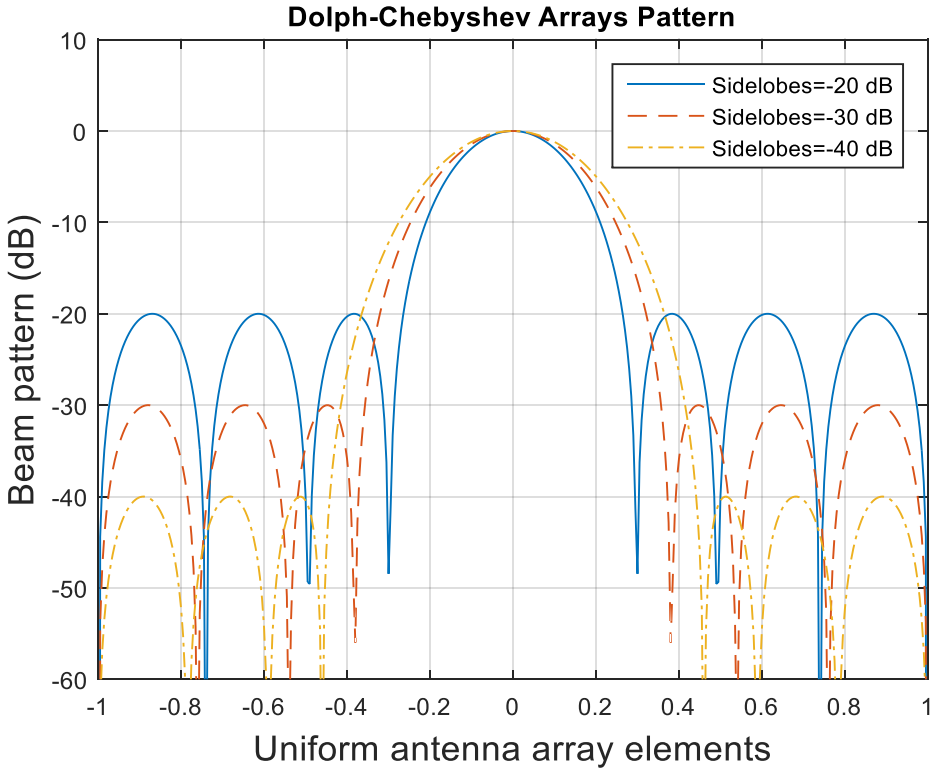

Figure 4.5. Patterns of Dolph-Chebyshev arrays with eight elements.

If the sidelobes S_{ll} (dB) is below the peak of the main beam, the value of the *Chebyshev* polynomial at the peak of the main beam must be equal to [42]:

$$T_{N-1}(x_{mb}) = 10^{\frac{S_{ll}}{20}} \tag{4.11}$$

Setting Equation (4.8) to (4.11), then we obtain of the main beam at

$$x_{mb} = \cosh\left[\frac{\pi A}{N-1}\right] \tag{4.12}$$

where

$$A = \frac{1}{\pi}\cosh^{-1}\left(10^{\frac{sll}{20}}\right) \tag{4.13}$$

From Equation (4.12) we observed that the main beam maps the Chebyshev polynomial, while the array factor zeros (nulls) map the zeros of the *Chebyshev polynomial*. The location of the zeros of the *Chebyshev polynomial* are at:

$$x_n = \cos\left[\frac{\pi(n-0.5)}{N-1}\right] \tag{4.14}$$

The zeros of the array factor mapping to the zeros of the *Chebyshev polynomial* can be obtained using:

$$x_n = x_{mb} \cos\left(\frac{\varphi_n}{2}\right) \tag{4.15}$$

The zeros of the array factor that match up with a sidelobe level (S_{ll}) can be given as:

$$\varphi_n = 2\cos^{-1}\left\{\frac{\cos\left(\frac{(n-0.5)\pi}{N-1}\right)}{\cosh\left(\frac{\pi A}{N-1}\right)}\right\} \tag{4.16}$$

For a specified number of elements and sidelobe level, we can simply get the null locations on the unit circle. Equation (4.16) can be used to design an *8-element* array ($d = 0.5\lambda$) with *-20-dB* sidelobes. It can also be repeated for *-30-sidelobe*, and *-40-sidelobes* levels as seen in Figure 4.5. From Equation (4.16),

$$\varphi_m = 2\cos^{-1}\left[\frac{\pi(m-0.5)}{\cosh(0.1)}\right] = \pm 73.2^0, \pm 120.5^0, 180^0$$

The factored polynomial in factored can be expressed as:

$$AF = (z - e^{j73.2})(z - e^{-j73.2})(z - e^{j120.5})(z - e^{-j120.5})(z - e^{j180})$$

The factors multiplication gives

$$AF = z^5 + 1.44z^4 + 1.85z^3 + 1.85z^2 + 1.44z + 1$$

The coefficients of AF are the amplitude weights for the 8-element array pattern in Figure 4.6. Figure 4.5 are the normalized weights for an 8-element Chebyshev array as a function of sidelobe level. The end element does not have the smallest amplitude for sidelobe levels above *-22 dB. At -22 dB* and below, the weights monotonically decrease from the centre to the edge.

4.3. Determination of Directivity and Gain for Improved Performance of Smart Antenna

This section of thesis deals with the analysis and design of smart antenna system that operates at THz frequency ranging from *0.3 THz* to *3 THz*. The efficiency of this adaptive array antennas system has been optimized and simulated with the aid of commercially available full-wave, Finite Element Method (FEM) based electromagnetic simulator Agilent's Advanced Design Software (ADS).This section proposed and examined smart/ adaptive antennas array at THz frequency range, which can be applied for far distance communications and can be extended to the far-field region of antenna.

Single antenna has a low gain or directivity, so there is need to increase the gain or directivity which can be achieved through antenna arrays. This is a method by which radiation

from groups of same antenna elements with interferences are combined together. As the number of elements in the antenna array increases, its radiated characteristics tend to be dominated by the geometric layouts and excitation of the component elements, rather than the elements themselves.

In wireless communication systems, antenna with high directivity and gain improves the network capacity and quality of service significantly. Antenna directivity $D(\theta, \phi)$ can be describes as a quantity that refer to the directional transmitting distinctive quality of the antenna element. Directivity $D(\theta, \phi)$ of an antenna in an indicated direction can be defined as the ratio of the radiation intensity of the antenna $U(\theta, \phi)$ in a specific direction in space over the antenna radiation intensity U of the source of isotropic power, to the identical radiated power. This is basically a direction in which the antenna is radiating:

$$D(\theta,\phi) = 4\pi \frac{\underline{u_{rad}(\theta,\phi)}}{\frac{p_{total}}{4\pi}} \tag{4.17}$$

where $U_{rad}(\theta, \phi)$ represents radiation intensity in the direction of (θ, ϕ) and P_{total} is the total power by the isotropic radiator. These quantities are related as:

$$p_{tot} = \int_{\phi=0}^{\theta=2\pi} \int_{\theta=0}^{\theta=\pi} u_{rad} \sin\theta d\theta d\phi \tag{4.18}$$

while gain and directivity are interrelated, but takes into consideration the antenna losses in conjunction with its directional capabilities. Usually, the losses are very insignificant. High gain indicates more directive. Sometimes, directivity and gain are used vice versa. The distinction is that directivity disregards antenna losses. The losses in antenna are dielectric, polarization, resistance, and VSWR. Since these losses in some antennas are typically relatively small, the gain and directivity will be nearly equal when unwanted pattern characteristics are disregarded. Regulating a radiation pattern by integrating the total power gives the antenna directivity as:

$$D(\theta) = 10\log\left[\frac{4\pi p(\theta,\phi)}{\iint p_{in}(\theta,\phi)\sin\theta d\theta d\phi}\right] \begin{matrix} 0 < \phi 360 \\ 0 < \theta 180 \end{matrix} \tag{4.19}$$

Directivity is a fundamental parameter directly associated with the chart of geographic coverage area of an antenna. This is basically directions at which the antenna is radiating. However, in the process that the antenna is radiating, losses do normally occur. The parameter that can accounts for losses and directivity is gain. Characteristically, the losses are little that we get proficient to deliberate of gain as directivity or vice versa. Therefore, low gain is equivalent to broader coverage. For antenna with high gain, a better directivity is achieved.

Most of the available antenna elements designed for smart antennas operates at low frequency range (GHz), and their directivity were not prioritized.

4.3.1 Design analysis for the antenna arrays

The antenna has been put together on a *Rogers_RT_Duroid* dielectric substrate of Svensson/Djordjevic loss type with dielectric permittivity (ε_r) = *2.33*, loss factor/tangent (*tanδ*) = $1.2*10^{-3}$, relative permeability (μ_r) =*1* and the thickness (*h*) = *0.80 mm*. In this work, Rogers_RT_Duroid dielectric substrate has been taken as substrate due to the low dielectric loss which make it suitable for high-frequency laminate over the FR-4 substrate as in appendix. Due to high loss of the FR-4 substrate, it exhibits low gain (low efficiency).

The interface of the substrate has been covered with a perfect conducting material layer of infinite width, and thickness of *0.01 mm*. The substrate has been computed from *40.92 GHz to 3.00 THz*. The antenna receives input power and radiated power at *15.55 Watts* in a specific direction, focusing the desired signals from where they come forth allowing for increased radiation efficiency of *100 %* and mitigate interfering signals from unwanted sources. The antenna has a peak directivity of *17.6 dB*, this made it possible for the maximum power transfer. The adaptive layout system of the antenna is shown in Figure 4.6. The system takes gain of its capability to efficiently detect and track various kinds of signals to dynamically curtail interference and exploit projected signal reception. The adaptive system offers optimal gain while concurrently detecting, tracking and reducing interfering signals.

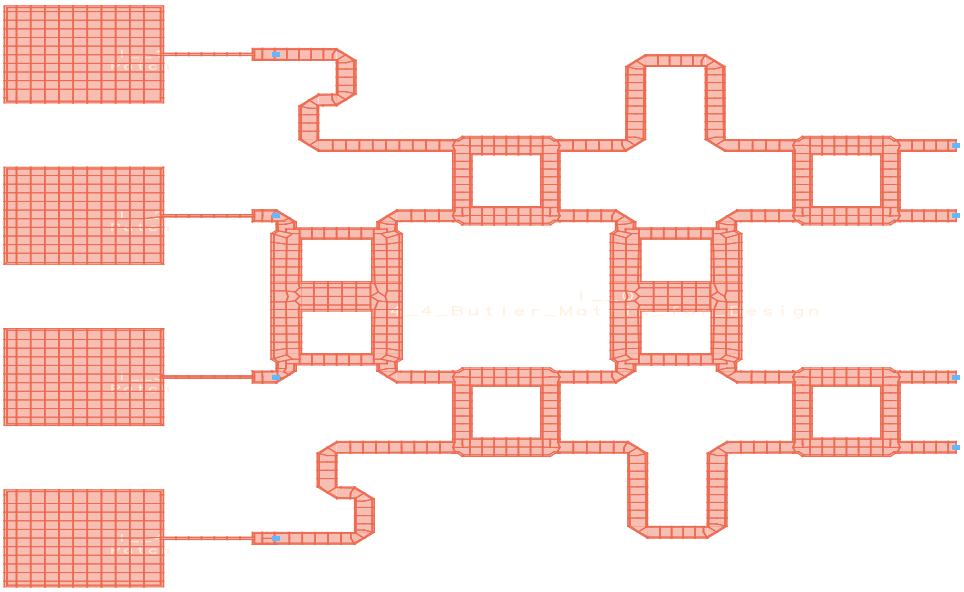

Figure 4.6. Array feed network layout design.

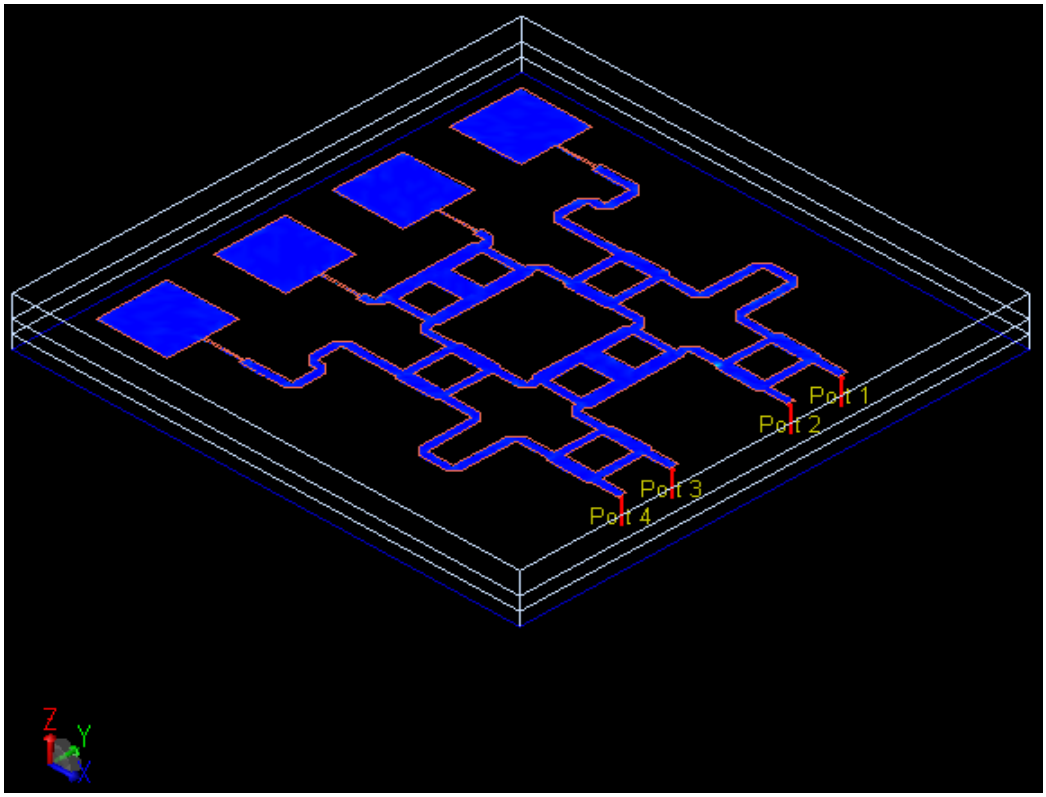

Figure 4.7. Isometric view of the array feed network.

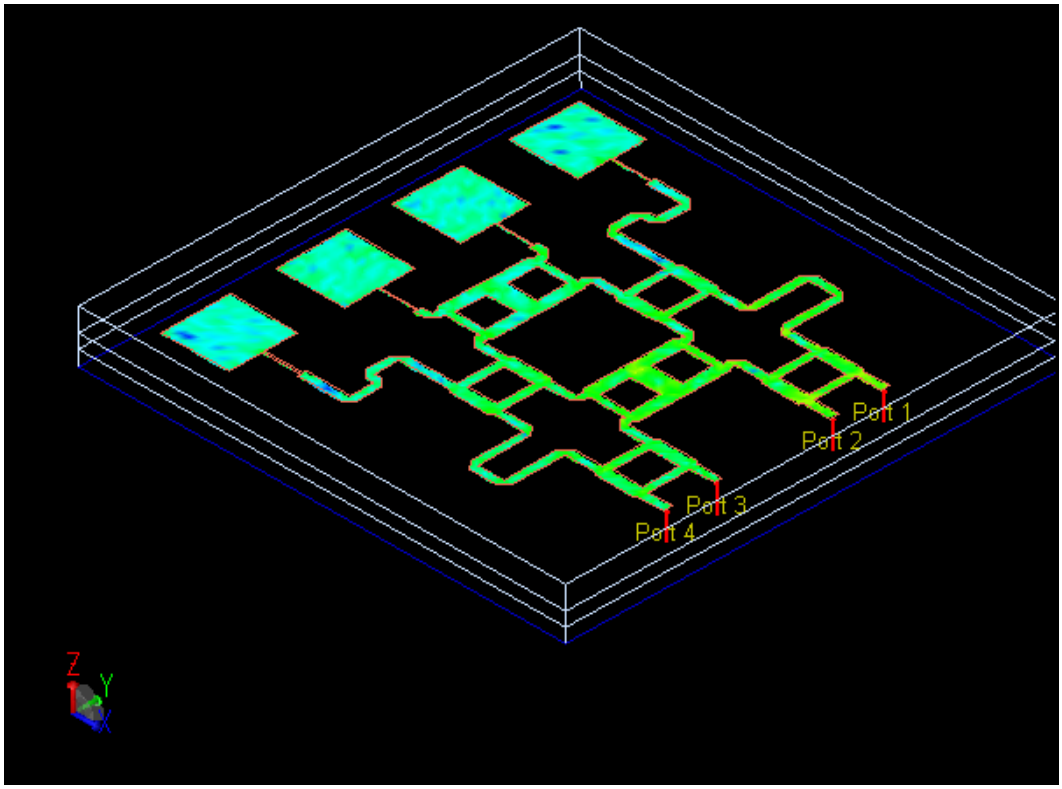

Figure 4.8. dB scale isometric preview of the array feed network.

Figure 4.7 shows the isometric view of the adaptive layout design. All the four radiating elements of the antenna array are equal. Each antenna element of the adaptive array is operated

within the frequency band between *300 GHz* to *3 THz*. We have analyzed the radiation features of the antenna array, they exhibits wide beams in specific directions by various phase at the ports. Figure 4.8 shows the isometric plot preview in dB of the design layout. This has a scale of relative power and angle selected to suit the antenna parameters.

4.3.2 Far-field of the adaptive array antenna

Far-field of the adaptive array antenna is a far-field that has an infinity range magnitude which is associated with the field E_a of the *far-zone* radiated by the antenna, with the current I_{in} in its terminals.

To calculate the gain and directivity of the array, its far field needs to be found. This can be estimated by multiplying the far field of the single patch by the array factor, which depends only on the spatial arrangement of the elements and the amplitude and phase of the feeding current of each element.

Optimization can then be used to adjust the spacing between the elements to maximize the gain of the antenna, and to change the magnitude of the feeding current to different patches to reduce the side lobes.

$$E_a = \hat{a}_\theta E_\theta + \hat{a}_\phi = -j\eta \frac{kI_{in}}{4\pi r} \mathrm{l}_e e^{-jkr} \tag{4.20}$$

Table 4.2. Antenna pattern parameters at the far-field region.

Dimension	**Value**
Frequency of operation	3.0 THz
Input Power	15.5515 watts
Power Radiated	15.5515 watts
Effective Angle	0.217413 steriadians
Directivity	17.6192 dB
Gain	17.6192 dBi
Radiation Efficiency	100 %
Maximum Intensity	71.5297 watts/steriadians
operational plot	E
minimum dBi	-40
Angle of U Max (θ, ϕ**)**	10, 122
E (theta) max (mag, phase)	84.75, 173.786
E (phi) max (mag, phase)	216.13, -124.257
E (z) max (mag, phase)	14.7167, -6.21413
E (y) max (mag, phase)	102.494, 93.2965

The vector effective length of the antenna can be determined by:

$$\mathrm{l}_e = \hat{a}_\theta \frac{l}{2} \sin\theta \tag{4.21}$$

This specifies, that the effective length of the antenna is a function of the direction of angle θ, and has a maximum value when $\theta = 90^0$.

The summation of the radiated array from the antenna far-fields E is [136]:

$$E = \sum_{i=1}^{N} E_i \tag{4.22}$$

E_i is the *i*th of the antenna far-field which can be expressed as:

$$E_i = \left[\hat{a}_\theta f_{\theta i}(\theta,\phi) + \hat{a}_\phi f_{\phi i}(\theta,\phi) \right] w_i k_i \mathrm{l}^{-jkr_i} \tag{4.23}$$

where $f_{\Theta i}$ is the θ component of the radiation pattern, while $f_{\phi i}$ is the ϕ component of the radiation pattern w_i *and* k_i are the excitation weighting factor of the source, and accounting for the continuous path loss, respectively. $f_{\Theta i(\theta,\ \phi)}$ and $f_{\phi \mathrm{i}(\theta,\ \phi)}$ are accomplished with the i_{th} for all *i* elements of the antenna positioned at the source. For equal antenna elements, the radiations element are equivalent and self-regulating of *i*. Therefore:

$$E_i = \left[\hat{a}_\theta f_{\theta i}(\theta,\phi) + \hat{a}_\phi f_{\phi i}(\theta,\phi) \right] w_i k_i \mathrm{l}^{-jkr_i} \tag{4.24}$$

$$r_i = r_o - \Delta r = r_o - \rho_i \bullet \hat{a}_r(\theta,\phi) \tag{4.25}$$

$$E = k\mathrm{l}^{-jkr_o} \left[\hat{a}_\theta f_{\theta i}(\theta,\phi) + \hat{a}_\phi f_{\phi i}(\theta,\phi) \right] \sum_i^N w_i \mathrm{l}^{jk\rho_i \bullet \hat{a}_r(\theta,\phi)} \tag{4.26}$$

The derivation in Equation (4.26) can be referred to as the principle of array pattern multiplication, which states that the array pattern is the multiplication of the antenna element pattern with $f_{array(\theta,\ \phi)}$ the array factor. In the same way, the relationship between signal impacting on the antenna array with equal number of element space and signal received can be written in the form of typical radiation parameters:

$$f(\theta,\phi) = \sum_{m=0}^{M} I_m \omega_m \exp(j\beta d_m (\cos\phi \sin\theta - \cos\phi_o) \tag{4.27}$$

where β, is the phase propagation factor, d_m is the space between antenna elements, and I_m is the complex amplitude at each element respectively. ϕ_o is the incident signal angle. The electric field generated by the antenna in the far field can usually be written as:

$$\overset{\mathrm{v}}{E} = \overset{\mathrm{v}}{E}_o F(\theta,\phi)\frac{\mathrm{l}^{-j\beta r}}{r} \tag{4.28}$$

The far-field pattern or the radiation pattern is referred to as the directional *(θ, ϕ)* on which the strength of radio waves from the antenna depends. This is can also be called the element pattern. For two identical antenna element spaced by d can be expressed as:

$$\overset{\mathrm{v}}{E}_{total} = \overset{\mathrm{v}}{E}_1 + \overset{\mathrm{v}}{E}_2 = F(\theta,\phi)\left[\overset{\mathrm{v}}{E}_1\frac{\mathrm{l}^{-j\beta R_1}}{R_1} + \overset{\mathrm{v}}{E}_2\frac{\mathrm{l}^{-j\beta R_2}}{R_2}\right] \tag{4.29}$$

Assuming that each antenna is excited with identical amplitudes but allowing for a phase-shift ξ between the antennas, that is, $E_2 = E_1\mathrm{l}^{-j\xi}$ gives:

$$\overset{\mathrm{v}}{E}_{total} = E_1 F(\theta,\phi)\left[\frac{\mathrm{l}^{-j\beta R_1}}{R_1} + \frac{\mathrm{l}^{j\xi}\mathrm{l}^{-j\beta R_2}}{R_2}\right] \tag{4.30}$$

In the far-field where *r >> d*, the two distances R_1 and R_2 are approximately the same. However, even a small difference could produce a significant phase-delay between the two signals, hence we must use a better approximation in the phase terms. To first order, we get $R_2 \approx R_1 - d.\sin\theta.\cos\phi$. We can still use $R_2 \approx R_1$ in the amplitude terms, however, using these far-field approximations gives the result:

$$\left|\overset{\mathrm{v}}{E}\right| = 2\frac{E_1}{r}\left|E_1 F(\theta,\phi)\right|\left|\cos\frac{\varphi}{2}\right| \tag{4.31}$$

where $\psi = \beta d\sin\theta\cos\phi + \xi$, the $|\cos(\varphi/2)|$ term is known as the array factor, since it describes the interference pattern for two antennas, regardless of what kind of antenna is used. This equation illustrates the principal of array multiplication pattern, which can be expressed as the total radiation pattern of an array is just the antenna element factor multiplied by the array factor (AF). Figure 4.10 to Figure 4.12 show the simulated far-field at $\phi = 43^0$ and $\theta = 44^0$.

In Figure 4.10 to Figure 4.11, *x*, *y*, and *z* represent the direction of radiation of the transmitted signals in their various directions. Electromagnetic waves equal to and as well as microwaves that have comparatively with high frequencies can transmit large amounts of data. As the frequency rises, the higher antenna increases the system capacity. Thus, the antenna tracking and targeting precision requirements will be increased. The adaptively fitted points is shown in blue, while the discrete frequency points are shown with red colour. Figure 4.13 shows the antenna parameters (gain is *17.6 dBi*, directivity is *17.6 dB*, efficiency is *100 %*, and the radiated power is *15.5* Watt) plotted against frequency at *3 THz*. It can be observed that directivity and gain are equal plotted against the frequency at *3 THz*. It can be observed that directivity and gain are equal because the efficiency is *100 %*.

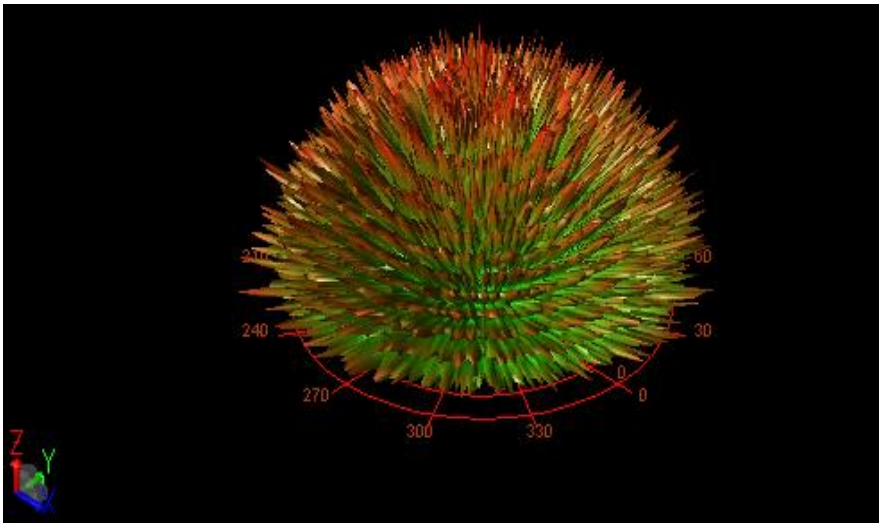

Figure 4.9. Far field at 3 THz.

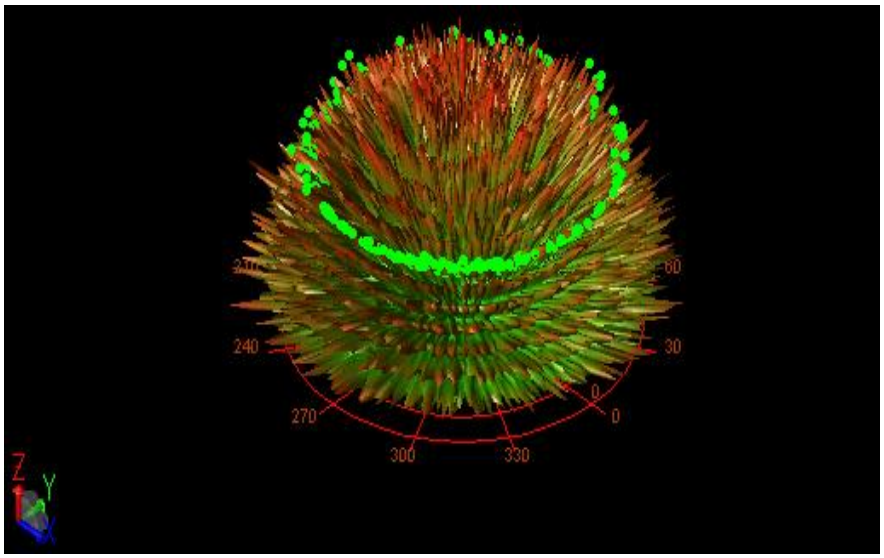

Figure 4.10. The far-field radiation pattern ($\theta = 44^0$).

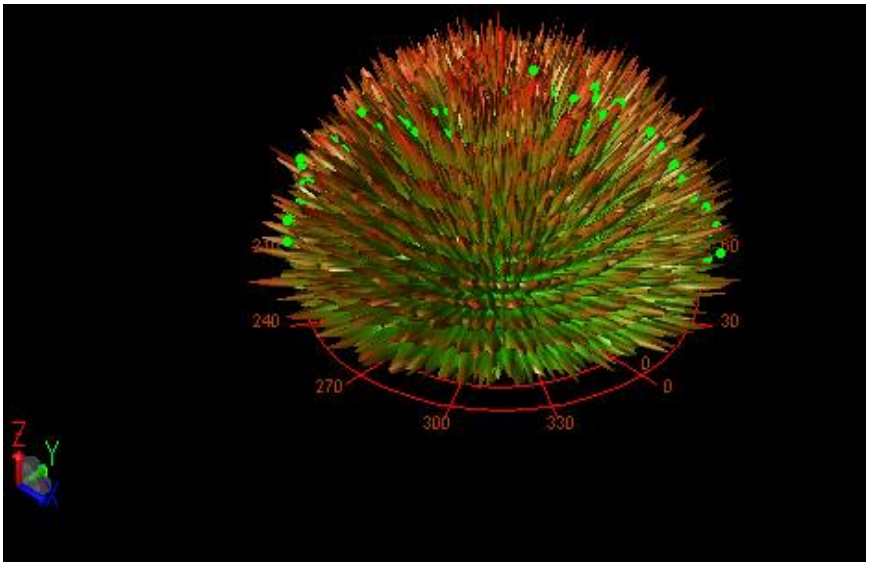

Figure 4.11. The far-field radiation pattern ($\phi = 43^0$).

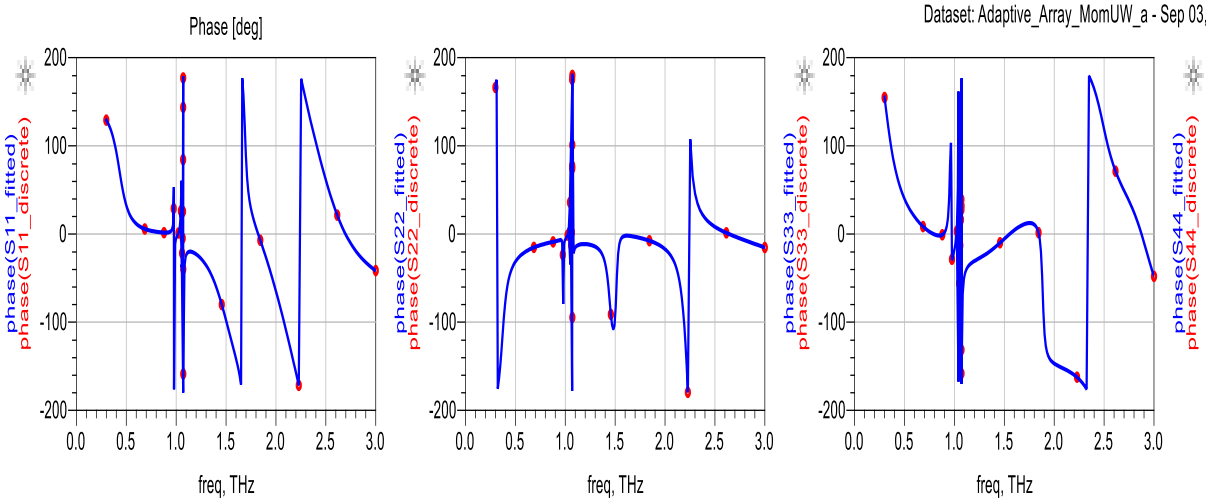

(a) Frequency from 300 GHz to 0.6 THz

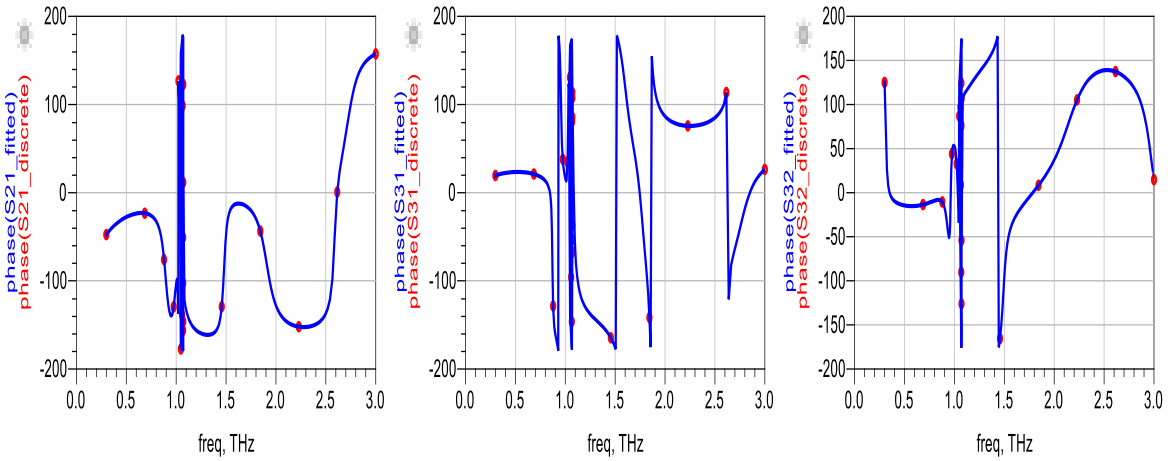

(b) Frequency from 0.7 THz to 1.7 THz

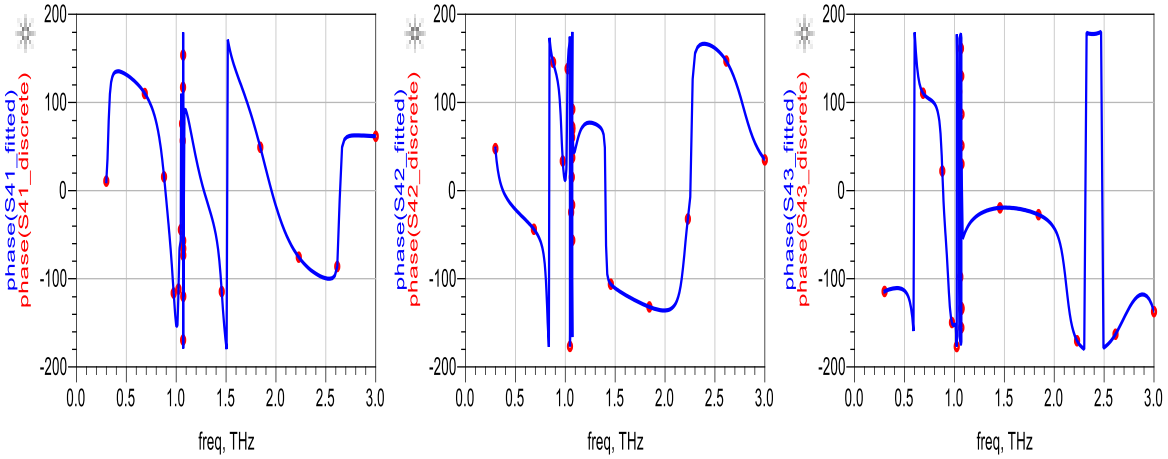

(c) Frequency from 1.8 THz to 3 THz

Figure 4.12. Discrete frequencies vs Fitted AFS of the adaptive array from 300 *GHz* to *3 THz*.

Figure 4.14 shows the s-parameters from *300 GHz* to *3 THz*. The S-paramters mostly depends on frequency during signal transmission. As the frequency is changing, the s-parameters change. A lossles network is achieved as it does not dissipate power. The power that is incident on the network is equal to the power reflected. The smith chart in Figure 4.14 acts as a graphical demonstrator of how radio frequency (RF) parameters behave. The real part of the reflection coefficient is the horizontal axis while the vertical/perpendicular axis displays the imaginary portion of the reflection coefficient. The starting point is $|\Gamma| = 0$ and $VSWR = 0$. The Figures shown on the smith chart is the normalized complex impedance as presented in Figure 4.14.

S-parameters are more appropriate for evaluating matching performance. The circles show the resistances, while the reactance is shown as arched lines. The inductive is the upper half-space, whilst the lower half space is capacitive. The middle line is pure resistance from *zero* to *infinity*. Since the frequencies are sufficiently close, the resulting Smith Chart (Figure 4.14) was joined by straight lines to create locus.

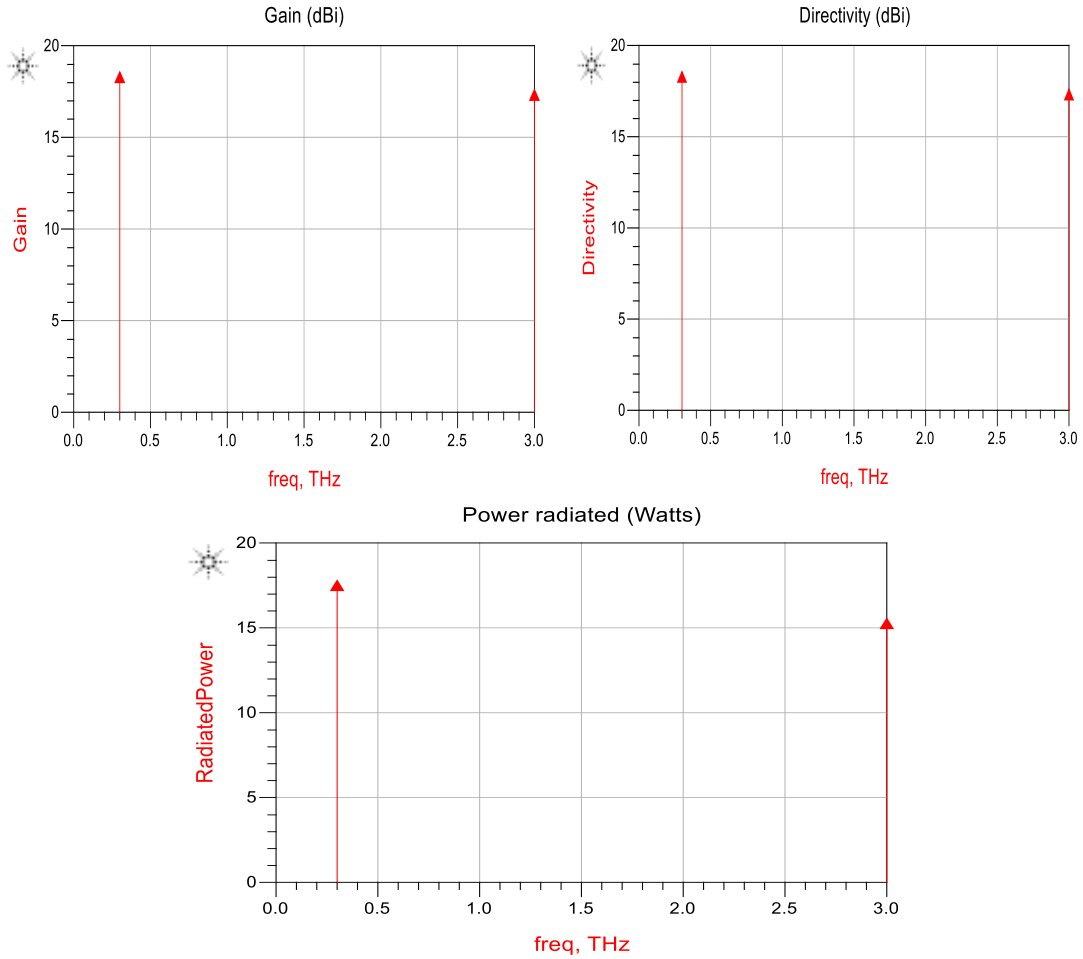

Figure 4.13. The parameters of antenna characteristics versus frequencies.

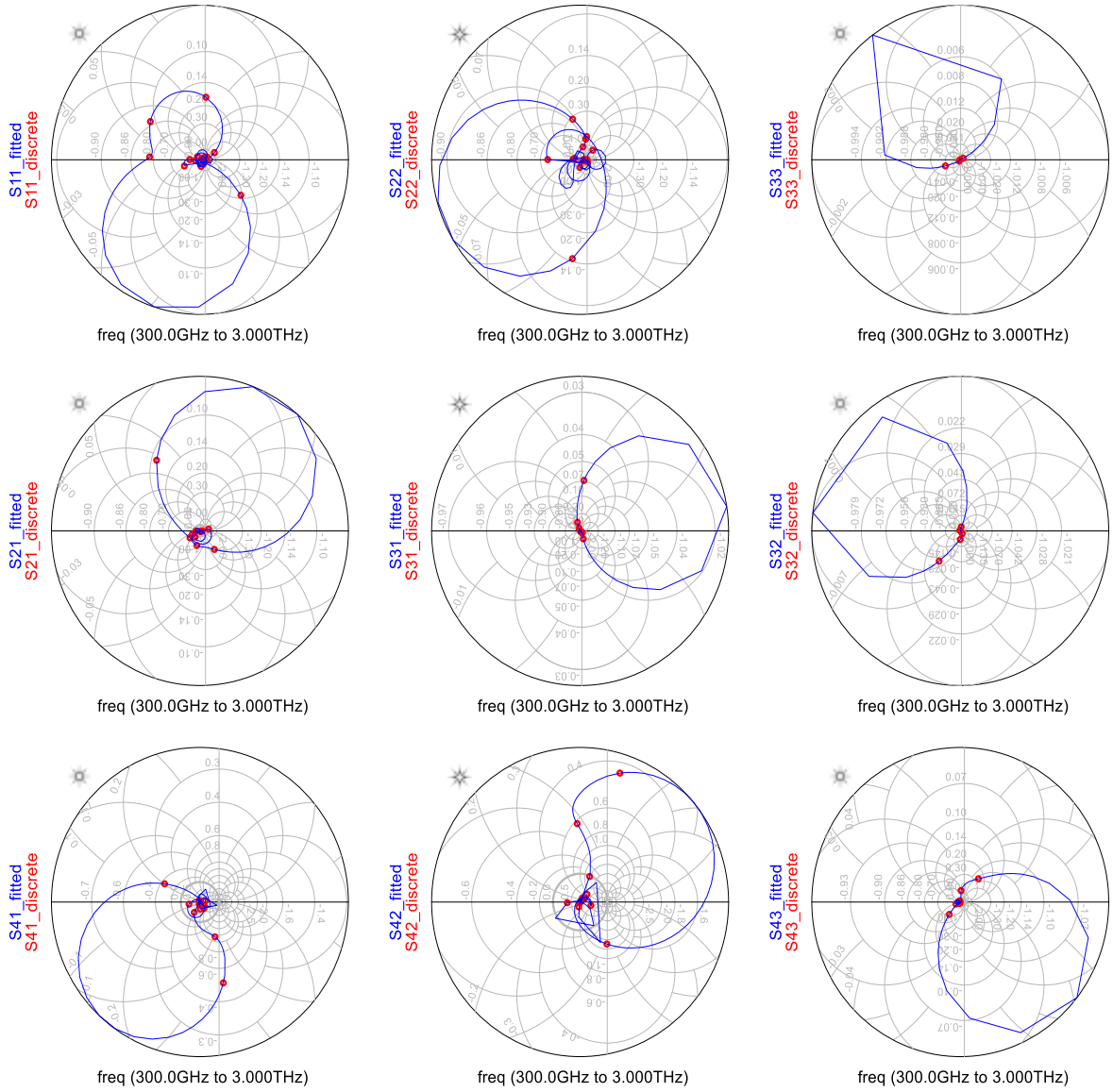

Figure 4.14. S-parameters from 300 GHz to 3 THz.

The locus on the Smith Chart covering range of frequencies (*300 GHz - 3 THz*) was employed to visually represent how capacitive or inductive a load is across the frequency range, and how difficult matching is likely to be at various frequencies. The $|\Gamma| = 0.9235$ as shown in Figure 4-14 with dash lines.

4.3.3 Radiation Intensity function of the antenna element

In this section, the theoretical model for the antenna arrays and some basic mechanism (radiation pattern) that allows the antenna to radiate has been discussed. Radiation pattern is an important function mechanism in antenna array's field. The far-field array's radiation pattern can be written as:

$$p(\varphi,\theta) = \sum_{k=1}^{L} I_k a_k(\varphi,\theta) \tag{4.32}$$

where I_k is the current on the k^{th} antenna's element, in the azimuthal angle φ and elevation angle θ, $a_k(\varphi, \theta)$ is the k^{th} element's array response, while L represents the total number of antenna elements. From Equation (4.32) regardless of the way these currents are produced, the array's radiation field pattern are influenced linearly by the individual antenna currents.

4.4. Signal Quality Improvement and Performance Analysis of designed Smart Antenna Bandwidth

In general, the performance of antenna depends on various characteristics such as antenna gain, sidelobe level, Standing Wave Ratio (SWR), antenna impedance, radiation patterns, antenna polarization, Front to Back (FBR) ratio etc. During the operation of antenna these requirements may change. Thus there is no unique definition for antenna bandwidth. The functional bandwidth of the antenna is generally limited by one or more factors mentioned above. So the antenna bandwidth can be specified in various ways such as

(a) Bandwidth over which the gain of the antenna is higher than the acceptance value, or
(b) Bandwidth over which the standing wave ratio of transmission line feeding antenna is below acceptable value, or
(c) Bandwidth over which the FBR is minimum equal to the specified value.

Thus in general we can define the bandwidth of antenna as the band of frequencies over which the antenna maintains required characteristics to the specified value. But as the requirements of antenna change during the operation, the specifications are set depending upon the application for which that antenna is used. This means for certain antenna where due to the increase in side lobe level, antenna gain decreases and resistance value changes, then the lower frequency limit is obtained by considering one of the parameters like pattern, gain or impedance. While the other parameters decide higher frequency limit.

In general, the antenna bandwidth mainly depends on impedance and pattern of antenna. At low frequency, generally impedance variation decides the bandwidth as pattern characteristics are frequency insensitive. Under such condition, bandwidth of the antenna is inversely proportional to Q factor of antenna. Thus bandwidth can be expressed mathematically as:

$$\text{Bandwidth (BW)}, \Delta\omega = \omega_2 - \omega_1 = \frac{\omega_0}{Q}$$

where $\Delta\omega = \frac{\omega_0}{Q}$ and $\Delta f = f_2 - f_1 = \frac{f_0}{Q} Hz$ in which f_o is the center frequency or design frequency or resonant frequency, while Q factor of antenna is given by:

$$Q = 2\pi \frac{\text{Total energy stored by antenna}}{\text{Energy radiated per cycle}}$$

Thus for lower Q antennas, the antenna bandwidth is very high and vice a versa.

4.5. Conclusions

This chapter deals with the analysis and design of smart antenna system that operates at THz frequency range from *0.3 THz - 3THz*. An array with high directivity is the focus with frequency range from *0.3 THz – 3 THz*. In this chapter, *Dolph-Chebyshev* and *Phase-Tapered* methods has been applied for the synthesis of antenna array radiation pattern. The normalized amplitude weights for an 8-element *Dolph-Chebyshev* array versus sidelobe level is shown in Figure 4.5 which are the normalized weights for an 8-element *Chebyshev array* as a function of sidelobe level. The end element does not have the smallest amplitude for sidelobe levels above at *-22 dB*. *At -22 dB* and below, the weights monotonically decrease from the center to the edge.

CHAPTER 5

Performance Evaluation of Optimal Smart Antenna Arrays

Basically, parameters for antenna arrays design are beamwidth, side lobe level, directivity, noise sensitivity, robustness, and the dynamic range of the element excitation inter alia. Some of the practically driven array antennas used as radiating systems forms are: (a) collinear array, (b) broadside array, (c) end-fire array, and (d) parasitic array. Collinear consists of two or more half wave dipoles mounted end to end are used for (UHF) and (VHF) bands.

5.1. Introduction

The synthesis of antenna arrays is vital in smart antennas in that it shapes the radiation pattern of the antenna array. To synthesize an antenna arrays, we need to determine the performance parameters such as the designing of the antenna element, determination of the space between each antenna element, and the evaluation of the amplitude and phases of all the antenna elements. For an antenna array with a given number of antenna elements and the space between them are known, it is easy to optimize the amplitudes and phase of the array elements [133].

5.2. Smart Antenna Design Procedure using Planar Phased-Array Antenna

The term phased array comes from the time-harmonic/steady-state analysis of antenna arrays [45]. A phased array is an array of multiple antenna elements, which scan a beam pattern to given angles in space through time-delay control of the element excitation phasing [61, 144]. Phased arrays can be used to steer the main beam of the antenna without physically moving the antenna [76]. In a particular array antenna, all the elements radiate coherently along a specified direction. In antenna theory, a phased array usually means an electronically scanned array; an array of antennas which creates a beam of radio waves which can be electronically steered to point in different directions, without moving the antennas. The planar phased array antenna is an antenna that composes a plane radiating elements or array of elements aligned over a plane.

This plane consists of two dimensional rectangular, square or circular apertures with different amplitude and phase controller installed between these elements [144].

Figure 5.1 consists the geometry of an *8 x 8* planar phased-array antenna located in the x-y plane of a rectangular coordinate system which offers the synthesis of a needed beam pattern which is not obtainable with a single patch antenna element [72, 145]. The planar phased-array antenna of high performance is analysed using an *8x8* square grid of z- controlled antenna monopoles with a length of *0.482λ*. The considered element spacing is *0.315λ* and the average directivity of *22.0 dBi*. The directivity cut across all various scanning angles at an average E-plane and H-plane antenna pattern's half power beamwidth of *39 degrees* and *25 degrees* with an efficiency of *99.8%*.

In antenna design system, the significant parameters are normally, the number of antenna elements, spacing that connects the antenna elements, amplitude and phase excitation, half-power beamwidth (HPBW), directivity and side lobe level (S_{11}). Aside from side-lobe level, additional imperative antenna array design specification typical feature is the complete magnitude and shape of the main beam [54, 144].

The elements are arranged in a rectangular grid of z-directed controlled.

From a characteristic mode theory, the generalized Eigen value problem can be expressed as:

$$[X]\{I\} = \lambda[R]\{I\} \tag{5.1}$$

To excite the arrays, we use the characteristics mode based excitation of finite arrays. For an array of N elements as the one shown in Figure 5.1, the N-port impedance matrix [Z_s]

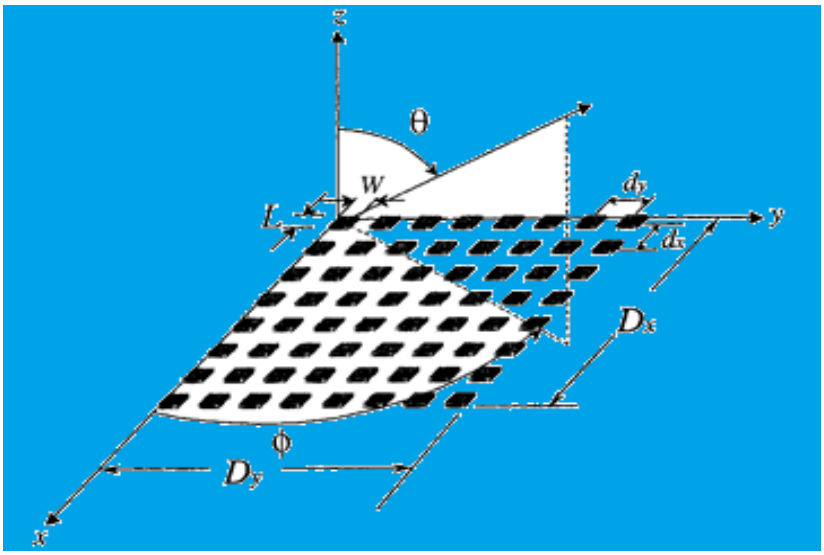

Figure 5.1. Planar-Phased array antenna system.

can be used in Equation (5.1) to excite the array, the induced port voltages $\{V_k\}$ are also real and in phase with the excitation. That is:

$$\begin{aligned}\{V_k\} &= [Z_s]\{I_k\} \\ &= [R_s]\{I_k\} + j[X_s]\{I_k\} \\ &= [R_s]\{I_k\} + j\lambda_k[R_s] \\ &\approx [R_s]\{I_k\}\end{aligned} \tag{5.2}$$

From Equation (5.1) the active impedance $\{Z_a\}$ for the array elements can then be expressed as:

$$\{Z_a\} = \{V_k\}./\{I_k\} \rightarrow [R_s]\{I_k\}./\{I_k\}$$

where "./" indicates element-wise division between the two vectors. The resulting active port impedances are real because both $\{V_k\}$ and $\{I_k\}$ are real valued. Hence, all array ports can be matched concurrently, provided each port is fed by a transmission line containing a characteristic impedance equal to the active port impedance.

5.3. Requirements and Specification for the Proposed Model Phased Array

In Figure 5.1, the array factor equation that meets the directive angle requirements for planar array is [72, 146]:

$$AF(\theta,\phi) = \sum_{m=1}^{M}\sum_{n=1}^{N} i_m \begin{bmatrix} e^{j(m-1)(kdx\sin\theta\cos\phi+\beta x)} \\ e^{j(n-1)(kdy\sin\theta\cos\phi+\beta y)} \end{bmatrix} \tag{5.3}$$

where $\beta x = -kdx\sin\theta_o\cos\phi_o$ and $\beta y = -kdy\sin\theta_o\cos\phi_o$. The ϕ and θ_0 are the angular variation in azimuth and elevation as seen from x and z-axis in degrees of Figure 5.1, θ_0 and ϕ_0 are scan angles in elevation and azimuth direction, d_x and d_y are elements design in x and y direction correspondingly ($d_x = d_y = \lambda/2$), the inter-element spacing of $\lambda/2$ was maintained to avoid grating lobes. The array factor was simplified by computing 0.1λ, 0.3λ, 0.5λ, and 1.0λ as analyzed in the following section. Where λ, M and N denote antenna's wavelength of operation, elements number in x and y-directions respectively. For the avoidance of grating lobes in the course of scanning, the inter-element configuration sandwiched in the middle of elements in x and y-axis. Antenna's elements number N is given as:

$$\frac{d_x}{\lambda} = \frac{d_y}{\lambda} = \frac{N}{N+1} \tag{5.4}$$

The Planar array is *N x M, N = M = 8*. Hence, antenna's elements *(8x8)* is equal to 64, operating frequency is *10 GHz*, the array length L_x/λ and L_y was calculated as *2.2 mm* with the aid of 3 dB beamwidth and scan angle versus linear array length. The element spacing is 0.351 λ, $d_x=d_y = 8.2$ *mm*, $D_x = D_y = 64.6$ *mm*.

The orthogonal direction of array's plane Z-axis for an array with combination of (*N*, *L*, and *d*) is *L=Nd*. This size gives us a concept for the breakdown of the phased array. To fill up the aperture, the required scan was maintained at an angle of $\pm 90^0$ while considering the frequency of operation. The inter element spacing (d) of 0.351λ was used so that the scan requirements are met at the operating frequency The element spacing decides the total number of sets of antenna array components due to the structure of maximum array area. The parameters calculated were approximated and the MATLAB simulation was done for dimensional optimization so as to meet the required specification. The inter element layout gives scan of up to sandwiched between 40^0 and 45^0. To minimize the side lobe level characteristic to a lower one of *-20 dB* in the direction of the main beam, the binomial current distribution is preferred for the work:

$$(AF)_{2M+1}(even) = \sum_{n-1}^{M} a_n \cos\left[(2n-1)\right]u \tag{5.5}$$

$$(AF)_{2M+1}(odd) = \sum_{n-1}^{M+1} a_n \cos\left[(2n-1)\right]u \tag{5.6}$$

$$u = \frac{\pi d}{\lambda}\cos\theta \tag{5.7}$$

The binomial array factor for the phase antenna is represented by Equations (5.5) to Equation (5.7), where the a_n's are the excitation coefficients. MATLAB simulations were performed to demonstrate the efficiency of the design. The array pattern for the two spatial planar arrays x and y possibly expressed as the multiplication of beam radiation array in the two planes which comprise the major axes of the antenna $G\ (\theta_a, \theta_e) = G_1\ (\theta_a)\ x\ G_2\ (\theta_e)$ *and*

Array separability: f(x, y) = f(x) * f(y) (5.8)

Since the antenna elements were arranged on a rectangular array, the normalized beam radiation configuration of an evenly lighted rectangular array is:

$$G(\theta_e,\theta_a) = \frac{\sin^2\left[N\pi\left(\frac{d}{\lambda}\right)\sin\theta_a\right]}{N^2\sin^2\left[N\pi\left(\frac{d}{\lambda}\right)\sin\theta_a\right]}\frac{\sin^2\left[M\pi\left(\frac{d}{\lambda}\right)\sin\theta_e\right]}{M^2\sin^2\left[N\pi\left(\frac{d}{\lambda}\right)\sin\theta_e\right]} \tag{5.9}$$

Both *N* and *M* are the number of antenna elements in θa and θe magnitude with d spacing respectively. During the design process, mutual phase coupling was included so that the pattern of radiation will not be weaken and experience an indigent match.

For a large array, having maximum array proximate to the broad side, the rise plane HPBW is approximately:

$$\theta_h = \sqrt{\frac{1}{\cos^2\theta_o\left[\Delta\theta_x^{-2}\cos^2\phi_o + \Delta\theta_y^{-2}\sin^2\phi_o\right]}} \tag{5.10}$$

(θ_o, ϕ_o) and $(\Delta\theta_x, \Delta\theta_y)$ the main-beam direction and HPBW of the linear broadside array having elements number *M*, *N* respectively. The amplitude distribution is equivalent to that of the x and y-axis linear arrays used for the designing the planar. The E and H-plane HPBW antenna pattern are 24.6^0 and 39.2^0 by simulation.

With the dimensions specify in section 5.2, MATLAB has been used to carry out the analysis as Figure (5.2) shows the three-dimensional shaded surface *z* directed antenna elements. In Figure 5.2, the three dimensional (3-D) contour surface plots for three (3) planes are created for the function values in matrix z-directed antenna element heights above a grid in the horizontal and vertical plane defined by the vertical and horizontal. The 3-D plot is defined

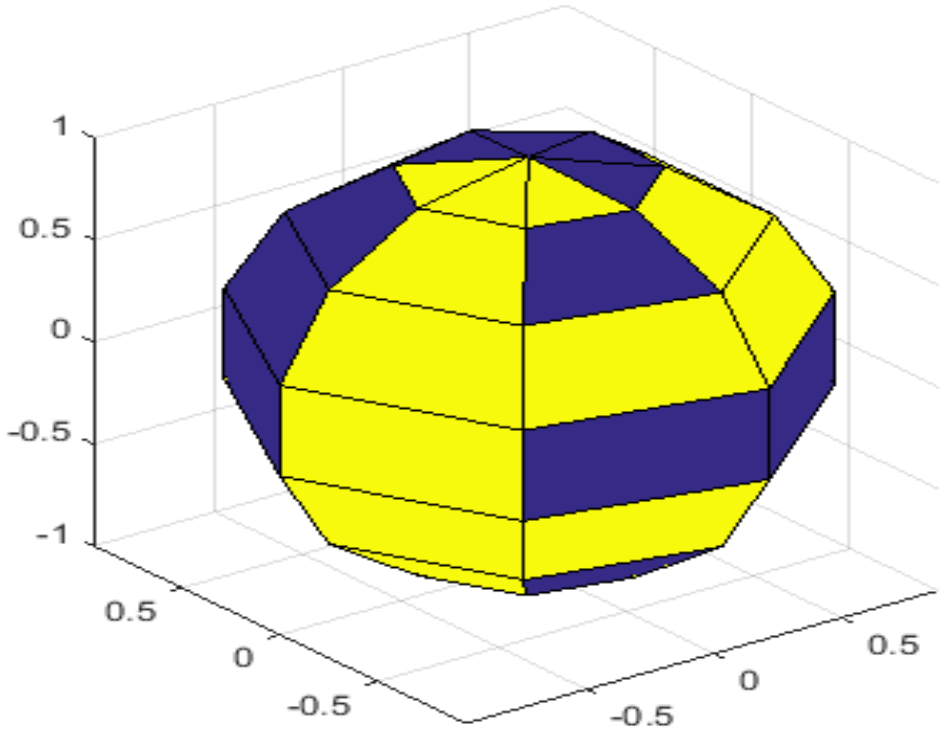

Figure 5.2. 3-D shaded surface plot of 8x8 planar array with contour plot of the z-directed antenna elements.

over a geometrically rectangular grid. The function uses z directed for the colour data as shown in Figure 5.2, which is also directly proportional to the height. The z is interpreted as heights with respect to the horizontal and vertical plane which is a single-valued function defined over a geometrically rectangular grid.

Figure 5.3 to Figure 5.5 shows the planar phased-array antenna configuration and its radiation pattern. The degree of accuracy azimuthally was loosed since the array is square arranged on a rectangular grid. Figure 5.3 shows the radiation pattern and the azimuth angle which shows the MATLAB simulation plot of the radiation pattern as a function of the angle measured off the z-axis for a fixed azimuth angle. Generally, when we increase the element spacing allows for better beamwidths (Figure 5.3), but when the element is greater than 0.5λ wavelength results in undesired grating lobes as it can be seen in Figure 5.3(c). Hence, the separation between feeding points vertically was optimized to avoid unnecessary grating lobes. The radiation pattern changes when the beam is not pointing horizontally.

The right hand side of Figure 5.3 shows the simulated polar plot radiation pattern consisting of lobes at various angles: (a) main lobe (lobe that shows the greatest field strength), sidelobes (unwanted radiation in undesired direction), and (b) back lobe (the sidelobe in the opposite direction of the main lobe). To achieve the objective of smart antenna, which is a directional antenna that emits the radio waves signal in one direction, the lobe in another direction is bigger nulls out the interference signal along the horizontal plane. This radiation pattern falls to zero Figure 5.3 (a) and (b). In Figure 5.3 (c), the element $d / \lambda = 1$ wavelength, that is why we experience grating lobes.

The effect of inter-spacing element can be felt on radiated power, in the sense that if same currents are applied to the number of antenna element N of an array. The utmost electric field strength of this array would be $N*E$. Where N is the number of antenna's element, while E is the electric field strength of the reference element. The power produced by these currents nevertheless fluctuates with the inter-element spacing as the power is determined by the electric field come across by the current. Deviation from the element spacing has an impact on the electric fields at the element positions and hence on the power produced by the array.

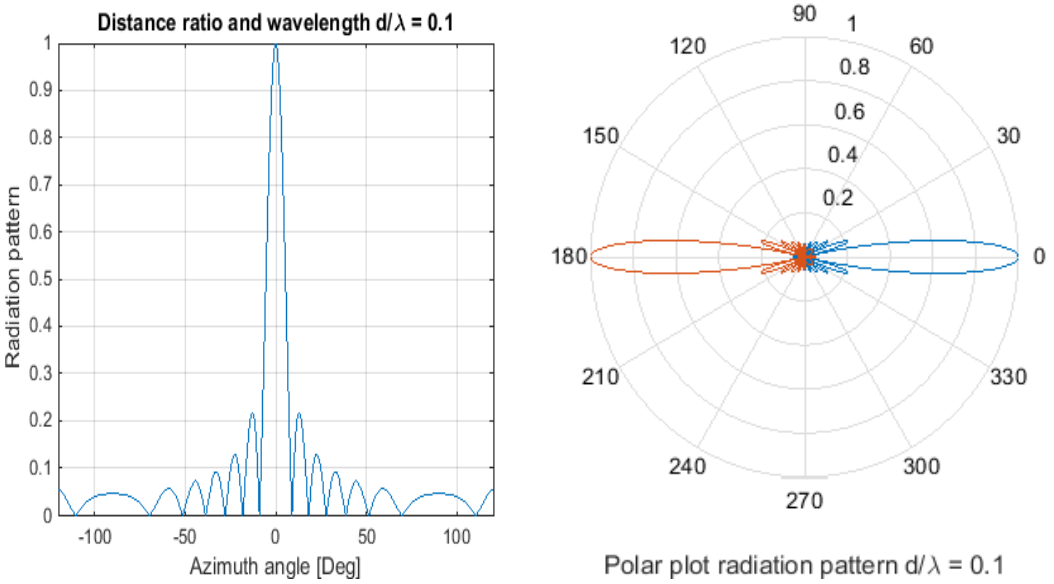

(a) For d/λ = 0.1

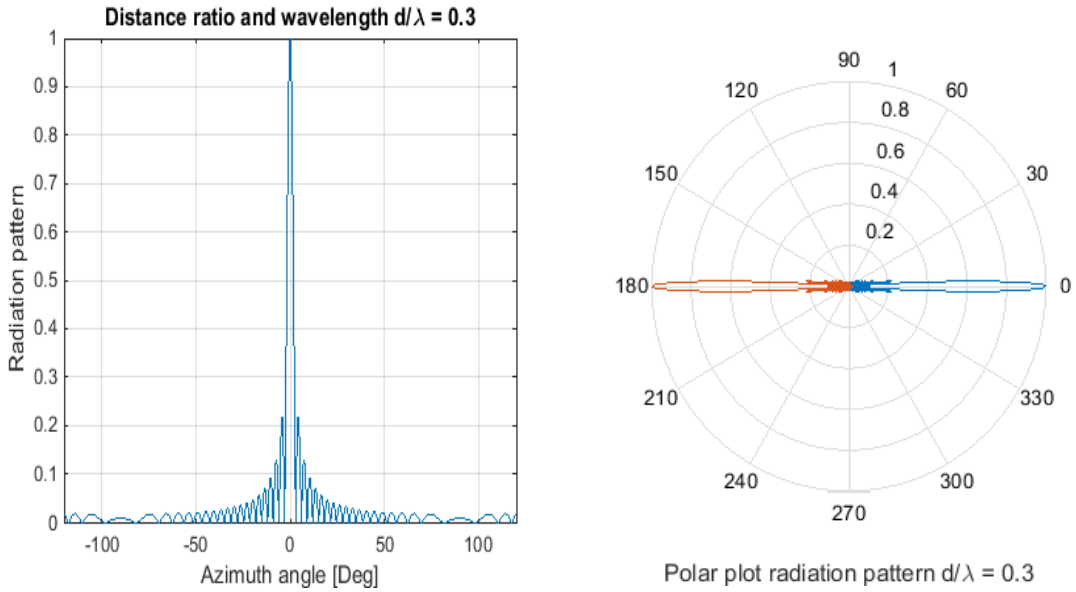

(b) For d/λ = 0.3

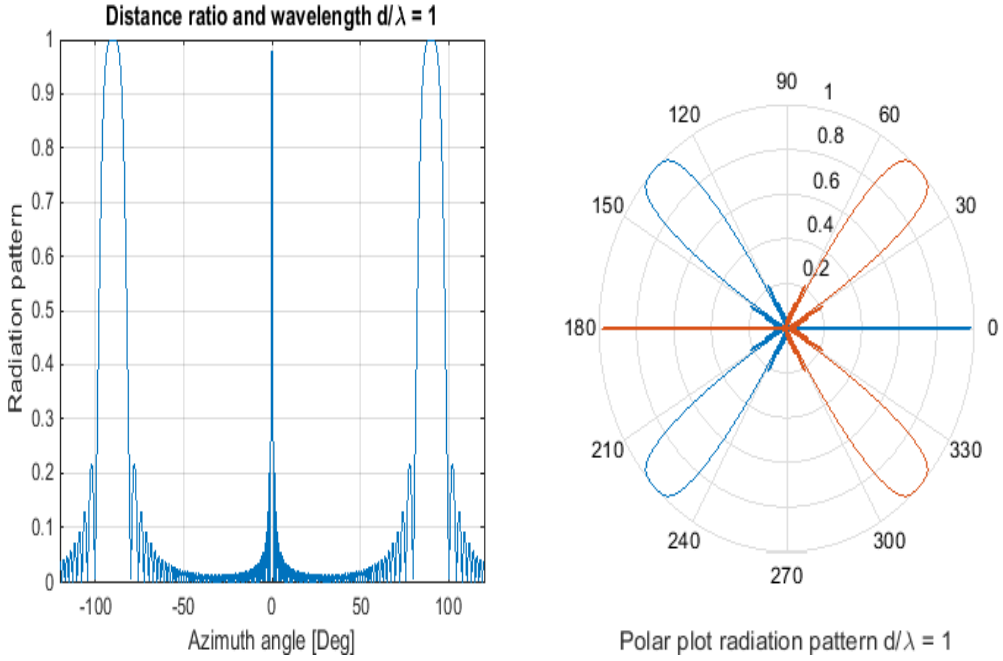

(c) For d/λ = 1

Figure 5.3. The inter element spacing and polar plot radiation pattern.

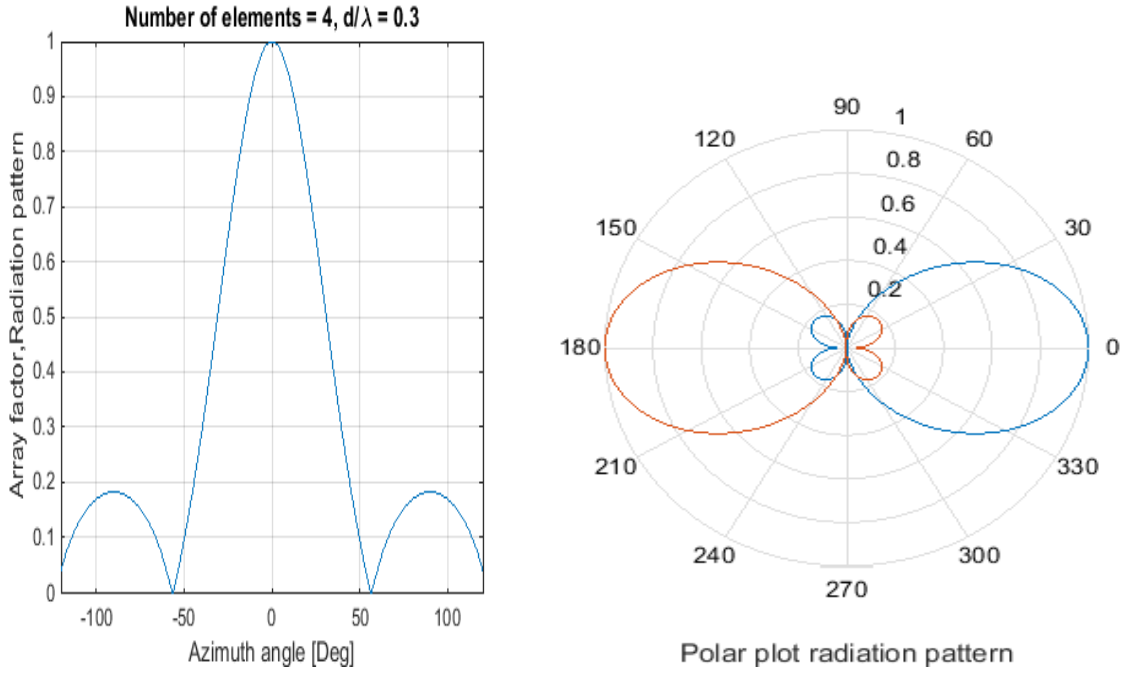

(a) for N=4 at d/λ=0.3

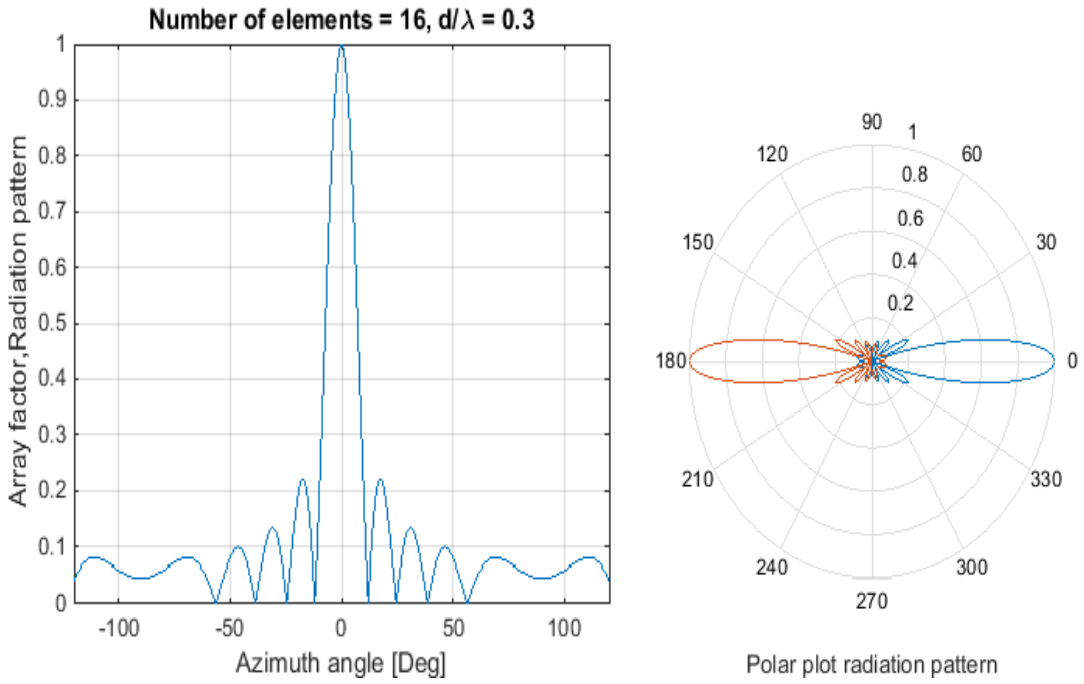

(b) for N=16 at d/λ=0.3

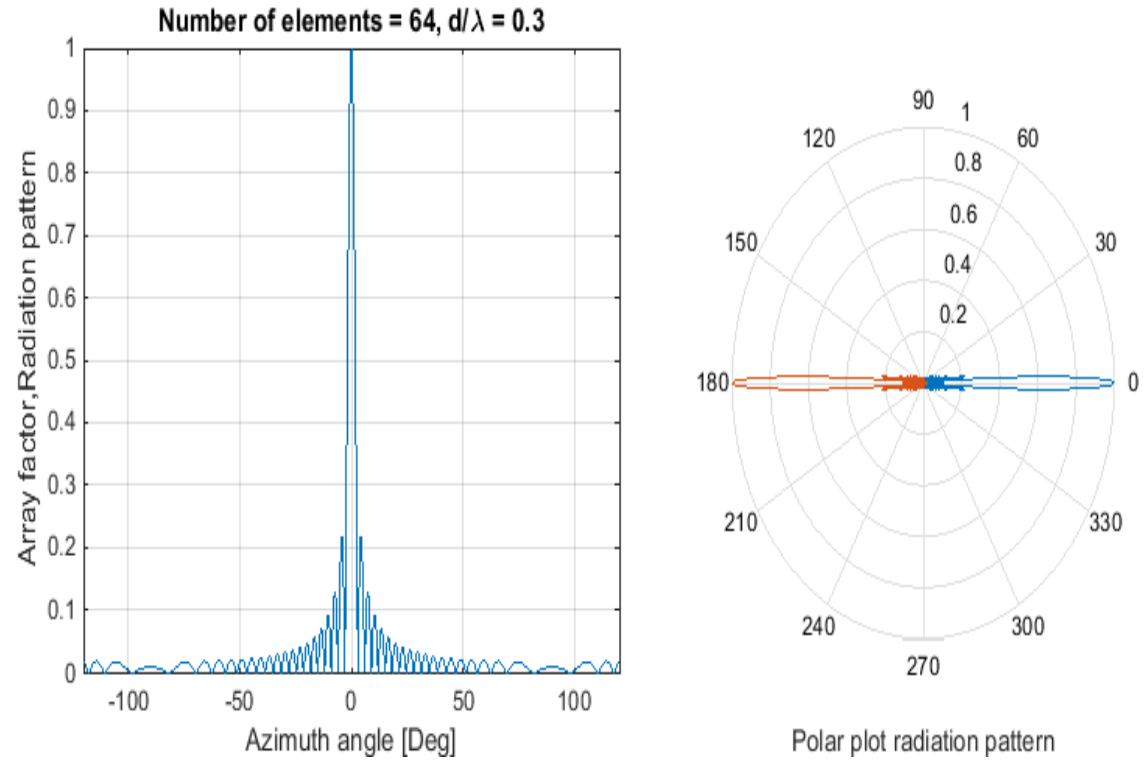

(c) for N=64 at d/λ=0.3

Figure 5.4. Simulation of number of elements and polar plot radiation.

Figure 5.4 shows the shows the simulated number of elements N and the polar radiation. As all antennas have directional characteristics, nevertheless they do not radiate power in the same way in all directions. These plots Figure 5.4 a-c, show a quick representation of the complete antenna response. On the other hand, radiation configurations can be confusing. Each antenna user has diverse criteria as well as plotting designs. Each organization has its own advantages and disadvantages. The array factor shown in Figure 5.5 consists of a set of *N* equal antenna components adapted to the same track. The signals originated from the elements in the

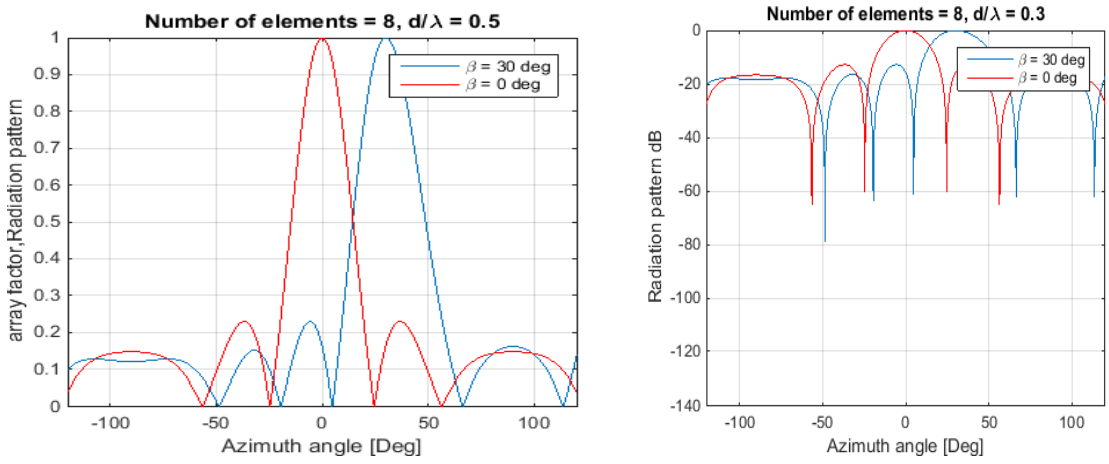

(a)

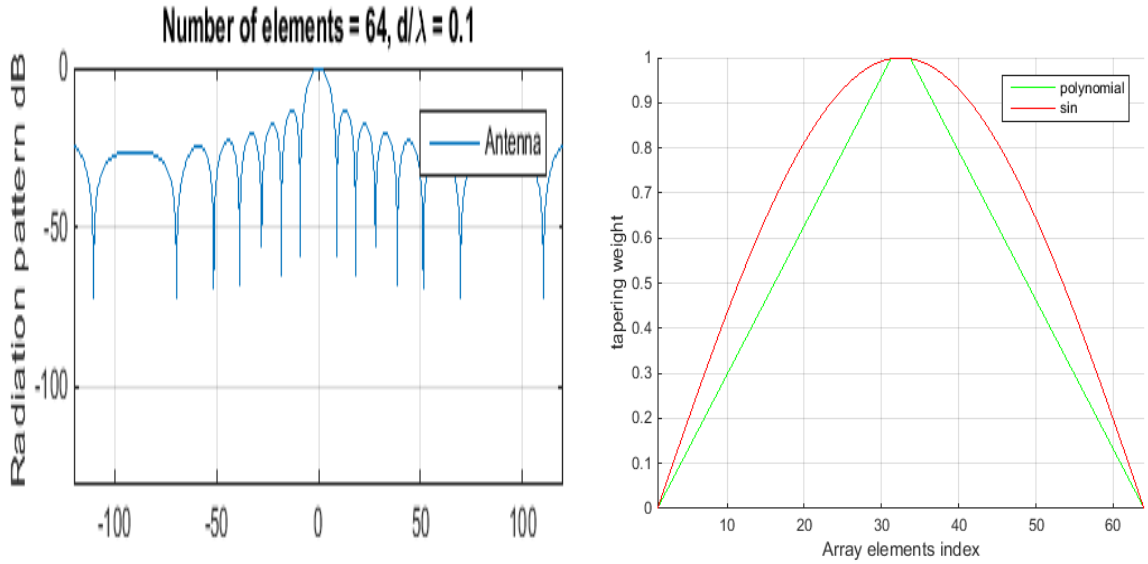

(b) (c)

Figure 5.5. Weighting Simulation (a) Simulation of array factor, radiation pattern versus azimuth angle, (b) Simulation of radiation pattern for N = 64, and (c) Simulation of the tapering weight and array index.

antenna array are multiplied by a complex weight and then added together to produce the phased array output. The array factor is a function of the points of the antennas in the array and the weights used, as it combines multiple antennas to permit for a greater flexibility in communicating with transmitting or receiving signals.

One of the advantages of a phased arrays associated with antenna element, is that the direction of the main beam can be automatically driven to a specific direction. This was realized by adapting the weights assigned to each element, also known as steering vector. Each weight is a complex number whose magnitude controls the sidelobe characteristics of the array and whose phase steers the beam. The simulated value is given by:

$$HPBW = I_n(\theta, \phi) = \sin^2 \theta \tag{5.11}$$

This is maximum at the element $N=8$ for $d / \lambda = 1$ wavelength that is Figure 5.5 (a). The highest point of $I_n = 1$ of the blue line is found at 30^0, the designed one is 39^0.

5.4. End-Fire Antenna Arrays for the Proposed Model

An end-fire array is a linear array having the peak of its main beam pointing in the same direction as the axis of the array [42]. The physical arrangement of end-fire array looks similar to that of the broad side array. The magnitude of currents in each element is same, but 180^0 out of phase between them (currents). This induction of energy differs in each element, which can be understood by the diagram shown in Figure 5.6.

Figure 5.6 and Figure 5.7 shows the arrangement of end-fire array in top and side views respectively. There is no radiation in the perpendicular directions to the array's plane because of cancellation. The first and third elements are fed out of phase and therefore cancel each other's radiation. Similarly, second and fourth are fed out of phase, to get cancelled. The usual dipole spacing are 0.2λ, 0.5λ, 1.0λ, and 1.5λ. This arrangement not only helps to avoid the radiation perpendicular to the antenna plane, but also helps the radiated energy get diverted to the direction of radiation of the full array. Hence, the minor lobes are avoided and the directivity is increased. The beam becomes narrower with the increased elements. If the spacing between the elements are very close to each other, then compactness of construction is feasible. Hence, an end-fire array is ideal when compared to other arrays when there is need for high gain or sharp directivity in a confined space.

For a four-dipole linear array with the element spacing *d=0.2λ, 0.5λ, 1.0λ*, and *1.5λ* (the offset in dB is set to zero). The dipole length always equals half-wavelength. The x-axis (the antenna axis) corresponds to the zero azimuthal angle.

The end-fire array of four-half-wavelength dipoles are considered at *0.2λ, 0.5λ, 1.0λ*, and *1.5λ*, and their polar plots are shown in Figure 5.8. It has been observed that the direction of the main lobe remain constant despite the fact that there are variation in spacing of the elements. The minor lobes are increasing while the main lobe becomes narrower as we increase the number elements. Hence, there is increase in directivity.

End-fire arrays has a uni-directional Radiation pattern. A major lobe occurs at one end, where maximum radiation is present, while the minor lobes represent the losses.

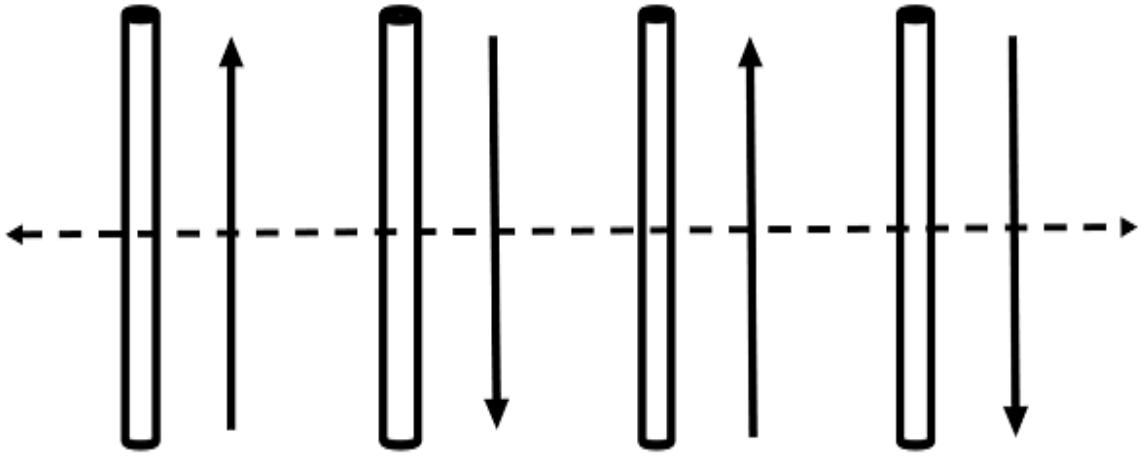

Figure 5.6. Top view of the dipole array.

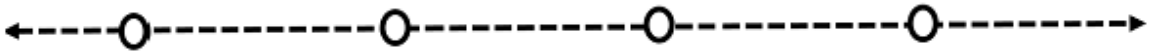

Figure 5.7. Dipole array side view.

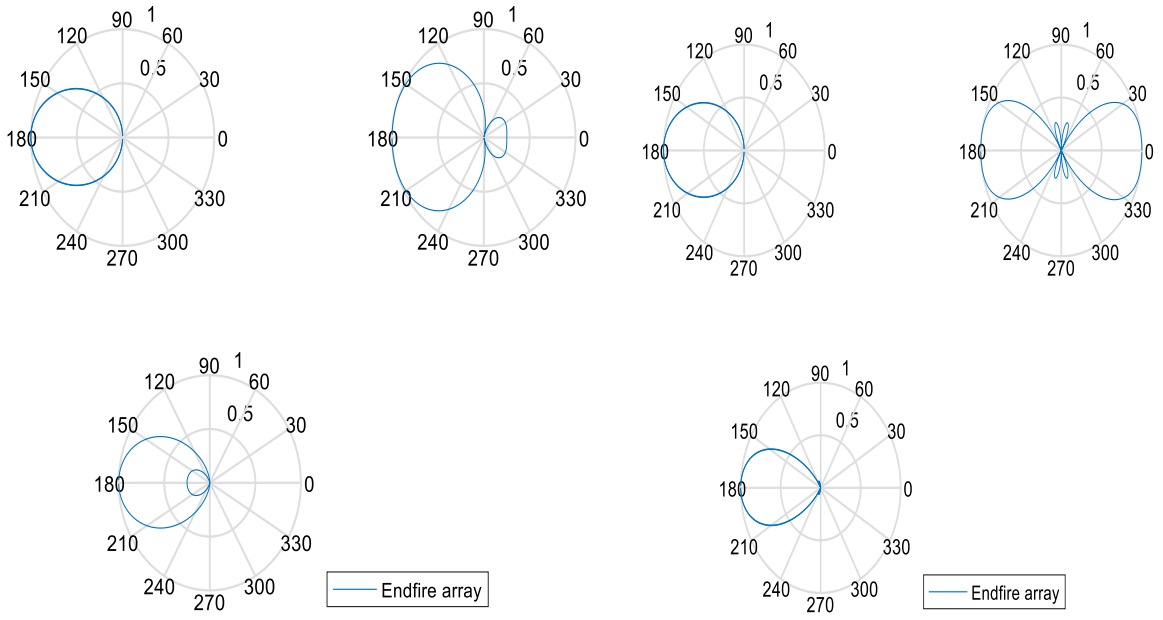

(a) d =0.2λ (b) d =0.5λ

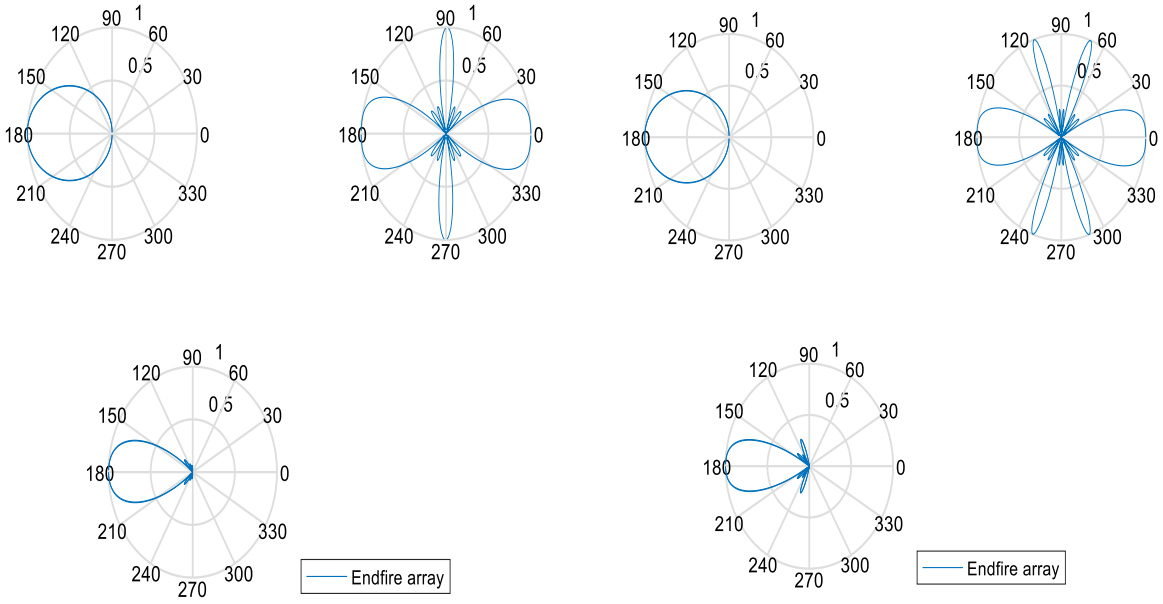

(c) d =1.0λ (d) d =1.5λ

Figure 5.8. Four elements end-fire array.

5.5. Broadside Linear Antenna Arrays for the Proposed Model

The most common mode of operation for a linear array is in the broadside mode. It is called a broadside array since the maximum radiation is broadside to the array geometry. As the array element spacing increases, the array physically is longer, thereby decreasing the main lobe width. The general rule for array radiation is that the main lobe width is inversely proportional to the array length [30]. The number of antenna elements have effects on the radiation pattern of broadside using half-wavelength dipole.

From Figure 5.9, there are grating lobes as the number of spacing between the elements is increasing i.e. $>\lambda/2$. Therefore, inter-element spacing should not exceed $\lambda/2$ so as to avoid the presence of grating lobes [147]. Practical antenna is often kept close to $\lambda/2$. For a beamforming applications, the relative displacements of $<\lambda/2$ is required.

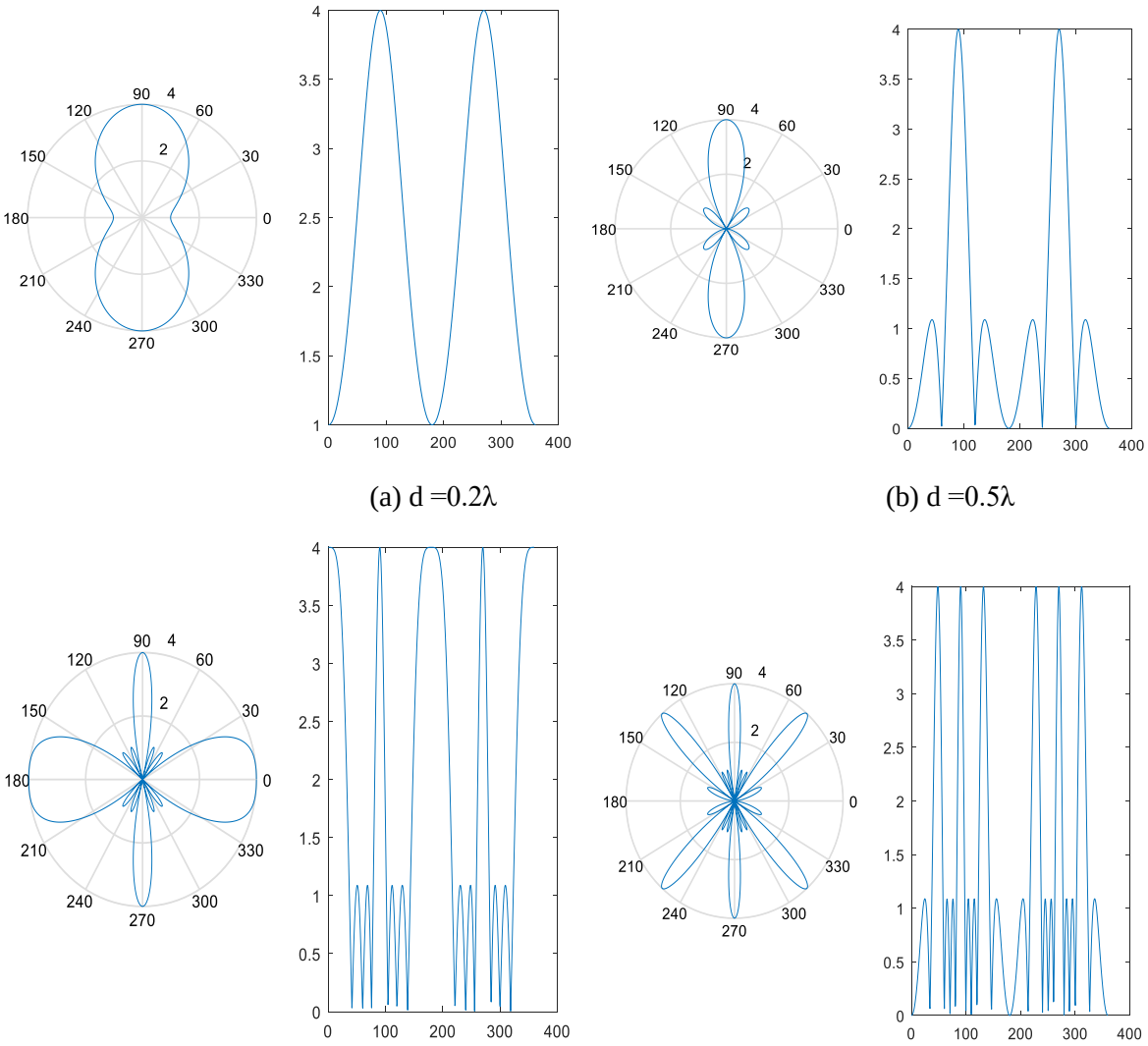

Figure 5.9. Four elements broadside antenna array with half-wavelength dipole antenna.

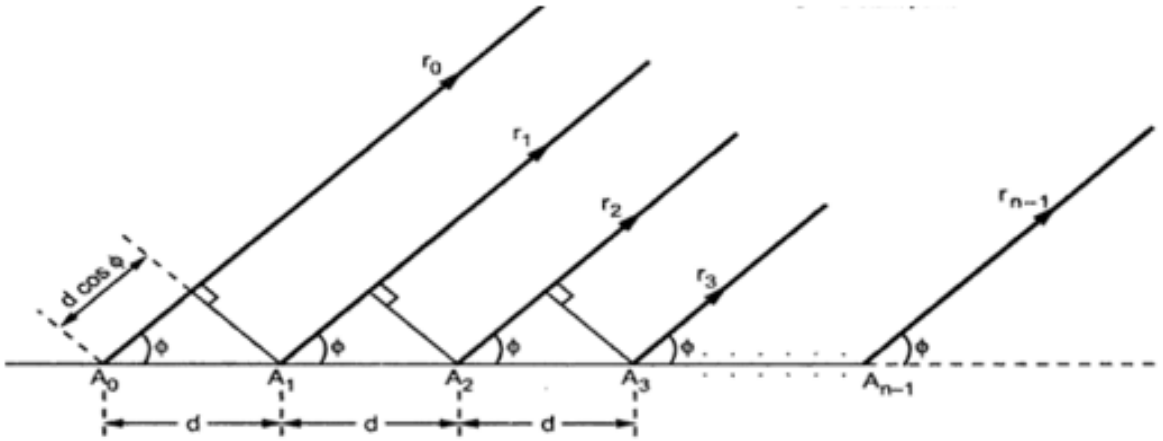

Figure 5.10. Broadside array with *n* identical radiators.

A broadside antenna arrays are arrays designed to radiate in a perpendicular direction to the array's axis direction. The maximum radiation direction is always orthogonal to the array's plane in accordance to the elements that lie on the plane. Broadside array is always in a ladder form and linear.

A broadside array is an arranged collinear antenna being made up of half-wave dipoles set apart from one another by one-half wavelengths. This antenna produces a highly directional radiation pattern that is perpendicular to the plane of the array. The broadside antenna is bidirectional in radiation, but the radiation pattern has a very narrow beam width and high gain.

$$\text{Path difference} = d\cos\phi$$

This path difference is normally written in wavelength form as,

$$\text{Path difference} = d/\lambda\cos\phi$$

From the optics, the phase angle is 2π times the path difference. Hence the phase angle is given by:

$$\text{Phase angle} = \varphi = 2\pi(\text{path difference})$$

$$\varphi = 2\pi\left(\frac{d}{\lambda}\cos\phi\right) rad$$

$$\therefore, \varphi = \left(\frac{2\pi}{\lambda}\right) d\cos\phi \qquad (5.12)$$

But phase shift = $\beta = 2\pi/\lambda$, so the Equation (5.12) becomes,

$$\varphi = \beta d\cos\phi$$

5.5.1 Properties of Broadside Array

(a) *Major Lobe*: In case of broadside array, the field is maximum in the direction normal to the axis of the array. Thus the condition for the maximum field at point P is given by:

$$\varphi = 0 \text{ i. e. } \beta d\cos\varphi = 0$$
$$\Rightarrow \cos\varphi = 0 \qquad (5.13)$$
$$\Rightarrow \phi = 90^0 \text{ or } 270^0$$

Thus $\phi = 90^0$ and $\phi = 270^0$ are called directions of principle maxima.

(b) *Magnitude of major lobe*: The maximum radiation occurs when $\varphi = 0$. Hence we can write:

$$|\text{Major lobe}| = \left|\frac{E_T}{E_o}\right| = \lim_{\varphi \to 0}\left\{\frac{\frac{d}{d\varphi}\left(\sin n\frac{\varphi}{2}\right)}{\frac{d}{d\varphi}\left(\sin\frac{\varphi}{2}\right)}\right\}$$
$$= \lim_{\varphi \to 0}\left\{\frac{\cos n\frac{\varphi}{2}\left(n\frac{\varphi}{2}\right)}{\left(\cos\frac{\varphi}{2}\right)\left(\frac{\varphi}{2}\right)}\right\}$$
$$|\text{Major lobe}| = n$$

where, n is the number of elements in the array.

Thus from $\phi = 90^0$ or 270^0 and |Major lobe| = n, it is clear that all the field components add up together to give total field which is 'n' times the individual field when $\phi = 90^0$ or 270^0.

(c) *Nulls*: The ratio of total electric field to an individual electric field is given by:

$$\left|\frac{E_T}{E_o}\right| = \frac{\sin n\frac{\varphi}{2}}{\sin\frac{\varphi}{2}}$$

The find direction of minima, equating ratio of magnitudes of the fields to zero.

$$\left|\frac{E_T}{E_o}\right| = \frac{\sin n\frac{\varphi}{2}}{\sin\frac{\varphi}{2}} = 0$$

Thus condition of minima is given by:

For $\varphi = 360^0$

$$\sin n\frac{\varphi}{2} = 0;$$

and when $\varphi = 180^0$,

$$\sin n\frac{\varphi}{2} \neq 0$$

Hence we can write:

$$\sin n\frac{\varphi}{2} = 0$$

i.e. $n\varphi/2 = \sin^{-1}(0) = \pm m\pi$, where m = 1, 2, 3, …

Now $\varphi = \beta d\cos\phi = 2\pi/\lambda(d)\cos\phi$

$$Therefore \frac{n}{2}\left(\frac{2\pi}{\lambda}d\right)\cos\phi_{\min} = \pm m\pi$$

$$i.e. \frac{nd}{2\lambda}\cos\phi_{\min} = \pm m$$

$$\phi_{\min}\cos^{-1}\left(\pm\frac{m\lambda}{nd}\right) \qquad (5.14)$$

where *n* is number of elements in array, d is the spacing between elements in meter, λ is the wavelength in meter, and m is the constant = 1, 2, 3, …Thus Equation (5.14) gives the direction of nulls

(d) *Subsidiary Maxima (or sidelobes):* The directions of the subsidiary maxima or sidelobes can be obtained if $\sin\left(n\frac{\varphi}{2}\right) = \pm 1$

$$In\left|\frac{E_T}{E_o}\right| = \frac{\sin n\frac{\varphi}{2}}{\sin\frac{\varphi}{2}}$$

Therefore $n\frac{\varphi}{2} = \pm\frac{3\pi}{2}, \pm\frac{5\pi}{2}, \pm\frac{7\pi}{2}, \text{L}$

Hence $\sin\left(n\frac{\varphi}{2}\right) = \pm 1$ is not considered. Because if $n\frac{\varphi}{2} = \frac{\pi}{2}$, then $\sin n\frac{\varphi}{2} = 1$ which is the direction of principle maxima Hence we can skip $n\frac{\varphi}{2} = \pm\frac{\pi}{2}$ value. Thus, we get:

$$\varphi = \pm\frac{3\pi}{n}, \pm\frac{5\pi}{n}, \pm\frac{7\pi}{n}, \text{L}$$

Now $\varphi = \beta d\cos\phi = (2\pi/\lambda)d\cos\phi$, Hence equation for φ can be written as:

$$\left(\frac{2\pi}{\lambda}\right)d\cos\phi = \pm\frac{3\pi}{n}, \pm\frac{5\pi}{n}, \pm\frac{7\pi}{n}, \text{L}$$

$$\therefore \cos\phi = \frac{\lambda}{2\pi d}\left[\pm\frac{(2m+1)}{n}\pi\right] \text{ where m = 1, 2, 3, …}$$

$$\therefore \phi = \cos^{-1}\left[\pm\frac{(2m+1)}{2\pi d}\right] \tag{5.15}$$

The Equation (5.15) represents the directions where certain radiation which is not maximum. Hence it represent directions of subsidiary maxima or sidelobes.

(e) *Beamwidth of major lobe*: The beamwidth is the angle equal to twice the angle between first null and the major lobe maximum direction. Hence the beamwidth between first nulls is given by: Beamwidth between first null (BWFN) = 2 x γ, where γ = 90^0-ϕ, But $\phi_{\min} = \cos^{-1}\left(\pm\frac{m\lambda}{nd}\right)$ where m = 1, 2, 3, …, Also 90^0-$\phi_{\min}$ = γ i. e. 90^0-γ = $\phi_{\min,}$ Hence

$$90^0 - \gamma = \cos^{-1}\left(\pm\frac{m\lambda}{nd}\right)$$

Taking cosine of angle on both sides, we get,

$$\cos\left(90^0 - \gamma\right) = \cos^{-1}\left(\pm\frac{m\lambda}{nd}\right)$$

$$\therefore \sin\gamma = \pm\frac{m\lambda}{nd} \tag{5.16}$$

If γ is very small, then sinγ can be substituted as γ in Equation (5.16). We get,

$$\gamma = \pm\frac{m\lambda}{nd} \tag{5.17}$$

For the first null, i.e. m =1,

$$\gamma = \pm\frac{\lambda}{nd}$$

$$\therefore BWFN = 2\gamma = \frac{2\lambda}{nd}$$

But $nd \approx (n-1)d$ if n is very large. This *nxd* indicates the total length of array in meter. This is denoted by *L*.

$$BWFN = \frac{2\lambda}{L} rad = \frac{2}{\left(\frac{L}{\lambda}\right)} rad \tag{5.18}$$

Converting BWFN in degrees, we can write:

$$BWFN = \frac{114.6\lambda}{L} = \frac{114.6}{\left(\frac{L}{\lambda}\right)} \deg rees \tag{5.19}$$

Now the half power beam width (HPBW) is given by,

$$HPBW = \frac{BWFN}{2} = \frac{1}{\left(\frac{L}{\lambda}\right)} rad$$

Expressing HPBW in degrees we can write:

$$HPBW = \frac{57.3}{\left(\frac{L}{\lambda}\right)} \deg rees$$

(f) *Directivity*: The directivity in case of broadside array is defined as,

$$G_{Dmax} = \frac{\text{Maximum radiation intensity}}{\text{Average radiation intensity}} = \frac{U_{max}}{U_{avg}} = \frac{U_{max}}{U_o} \tag{5.20}$$

Where, U_o is average radiation intensity which is given by,

$$U_o = \frac{P_{rad}}{4\pi} = \frac{1}{4\pi} \int_{\phi=0}^{2\pi} \int_{\theta=0}^{\pi} \left|E(\theta,\phi)\right|^2 \sin\theta d\theta d\phi \tag{5.21}$$

From the expression of ratio of magnitudes we can write:

$$\left|\frac{E_T}{E_o}\right| = n$$

or

$$\left|E_T\right| = n\left|E_o\right|$$

for the normalized condition, let us assume $E_o = 1$, then $|E_T| = n$, Thus field from array is maximum in any direction of θ when $\varphi = 0$, hence normalized field pattern is given by:

$$E_{Normalized} = \left|\frac{E_T}{E_{T\max}}\right| = \frac{1}{n}\left|\frac{E_o}{E_o}\right| = \frac{1}{n}$$

Hence the field is given by:

$$\therefore E_{Normalized} = \frac{\sin n\frac{\varphi}{2}}{n\left(\sin\frac{\varphi}{2}\right)}$$

where $\varphi = \beta d\cos\phi$. The Equation (5.20) indicates array factor, hence we can write, the electric field due to n arrays as:

$$E = \frac{1}{n}\left[\frac{\sin\frac{n\beta d\cos\phi}{2}}{\sin\frac{\beta d\cos\phi}{2}}\right]$$

Assuming *d* very small as compared to length of array, we can approximate

$$\sin\frac{\beta d\cos\phi}{2} \approx \frac{\beta d\cos\phi}{2}$$

Then:

$$E = \frac{1}{n}\left[\frac{\sin\frac{n\beta\cos\phi}{2}}{\sin\frac{\beta\cos\phi}{2}}\right]$$

Substituting value of E in Equation (5.21), we get,

$$U_o = \frac{1}{4\pi}\int_{\phi=0}^{2\pi}\int_{\theta=0}^{\pi}\left[\frac{\sin\frac{n\beta d\cos\phi}{2}}{\sin\frac{\beta d\cos\phi}{2}}\right]^2 \sin\theta d\theta d\phi$$

$$= \frac{1}{4\pi}\int_{\phi=0}^{2\pi} d\phi.\int_{\theta=0}^{\pi}\left[\frac{\sin\frac{n\beta d\cos\phi}{2}}{\frac{n}{2}\beta d\cos\phi}\right]^2 \sin\theta d\theta$$

$$= \frac{1}{4\pi}[2\pi].\int_{\theta=0}^{\pi}\left[\frac{\sin z}{z}\right]^2 \sin\theta d\theta$$

Let z = n/2βdcosθ

$$\therefore dz = -\frac{n}{2}\beta d\sin\theta d\theta$$

$$\therefore n\sin\theta d\theta = -\frac{dz}{\frac{n}{2}\beta d}$$

$$\therefore \text{n}\sin\theta\text{d}\theta = -\frac{\text{dz}}{\frac{\text{n}}{2}\beta\text{d}}$$

Also when θ = π, z = -n/2βd, and when θ = 0, z = ±n/2βd

Rewriting above equation we get:

$$U_o = \frac{1}{2}\int_{+\frac{n}{2}\beta d}^{-\frac{n}{2}\beta d}\left[\frac{\sin z}{z}\right]^2 .\frac{dz}{-\frac{n}{2}\beta d}$$

$$\therefore U_o = -\frac{1}{n\beta d}\int_{+\frac{n}{2}\beta d}^{-\frac{n}{2}\beta d}\left[\frac{\sin z}{z}\right]^2 dz$$

For large array, n is large hence nβd is also very large (assuming tending to ∞). Hence rewriting above equation:

$$U_o = -\frac{1}{n\beta d}\int_{+\infty}^{-\infty}\left[\frac{\sin z}{z}\right]^2 dz$$

Interchanging limits of integration, we get:

$$U_o = +\frac{1}{n\beta d}\int_{-\infty}^{\infty}\left[\frac{\sin z}{z}\right]^2 dz$$

By integration formula:

$$\int_{-\infty}^{\infty}\left[\frac{\sin z}{z}\right]^2 dz = \pi$$

Thus using this property in above equation we can write:

$$U_o = \frac{1}{n\beta d}\pi = \frac{\pi}{n\beta d} \tag{5.22}$$

From Equation (5.20), the directivity is given by:

$$G_{D\max} = \frac{U_{\max}}{U_o}$$

But $U_{max} = 1$ at $\phi = 90^0$ and substituting value of U_o from Equation (5.22), we get:

$$G_{D\max} = \frac{1}{\left(\frac{\pi}{n\beta d}\right)} = \frac{n\beta d}{\pi}$$

$$\beta = \frac{2\pi}{\lambda}$$

$$G_{D\max} = \frac{n(2\pi)d}{\pi}$$

hence,

$$G_{D\max} = \frac{2nd}{\lambda} = 2n\left(\frac{d}{\lambda}\right)$$

The total length of the array is given by: L = (n-1)d≈nd, if n is very large. Hence the directivity can be written in total length form of the array as:

$$G_{D\max} = 2\left(\frac{L}{\lambda}\right)$$

5.5.2 Directivity control

Large antennas are problematic during fabrication and difficult to manoeuvre because of their large structures, but are directional in relative to a wavelength. An additional problem is that the antennas rarely offer as much freedom as we would like in shaping the precise parameters of the radiation patterns, for instance their directivity and side-lobe characteristics.

An attractive way around these limitations is to design arrays of small, simple elements, such as dipoles. By locating and feeding respective element correctly, large directivities could be achieved, despite when the radiation pattern of each element (alone) is relatively poor. Furthermore one can change the direction of maximum radiation by changing the phases of the feed voltages (electronic beam steering). The beam-steering mechanism (scanning array) [80].

Three major factors must be considered when controlling the directivity of an antenna arrays: (a) geometry, (b) phase factor, and (c) number of array elements. Consequently, broadside and end-fire arrays can be controlled either by element spacing or by relative phases of the fed voltages. Broadside arrays generate their maximum radiation perpendicular to the array axis. On the contrary, an end-fire array directs its main lobe along the array axis [80].

5.6. Conclusions

The consideration of smart antenna system using an *8 x 8* planar phased-array antenna offers the synthesis of a needed beam pattern which is not obtainable with a single patch antenna element. In this research work, a high performance planar phased-array antenna has been designed using an *8 x 8* square grid of z-controlled antenna monopoles with a length of *0.482λ*. The considered element spacing is *0.315λ* and the average directivity of *22.0 dBi*. Using a planar phased array antenna yields various, concurrent readily obtainable beams. These beams can have high gain directivity, optimum side lobe suppression, and beam width controlled. Planar phased array antenna can automatically adjust the array pattern to optimize some typical features of the received signal i.e. phases and amplitudes. These multiple beams formed by planar array antenna are steered by means of electronic control.

CHAPTER 6

Spatial Signal Processing and Adaptive Beamforming Algorithms for Smart Antenna Arrays

The effective design of smart antennas is normally determined by the selection and performances of the adaptive beamforming algorithms used for radiation diagram adaptation and adjustment to the specific scenario of incoming signals dynamically. Spatial filtering of desired signals and provision of higher Signal to Interference plus Noise Ratio (SINR) in smart antenna arrays are necessary in order to achieve improvements of the transmission quality and the wireless communication systems capacity [60]. Three types of beamforming algorithms are:

(a) Estimation of Angle Of Arrival (AOA) algorithms (MUSIC and ESPRIT),

(b) Blind algorithm, and

(c) Non-blind algorithms (maximum likelihood and minimum variance distortionless response).

6.1 Spatial Signal Processing for the Smart Antenna Arrays

To realize smart antennas necessity with wide-band in wireless communication systems, three main approaches are fundamental, (a) space-time signal processing, (b) spatial-frequency signal processing (filtering of signals that overlay with noise in space and frequency), and (c) spatial signal processing (beamforming).

Using a spatial signal processing, the signals received are first converted to base band and then sampled. One of the advantages of spatial signal processing is that wideband beamforming can be successfully performed without tapped-delay lines or frequency filters. This can also be referred as wideband spatial beamformer.

6.1.1 Introduction of Smart Antenna

Figure 6.1 consists of an array of antenna elements (N). The output $y(t)$ is a summation of multiplication of signals from each antenna elements and the complex weight.

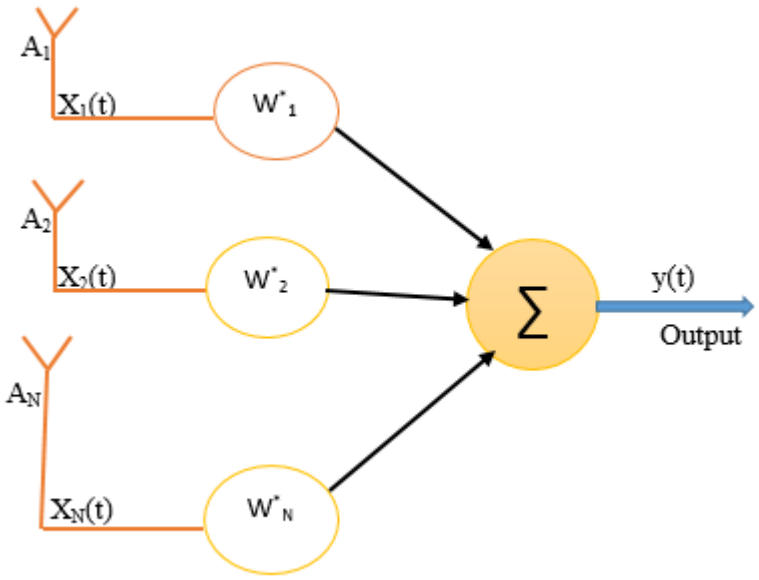

Figure 6.1. Antenna array system.

The output *y(t)* in Figure 6.1 is written as [46, 55, 132]

$$y(t) = \sum_{i=1}^{N} w_1^* x_1(t) \tag{6.1}$$

where * represents the complex conjugate and used to solve mathematical symbols in Equation (6.1). The weights of systems array can be represented using a vector sign and written as:

$$w = \left[w_1, w_2, \mathrm{K}\, , w_N \right]^T \tag{6.2}$$

Superscript *T* represents the transpose operator [103]. The signals on the elements are expressed as [148]:

$$x(t) = \left[x_1(t), x_2(t), \mathrm{K}\, , x_N(t) \right]^T \tag{6.3}$$

Adaptive array processing output of the system is [90, 92, 103]:

$$\mathrm{y(t)} = \mathbf{w}^{\mathrm{H}}\mathbf{x}(\mathrm{t}) \tag{6.4}$$

minimize output power dependent on look-direction control [129]:

$$\mu = \mathbf{w}^{\mathrm{H}}\mathrm{c(t)}$$

The output power of the array at any time *t* can be expressed as the square of magnitude of the array output, i.e.,

$$\mathrm{P(t)} = \left|\mathrm{y(t)}\right|^2 \tag{6.5}$$

$$= \mathrm{y(t)y^*(t)}$$

P(t) can be written as Equation (6.6) if y(t) is substituted in Equation (6.4):

$$P(t) = w^H x(t) x^H(t) w \tag{6.6}$$

Modelling of vector **x**(t) equal to summation of vector entries as zero, the mean output power for a specified **w** of the system array is achieved by taking conditional expected value of **x**(t)

$$\begin{aligned} P(w) &= E\left[w^H x(t) x^H(t) w \right] \\ &= w^H E\left[x(t) x^H(t) \right] w \\ &= w^H R w \end{aligned} \tag{6.7}$$

Assuming we have a wanted signal in the presence of unwanted interference and random noise, we can write xS(t), xI(t), and n(t) as the signal vector due to the desired signal source, unwanted interference, and random noise, while yS(t), yI(t), and yn(t) represents the output components of signal, interference, and random noise.

The inner product of the weight vector with xS(t), xI(t), and n(t) can be expressed as:

$$y_s(t) = \mathbf{W}^H X_s(t) \tag{6.8}$$

$$y_I(t) = \mathbf{W}^H X_I(t) \tag{6.9}$$

$$y_n(t) = \mathbf{W}^H \mathbf{n}(t) \tag{6.10}$$

The array correlation matrix as a result of the signal source is expressed in Equation (6.11), while that of the unwanted interference signal is written as Equation (6.12), and the array correlation matrix for the random noise can be expressed as Equation (6.13) respectively:

$$R_s = E\left[x_s(t) x_s^H(t) \right] \tag{6.11}$$

$$R_1 = E\left[x_1(t) x_1^H(t) \right] \tag{6.12}$$

$$R_n = E\left[\mathbf{n}(t) \mathbf{n}^H(t) \right] \tag{6.13}$$

From Equation (6.7), the mean output power P_s, P_I and P_n for the signal source, unwanted interference, and random noise, can be expressed as:

$$P_s = \mathbf{W}^H R_s \mathbf{W} \tag{6.14}$$

$$P_I = \mathbf{W}^H R_I \mathbf{W} \tag{6.15}$$

$$P_n = \mathbf{W}^H R_n \mathbf{W} \tag{6.16}$$

From Equation (6.15) and (6.16), we have:

$$P_N = \mathbf{w}^H R_I \mathbf{w} + \mathbf{w}^H R_n \mathbf{w} \tag{6.17}$$

$$= \mathbf{w}^{H}(R_I + R_n)w \tag{6.18}$$

where P_N represents the mean output power noise of the system array and noise array correlation matrix

$$R_N = R_1 + R_n \tag{6.19}$$

where R_N represents the noise array correlation matrix.

From Equation (6.18), P_N can be written as Equation (6.20) in terms of R_n

$$P_N = \mathbf{w}^{H}R_n w \tag{6.20}$$

The ratio of (P_s) to (P_N) at the output of the array system is called signal to noise ratio (SNR), and is written as,

$$SNR = \frac{p_s}{p_N} \tag{6.21}$$

From Equation (6.14) and (6.17), we have:

$$SNR = \frac{\mathbf{w}^{H}R_s w}{\mathbf{w}^{H}R_n w} \tag{6.22}$$

6.1.2 Preliminaries of the mathematical signal processing array model

Assuming a uniform linear antenna array system of *N* units having an omni-directional antenna elements with half wavelength distance. The mathematical expression of the received signal by this narrowband antenna element array at any time *k* is [36, 149]:

$$z_n(k) = x_n(k) + j(k) + q_n(k)$$

$$= (k)\left[x_n + j + q_n\right] \tag{6.23}$$

where $x_n(k)$ represents the *Nx1* signal vector, $j(k)$ denotes the *Nx1* interference signal's vector, and $q_n(k)$ represents the noise vector output of the array. The received signals in vector form can be represented as:

$$z_n(k) = \left[z_{n11} \ldots z_{n1L}(k) \ldots z_{nN1}(k) \ldots z_{nNL}(k)\right]^{T}$$

If the required signal, interference and noise are statistically independent, then the desired signal can be expressed as [36]:

$$\mathbf{Z_n}(k) = Z_n(k)\mathbf{a}_s \tag{6.24}$$

where $z(k)$ is the preferred received signal waveform, $\boldsymbol{a}_s$ is the steering vector connected to the spatial signature and if substituted in Equation (6.23), it becomes the oriented vector. The beamformer output for the narrowband is written as [36]:

$$z(k) = \mathbf{K}^{H}\mathbf{N}(k) \tag{6.25}$$

The beamforming algorithm for the weight vector *(K)* is $(k_1, k_2, \ldots, k_x)^T$, where *k*, $(.)^H$, and *k(t)* are the *Kx1* beamformer complex weight vector of the array, the Hermitian transpose, and the *kx1* array shot vector respectively. The signal output for the SINR beamforming problem is [36]:

$$\text{SINR} = \frac{\text{P}}{\text{N}+1} \tag{6.26}$$

where *P, N and I* are the array output signal power, noise power output of the array signal, and the interference power, respectively.

The fundamental issue is the interference (*I*), taken at a point source $x \in \mathbb{R}^k$ expressed as [36]:

$$I(x) = \sum_{y \in \tau} p_y h_y \mathrm{l}(\|x - y\|) \tag{6.27}$$

where $\tau \subset \Re^k \Rightarrow$ set of all receiving signals, p_y is the power received by the signal *y*, h_y is the fading coefficient of the signal power, and l the path loss function. We assumed $\|x - y\|$ to depend on the distance from the antenna element y to another point of antenna element x. Therefore,

$$\text{SNR} = \frac{\text{w}^{\text{H}}\text{R}_{\text{s}}\text{w}}{\text{w}^{\text{H}}\text{R}_{\text{i+n}}\text{w} + \text{I}} \tag{6.28}$$

Hence, SNR

$$= \frac{\text{w}^{\text{H}}\text{E}\left\{\text{x(k)s}^{\text{H}}\text{(k)}\right\}\text{w}}{\text{w}^{\text{H}}\text{E}\left\{\varepsilon\right\}\text{w} + \text{I(x)}} \tag{6.29}$$

Hence,

$$\text{SNR} = \frac{w^H E\left\{x(k)s^H(k)\right\}w}{w^H E\left\{(j(k)+n(k))(j(k)+n(k))^H\right\}w + \sum_{y \in \tau} p_y h_y \mathrm{l}\left(\|x-y\|\right)} \tag{6.30}$$

$E\{x(k)x^H(k)\}$, and $E(\varepsilon)$ are the desired signal, while $\sum_{y \in \tau} p_y h_y \mathrm{l}\left(\|x-y\|\right)$, is the fundamental issue of the interference power taken into consideration for this work, respectively, $E\{\bullet\}$ is the statistical expectation [7, 103, 148, 149]. Considering an extensive wireless system, τ , h_y, and P_y are the unknowns. The interfering signal points and the path loss can control the interference to the first order. The covariance matrix of the corresponding desired signal in Equation (6.28), can be of an arbitrary rank as shown in reference, i.e. $1 \leq rank\{R_s\} \leq M$. $rank\{R_s\} > 1$ for signals that have randomly fluctuating wavefronts. This might occur frequently in wireless communications. For a point source signal, $R_s = 1$. From Equation

(6.28), R_{i+n} is known as the interference plus noise covariance matrix. The substitution of R_{i+n} using the covariance matrix for the data sample as in [36, 149].

$$\hat{z} = \frac{1}{n}\sum_{i=1}^{n} y_i(x)y_i^H(x) \tag{6.31}$$

where *n* in Equation (6.31) is the number of samples of training data.

6.1.3 Array Signal Processing Model

Consider a plane wave signal for random antenna array as in Figure 6.2 receives signal in the direction $-\hat{s}_r(\theta,\phi)$, the analytical signal of the plane wave signal is:

$$x(t) = y(t)e^{j\omega t} \tag{6.32}$$

where *x(t)* is the signal along the plane wave, *y(t)* is the signal along the base-band or the real signal, and ω is the frequency carrier, and *t* is the measured time respectively. q_1, q_2, q_i, and q_m are the antenna elements in Figure 6.2. Taking the real part of the analytical signal, the real signal r(t) is written as:

$$r(t) = \mathrm{Re}\{x(t)\} = y(t)\cos(\omega t) \tag{6.33}$$

The mathematical correlation between the Phasor-form signal b(t) and the analytical signal a(t) can be written as: $x(t) = Xe^{j\omega t} \Rightarrow X = y(t)$. The power of r(t) is $r(t) - \frac{1}{2}|z(t)|^2$

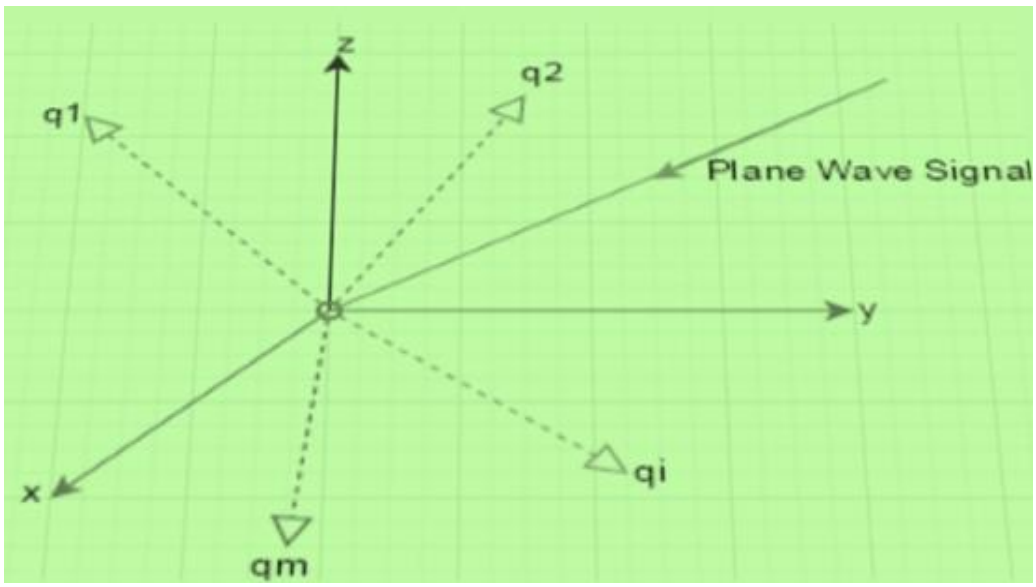

Figure 6.2. System coordinate signal for the random antenna array.

The phasor-form signal for the r(t) can be expressed as:

$$\frac{1}{2}\mathrm{E}\{\mathrm{s(t)s^*(t)}\} = \frac{1}{2}\mathrm{SS^*}$$

The Phasor-form signal "s is a function of (*x, y, z*) and *t"* and also a complex quantity. Mathematically,

S = s(x, y, z) and s = s(t).

Characterization of antenna element's time domain can be normalized by the impulse response. Fast transient pulses are responsible for antenna-excitation in time domain systems. Firstly, we have considered the impulse and frequency response of the system. The impulse response and *k(t)* relates the antenna elements to the plane wave signal *z(t).* The input to the system is *z(t*), while the antenna elements act as the output *q(t).* From the convolution integral,

$$q(t) = \int_{-\infty}^{+\infty} k(\tau)z(t-\tau)d\tau \tag{6.34}$$

Using the convolution operator $\otimes$, Equation (6.34) is:

$$q(t) = k(t) \otimes z(t)$$

If the system is excited by $\delta(t)$, i.e. the Dirac impulse, then

$$q(t) = k(t) \otimes z(t) = k(t) \tag{6.35}$$

$$q_i(t) = f_i(\theta,\phi)\delta k \tag{6.36}$$

where $f_i(\theta,\phi)$ is the radiation pattern for the *ith* antenna element [27], δk is the Dirac impulse response changes with $K=(t-\tau_i)$, where

$$\tau_i = \frac{q_i \cdot (-\hat{s}_r(\theta,\phi))}{v}$$

and *v* is the propagation speed. Hence the impulse response (IR) of the antenna elements in relation to the signal plane wave *z(t)* is:

$$q_i(t) = f_i(\theta,\phi)\delta\left[t - \frac{q_i \cdot (-\hat{s}_r(\theta,\phi))}{v}\right]$$

i = 1, 2, … N, where *N* is the total number of antenna elements in the array and *t* is the reference time of the coordinate system. If the radiation patterns of the system is isotropic, $f_i(\theta,\phi)$ will be equal to one, and

$$q_i(t) = \delta\left[t - \frac{q_i \cdot (-\hat{s}_r(\theta,\phi))}{v}\right] = \delta(t-\tau_i)$$

Signal received at the i[th] elements will be:

$$z_i(t) = k_i(t) * s(t) + n_i(t)$$

$$= \delta\left[t - \frac{q_i \cdot (-\hat{s}_r(\theta,\phi))}{v}\right] * s(t)e^{j\omega t} + n_i(t)$$

$$= s(t-\tau_i)e^{j\omega t}e^{jkp_i.\hat{a}_r(\theta,\phi)} + n_i(t)$$

$$\approx z(t)e^{jkq_i.\hat{s}_r(\theta,\phi)} + n_i(t)$$
$$= s(t) + n_i(t)$$

where $n_i(t)$ is the noise in the antenna array elements. Hence, signal array vector received by the antenna elements is:

$$\mathbf{q} = \mathbf{s} + \mathbf{n}$$

$$= s(t)\mathbf{b} + \mathbf{n} \qquad (6.37)$$

where

$$\mathbf{q} = \begin{bmatrix} q_1(t) \\ q_2(t) \\ \text{M} \\ q_N(t) \end{bmatrix}, \mathbf{b} = \begin{bmatrix} e^{jkq_1.\hat{s}_r(\theta,\phi)} \\ e^{jkq_2.\hat{s}_r(\theta,\phi)} \\ \text{M} \\ e^{jkq_m.\hat{s}_r(\theta,\phi)} \end{bmatrix}, \mathbf{n} = \begin{bmatrix} n_1(t) \\ n_2(t) \\ \text{M} \\ n_N(t) \end{bmatrix}$$

If there are sets of signals k, $x_j(t) = s_j(t)e^{j\omega t}$ entering the system in the direction (θ_j, ϕ_j), $j = 1, 2, \ldots, k$, the array signals received is the array signal vector received by the antenna elements in Equation (6.36):

$$\boldsymbol{q} = \boldsymbol{s} + \boldsymbol{n}$$

$$= s_1(t)\boldsymbol{b_1} + s_2(t)\boldsymbol{b}_2 + \cdots + a_k(t)\boldsymbol{b}_k + \boldsymbol{n}$$

$$= [b_1, b_2, \ldots b_k][s_1(t), s_2(t), \ldots s_k(t)]^T + n$$

$$= \boldsymbol{B}_a + \boldsymbol{n}$$

where

$$B_a = [b_1, b_2, \text{L}\ , b_k] = \begin{bmatrix} e^{jkq_1.\hat{s}_r(\theta_1,\phi_1)} & e^{jkq_1.\hat{s}_r(\theta_2,\phi_2)} & \text{L} & e^{jkq_1.\hat{s}_r(\theta_k,\phi_k)} \\ e^{jkq_2.\hat{s}_r(\theta_1,\phi_1)} & e^{jkq_2.\hat{s}_r(\theta_2,\phi_2)} & \text{L} & e^{jkq_2.\hat{s}_r(\theta_k,\phi_k)} \\ \text{M} & \text{M} & \text{O} & \text{M} \\ e^{jkq_m.\hat{s}_r(\theta_1,\phi_1)} & e^{jkq_m.\hat{s}_r(\theta_2,\phi_2)} & \text{L} & e^{jkq_m.\hat{s}_r(\theta_k,\phi_k)} \end{bmatrix}$$

$$s = \begin{bmatrix} s_1(t) \\ s_2(t) \\ \mathrm{M} \\ s_k(t) \end{bmatrix}$$

Figure 6.3 shows a uniform linear antenna array having an equal inter-element spacing *d*, taken the first element from the origin, we can have the matrix **B** in the form of:

$$B = \left[b_1,\ b_2,\ \ldots,\ b_k\right] = \begin{bmatrix} 1 & 1 & \mathrm{L} & 1 \\ e^{jkd\sin\theta_1\cos\phi_1} & e^{jkd\sin\theta_2\cos\phi_2} & \mathrm{L} & e^{jkd\sin\theta_k\cos\phi_k} \\ \mathrm{M} & \mathrm{M} & \mathrm{O} & \mathrm{M} \\ e^{jk(2m-1)d\sin\theta_1\cos\phi_1} & e^{jk(2m-1)d\sin\theta_2\cos\phi_2} & \mathrm{L} & e^{jk(2m-1)d\sin\theta_k\cos\phi_k} \end{bmatrix}$$

Figure 6.3. Inter-element spacing for uniform linear array.

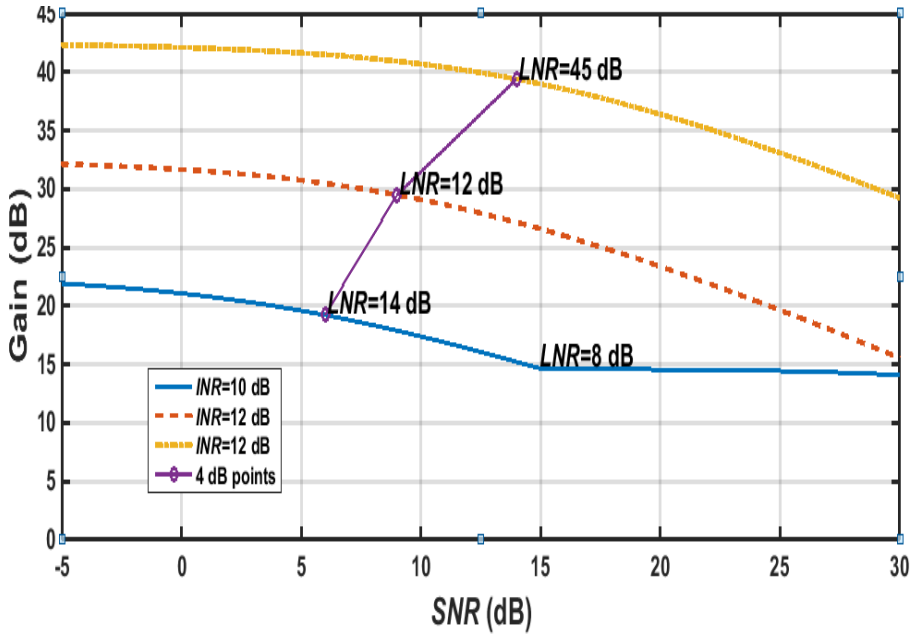

Figure 6.4. Gain versus SNR for the designed smart antenna element.

The average array gain when the signal direction is uniform at *[-0.1 0.1]* is studied in relation to the SNR in Equation (6.28). The result is shown in Figure 6.4. The total antenna elements considered for the simulation of the array gain is *16*, while the sigma range *[-0.1:1/1000:0.1]*. For the *4 dB* points observed in the simulation, when *INR = 10 dB*, it has an optimum gain of 18 dB and SNR of 6 dB, while for INR of 12 dB, its optimum gain is *29 dB* while its SNR is 8 dB, and for INR of *12 dB*, optimum gain is *39 dB* and SNR is *14 dB*.

6.2 Wideband Beamforming

In wideband beamforming, generally two techniques are used for the signal processing analysis. (a) Time-Domain (TD) processing, and (b) Frequency-Domain (FD) processing. These methods can generate frequency invariant beam patterns for wideband signal. One of the advantages of frequency-domain approach over the time-domain for signals with large bandwidths is the computational approach. Figure 6.5 shows the simulation of a frequency invariant beam-pattern in the normalized frequency band of fractional bandwidth of 120%.
Some of the advantages of frequency invariant wideband beamforming are: (i) faster convergence speed and (ii) lower computational complexity. The effective approach to solve the blind wideband beamforming problem is the frequency invariant beamforming technique. In general, processing of array signal is useful in detection and elimination of difficulties being encountered when a desired signal is taken, interference and noise may likely occurs. The bandwidth ratio to centre frequency of the narrowband incoming signal is ≤ 1%. Wideband applications are recommended in the work for fractional bandwidth up to 100-150%.

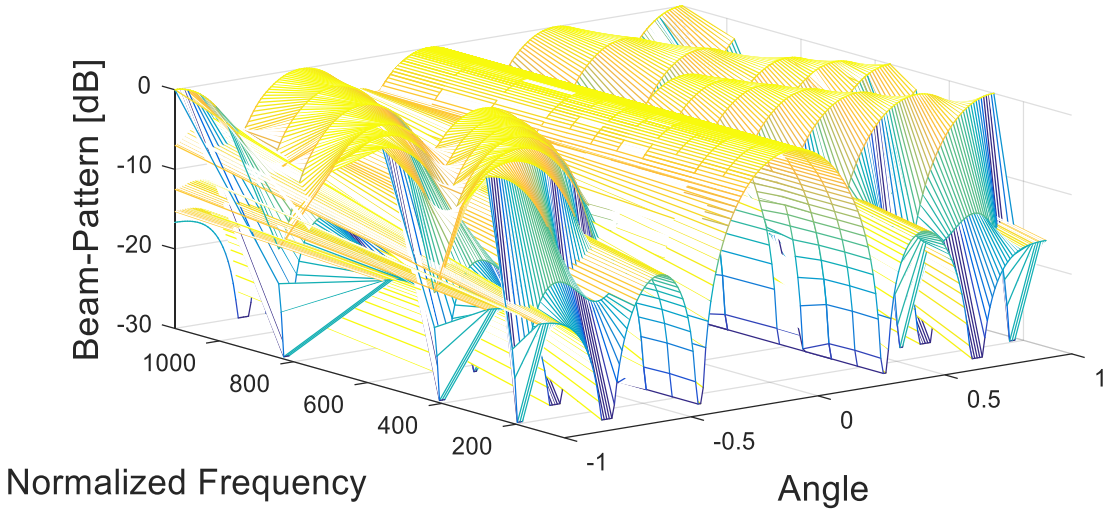

Figure 6.5. Frequency invariant wideband beamforming pattern.

6.2.1 Broadband signal beam pattern

The source of an antenna array system can be modelled in a wideband manner and potentially non-stationary random process. Assuming a discrete aperture of an array of *N* sensors in which the wave field is sampled in space and time. Assumed in the direction of θ_0, the source lies on the plane of the array, and plane wave impinged signal on the array. For a broadband signal (for the plane wave), response to this signal from the plane wave will characterize the beampattern for broadband signal of the array. Therefore, n^{th} sensor output modelled at time *t* is $\mathbf{x_n(k)=\delta[k-\tau_n(\Theta_o)]}$, where $n = 1, 2, ..., N$, $x_n(k)$ is the output sensor *n* at time *k*, and $\delta(k)$ is the corresponding of $n = 1, 2, ..., N$ signal that processes distinguishing source signal, $\tau_n(\theta_0)$ is the time propagation from the signal source to sensor *n*, while θ_0 is the direction of signal of the source [150]. The output noise power and output signal power for the array is mathematically expressed as [36]:

$$\begin{aligned} p &= E\left\{y_x^* y_x\right\} = w^H E\left\{x^* x^T\right\} w \\ N &= E\left\{y_n^* y_n\right\} = w^H E\left\{nn^H\right\} w = \sigma^2 w^H I_N w = \sigma^2 w^H w \\ &= \sigma^2 \sum_{i=1}^{N} \left|w_i\right|^2 \end{aligned} \tag{6.38}$$

Therefore, SNR for the sensors will be [73]:

$$SNR = \frac{P}{N} = \frac{w^H E\left\{x^* x^T\right\} w}{\sigma^2} * \left(\sum_{i=1}^{N} \left|w_i\right|^2\right)^{-1}$$

From Equation (6.38):

$$\begin{aligned} & w^H E\left\{x^* x^T\right\} w \\ &= w^H E\left\{x^*(k) x^* x(k) x^T\right\} w \\ &= p w^H x^x x^T w \\ &= p\left(\sum_{j=1}^{N} w_j z_j\right)^* \left(\sum_{j=1}^{N} w_j z_j\right) \\ &= \left|\sum_{j=1}^{N} w_j z_j\right|^2 \\ &\le p \sum_{j=1}^{N} \left|w_j\right|^2 \sum_{j=1}^{N} \left|z_j\right|^2 \end{aligned} \tag{6.39}$$

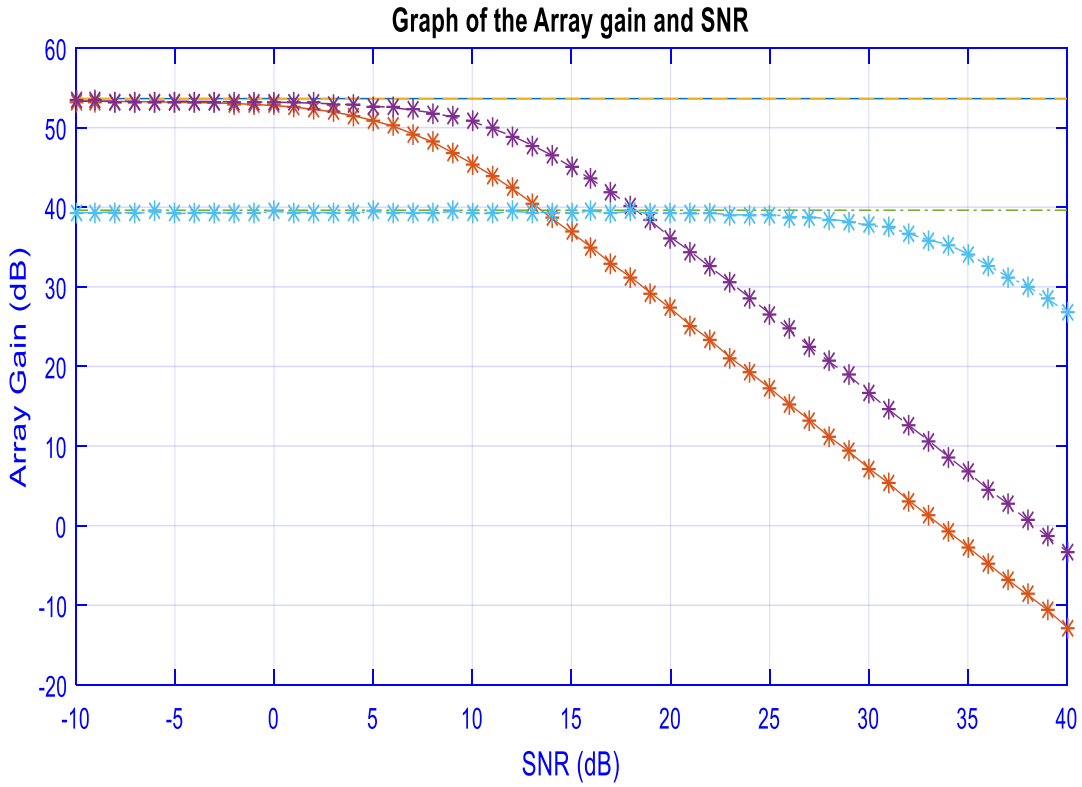

Figure 6.6. Simulaed results for the propsed antenna array gain and SNR.

Equation (6.39) is achieved using *Schwarz inequality*. Hence, *(p = E{s·(t)s(t)}* where *p* is the baseband signal power. Therefore,

$$SNR = \frac{w^H E\left\{s^* s^T\right\} w}{\delta^2 \sum_{j=1}^{N} |w_j|^2} \le \frac{p \sum_{j=1}^{N} |w_j|^2 \sum_{j=1}^{N} |z_j|^2}{\delta^2 \sum_{j=1}^{N} |w_j|^2} = \frac{p}{\delta^2} \sum_{j=1}^{N} |z_j|^2$$

From Equation (6.39): $P = w^H E\left\{x^* x^T\right\} w = {}_w{}^H E\left\{xx^T\right\}^* {}_w = {}_w{}^H R_{xx}^* w$, where

$$R_{xx} = E\left\{xx^H\right\} = \begin{bmatrix} E\left\{x_1 x_1^*\right\} & E\left\{x_1 x_2^*\right\} & \text{L} & E\left\{x_1 x_N^*\right\} \\ E\left\{x_2 x_1^*\right\} & E\left\{x_2 x_2^*\right\} & \text{L} & E\left\{x_2 x_N^*\right\} \\ \text{M} & \text{M} & \text{O} & \text{M} \\ E\left\{x_N x_1^*\right\} & E\left\{x_N x_1^*\right\} & \text{L} & E\left\{x_2 x_N^*\right\} \end{bmatrix}$$

R_{xx} is the data correlation matrix if the average values of $x_1(t), x_1(t), ..., x_N(t)$ are zero. The data correlation matrix can be used to analyze wave propagation.

6.3 Spatial Techniques of Antenna Arrays

A smart antenna is spatially sensitive and has inherent intelligence to create a beam with high gain in the preferred direction. It can change the beam pattern actively and can find and track the users as necessary. Higher degrees of freedom can be achieved in smart antenna design system using a spatial processing, which improves the performance of smart antennas [30]. Various signal processing applications are employed for estimating some parameters or the whole waveform of the received signals.

6.3.1 Spatial Smoothing Technique

Spatial smoothing processing of antenna arrays is one of the conventional methods for improving Multiple Signal Classification (MUSIC) algorithm [151]. This method makes the algorithm to work even in existence of coherent signals. Among the recommended methods to de-correlate coherent signals, spatial smoothing is one of the effective techniques, widely use in wireless communication systems. This technique has been established on a preprograming structure that distributes the entire array into corresponding subarrays, and then find the arithmetic mean of the subarrays output covariance matrices. This resulted in spatially smoothed covariance matrix [28-30].

6.3.2 Spatial filtering

Spatial sampling in one dimension which can be written as:

$$Z(\omega\overset{\mathrm{v}}{\delta}_j^o,\omega)=\sum_i S_i(\omega)w(\omega\overset{\mathrm{v}}{\delta}_j^o-\omega\overset{\mathrm{v}}{\delta}_i^o)$$
$$=S_j(\omega)w(0)+\sum_{i\neq j}S_i(\omega)w(\omega[\overset{\mathrm{v}}{\delta}_j^o-\overset{\mathrm{v}}{\delta}_i^o])$$

If we can design *w* so that we have a spatial filter for direction α_j

$$w\left(\omega\left[\overset{\mathrm{v}}{\alpha}_j^o-\overset{\mathrm{v}}{\alpha}_i^o\right]\right)\Delta w(0)$$

for $i\neq j$

Aperture is a spatial region that transmits or receives propagating waves. For space-time field through aperture:

$$z(\overset{\mathrm{v}}{x},k)=\omega(\overset{\mathrm{v}}{x})\,f(\overset{\mathrm{v}}{x},k)$$

Spatial domain multiplication is a convolution in wavenumber domain

$$z(\overset{\mathrm{v}}{k},\omega)=\frac{1}{(2\pi)^3}\int_{-\infty}^{\infty}W(\overset{\mathrm{v}}{k}-\overset{\mathrm{v}}{l})F(\overset{\mathrm{v}}{l},\omega)d\overset{\mathrm{v}}{l}$$

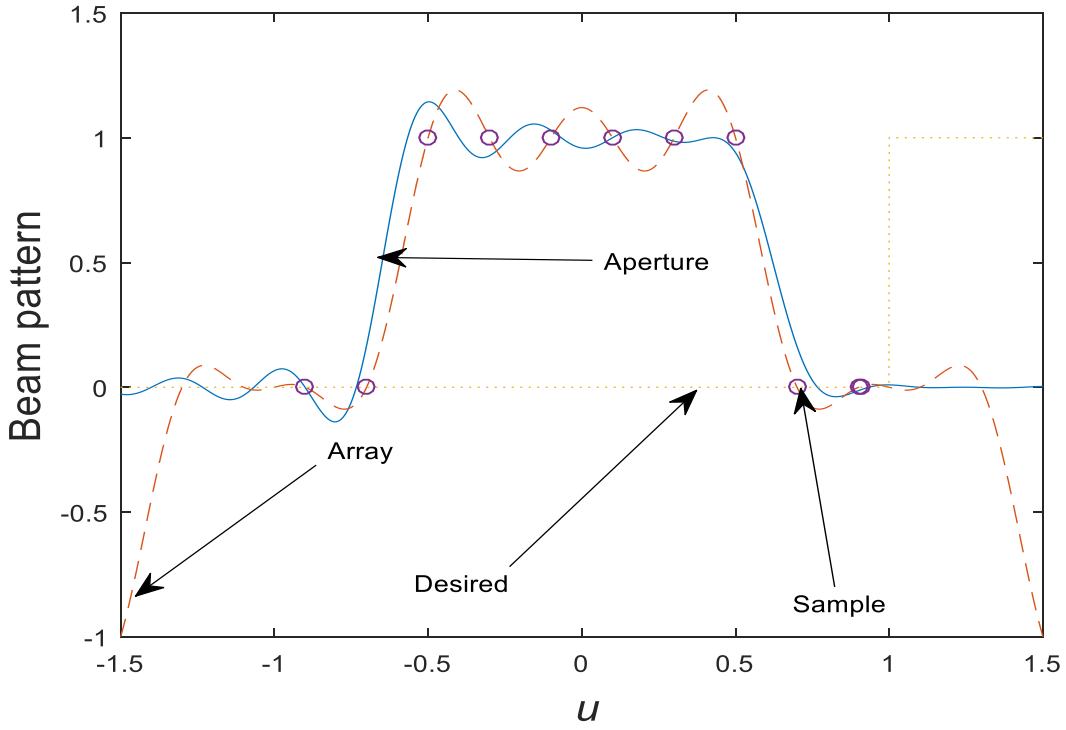

(a)

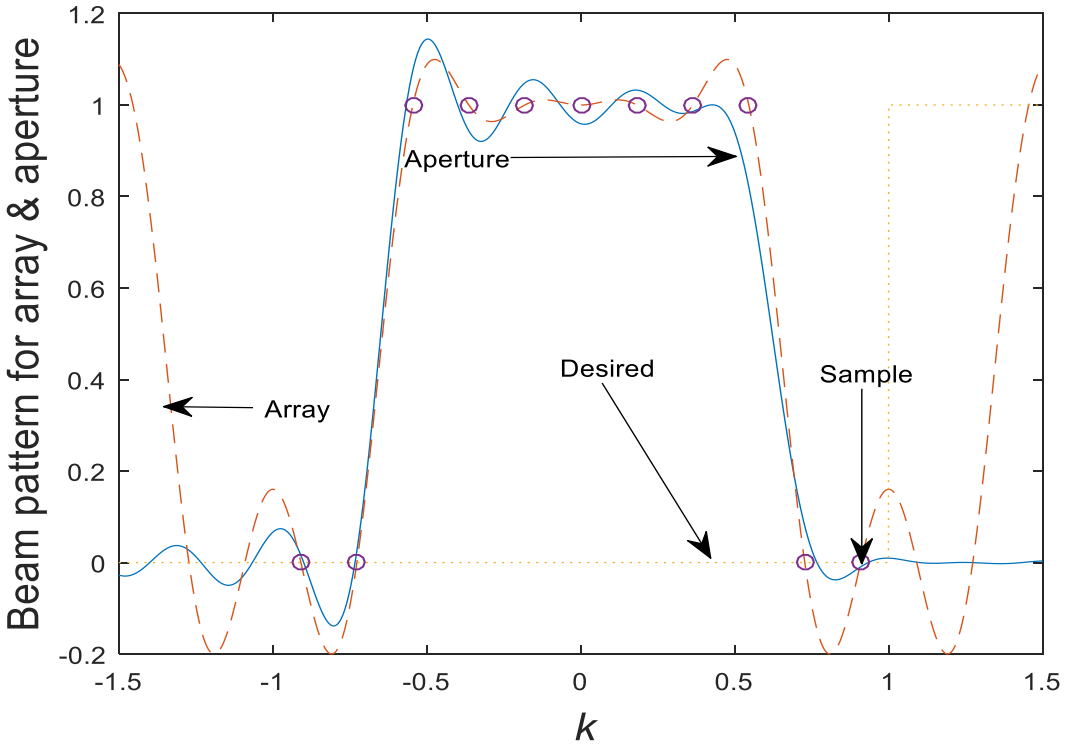

(b)

Figure 6.7. Beam pattern array aperture and their corresponding angles.

where $W(\vec{k}-\vec{l})$ is the spatial FT of w,

$F(\vec{l},\omega)$ is the spatiotemporal FT of f, $W(\vec{k})=\int_{-\infty}^{\infty} w(\vec{k})\exp\left\{\oplus j\vec{k}.\vec{x}\right\}d\vec{x}$

$W(\vec{k})$ =aperture smoothing and $\otimes$ =Mathematician's FT

For plane wave,

$$f(\vec{x},t)=s(t-\vec{\alpha}^{o}\cdot\vec{x})$$
$$F(\vec{k},\omega)=S(\omega)(2\pi)^{3}\delta(\vec{k}-\omega\vec{\alpha}^{o})$$

Smoothed in wavenumber space:

$$Z(\vec{k},\omega)=\frac{1}{(2\pi)^{3}}(W*\vec{x}F)(\vec{k},\omega)$$
$$=s(\omega)W(\vec{k}-\omega\vec{\alpha}^{o})$$

One of the elements that determines the performances of an array is beampattern [79]. Here we have developed the beam patterns for a uniformly weighted linear array.

6.4 Delay-Sum-Beamforming Technique

Delay-and-sum beamforming method [129] is a conventional methods for DOA estimation of array of antenna signals also known as classical beamformer, having equal magnitudes in weights [30]. The ideology behind delay and sum beamformer is that if a uniform linear array is being used, then each sensor output will be the same, with the exception of each one delaying by a different amount. So, if there is appropriate delay in output of each sensor, then we add all the outputs together the signal that was propagating through the array will reinforce, while noise will tend to cancel.

The selected array phases are steered in a specified direction, called the look direction or the main lobe [60]. In the look direction, the source power is equivalent to the mean output power of classical beamformer driven in the look direction. Consider a sensors of *M* positioning at $\vec{x}_0 \mathrm{K}\ \vec{x}_{M-1}$. If the phase center is put at the origin, the proposed model can be expressed as [36]:

$$\sum_{m=0}^{M-1}\vec{x}_m=\vec{0}$$

Its delay-and-sum beamforming can be found as:

$$z(t) = \sum_{m=0}^{M-1} w_m e^{-j\omega\Delta_m} y_m(t)$$

w_m: weight on signal, m ⇒ shading = apodization

Delay-and-sum on vector form

Monochromatic:

$$y_m(t) = e^{j(wt - \underset{\sim}{k}^o . \underset{\sim}{x}_m)}$$

Delayed signal:

$$y_m(t - \Delta_m) = y_m(t) e^{-j\omega\Delta_m}$$

Let us consider the Monochromatic plane waves,

$$f(\underset{\sim}{x}, k) = \exp\left\{ j\omega^0 (k - \underset{\sim}{\alpha}^o . \underset{\sim}{x}) \right\}$$

$$= s(k - \alpha^o \cdot \underset{\sim}{x})$$

where $s(k) = \exp(j\omega^o k)$

For a plane wave, the delay-and-sum beamformer response is

$$z(t) = \sum_{m=o}^{M-1} w_m s(k + (\underset{\sim}{\alpha} - \underset{\sim}{\alpha}^o) \cdot \underset{\sim}{x}_m)$$

$$= \sum_{m=o}^{M-1} w_m \exp(j\omega^o [k + (\underset{\sim}{\alpha} - \underset{\sim}{\alpha}^o) \cdot \underset{\sim}{x}_m])$$

$$= \left[\sum_{m=o}^{M-1} w_m \exp(j\omega^o (\underset{\sim}{\alpha} - \underset{\sim}{\alpha}^o) \cdot \underset{\sim}{x}_m) \right] \exp(j\omega^o t)$$

$$\underset{\sim}{k}^o = \omega^o \alpha^o$$

$$= \left[\sum_{m=o}^{M-1} w_m \exp(j(\omega^o \underset{\sim}{\alpha} - \underset{\sim}{k}^o) \cdot \underset{\sim}{x}_m) \right] \exp(j\omega^o t)$$

$$= W(\omega^o \underset{\sim}{\alpha} - \underset{\sim}{k}^o) \exp(j\omega^o t)$$

Where the discrete aperture smoothing function is

$$W(\underset{\sim}{k}) = \sum_{m=o}^{M-1} w_m \exp(j\underset{\sim}{k} . \underset{\sim}{x}_m)$$

From Equation (3.18) using the array factor, this can be applied to delay-and-sum beamformer. Assuming we have *J* as our space, the beam pattern can be:

$$B_j = \frac{1}{x}\frac{\sin\left(\frac{\pi x d}{\lambda} j\right)}{\sin\left(\frac{\pi d}{\lambda} j\right)} \; for -1 \le j \le 1$$

There will be null when the numerator is zero and the denominator is not zero. Note that $\sin\left(\frac{\pi x d}{\lambda} j\right) = 0$ when $\frac{\pi x d}{\lambda} j = k\pi$ for k = 1,2, … The nulls occur when both $j = k\frac{\lambda}{jd}$ for k = 1, 2, …and $j \neq k\frac{\lambda}{d}$ for k = 1, 2, …

Hence, the first null occurs at $j = k\frac{\lambda}{xd}$ and the null-to-null beamwidth BW_{xx} is $\Delta j_2 = 2\frac{\lambda}{xd}$. Assuming we have an *M* equally spaced of linear antenna array units of omni-directional antenna, and the inter-element spacing along the x-direction is *d*. The spatial aliasing exist if *x* is relative to λ. If the plane wave for a uniform linear array is changed from the plane wave considered before to a monochromatic plane, its response delay-and-sum beamformer tuned to $\overset{1}{\alpha}$ can be expressed as:

$$z(t) = w(\omega^o \overset{r}{\alpha} - \overset{r}{k}^o) \mathrm{l}^{j\omega^o t}$$

$$w(\overset{r}{k}) = \frac{\sin\left(mk_x \frac{d}{2}\right)}{\sin\left(k_x \frac{d}{2}\right)}$$

$$w(\omega^o \overset{r}{\alpha} - \overset{r}{k}^o) = \frac{\sin\left(m[\omega^o \alpha_x - k_x^o]\frac{d}{2}\right)}{\sin\left([\omega^o \alpha_x - k_x^o]\frac{d}{2}\right)}$$

Using $k_x = \omega^o \alpha_x$ $\quad W(\omega^o \overset{r}{\alpha} - \overset{r}{k}^o) = \frac{\sin\left(M\left[k_x - k_x^o\right]\frac{d}{2}\right)}{\sin\left(\left[k_x - k_x^o\right]\frac{d}{2}\right)}$

Let us consider it n terms of angles, let $k_x = \left(\frac{2\pi}{\delta}\right)\sin(\phi)$

$$W(k_x - \overset{r}{k}^o) = \frac{\sin\left(M\frac{\pi}{\delta}\left[\sin\phi^o - \sin\phi\right]d\right)}{\sin\left(\frac{\pi}{\delta}\left[\sin\phi^o - \sin\phi\right]d\right)}$$

The beam patterns for the uniform array are illustrated in Figure 6.8.

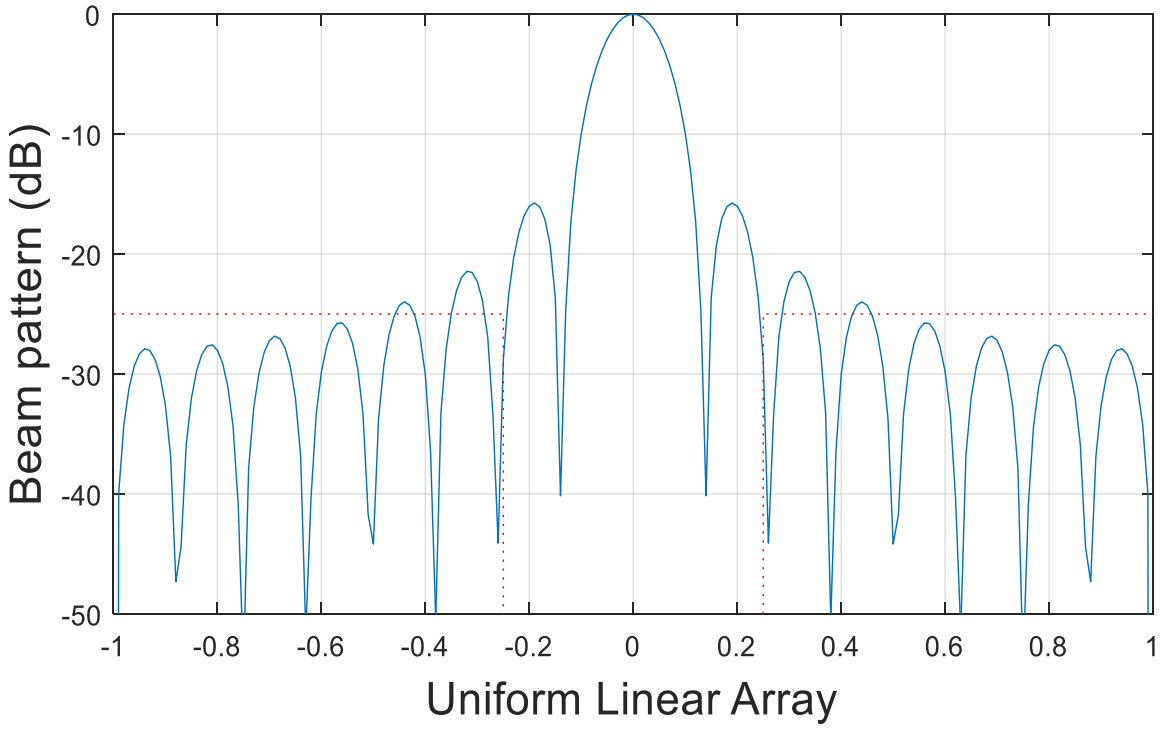
Beam pattern (dB)
0
-10
-20
-30
-40
-50
-1
-0.8
-0.6
-0.4
-0.2
0
0.2
0.4
0.6
0.8
1
Uniform Linear Array

(a)

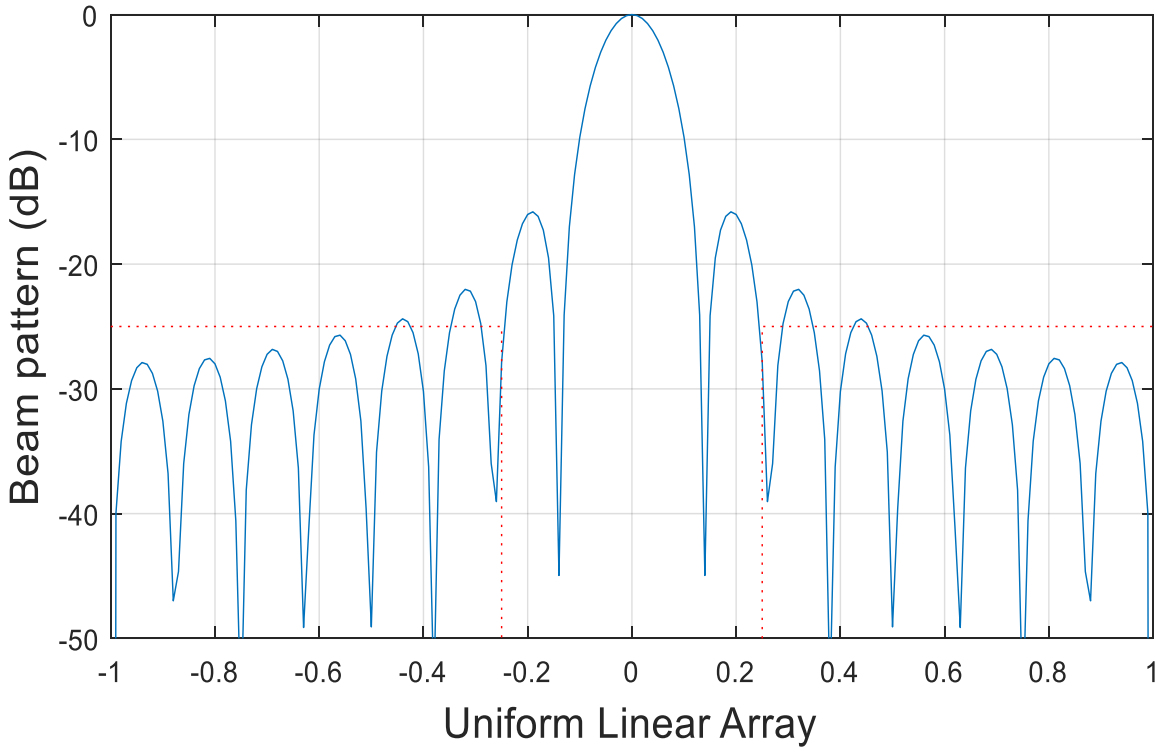
Beam pattern (dB)
0
-10
-20
-30
-40
-50
-1
-0.8
-0.6
-0.4
-0.2
0
0.2
0.4
0.6
0.8
1
Uniform Linear Array

(b)

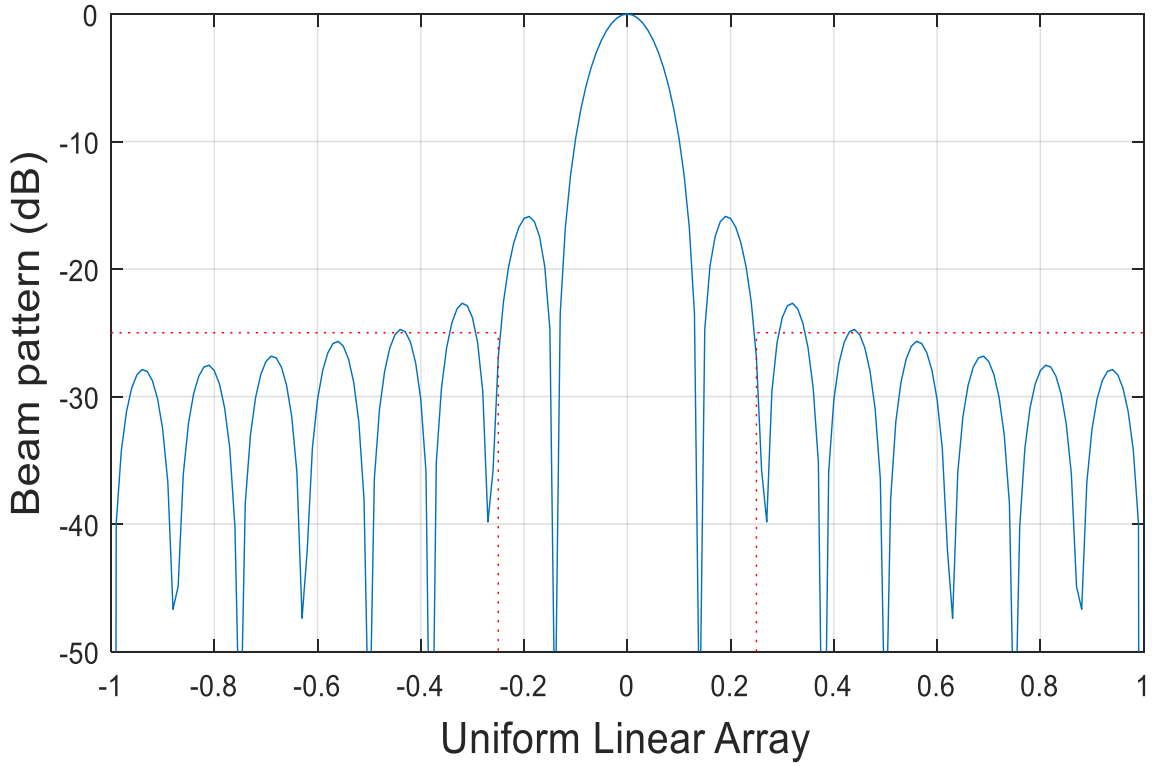
Beam pattern (dB)
0
-10
-20
-30
-40
-50
-1
-0.8
-0.6
-0.4
-0.2
0
0.2
0.4
0.6
0.8
1
Uniform Linear Array

(c)

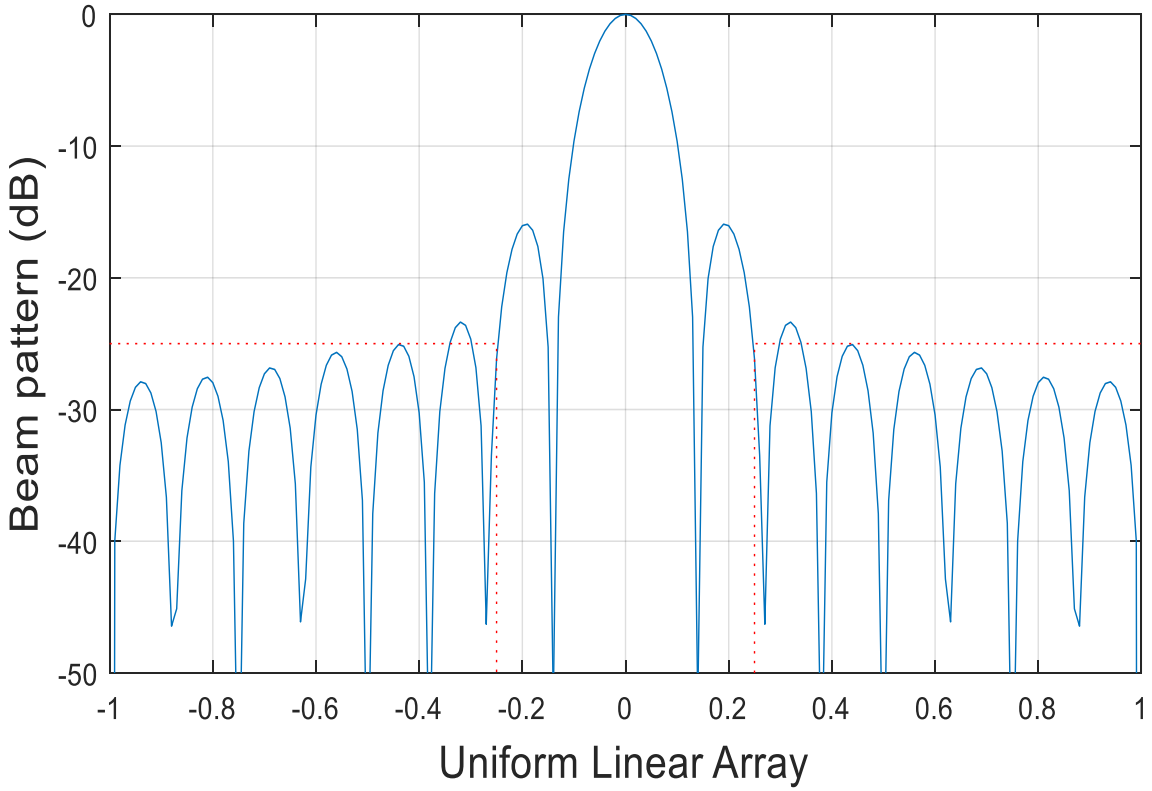
Beam pattern (dB)
0
-10
-20
-30
-40
-50
-1
-0.8
-0.6
-0.4
-0.2
0
0.2
0.4
0.6
0.8
1
Uniform Linear Array

(d)

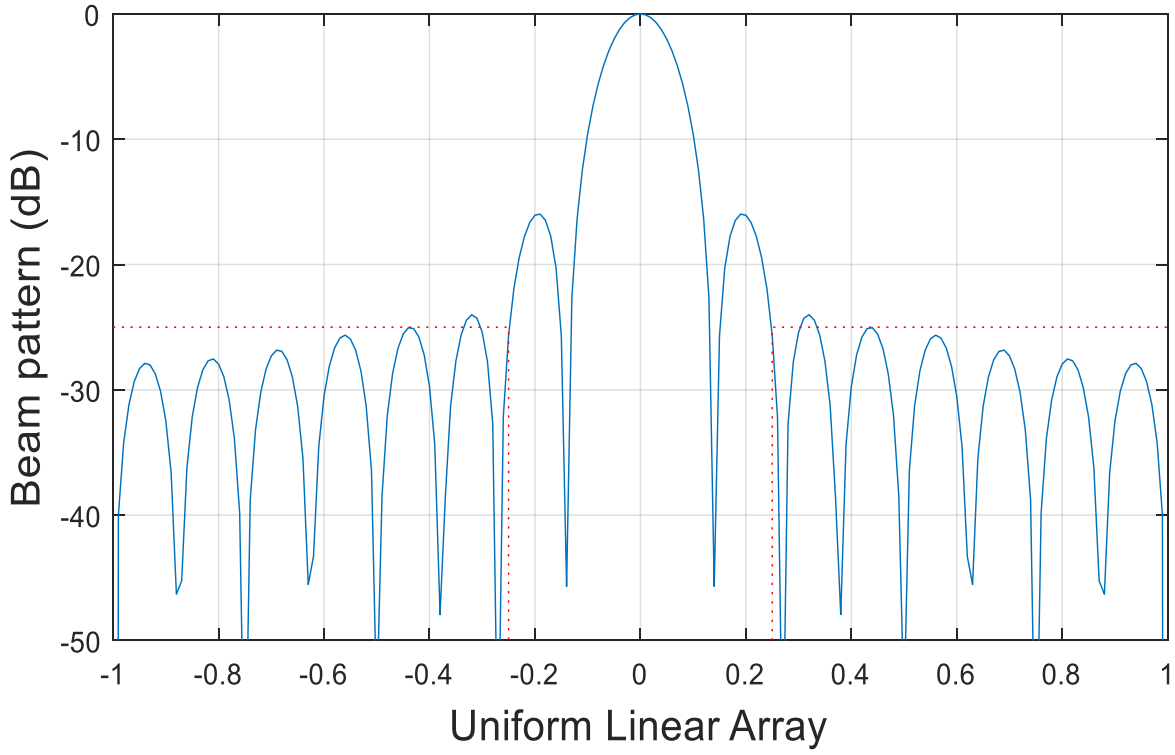

(e)

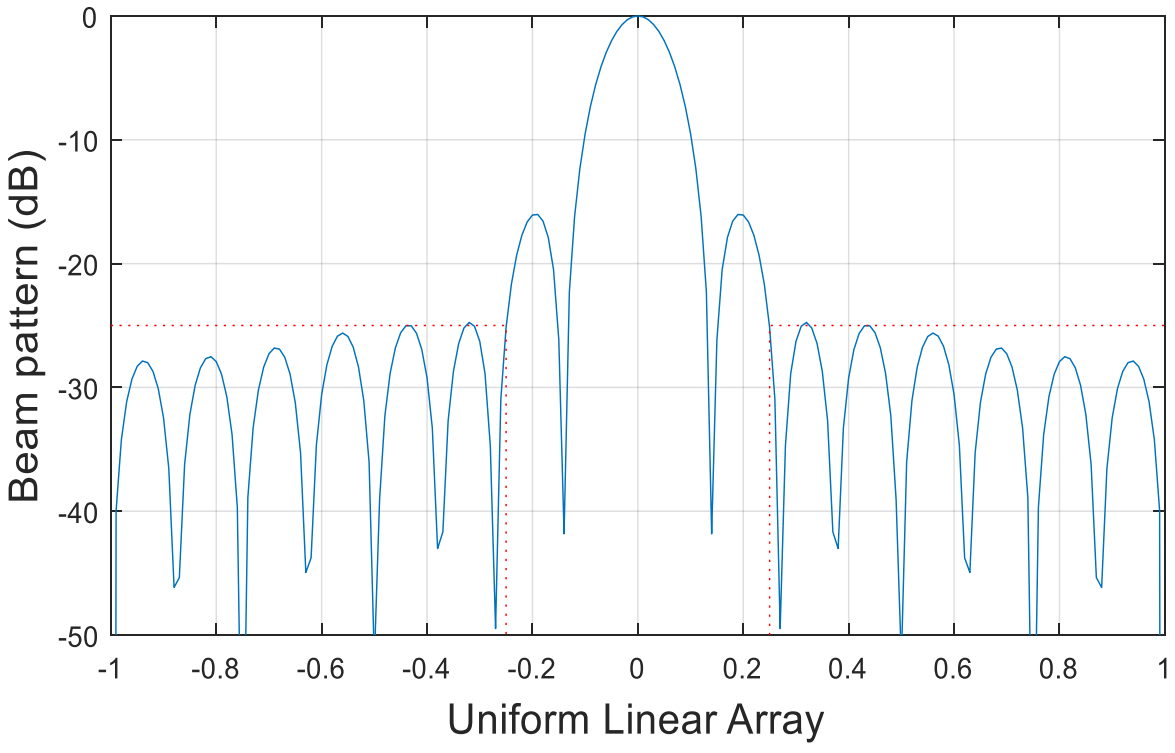

(f)

Figure 6.8. Beam patterns and the uniform linear array. Beam pattern evolution for 10-element non-uniform linear array and -25 dB sidelobes. (a) first iteration; (b) third iteration; (c) fifth iteration; (d) seventh iteration; (e) ninth iteration; (f) tenth iteration.

6.5 Direction Of Arrival (DOA) Approximation

Some optimum beamformers need the DOA information to control the optimum weight vector. Smart antennas performance and optimization depends on the idea that the DOA of desired signal is recognized to the system. The DOA of signals must match the phase delay variances of signals at the outputs of receiving antenna array elements to avoid loss of signals. The level of uncertainty in determining DOA depends on array geometry, parameters, and characteristics of the array sensors.

The array of interest is presumed to comprise of *N* isotropic elements that receive directional signals from the far field. All propagating signals are modelled as narrowband. The DOA of a signal is mainly calculated by using sensors or arrays of antenna [36]. The DOA estimation process are described in detail for uncorrelated signal sources. In Figure 6.3, the direction of signal from the received signals can be estimated using the following description: the set of incoming signal direction is θ_1, the elements *N* of the antenna array are in a linear equispaced. Here, the number of incoming signals are unknown, likewise the direction and the amplitude. The signals are normally corrupted by noise. Let the number of the unknown signals be *M*, *M*<*N*, and with the assumption of white Gaussian noise,

$$x = v(\theta) + n$$

where *x* is the length of *N* vector of the received signals, $\theta = \left[\theta_1, \mathrm{K}\ , \theta_p\right]^T$ is the set of parameters, and ***v*** is a known function of parameters, $\mathrm{var}(\theta_p) \geq J_{pp}^{-1}$

$$J_{ij} = E\left\{\frac{\partial^2}{\partial_{\theta i}\partial_{\theta j}}[\ln\ fx(x/\theta]\right\}$$

where ***J*** is known as the Fischer Information Matrix. Single signal corrupted is written as:

$$x = \alpha \boldsymbol{s}(\theta) + \boldsymbol{n}$$

where **s** is the direction-finding vector of the signal, **n** is zero mean Gaussian with covariance $\delta^2 I$

Assuming $\alpha = ae^{jb}$

$\theta = [a, b, \theta]^T$

In this situation,

$$v(\theta) = \alpha s(\delta)$$

$$fx(x/\phi) = Ce^{-(x-v)^H R^{-1}(x-v)}$$

$$\ln\ fx(x/\theta) = \ln C + \frac{-x^H x + \alpha^* s^H(\phi)x + \alpha x^H s(\phi) - |\alpha|^2 s^H(\phi)s(\phi)}{\sigma^2}$$

$$g(\theta) = \frac{1}{\sigma^2}\left[ae^{-jb}s^H(\phi)x + ae^{jb}x^H s(\phi) - a^2 s^H(\phi)s(\phi)\right]$$

Therefore, CRB estimation problem for the DOA is:

$$\text{var}(\theta) \geq \left[E\left(\frac{\partial^2 g}{\partial\theta^2}\right)\right]^{-1} \tag{6.40}$$

$$\geq \frac{6\delta^2}{|\alpha|^2 N(N^2-1)(kd)^2\sin^2\phi}$$

Equation (6.40) gives the derivation for the estimation of some optimum beamformers that need the Direction of Arrival (DOA) information to control the optimum weight vector. The performance and optimization depends on the idea that the DOA of desired signal is recognized to the system.

6.6 Deterministic Beamformer

Adaptive algorithms proposed for beamforming are the Howells-Applebaum adaptive loop. If an array consist of *M* as odd antenna elements evenly spaced along the x-axis, centered at the origin, with spacing *d*. The twist here is that each element, instead of being a point, is actually a small linear segment of length *L* along the x-axis (where $L<d$, so the segments don't overlap), centered at the element locations. The wave number-frequency response of the resulting filter and sum beamformer can be found if the sensor delays are adjusted to steer the beam to look for plane waves propagating with a slowness vector $\vec{\alpha}$. We have observed a space-time field m^{th} sensor position, $\vec{x}_m.f(\vec{x}_m,k)$, our sensors can only gather energy over a finite area, indicated by the (spatial) aperture function $\omega(\vec{x}).f(\vec{x},k),$ is the field values. Therefore,

$$\omega(\vec{x}) = \begin{cases} \neq 0 \text{ inside aperture} \\ = 0 \text{ outside aperture} \end{cases}$$

where $y_m(t)$ is the sensors output. If sensor is perfect, $y_m = \kappa f(x_m,k)$

Directional sensors have significant spatial extent. They spatially integrate energy over the aperture, i.e. they focus a particular propagation direction. e.g. parabolic dish. They are described by the aperture function, $\omega(\vec{x})$, which describes: (a) spatial extent reflects size and

shape, (b) aperture weighting: relative weighting of the field within the aperture (also known as shading, tapering, apodization). For places where $\omega(\overset{\vee}{x}) \neq 0$, we sometimes get to pick $\omega(\overset{\vee}{x})$ called aperture weighting, or apodization, shading, or tapering.

6.7 Uncorrelated Signal Sources Estimation

The DOAs estimation of the uncorrelated signal sources must be estimated in the first instance. Let us consider a group of coherent sources equivalent to a virtual source. The Eigen decomposition can be expressed as [79, 148]

$$R_s = U\sum U^H = U_s\sum_s U_s^H + U_n\sum_n U_n^H$$

$$\lambda_Q = diag\left\{\lambda_1,\mathrm{K}\ \lambda_m\right\} with \lambda_1 \geq \mathrm{L}\ \geq \lambda_{Q+L} > \lambda_{Q+L+1} = \mathrm{L}\ \lambda_m = \sigma_n^2$$

$$\boldsymbol{U}_s = \left[\boldsymbol{U}_1, \ldots \boldsymbol{U}_{Q+L}\right], \Sigma_s = diag\{\lambda_1, \ldots, \lambda_{Q+L}\}, \boldsymbol{U}_n = \left[\boldsymbol{U}_{Q+L+1}, \ldots \boldsymbol{U}_M\right]$$

and

$$\sum_n = diag\left\{\lambda_{Q+L+1},\mathrm{K}\ ,\lambda_M\right\}$$

Assuming $R_s = Q \wedge Q^H$, then $R = Q[\wedge + \sigma^2 I]Q^H$. Therefore,

$$R = QQ^H \begin{bmatrix} \lambda_m+\sigma^2 & 0 & \mathrm{L} & 0 & 0 & \mathrm{L} & 0 \\ 0 & \lambda_m+\sigma^2 & \mathrm{L} & 0 & 0 & \mathrm{L} & 0 \\ \mathrm{M} & \mathrm{M} & \mathrm{O} & \mathrm{M} & \mathrm{M} & \mathrm{M} & \mathrm{M} \\ 0 & 0 & \mathrm{L} & \lambda_m^2+\sigma^2 & 0 & \mathrm{L} & 0 \\ 0 & 0 & \mathrm{L} & 0 & \sigma^2 & \mathrm{L} & 0 \\ \mathrm{M} & \mathrm{M} & \mathrm{M} & \mathrm{M} & \mathrm{M} & \mathrm{O} & \mathrm{M} \\ 0 & 0 & \mathrm{L} & 0 & 0 & \mathrm{L} & \sigma^2 \end{bmatrix}$$

The Eigen vector matrix (Q) can be partitioned into noise subspace (Q_n) and signal matrix (Q_s), columns M of Q_s » signal Eigen values of M, N-M columns of Q_n » noise Eigen values The m-th signal Eigen value is written as

$$\lambda_m + \sigma^2 = N\left|\alpha_m\right|^2 + \sigma^2$$

By orthogonality, Q and Q_s is ⊥ (perpendicular) to Q_n. Hence, noise Eigen vectors are ⊥ to the steering signal vectors. The Eigen values for the uncorrelated sources is shown in Figure 6.9.

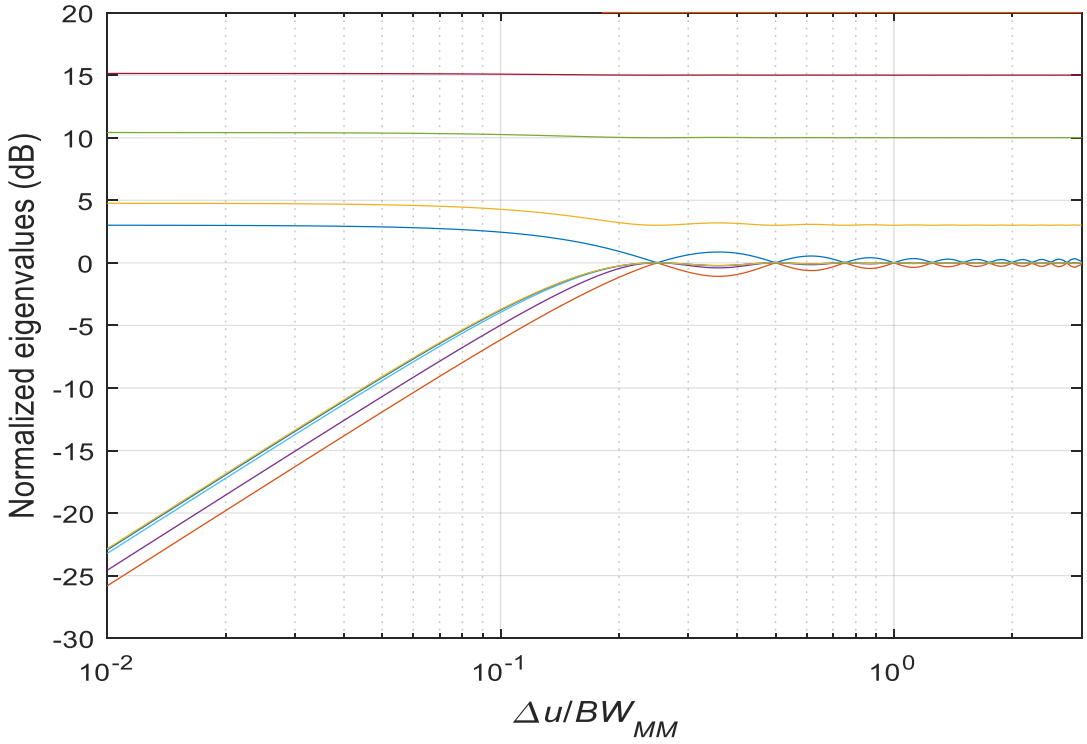

Figure 6.9. Eigen values for uncorrelated sources.

An array of ten omnidirectional sensors/antennas that involves three linear subarrays are used. The first subarray involves of four sensors that has an inter-element spacing of: (i) 0.42λ, (ii) 0.53λ, and (iii) 0.32λ, where λ is the signal wavelength. The plot shown indicates that the beamformer can be steered to the desired direction of the main beam. The plot also shown the simulation results when the interference signals are coming from different directions.

6.8 Adaptive Beamforming: An Excellent Performance for Smart Antennas in Wireless Communication Systems

A smart antenna arrays system geometry Figure 6.10 comprises of uniform linear antenna array *M* at the cellular sites. The adaptive beamforming algorithms of the array adjust the amplitudes current by the complex weights. The array output beam pattern is optimized by the algorithm so as to produce the radiated power in the directions of signals of interest and put nulls in the direction of co-channel interference. With beamforming algorithms, antenna arrays' weight are adjusted to generate adaptive beam so as to locate corresponding users dynamically and concurrently reduce any interference coming from other consumers by putting nulls in their respective directions [14]. In this work, the LMS and RLS algorithms results have been evaluated for their convergence rate and beamforming. The performance of null steering such as: beamwidth, null depths and maximum sidelobe level has been examined and computed. Here, m_1, m_2, and m_3 are the number of antenna array elements used for the analysis respectively. While w_1, w_2, and w_3 are the weights of the beamforming antenna array elements. Also, the α is the direction of arrival of signals on the antenna arrays.

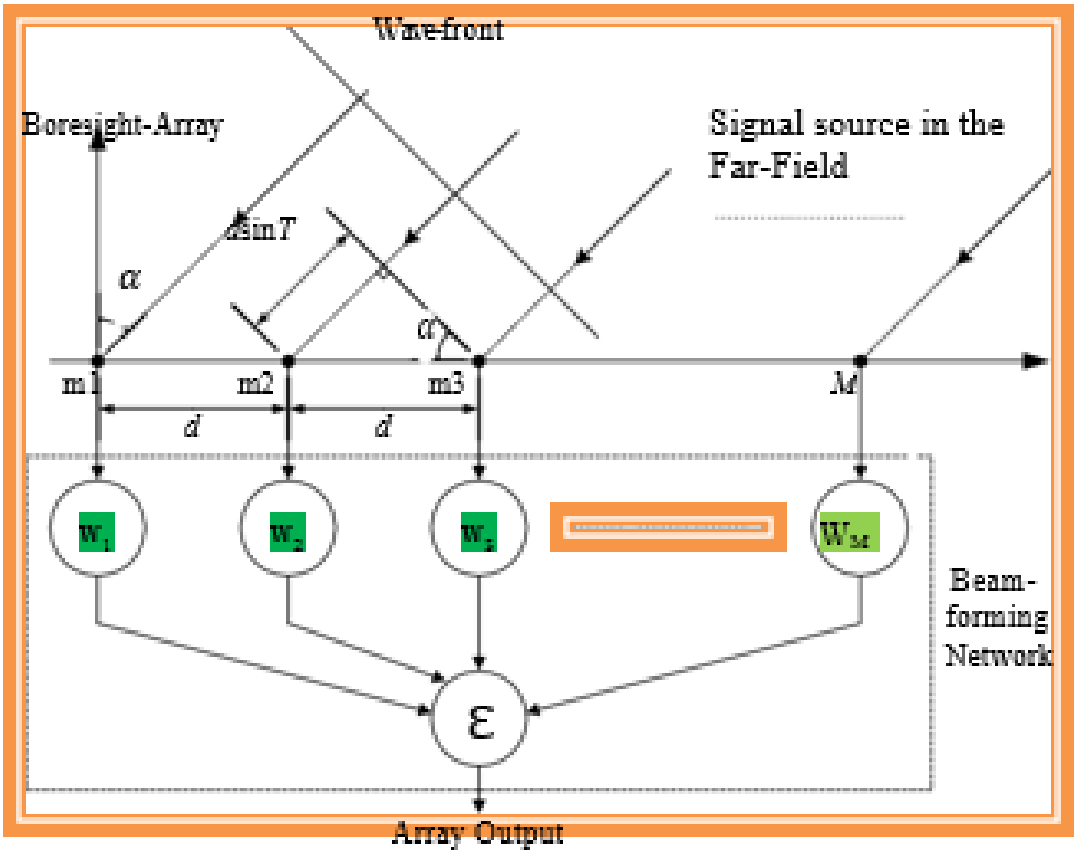

Figure 6.10. Uniform linear array (M) geometry.

6.8.1 Adaptive beamforming algorithm

Adaptive beamforming is a process by which an adaptive spatial signal processing are performed on array of antennas. By the addition of the signals weights constructively in the preferred direction of signal, adaptive beamforming technique creates radiation pattern on antenna array thereby nulling pattern in the unwanted direction that is interference [25]. These arrays are antennas in the smart antenna context. Adaptive beamforming are normally used to achieve spatial selectivity at transmitting and receiving ends.

The adaptive beamforming is a combination of several antenna elements inputs from the antennas array using the signal processing capacity to produce a narrow beams so as to allow certain frequency range for separate users within the cell at a particular point in time. To improve a system capacity, one of the factors to consider is to suppress the co-channel interference. This can be achieved through the implementation of adaptive beamforming. Hence, system immunity to multipath fading is improved. To achieve a better SNR through adaptive beamforming, each antennas weights are varied in the array.

Adaptive beamformer is a device that has the capacity to filter out signals that are located in the frequency band but separated in the spatial domain; separating a desired signal from interfering signals.

Adaptive beamforming algorithm can be used to track non-stationary channels, and smart antennas users in a wide angle spread environment when there are random variations in both eigenvalues of the autocorrelation matrix of the received signal [57]. It has the capacity to operate in any of the block mode or recursive mode approximation. In block approximation mode, the input data stream is arranged in the form of blocks of the same length (duration), and the current weight vector *G(i)* is in sync on a block-by-block basis. In recursive approximation mode, conversely, the tap weights of spatial processor are updated on a sample-by-sample basis [25], [44], [52-53]. An adaptive solution which minimizes the cost function is

$$G_{i+1} = G_i - \frac{\mu}{2}\nabla j(G_i)$$

where μ is the convergence factor which controls the rate of adaptation, and $\nabla j(G_i)$ is the gradient of a function *H(ρ)* which is given as

$$H(\rho) = B\left[\left|\tau(\rho)\right|^2\right]$$

where *τ(ρ)* is the a priori estimation error defined by

$$\tau(\rho) = d(\rho) - \boldsymbol{G}^H(\rho - 1)\boldsymbol{r}(k)$$

The function *H(G)* is the cost function which describes the error performance surface.

6.9 Signal Modelling Formulation for the Adaptive Beamforming

Figure 6.10 comprises of linear array of *M* antennas (uniform), $S_m(u)$ signal source with *k* narrowband from signal of interest directions ($\alpha_1, \alpha_2, \ldots, \alpha_k$,), and interferers from directions ($\alpha_1, \alpha_2, \ldots, \alpha_I$) as it receives source signals $S_i(u)$ of narrowband *I*. At specific time, u = 1, 2, …, J, where J is the sum of time taken. Mathematically, the desired users signal vector $\mathbf{X}_n(v)$ can be written as [15].

$$\mathbf{X}_n(u) = \sum_{n=1}^{N} \mathbf{q}\,(\alpha_n) S_n(v)$$

α_k (array response) can be written as:

$$\mathbf{q}(\alpha_n) = e^{[i(k-1)\varphi_n]^v}$$

φ_n (electrical phase shift) is:

$$\varphi_n = 2\pi\left(\frac{d}{\lambda}\right)\sin(\alpha_n)$$

From Equation (1), $\mathbf{X}_n(v)$

$$\mathbf{X}_n(v) = \mathbf{A}_n\,\mathbf{S}(v)$$

$\mathbf{X}_n(v)$ direction vectors

$$\mathbf{A}_n = [\mathbf{q}(\alpha_1), \mathbf{q}(\alpha_2),\ldots, \mathbf{q}(\alpha_k)]$$

$\mathbf{S}(v)$ waveform vector is written as

$$\mathbf{S}(v) = [s_1(v)\ s_2(v)\ ..\ \ ..\ \ s_k(v)]^V$$

The interference users signal vector $\mathbf{X}_I(v)$ is

$$\mathbf{X}_I(v) = \mathbf{A}_I\mathbf{i}(v)$$

$$\mathbf{A}_I = [\mathbf{q}(\alpha_1), \mathbf{q}(\alpha_2), \ldots, \mathbf{q}(\alpha_I)]$$

The interference users' source waveform vector defined is

$$\mathbf{I}(v) = [i_1(v)\ \ i_2(v)\ ..\ ..\ i_I(v)]^V$$

Combining $\mathbf{X}_I(v)$, $\mathbf{A}_I$, and $\mathbf{I}(v)$ from above, we have

$$\mathbf{x}(v) = q_o\mathbf{S}(v)[q_1\ q_2\ \cdots q_N]\cdot\begin{bmatrix}\mathbf{I}_1(v)\\ \mathbf{I}_2(v)\\ \vdots\\ \mathbf{I}_N(v)\end{bmatrix} + \mathbf{n}(v)$$

Where $\begin{bmatrix}\mathbf{I}_1(v)\\ \mathbf{I}_2(v)\\ \vdots\\ \mathbf{I}_N(v)\end{bmatrix}$ is our reference correlation vector and $\mathbf{I}_N(v)$ is the Lx1 correlation for the nth antenna element [103]. Hence,

$$\mathbf{X}(v) = \mathbf{X}_k(v) + \mathbf{n}(v) + \mathbf{X}_I(v)$$

Its covariance matrix is expressed as

$$\mathbf{R}_{k+1} = E\{\mathbf{X}_{K+1}(v)\mathbf{X}^H_{k+1}(v)\} \qquad (6.41)$$

To approximate Equation (6.41), averaging process over D snapshots taken from signals that are incident on the antenna array leads to form a spatial correlation matrix $\mathbf{R}_{k+1}$ given by [149]:

$$\mathbf{R}_{k+1} = \boldsymbol{D^{-1}}\sum_{d=1}^{J}\mathbf{X}(d)\mathbf{X}^H_{k+1}(d)$$

$$\mathbf{R} = \mathbf{A}_k\mathbf{R}_{ss}\mathbf{A}^H_k + \mathbf{n}(k) + \mathbf{A}_I\mathbf{R}_{ii}\mathbf{A}^H_I$$

The summation of the array antenna in direction α, Figure 6.10 is given as:

$$y_k(v) = \sum_{n=1}^{M} w_{N-1}e^{j(2\pi fv+\varphi_n k)}$$

The output of the narrowband beamforming is [152]:

$$Y(v) = \mathbf{W}^{H}\mathbf{X}(v)$$

The defined SINR is [24, 103, 149]:

$$SINR = \frac{W^{H}R_{s}W}{W^{H}\left(R_{i} + R_{n}\right)W}$$

$$= \frac{W^{H}R_{s}W}{W^{H}R_{i+n}W}$$

Smart antenna power comes from the fact that it can steer and reshape its radiation pattern to maximize signal to interference and noise ratio (SINR) [4]. Hence to achieve optimum (SINR), the optimal weight vector *W* is needed. Hence optimal weight vector *W* can be expressed as:

$$W_{opt} = \frac{R_{i+n}^{-1}A}{A^{H}R_{i+n}^{-1}A}$$

At this time the corresponding $SINR_{opt}$ is:

$$SINR_{opt} = P_{s}^{2}A^{H}R_{i+n}^{-1}A \qquad (6.42)$$

6.10 Least Mean Square (LMS) Algorithm Formulation

The Least Mean Square (LMS) algorithm [10, 91] is the simplest and most robust for adaptive signal processing technique adopted in many applications especially adaptive beamformers [4, 87]. This estimate the covariance matrix of the desired signal from the measurements of the received signal. For the adaptive algorithm, the minimization of mean-square error (MSE) by (LMS) algorithm is now utilized as an example to introduce the digital adaptive beamforming [44]. LMS is based on the cost function minimization which is defined as the error between the reference signal and the received signal. The algorithm is based on maximization of SNR at the array output and least mean squares errors. The LMS algorithm generates better main lobes in desired user direction but do not nullify co-channel interference. The LMS algorithms are used in adaptive filters to find the filter coefficients that relate to producing the least mean squares of the error signal *(e)* (difference between the desired and the actual signal). It is a stochastic gradient descent method in that the filter is only adapted based on the error at the current time. The idea behind LMS filters is to use the methods of steepest descent to find a coefficient vector ***h****(n)* which minimizes a cost function.

The LMS algorithm updates its weights at each iteration by computing nearly the quadratic MSE gradient at the instant time. The updated weights are moved in the negative direction of the gradient by the step size parameter [10, 91]. Let the weights for the mathematical analysis be equal to *G*.

Consider the output of the beamformer at time u, *y(u)* is specified through a linear summation of the numbers of *M* antennas [$X_1, X_2, X_3, \ldots, X_{N-1}$] , with ***c(u)*** as input vector and ***G(u)*** as weight vector. Adaptive techniques are frequently used by means of iterative technique which gives an updated weight vector **w,** after each calculation. The output response for the array can be expressed as

$$y(u) = \mathbf{G}^{H}\mathbf{C}(u),$$

$$e(u) = d(u)-\mathbf{G}^{H}\mathbf{c}(u)$$

To avoid matrix inverse operation for the LMS algorithm, the gradient vector $\nabla \boldsymbol{J}(t)$ for weight vector upgradation can be used. The weight vector at time *(u+1)* can be expressed as [91, 93]

$$\boldsymbol{G}(u+1) = \boldsymbol{G}(u) + \frac{1}{2}\mu[-\nabla \boldsymbol{J}(u)]$$

where μ operates on the adoption rate and is being referred to as the step-size parameter, correlation matrix, and determines how close the weights are moving. Its value is in the range of 0 and 1. For small values of step-wise parameter, there will be slow convergence. Hence, cost function are approximately in a good sense. However, large values of step-wise parameter leads to a faster convergence but the stability could be lost at the lowest value. When LMS algorithm is started with random weight vector, it converges and stable in the range of $0 < \mu < \frac{1}{\lambda_{\max}}$ [10]. For slow convergence values, it means the eigenvalues of the correlation matrix is widespread. From Equation (6.42), to estimate the instantaneous gradient vector $\nabla \boldsymbol{J}(u)$. Covariance matrix **X** and cross-correlation vector **Y** previous information is required. The LMS algorithm conversely simplifies this with the help of instantaneous values of covariance matrices **X** and **Y** in preference to their actual values.

$$\nabla(u) = \partial\left(\frac{J(u)}{\partial(G(u)}\right)$$

J(u) is a squared error [93]:

Hence,

$$\nabla \mathbf{J}(u) = -2\mathbf{Y}(u) + 2\mathbf{X}(u)\mathbf{G}(u)$$

The weight vector update is found to be

$$\mathbf{G}(u+1) = \mathbf{G}(u) + \mu[\mathbf{Y}(u) - \mathbf{X}(u)\mathbf{G}(u)] \quad (6.43)$$

$$= \mathbf{G}(u) + \mu\mathbf{c}(u)[\mathbf{d}^*(u)(u) - \mathbf{c}^H(u)\mathbf{G}(u)]$$

$$= \mathbf{G}(u) + \mu\mathbf{c}(u)\mathbf{e}^*(u) \quad (6.44)$$

Equation (6.43) and (6.44) are the estimated weight vector and reference signal used for weights update at individual iteration [6]. This weight vector correction gives the minimum value of the mean square error. Stability is determined by [10]: $0 \le \mu \le \frac{1}{2\lambda_{max}}$.

In practice, **X** is normally used as optimal beamformer above for the estimation of the array optimal weights [90, 152]. $y(t) = \mathbf{w}^H\mathbf{x}(t)$ minimize output power subject to look-direction constraint $\mu = \mathbf{w}^H\mathbf{c}(\theta)$. For the least squares solution, minimize:

$$E(n) = \sum_{t=1}^{n} |e(t)|^2 = \mathbf{w}^H\mathbf{M}(n)\mathbf{w} \quad (6.44a)$$

Subject to $\mu = \mathbf{w}^H\mathbf{c}(\theta)$

Least squares solution (Gauss normal equations):

$$\mathbf{M}(n)\mathbf{w}(n,\theta) = \lambda\mathbf{c}(\theta) \quad (6.44b)$$

where

$$M_{ij}(n) = \sum_{t=1}^{n} x_i(t)x_j^*(t) \quad (6.44c)$$

For the LMS algorithm, Minimize:

$$E\left\{|e(t)|^2\right\}$$

$$e(t) = \mathbf{w}^H\mathbf{x}(t) + y(t) \quad (6.44d)$$

Stochastic gradient updates

$$\mathbf{w}(t+1) = \mathbf{w}(t) - \mu e^*(t)\mathbf{x}(t) \quad (6.44e)$$

Iterative process defined by the LMS [27, 93]

$$\mathbf{w}(n+1) = \mathbf{w}(n) - 2\mu\mathbf{w}(n+1)\varepsilon^*\big(\mathbf{x}(t)\big) \quad (6.44f)$$

$$\varepsilon\big(\mathbf{w}(n)\big) = \mathbf{w}^H(n)\mathbf{x}(n+1) - r(n+1) \quad (6.44g)$$

By the quadratic characteristics of the mean square-error function $\varepsilon\{|e(k)|^2\}$ that has only one minimum, the steepest descent is guaranteed to converge. At adaptation index *k*, given a Mean-Square Error (MSE) function $\varepsilon\{|e(k)|^2\} = \varepsilon\{|d(k) - \boldsymbol{w}^H\boldsymbol{x}(k)|^2\}$, the LMS algorithm updates the weight vector according to

$$\mathbf{w}(k+1) = \mathbf{w}(k) - \frac{\mu}{2}\frac{\delta J_{\mathbf{w},\mathbf{w}^*}}{\delta \mathbf{w}^*}$$

$$= \mathbf{w}(k) + \mu e^{*}(k)\mathbf{x}(k) \quad (6.44h)$$

where $J_{\boldsymbol{w},\boldsymbol{w}^*}$ is the rate of change of the objective function, and is equal to $|e(k)|^2$ and μ is a scalar constant which controls the rate of convergence and stability of the algorithm. In order to guarantee the stability in the mean-squared sense, the step size μ should be restricted in the interval [10, 93]

$$0 < \mu < \frac{2}{\lambda_{max}} \quad (6.44i)$$

where λ_{max} is the maximum eigenvalue of R_{xx}. On the other hand, in terms of the total power of the vector **x** [10]:

$$\lambda_{max} \leq trace\{\boldsymbol{R}_{xx}\} \quad (6.44j)$$

where

$$trace\{\boldsymbol{R}_{xx}\} = \sum_{i=1}^{N} \varepsilon\{x_i^2\} \quad (6.44k)$$

is the total input power. Therefore, a condition for satisfactory Wiener solution convergence of the mean of the LMS weight vector is [10]

$$0 < \mu < 2\sum_{i=1}^{N} \varepsilon\left\{x_i^2\right\}^{-1} \quad (6.44l)$$

6.10.1 Simulation results for the proposed LMS algorithm

LMS and RLS nearly show equal dependence on SNR and SIR. The weights of the estimated system is nearly identical with the real one.

Table 6.1. LMS and RLS Algorithms Results

Beamforming Algorithm Analysis	M	Beamwidth	Sidelobe Level	Null depth (-18^0)	Null depth (35^0)
LMS	10	14^0	-9.5dB	-32dB	-38dB
	15	6^0	-9.8dB	-28dB	-32dB
	20	7^0	-13dB	-29dB	-27dB
RLS	10	13.57^0	-5.3dB	-21.37dB	-38.25dB
	15	6^0	-5.5dB	-25.23dB	-36.73dB
	20	7^0	-10.7dB	-16.31dB	-48.37dB

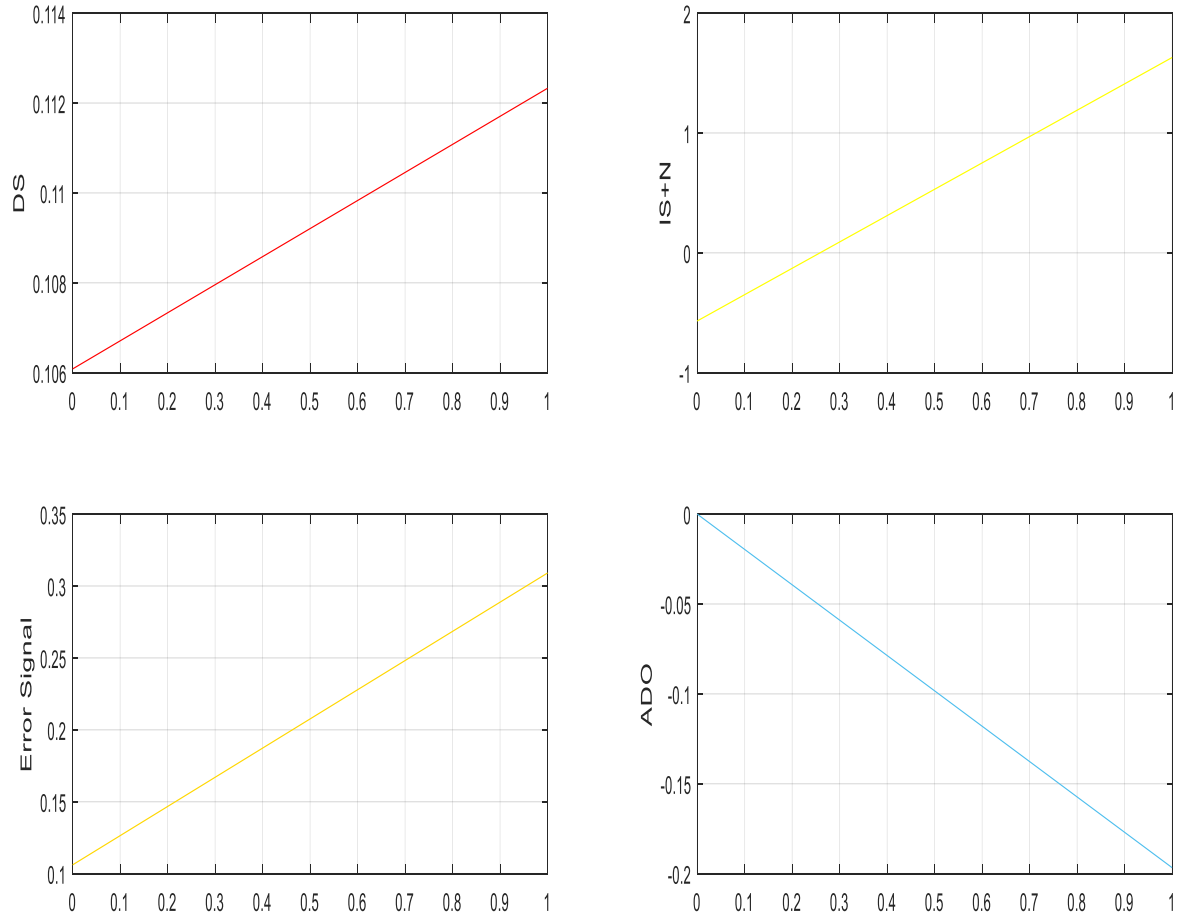

(a) LMS adaptive algorithm simulated curve.

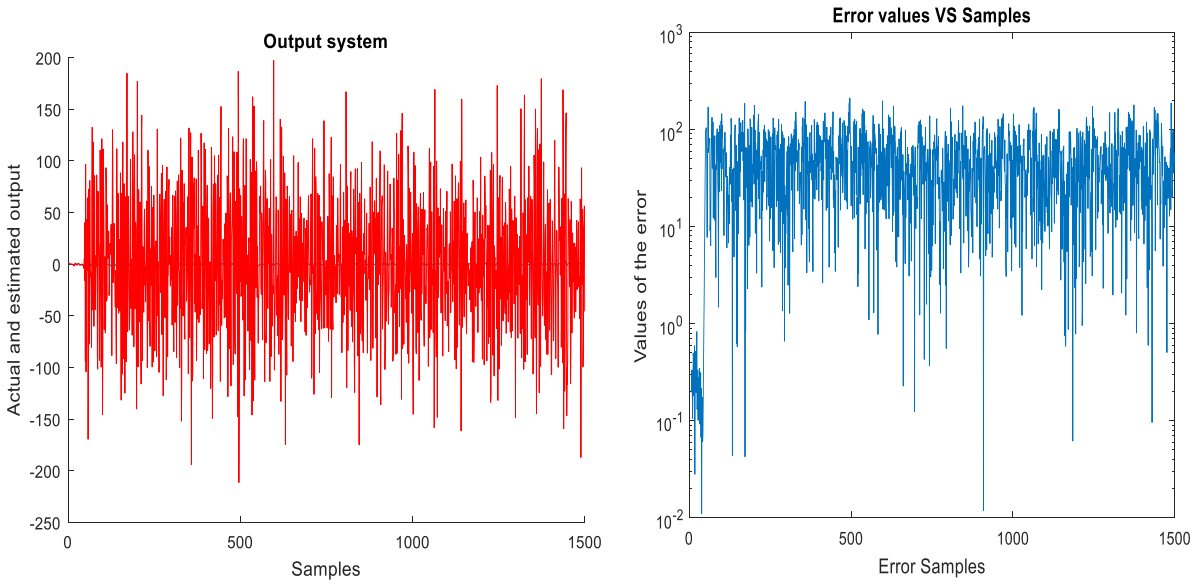

(b) LMS adaptive algorithm filtering curve.

Figure 6.11. LMS adaptive algorithm and filtering curve.

We have observed in Figure (6.11a) that equal number of antenna elements inputs (*N and mu*), the Desired Signal (DS) and the Adaptive Desired Output (ADO) starts from the origin and takes the same shape i.e. a straight line curve. If *N* > *mu*, all the shapes takes zig-zag curve. If *mu* > *N*, only the desired signal takes a straight line curve.

To minimize the error signal, we need adaptive filtering. This process is referred to as convergence. It is observed in Figure (6.11b) that adaptive filter takes a short time to calculate the error signal.

6.11 Recursive Least Square (RLS) Algorithm for the Proposed Model

The RLS is one of the greatest adaptive filter algorithms. It computes the requisite correlation matrix and vector repeatedly to lessen the computational intricacy with fast conversion rate [7]. For the tap input vector ***c(u)*** the autocorrelation of the order *M* x *M* is given by [91]

$$\boldsymbol{\vartheta} = \sum_{k=1}^{u} \lambda^{n-1}\, \mathbf{c}(b)\mathbf{c}^{H}(b) + \delta\lambda^{n}\mathbf{I}$$

where λ and δ are forgetting factor (positive constant) and the regularizing term. The tap input vector autocorrelation matrix and desire response can be expressed as

$$\mathbf{Y}(u) = \sum_{b=1}^{u} \frac{1}{\lambda} \cdot [\mathbf{c}(b)d^{*}(b)]$$

For RLS tricky, tap weight vector ***G(u)*** could be approached as

$$\boldsymbol{\vartheta}(u) = \frac{\mathbf{Y}(u)}{\mathbf{G}(u)}$$

Matrix inversion Lemma is applied to avoid computationally inefficient calculations of $\boldsymbol{\vartheta}^{-1}(n)$ [13]. Hence,

$$\boldsymbol{\vartheta}^{-1}(u) = \lambda^{-1}\frac{\mathbf{G}(u)}{\mathbf{Y}(u)}(u-1) - \frac{\lambda^{-2}\frac{\mathbf{G}(u)}{\mathbf{Y}(u)}(u-1)\mathbf{c}(u)\mathbf{c}^{H}(u)\frac{\mathbf{G}(u)}{\mathbf{Y}(u)}(u-1)}{1+\lambda^{-1}\mathbf{c}^{H}(u)\frac{\mathbf{G}(u)}{\mathbf{Y}(u)}(u-1)\mathbf{c}(u)}$$

Let ***b(u)*** represents M x 1 vector defined by the tap input vector as ***c(u)***. This can also be referred to as gain vector. The transformed inverse of the correlation matrix of $\frac{\mathbf{G}(u)}{\mathbf{Y}(u)}(u)$ results in

$$\mathbf{b}(u) = \boldsymbol{\vartheta}^{-1}(u)\boldsymbol{u}(u)$$

The weight upgradation equation in RLS is obtained [13]:

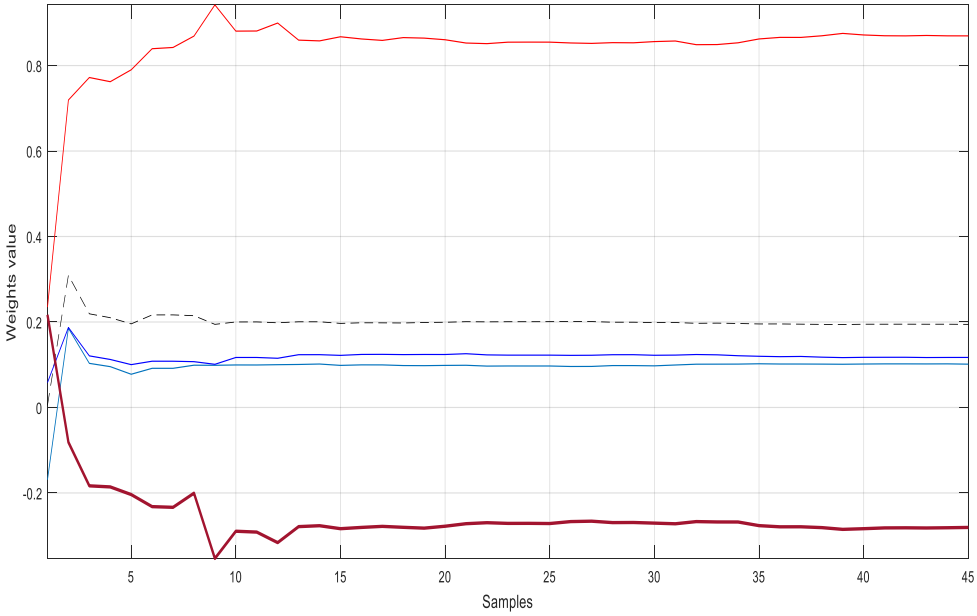

Figure 6.12. RLS adaptive algorithm curve for the proposed model.

$$\mathbf{G}(u) = \frac{\mathbf{G}(u)}{\sum_{b=1}^{u} \frac{1}{\lambda} \cdot [\mathbf{c}(b)d^{*}(b)]}(u)\mathbf{z}(u-1)$$

$$+\frac{\mathbf{G}(u)}{\sum_{b=1}^{u} \frac{1}{\lambda} \cdot [\mathbf{c}(b)d^{*}(b)]}(u)\mathbf{c}(u)d^{*}(u) - \mathbf{b}(u)\mathbf{c}^{H}(u)\frac{\mathbf{G}(u)}{\sum_{b=1}^{u} \frac{1}{\lambda} \cdot [\mathbf{c}(b)d^{*}(b)]}(u-1)\mathbf{z}(u-1)$$

Figure 6.12 shows the estimated weights convergence of the weights value and samples for the (RLS) algorithm. The RLS algorithm takes less number of iteration to achieve a steady state error with mean square error.

6.11.1 Recursive Least Square Algorithm with Adaptive Memory

The recursive least square algorithm with adaptive memory defined gradient can be expressed as [91]:

$$\varphi(x) = \frac{\delta G(x)}{\delta \tau} \tag{6.45}$$

Differentiating the cost function *B(x)* in regard to τ gives

$$\tilde{N}_{\tau} = \frac{\delta B(x)}{\delta \tau} = -\frac{1}{2} C\left[\tau^{H}(x-1)p(x)\xi^{*}(x) + p^{H}(x)\varphi(x-1)\xi(x)\right] \tag{6.46}$$

The updated weight vector for time x is given by gain vector **Q**(x) = **T**(x) **p**(x)

$$G(x) = G(x-1) + \mathbf{Q}(x)\xi^{*}(x) \tag{6.47}$$

where $\mathbf{Q}(x)$ is gain vector

$$\mathbf{Q} = \frac{\tau^{-1}T(x-1)p(x)}{1+\tau^{-1}p^{H}(x)T(x-1)p(x)} \tag{6.48}$$

and

$$\mathbf{T}(x) = \tau^{-1}\mathbf{T}(x-1) - \tau^{-1}\mathbf{Q}(x)\mathbf{p}^{H}(x)\mathbf{T}(x-1) \tag{6.49}$$

Let $\mathbf{O}(x)$ denote the derivative of the inverse correlation matrix T(x) with respect to τ:

$$\mathbf{O}(x) = \frac{\delta T(x)}{\delta \tau} \tag{6.50}$$

Differentiating Equation (6.49) with respect to τ

$$\mathbf{O}(x) = \tau^{-1}\left[\mathbf{K} - \mathbf{Q}(x)\mathbf{p}^{H}(x)\right]\mathbf{O}(x-1)\left[\mathbf{K} - \mathbf{p}(x)\mathbf{Q}^{H}(x) + \tau^{-1}\mathbf{Q}(x)\mathbf{Q}^{H}(x) - \tau^{-1}\mathbf{T}(x)\right]$$

Then using Equations (6.47) and (6.50) in Equation (6.45) yields

$$\varphi(x) = \left[\mathbf{K} - \mathbf{Q}(x)\mathbf{p}^{H}(x)\right]\varphi(x-1) + \mathbf{O}(x)\mathbf{p}^{H}(x)\xi^{*}(x) \tag{6.51}$$

According to Equation (6.46) , the forgetting factor $\tau(x)$ is adaptively computed

$$\tau(x) = \tau(x-1) + \omega \mathrm{Re}\left[\tau^{H}(x-1)\mathbf{p}(x)\xi^{*}(x)\right]$$

where ω is a small positive learning – rate parameter. The applicability of the RLS algorithm requires that we initialize the recursion of the equation (6.49) by choosing a starting value *T(0)* that assures the non-singularity of the correlation matrix [91]. To meet this requirement we may choose the initial value of T(x) with $\mathbf{T}(0) = \tau^{-1}\mathbf{K}$, where δ is the small positive constant and the initial value of weight vector is set to $\mathbf{G}(0) = \mathbf{0}$, where ***0*** is the *N x 1* null vector.

6.12 Conventional and Optimum Adaptive Beamforming Schemes for the Proposed Model

Several beamforming approaches exist, with varying degrees of complexity. A conventional beamformer, has equal weights and equal magnitudes [67]. Its algorithms depend on the notion of decreasing the output power of the array subject to a distortionless constriction.

For conventional beamformer, all the weights are given a magnitude of *1/N* but the individual weight has different phase [90, 91], i.e.

$$\mathbf{w} = \frac{1}{N}\mathbf{a}(\omega) = \frac{1}{N}\left[1, e^{-j\omega}, e^{-j2\omega} \ldots, e^{-j(N-1)\omega}\right]^{T}$$

where ***a****(ω)* is the steering vector.

For a uniform linear array (Figure 6.1), the relationship between θ and ω is given by

$$w(\theta_o) = \frac{1}{N}\sum_{n=0}^{N-1} w_n e^{-jn\omega}$$

where *w(θ)* is known as the array factor or beampattern, and $\omega = 2\pi d \sin\theta$. The beampattern can be written in vector notation as follows:

$$w(\theta_o) = \frac{1}{N}\sum_{n=0}^{N-1} w_n e^{-jn\omega} = w^H \mathbf{a}(\theta)$$

In a situation whereby only one signal is present and ignoring noise, the beamformer output with the conventional beamformer can be expressed as:

$$y_k = \mathbf{w}^H \mathbf{x}_k = s_o[k]\mathbf{w}^H\mathbf{a}(\theta) = s_o[k]\left(\frac{1}{N}\right)\mathbf{a}(\theta)\mathbf{a}(\theta)^H = s_o[k]$$

The beamformer output is said to be phase-aligned with the signal of interest and this seems undistorted at the output. The Signal to Noise Ratio (SNR) gain of the conventional beamformer can be computed by comparing the SNR at the output of a single element with the overall beamformer output. Assuming $E|v_n[k]|^2 = \sigma^2$ and knowing $|a_n(\theta)|^2 = 1$, the SNR of the signal received by the k[th] element can be computed by first considering the signal model for element k:

$$x_k[k] = a_k(\theta)s_o[k] + v_k[n]$$

The signal power is given by:

$$E_s = E\left[|a_k(\theta)s_o[k]|^2\right] = E\left[|s_o[k]|^2\right]$$

and the noise power is:

$$E_n = E\left[|v_n[k]|^2\right] = \sigma^2$$

Assuming $E\left[\mathbf{v}_k\mathbf{v}_k^H\right] = \sigma^2\mathbf{I}$ and knowing $\mathbf{a}(\theta)^H\mathbf{a}(\theta) = N$, the SNR of the signal at the beamformer output can be computed by first examining the beamformer output, i.e.,

$$y_k = \mathbf{w}^H\left(\mathbf{a}(\theta)s_o[k] + \mathbf{v}_k\right) = s_o[k] + \mathbf{w}^H\mathbf{v}_k$$

The signal power is given by,

$$E_s = E\left[|s_o[k]|^2\right]$$

And the noise power is given by,

$$E_n = E\left[\left|\mathbf{w}^H\mathbf{v}_k\right|^2\right] = \frac{1}{N^2}E\left[\mathbf{a}(\theta)^H\mathbf{v}_k\mathbf{v}_k^H\mathbf{a}(\theta)\right] = \frac{N\sigma^2}{N^2}$$

Hence, the SNR for the overall beamformer output is $\left(\frac{E_s}{E_n}\right) = \left(\frac{NE_s}{\sigma^2}\right)$. The SNR has increased by a factor of N over the SNR at the output of a single element.

In optimum beamforming, the knowledge of directions and power levels of interferences source is neither required nor the level of the background noise power, but requires the knowledge of the directions of the desired signal characteristic [44]. This can be based on either its statistics of; (a) Maximum SNR, and (b) Reference signal method. If the knowledge of the desired signal required is inaccurate, the desired signal will be attenuated by the optimum beamformer as if it were interference. Optimal beamformer is also referred to as the Minimum Variance Distortionless Response (MVDR) beamformer [14]. For optimum beamformer array, the outputs sensor are joined by a weight vector in order to receive desired signal without distortion, while simultaneously rejecting interfering signals to the barest minimum. A satisfactory quality of service at economical rate is always delivered by the optimum beamforming system. This continually serve numerous users. Whenever the broadband signals is of reference point, beamforming can be implemented in the frequency domain.

From Figure 6.1, let L-dimensional complex vector *w* represents the weights of the beamformer shown that maximizes the output SNR. The unconstrained array, *w* can be expressed as:

$$\hat{w} = \mu_0 R_N^{-1} S_o \tag{6.52}$$

The array correlation matrix R can be expressed as

$$R = P_s\mathbf{S}_o\mathbf{S}_o^H + P_I\mathbf{S}_I^H R_N^{-1} + \sigma_n^2 I$$

For the processor, the mean output power can be expressed as

$$\hat{p} = \hat{w}^H R\hat{w}$$

$$\hat{p} = P_s S_o S_o^H\hat{w} + P_I\hat{w}^H S_I S_I^H\hat{w} + \sigma_n^2\hat{w}^H\hat{w}$$

so, $\hat{p}_s = P_s\hat{w}^H S_o S_o^H\hat{w}$

$$\hat{p}_I = P_I\hat{w}^H S_I S_I^H\hat{w} \ = \sigma_n^2\hat{w}^H\hat{w}$$

Substituting for w:

$$\hat{p}_s = P_s\mu_o^2\left(S_o^H R_N^{-1} S_o\right)^2$$

$$\hat{p}_I = \mu_o^2 S_o^H R_N^{-1} R_I R_N^{-1} S_o \tag{6.53}$$

$$\hat{p}_n = \sigma_n^s \hat{\beta} \mu_o^2 \left(S_o^H R_N^{-1} S_o \right)^2 \tag{6.54}$$

where R_I is the correlation matrix of interference and

$$\beta = \frac{S_o^H R_N^{-1} R_N^{-1} S_o}{\left(S_o^H R_N^{-1} S_o \right)^2}$$

The total noise at the output is given by $\hat{P}_N = \hat{P}_I + \hat{P}_n$

Substituting from (6.53) and (6.54), total noise becomes:

$$\begin{aligned}
\hat{P}_N &= \mu_o^2 \left(S_o^H R_N^{-1} R_I R_N^{-1} S_o + \sigma_n^2 S_o^H R_N^{-1} R_N^{-1} S_o \right) \\
&= \mu_o^2 S_o^H R_N^{-1} \left(R_I + \sigma_n^2 I \right) R_N^{-1} S_o \\
&= \mu_o^2 S_o^H R_N^{-1} R_N R_N^{-1} S_o \\
&= \mu_o^2 S_o^H R_N^{-1} S_o
\end{aligned}$$

For two identical processor without errors, the processor has the same performance in both cases. This fact can be proved as follows. The matrix inversion lemma states that

$$(\mathbf{A} + \mathbf{XYZ})^{-1} = \mathbf{A}^{-1} - \mathbf{A}^{-1}\mathbf{X}(\mathbf{ZA}^{-1}\mathbf{X} + \mathbf{Y}^{-1})^{-1}\mathbf{ZA}^{-1}$$

An important special case is where **X** is an Mx1 column vector **X**, **K** is a scalar c, and **Z** = $\mathbf{X}^H$:

$$(\mathbf{A} + k\mathbf{X}\mathbf{X}^H)^{-1} = \mathbf{A}^{-1} - \frac{\mathbf{A}^{-1} + \mathbf{X}\mathbf{X}^H\mathbf{A}^{-1}}{k^{-1} + \mathbf{X}^H\mathbf{A}^{-1}\mathbf{X}}$$

Therefore, for Matrix Inversion Lemma for an invertible matrix **A** or Woodbury's identity is obtained by setting k =1 such that

$$(\mathbf{A} + \mathbf{X}\mathbf{X}^H)^{-1} = \mathbf{A}^{-1} - \frac{\mathbf{A} + \mathbf{X}\mathbf{X}^H\mathbf{A}^{-1}}{1 + \mathbf{X}^H\mathbf{A}^{-1}\mathbf{X}}$$

since $R = P_s \mathbf{S}_o \mathbf{S}_o^H + R_N$

$$R^{-1} = R_N^{-1} - \frac{P_s R_N^{-1} \mathbf{S}_o \mathbf{S}_o^H R_N^{-1}}{1 + \mathbf{S}_o^H R_N^{-1} \mathbf{S}_o P_s}$$

and

$$R^{-1}\mathbf{S}_o = R_N^{-1}\mathbf{S}_o - \frac{P_s R_N^{-1} \mathbf{S}_o \mathbf{S}_o^H R_N^{-1} \mathbf{S}_o}{1 + \mathbf{S}_o^H R_N^{-1} \mathbf{S}_o P_s}$$

$$= \frac{R_N^{-1}\mathbf{S}_o (1 + \mathbf{S}_o^H R_N^{-1} \mathbf{S}_o P_s) - P_s R_N^{-1} \mathbf{S}_o \mathbf{S}_o^H R_N^{-1} \mathbf{S}_o}{1 + \mathbf{S}_o^H R_N^{-1} \mathbf{S}_o P_s}$$

$$= \frac{R_N^{-1} S_o}{1 + S_o^H R_N^{-1} S_o P_s} \tag{6.55}$$

P_s and R_N^{-1} are scalar, $\boldsymbol{S}_o$ and $\boldsymbol{S}_o^H$ are vector matrix.

and

$$S_o^H R_N^{-1} S_o = \frac{S_o^H R_N^{-1} S_o}{1 + S_o^H R_N^{-1} S_o P_s} \tag{6.56}$$

P_s and R_N^{-1} are scalar, $\boldsymbol{S}_o$ and $\boldsymbol{S}_o^H$ are vector matrix.

Equations (6.51), (6.55), and (6.56) imply

$$\hat{w} = \frac{R_N^{-1} S_o}{1 + S_o^H R_N^{-1} S_o}$$

Thus,

$$\hat{w} = \hat{w}$$

6.13 Conclusions

The closed-form expression for the smart antennas adaptive beamforming algorithms has been derived in this chapter. The adaptive beamforming are used as a technique to create the radiation pattern on antenna array by the addition of the signals weights constructively in the preferred direction of signal and nulling pattern in the interference direction. The following are the observation as the antenna element spacing are increasing; narrower main lobe, grating lobes, reduction in beamwidth thus making the array more directional, and reduction in sidelobe level, thus improving beamforming. It is also observed that there is no grating lobe when $d/\lambda = 0.5$, which we considered as the optimal design spacing for the array antenna elements in the smart antenna. The LMS and RLS algorithms results were evaluated for their convergence rate and beamforming.

CHAPTER 7

Conclusions and Future Scope

This chapter presents a succinct of this thesis and possible future research works has been suggested.

7.1 Conclusions

Various methods and approaches by which smart antenna arrays could be analysed and design has been highlighted in this research work. Circular pin-fed linearly polarized patch antenna and waveguide-fed pyramidal horn antenna are used as antenna elements. The design of smart antenna using waveguide-fed pyramidal horn antenna gives a better system performance of directional radiation beam pattern with a high gain and wide impedance bandwidth. The mathematical model for uniform and circular array radiation synthesis has been established. The analysis and design of smart antenna system with directivity that operates at frequency range from *0.3 THz* to *3 THz* has been considered. Dolph-Chebyshev has been applied for the synthesis of antenna array radiation pattern model.

Also, smart antenna system using an *8 x 8* planar phased-array antenna has been considered in this research work. Therefore, it offers the synthesis of a needed beam pattern which is not obtainable with a single patch antenna element. Using a planar phased array antenna yields various, concurrent readily obtainable beams. These beams have high gain directivity, optimum side lobe suppression, and beam width controlled. However, Planar phased array antenna can automatically adjust the array pattern to optimize some typical features of the received signal i.e. phases and amplitudes.

The adaptive beamforming has been used as a technique to create the radiation pattern on antenna array by the addition of the signals weights constructively in the preferred direction of signal and nulling pattern in the interference direction. The closed-form expression for the smart antennas adaptive beamforming algorithms has been derived.

With the model developed in this research, smart antenna arrays has been able to improve radiation in one direction and null out interference in other direction through its distinctive increase in directivity, which leads to gain in a specific direction. This research work has been applied in the RF security systems for security purpose. Higher degree of freedom has been achieved in the smart antenna arrays using a spatial signal processing, which improved system

performance. The derived smart antenna power has been able to steer and reshape its radiation pattern to maximize Signal to Interference and Noise Ratio (SINR). With the adaptive beamforming model developed in this research work, co-channel interference has been suppressed. Hence, system immunity to multipath has been improved.

7.2 Recommendations for Future Research Works

It will be of optimum interest if the geometries and weights of different antenna elements could be optimized. Antenna array are normally performed with identical elements, and it will be a research break-through provided gains could be made through exploiting of radiation pattern with different elements.

Moreover, when a smart antenna is being implemented on the wireless communication area, some new areas of concentration that may be considered for future works are:

- Modeling of the nonlinearities at the receiving and transmitting end in order to incorporate instabilities and mutual antenna coupling of the antenna arrays. To convert noise in some of the nonlinear devices for multicarrier applications is worrisome and call for research.
- Spatial-temporal multiuse algorithms to significantly improve the signal processing power at affordable cost at the user ends.
- Reduction in size for terminal applications is another issue that must be well care for in design.
- Fabrication and implementation factors were not considered for smart antennas security in chapter two of this thesis, it will be of optimum interest if this could be considered for commercial purpose.
- In order to evaluate the validity of the developed theoretical model, extensive measurements need to be carried out. Furthermore, the effect user's hand and head on the performance of handheld smart antenna arrays is a topic of interest. Use of phantom heads and hands in theoretical and experimental work results in gain imbalance between antenna elements in the array as one of more antennas could be covered by the user's head or hand. This will provide the important design information for smart antenna arrays such as the use of different antenna elements and positioning of antenna elements on the handset so that the radiation pattern of the element can be directed away from user's head and hand.

- In multiple user and multiple Base Station (BS) investigations, effort can also be given to the consideration on how spatial interference cancellation techniques can be used in compact smart antenna arrays. Such investigation is vital in interference limited scenarios particularly on the cell edges where there is strong interference from adjacent cells.

REFERENCES

1. A. S. Oluwole and V. M. Srivastava, "Designing of smart antenna for improved directivity and gain at terahertz frequency range," *Progress in Electromagnetics Research Symposium (PIERS),* Shanghai, China, pp. 473, Aug. 2016.
2. A. S. C. Svendsen and J. J. Gupta. "The effect of mutual coupling on the nulling performance of adaptive antennas," *IEEE Antennas and Propagation Magazine*, vol. 54, no. 3, pp. 17-38, June 2012.
3. I. Tzanidis, K. Sertel, and J. L. Volakis, "Characteristic excitation taper for ultrawideband tightly coupled antenna arrays," *IEEE Transactions on Antennas and Propagation,* vol. 60, no. 4, pp. 1777-1784, April 2012.
4. A. N. Jabbar, "A novel ultra-fast ultra-simple adaptive blind beamforming algorithm for smart antenna arrays," *Progress in Electromagnetics Research B,* vol. 35, pp. 329-348, 2011.
5. S. A. Schelkunoff, "A mathematical theory of linear arrays," *Bell System Technical Journal*, vol. 22, pp. 80-107, 1943.
6. B. Goswami and D. Mandal, "A genetic algorithm for the level control of nulls and side lobes in linear antenna arrays," *Journal of King Saud University-Computer and Information Sciences,* vol. 25, pp. 117-126, July 2012.
7. H. Gazzah and J. P. Delmas, "Direction finding antenna arrays for the randomly located sources," *IEEE Transactions on Signal Processing*, vol. 60, no. 11, pp. 6063-6068, Nov. 2012.
8. A. S. S. Rao and P. M. Rao, "Design and analysis of array weighted wideband antenna using FRFT," *International Arab Journal of Information Technology,* vol. 10, no. 4, pp. 373-377, July 2013.
9. A. Kalis, A. G. Kanatas, and C. B. Papadias, *Parasitic Antenna Arrays for Wireless MIMO Systems,* Springer New York, (Oct. 2013).
10. C. A. Balanis and P. I. Ioannides, *Introduction to Smart Antennas,* Morgan & Claypool, 2007.
11. F. R. Farrokhi, K. J. R. Liu, and L. Tassiulas, "Transmit beamforming and power control for cellular wireless systems," *IEEE Journal on Selected Areas in Communication,* vol. 16, no. 8, pp. 1437-1450, Oct. 1998.

12. R. M. Radaydeh and M. S. Alouini, “Comparisons of receive array interference reduction techniques under erroneous generalized transmit beamforming,” *IEEE Transactions on Communication,* vol. 62, no. 2, pp. 600-615, Feb. 2014.
13. J. Liu, H. Li, and B. Himed, “Joint optimization of transmit and receive beamforming in active arrays,” *IEEE Signal Processing Letters*, vol. 21, no. 1, pp. 39-42, Jan. 2014.
14. B. Friedlander and B. Porat, “Performance analysis of a null-steering algorithm based on direction-of-arrival estimation,” *IEEE Transactions on Acoustics, Speech, and Signal Processing,* vol. 37, no. 4, pp. 461-466, April 1989.
15. H. Krim and M. Viberg, “Two decades of array signal processing research: the parametric approach,” *IEEE Signal Processing Magazine,* vol. 13, no. 4, pp. 67-94, July 1996.
16. M. Y. Khattak and P. Akhtar, “Fully automatic gain control beamformer for smart antenna array system,” *The International Journal for Computation and Mathematics in Electrical and Electronic Engineering*, vol. 35, no. 3, pp. 1086-1097, 2016.
17. Z. D. Zaharis, C. Skeberis, and T. D. Xenos, “Improved antenna array adaptive beamforming with low side lobe level using a novel adaptive invasive weed optimization method,” *Progress in Electromagnetics Research,* vol. 124, pp. 137-150, 2012.
18. T. S. G. Basha, P. V. Sridevi, and M. N. G. Prasad, “Beam forming in smart antenna with precise direction of arrival estimation using improved MUSIC,” *Wireless Personal Communication,* vol. 71, no. 2, pp. 1353-1364, July 2013.
19. X. Wang, E. Aboutanios, M. Trinkle, and M. G. Amin, “Reconfigurable adaptive array beamforming by antenna selection,” *IEEE Transactions on Signal Processing*, vol. 62, no. 9, pp. 2385-2396, May 2014.
20. L. Desheng, L. Songtao, S. Jinping, and W. Jun, “Coordinated adaptive beamformer over distributed antenna network,” *Chinese Journal of Aeronautics,* vol. 26, no. 2, pp. 357-362, April 2013.
21. Q. Zhou, H. Gao, H. Zhang, and F. Wang, “Robust superdirective beamforming for HF circular receive antenna arrays,” *Progress In Electromagnetics Research,* vol. 136, pp. 665-679, 2013.
22. Y. L. Chen and J. H. Lee, “Performance evaluation of DFT beamforminers for broadband antenna array processing,” *Progress In Electromagnetics Research,* vol. 139, pp. 57-86, 2013.

23. R. G. Lorenz and S. P. Boyd, “Robust minimum variance beamforming,” *IEEE Transactions on Signal Processing*, vol. 53, no. 5, pp. 1684-1696, May 2005.
24. S. A. Vorobyov, A. B. Gershman, and Z. Q. Luo, “Robust adaptive beamforming using worst-case performance optimization: a solution to the signal mismatch problem,” *IEEE Transactions on Signal Processing*, vol. 51, no. 2, pp. 313-324, Feb. 2003.
25. B. D. V. Veen and K. M. Buckley, “Beamforming: a versatile approach to spatial filtering,” *IEEE ASSP Magazine*, vol. 5, no. 2, pp. 4-24, April 1998.
26. K. Slavakis and I. Yamada, “Robust wideband beamforming by the hybrid steepest descent method,” *IEEE Transactions on Signal Processing*, vol. 55, no. 9, pp. 4511-4522, Sept. 2007.
27. F. Babich, M. Comisso, M. D. Orlando, and L. Mania, “Interference mitigation on WLANs using smart antennas,” *Wireless Personal Communication*, vol. 36, no. 2, pp. 387-401, March 2006.
28. H. T. Liu, S. Gao, and T. H. Loh, “Electrically small and low cost smart antenna for wireless communication,” *IEEE Transactions on Antennas and Propagation*, vol. 60, no. 3, pp. 1540-1549, March 2012.
29. J. Fuhl and E. Bonek, “Temporal reference algorithms versus spatial reference algorithms for smart antennas,” *Wireless Personal Communication*, vol. 9, pp. 271-293, 1998.
30. F. B. Gross. *Smart Antennas for Wireless Communications with MATLAB*. 1st Ed., McGraw-Hill, New York, (2005).
31. J. A. Stine, “Exploiting smart antennas in wireless mesh networks using contention access,” *IEEE Wireless communication*, vol. 13, no. 2, pp. 38-49, April 2006.
32. M. Uthanksul and M. E. Bialkowski, “A wideband smart antenna employing spatial signal processing,” *Journal of Telecommunications and Information Technology*, pp. 13-17, 2007.
33. J. Hong, S. Kawakami, C. N. Nyirenda, and T. Ohtsuki, “Array antenna based localization using spatial smoothing processing,” *Journal of Communication*, vol. 7, no. 6, pp. 427-435, June 2012.
34. F. Hutu, D. Cordeau, and J. M. Paillot, “2.4 GHz antenna array using vector modulator-based active phase shifters for beamforming,” *IET Microwaves Antennas and Propagation*, vol. 5, no. 2, pp. 245-254, 2011.
35. K. R. Jha and G. Singh, “Terahertz planar antennas for wireless communication: a technical review” *Infrared Physics and Technology*, vol. 60, pp. 71-80, Sept. 2013.

36. A. S. Oluwole and V. M. Srivastava, “Smart antenna for wireless communication systems using spatial signal processing,” *Journal of Communications*, vol. 12, no. 6, pp. 328-339, June 2017.
37. T. D. Hong and P. Russer, “Signal processing for wideband smart antenna array applications,” *IEEE Microwave Magazine*, vol. 5, no. 1, pp. 57- 67, March 2004.
38. S. Lu, J. Sun, G. Wang, and J. Tian, “A novel GSC beamformer using a combination of two adaptive filters for smart antenna array,” *IEEE Antennas and Wireless Propagation Letters*, vol. 11, pp. 377-380, April 2012.
39. J. Dmochowski, J. Benesty, and S. Affes, “On spatial aliasing in microphone arrays,” *IEEE Transactions on Signal Processing*, vol. 57, no. 4, pp. 1383-1395, April 2009.
40. D. C. Chang and C. N. Hu, “Smart antennas for advanced communications,” *Proceedings of the IEEE*, vol. 100, no. 7, pp. 2233-2249, July 2012.
41. X. Huang, J. Guo, and J. D. Bunton, “A hybrid adaptive antenna array,” *IEEE Transactions on Wireless Communications*, vol. 9, no. 5, pp. 1770-1779, May 2010.
42. R. L. Haupt, *Antenna Arrays: A Computational Approach*. New Jersey: John Wiley and Sons, 2010.
43. J. Dmochowski, J. Benesty, and S. Affes, “An information-theoretic view of array processing,” *IEEE Transactions on Audio, Speech, and Language Processing*, vol. 17, no. 2, pp. 392-401, Feb. 2009.
44. H. Sing and R. M. Jha, “Trends in adaptive array processing,” *International Journal of Antennas and Propagation*, pp. 1-20, 2012.
45. R. L. Haupt, “Antenna arrays in the time domain: an introduction to timed arrays,” *IEEE Antennas & Propagation Magazine*, vol. 59, no. 3, pp. 33-41, June 2017.
46. R. A. Monzingo, R. L. Haupt, and T. W. Miller, *Introduction to Adaptive Arrays*, 2nd Ed., SCITECH Publishing, Inc., 2011.
47. S. Bellofiore, C. A. Balanis, J. Foutz, and A. S. Spanias, “Smart-antenna systems for mobile communication networks part 1: overview and antenna design,” *IEEE Antennas and Propagation Magazine*, vol. 44, no. 3, pp. 145-154, June 2002.
48. S. Bellofiore, J. Foutz, C. A. Balanis, and A. S. Spanias, “Smart antenna system for mobile communication networks part 2: beamforming and network throughput,” *IEEE Antennas and Propagation Magazine*, vol. 44, no. 4, pp. 106-114, Aug. 2002.
49. H. Elkamchouchi and M. Hassan, “A wideband direct data domain genetic algorithm beamforming,” *Radioengineering*, vol. 24, no. 1, pp. 80-86, April 2015.

50. A. U. Bhobe and P. L. Perini, “An overview of smart antenna technology for wireless communication,” *IEEE Aerospace Conference*, Montana, USA, vol. 2, pp. 875-883, March 2001.
51. H. Liu, S. Gao, T. H. Loh, and F. Qin, “Low-cost intelligent antenna with low profile and broad bandwidth,” *IET Microwaves Antennas and Propagation,* vol. 7, no. 5, pp. 356-364, 2013.
52. C. Bunsanit, P. Uthansakul, and M. Uthansakul, “Refinement method for weighting scheme of fully spatial beamformer,” *International Journal of Antennas and Propagation,* vol. 2012, pp. 1-13, June 2012.
53. S. Bellofiore, J. Foutz, C. A. Balanis, and A. S. Spanias, “Smart-antenna system for mobile communication networks part 2: beamforming and network throughput,” *IEEE Antenna Propagation, Magazine,* vol. 44, no. 4, pp. 106-114, Aug. 2002.
54. C. A. Balanis, *Antenna Theory: Analysis and Design,* 3rd ed., John Wiley & Sons, Inc., Hoboken, New Jersey, (2005).
55. J. R. Mohammed and K. H. Sayidmarie, “Null steering method by controlling two elements,” *IET Microwaves Antennas Propagation*, vol. 8, no. 15, pp. 1348-1355, 2014.
56. H. Tong and W. Geyi, “Optimal design of smart antenna systems for handheld devices,” *IET Microwaves, Antennas and Propagation*, vol. 10, no. 6, pp. 617-623, April 2016.
57. F. G. Khodaei, J. Nourinia, and C. Ghobadi, “Adaptive beamforming algorithm with increased speed and improved reliability for smart antennas,” *Journal of Computers and Electrical Engineering,* vol. 36, no. 6, pp. 1140-1146, Nov. 2010.
58. H. Wang, Z. Zhang, Y. Li, and M. F. Iskander, “A switched beam antenna with shaped radiation pattern and interleaving array architecture,” *IEEE Antennas and Wireless Propagation,* vol. 63, no. 7, pp. 2914-2921, July 2015.
59. M. Haardt and Q. Spencer, “Smart antennas for wireless communications beyond the third generation,” *Computer Communication,* vol. 26, pp. 41-45, 2003.
60. T. S. G. Basha, M. N. G. Prasad, and P. V. Sridevi, “Beamforming in smart antenna with improved gain and suppressed interference using genetic algorithm,” *Central European Journal of Computer Science*, vol. 2, no. 1, pp. 33-46, March 2012.
61. R. S. Dhanaraj, L. Gudino, and J. Rodrigues, “Development of adaptive beamforming algorithms for wireless communication networks,” *IEEE International Conference on Recent Trends in Information Technology (ICRTI),* Tamil Nadu, pp. 18-23, June 2011.

62. C. H. Hsu, “Uplink MIMO-SDMA optimization of smart antennas by phase-amplitude perturbations based on memetic algorithms for wireless and mobile communication systems,” *IET Communications*, vol. 1, no. 3, pp. 520-525, June 2007.
63. M. D. Filippo, L. Lucci, D. Marabisi, and S. Selleri, “Design of a smart antenna for mobile ad hoc network applications,” *International Journal of Antennas and Propagation*, vol. 2015, pp. 1-7, 2015.
64. S. Goel and R. Negi, “Guaranteeing secrecy using artificial noise,” *IEEE Transaction on Wireless Communications*, vol. 7, no. 6, pp. 2180-2189, June 2008.
65. A. S. Oluwole and V. M. Srivastava, “Modeling of RF security system using smart antennas,” *IEEE International Conference on Cyberspace Governance (Cyber-Abuja)*, Abuja, Nigeria, pp. 118-112, Dec. 2015.
66. A. Alexiou and M. Haardt, “Smart antenna technologies for future wireless systems: trends and challenges,” *IEEE Communications Magazine*, pp. 90-97, Sept. 2004.
67. N. Herscovici and C. Christodoulou, “Potentials of smart antennas in CDMA systems and uplink improvement,” *IEEE Antennas and Propagation Magazine*, vol. 43, no. 5, pp. 172-177, Oct. 2001.
68. A. S. Oluwole and V. M. Srivastava, “Design of smart antenna using waveguide-fed pyramidal horn antenna for wireless communication systems,” *Annual IEEE India Conference (INDICON)*, New Delhi, India, pp. 1-5, Dec. 2015.
69. A. S. Oluwole and V. M. Srivastava, “Design of smart antenna by circular pin-fed linearly polarized patch antenna,” *International Journal of Wireless and Microwaves Technologies*, vol. 6, no. 3, pp. 40-49, May 2016.
70. Ayodele S. Oluwole and Viranjay M. Srivastava, “Determination of directivity and gain for improved performance of smart antenna,” *International Journal on Communications Antenna and Propagation*, vol. 7. no. 4, Sept. 2017.
71. K. R. Jha and G. Singh, “Design of highly directive cavity type terahertz antenna for wireless communication,” *Optics Communications*, vol. 284, no. 20, pp. 4996-5002, Jan 2011.
72. A. S. Oluwole and V. M. Srivastava, Design of smart antenna using planar phased-array antenna for wireless communication systems, *IEEE International Conference on Trends in Automation, Communications and Computing Technology (ITACT-15)*, Bangalore, India, pp. 113-119, Dec. 2015.

73. D. Inserra and A. M. Tonello, “A multiple antenna wireless testbed for the validation of DOA estimation algorithms,” *International Journal of Electronics and Communications*, vol. 68, no. 1, pp. 10-18, Jan. 2014.
74. M. Mizuno and T. Ohgane, “Application of adaptive array antennas to radio communications,” *Electronics and Communications in Japan*, vol. 77, no. 2, pp. 733-741, Nov. 1994.
75. K. R. Jha and G. Singh, “Comparison method to predict the directivity of terahertz patch antenna,” Terahertz Planar Antennas for Next Generation Communication, Springer International Publishing Switzerland, pp. 147-166, Jan. 2014.
76. R. L. Haupt and Y. R. Samil, “Antenna array developments: a perspective on the past, present and future,” *IEEE Antennas and Propagation Magazine*, vol. 57, no. 1, pp. 86-96, Feb. 2015.
77. J. Babu and G. S. N. Raju, “Generation of cosecant beams from circular arrays,” *International Journal of Electronics and Communications*, vol. 67, no. 2, pp. 81-87, Feb. 2013.
78. A. Sharaqa and N. Dib, “Position-only side lobe reduction of a uniformly excited elliptical antenna array using evolutionary algorithms,” *IET Microwaves Antennas Propag*ation, vol. 7, no. 6, pp. 452-457, 2013.
79. H. L. V. Trees. *Optimum Array Processing (Part IV of Detection, Estimation, and Modulation Theory)*. 1st Ed., Wiley-Interscience, March 2002.
80. S. N. Makarov, *Antennas and EM Modeling with MATLAB*, John Wiley & Sons, Inc., Canada, (2002).
81. S. Das, D. Mandal, R. Kar, and S. P. Ghoshal, “A generalized closed form expression of directivity of arbitrary planar antenna arrays,” *IEEE Trans. on Antennas and Propag*., vol. 61, no. 7, pp. 3909-3912, July 2013.
82. G. Ram, D. Mandal, R. Kar, and S. P. Ghoshal, “Directivity maximization and optimal far-field pattern of time modulated linear antenna arrays using evolutionary algorithms,” *International Journal of Electronics Communications*, pp. 1-10, Sept. 2015.
83. C. T. Chang, C. Y. Chang, T. L. Wang, and Y. J. Lu, “Throughput enhancement by exploiting spatial reuse opportunities with smart antenna systems in wireless ad hoc networks,” *Computer Networks*, vol. 57, no. 13, pp. 2483-2498, Sept. 2013.
84. N. U. Saqib and M. Khan, “A hybrid antenna array design for 3-D direction of arrival estimation,” *PLoS One*, vol. 10, no. 3, pp. 1-12, March 2015.

85. M. A. Panduro, D. H. Covarrubias, C. A. Brizuela, and F. R. Marante, “A multi-objective approach in the linear antenna array design,” *International Journal of Electronics and Communications*, vol. 59, no. 4, pp. 205-212, June 2005.
86. D. Mandal, S. P. Ghoshal, and A. K. Bhattacharjee, “Optimized radii and excitations with concentric circular antenna array for maximum sidelobe level reduction using wavelet mutation based particle swarm optimization techniques,” *Telecommunication Systems* vol. 2013, no. 52, pp. 2015-2025, June 2011.
87. J. A. Srar, K. S. Chung, and A. Mansour, “Adaptive array beamforming using a combined LMS-LMS algorithm,” *IEEE Transactions on Antennas and Propagation* vol. 58, no.11, pp. 3545-3557, Nov. 2010.
88. T. S. G. Basha, G. Aloysius, B. R. Rajakumar, M. N. G. Prasad, and P. V. Sridevi, “A constructive smart antenna beam-forming technique with spatial diversity,” *IET Microwaves Antennas Propagation*, vol. 6, no. 7, pp. 773-780, 2012.
89. T. S. G. Basha, G. Aloysius, B. R. Rajakumar, M. N. G. Prasad, and P. V. Sridevi, “A constructive smart antenna beam-forming technique with spatial diversity,” *IET Microwaves Antennas Propagation*, vol. 6, no. 7, pp. 773-780, 2012.
90. J. Foutz, A. Spanias, and M. K. Banavar, *Narrowband Direction of Arrival Estimation for Antenna Arrays*, 1st ed. Arizona State University: Morgan & Claypool, 2008.
91. S. Haykin, *Adaptive Filter Theory*, 5th Ed. Pearson Education Ltd., England, 2014.
92. C. B. Dietrich, W. L. Stutzman, B. K. Kim, and K. Dietze, “Smart antennas in wireless communications: base-station diversity and handset beamforming,” *IEEE Antennas and Propagation Magazine*, vol. 42, no. 5, pp. 142-151, Oct. 2000.
93. R. L. Ali, S. A. Khan, A. Ali, A. U. Rehman, and S. A. Malik, “A robust least mean square algorithm for adaptive array signal processing,” *Wireless Personal Communications*, vol. 68, pp. 1449-1461, vol. 2013, no. 68, Feb. 2012.
94. R. H. Kwong and E. W. Johnston, “A variable step size LMS algorithm,” *IEEE Transactions on Signal Process*ing vol. 40, no. 7, pp. 1633-1642, July 1992.
95. B. Wang, Y. Chang, and Y. Sun, “Performance of the large-scale adaptive array antennas in the presence of mutual coupling,” *IEEE Transactions on Antennas and Propagation*, vol. 64, no. 6, pp. 2236-2245, June 2016.
96. I. J. Gupta and A. A. Ksienski, “Effect of mutual coupling on the performance of adaptive arrays,” *IEEE Transactions on Antennas and Propagation*, vol. AP-31, no. 5, pp. 785-791, Sept. 1983.

97. H. T. Hui, “A practical approach to compensate for the mutual coupling effect in an adaptive dipole array,” *IEEE Transactions on Antennas and Propagation*, vol. 52, no. 5, pp. 1262-1269, May 2004.

98. G. Babur, P. J. Aubry, and F. L. Chevalier, “Antenna coupling effects for space-time radar waveforms: analysis and calibration,” *IEEE Transactions on Antennas and Propagation*, vol. 62, no. 15, pp. 2572-2586, May 2014.

99. M. A. Abdala and A. M. Abdelraheem, “Compact transmit receive hybrid electromagnetic isolation in antenna array transceiver system for full duplex applications,” *IET Microwaves Antennas Propagation*, vol. 11, no. 3, pp. 417-425, 2017.

100. H. M. Bernety and A. B. Yakovlev, “Reduction of mutual coupling between neighboring strip dipole antennas using confocal elliptical metasurface cloaks,” *IEEE Transactions on Antennas and Propagation*, vol. 63, no. 4, pp. 1554-1563, April 2015.

101. S. M. Mikki and Y. M. M. Antar, “A new technique for the analysis of energy coupling and exchange in general antenna systems,” *IEEE Transactions on Antennas and Propagation*, vol. 63, no. 12, pp. 5536-5547, Dec. 2015.

102. R. Wang, B. Z. Wang, X. Ding, and X. S. Yang, “Planar phased array with wide-angle scanning performance based on image theory,” *IEEE Transactions on Antennas and Propagation*, vol. 63, no. 9, pp. 3908-3917, Sept. 2015.

103. A. S. C. Svendsen and I. J. Gupta, “The effect of mutual coupling on the nulling performance of adaptive antennas,” *IEEE Antennas and Propagation*, vol. 54, no. 3, pp. 17-38, June 2012.

104. S. Bellofiore, et al., “Smart antenna system analysis, integration and performance for mobile ad-hoc networks (MANETs),” *IEEE Transactions on Antennas and Propagation*, vol. 50, no. 5, pp. 571-581, May 2002.

105. M. A. Gondal and A. Anees, “Analysis of optimized signal processing algorithms for smart antenna system,” *Neural Computing & Applications*, vol. 23, no. 3, pp. 1083-1087, Sept. 2013.

106. M. Yasin and P. Akhtar, “Mathematical model of Bessel beamformer with automatic gain control for smart antenna array system,” *Arabian Journal for Science and Engineering*, vol. 2014, no. 39, pp. 4837-4844, April 2014.

107. H. Boche, et al., “Smart antennas: state of art,” *IEEE Vehicular Technology Magazine*, vol. 1, no. 1, pp. 8-17, March 2006.

108. T. Kaiser, “When will smart antennas be ready for the market? Part I,” *IEEE Signal Processing Magazine*, pp. 87-92, March 2005.
109. B. R. Jackson, S. Rajan, B. J. Lio, and S. Wang, “Direction of arrival estimation using directive antennas in uniform circular arrays,” *IEEE Transactions on Antennas and Propagation*, vol. 63, no. 2, pp. 736-747, Feb. 2015.
110. P. H. Lehne and M. Pettersen, “An overview of smart antenna technology for mobile communications systems,” *IEEE Communications Surveys*, vol. 2, no. 4, pp. 1-12, 1999.
111. G. V. Tsoulos, “Smart antennas for mobile communication systems: benefits and challenges,” *Electronics & Communications Engineering Journal*, vol. 11, no. 2, pp. 84-94, April 1999.
112. C. M. Li, J. C. Wu, and I. T. Tang, “An analytic analysis of W-CDMA smart antennas beamforming using complex conjugate and DOA methods,” *Journal of Marine Science and Technology*, vol. 15, no. 4, pp. 287-294, 2007.
113. K. C. J. Lin, T. W. Kuo, P. J. Yan, W. J. Chen, and S. K. Jeng, “Beam configuration and client association for access points with switched beam antennas,” *IEEE Transactions on Mobile Computing*, vol. 15, no. 9, pp. 2179-2192, Sept. 2016.
114. H. T. Chou and C. T. Yu, “Design of phased array antennas with beam switching capability in the near-field focus applications,” *IEEE Microwaves Antennas Propagation*, vol. 9, no. 11, pp. 1120-1127, 2015.
115. I. Slomian, K. Wincza, and S. Gruszezynski, “Circularly polarized switched-beam antenna arrays with reduced sidelobe level,” *IEEE Antennas and Wireless Propagation Letters* vol. 15, pp. 1213-1216, 2016.
116. C. Gu, et al., “Compact smart antenna with electronic beam-switching and reconfigurable polarizations,” *IEEE Transactions on Antennas and Propagation*, vol. 63, no. 12, pp. 5325-5333, Dec. 2015.
117. N. A. Muhammad, et al, “Beam forming networks using reduced size Butler matrix,” *Wireless Personal Communications*, vol. 63, no. 4, pp. 765-784, Oct. 2010.
118. M. Elhefnawy and W. Ismail, “A microstrip antenna array for indoor wireless dynamic environments,” *IEEE Transactions on Antennas and Propagation*, vol. 57, no. 12, pp. 3998-4002, Dec. 2009.
119. J. He, B. Z. Wang, Q. Q. He, Y. X. Xing, and Z. L. Yin, “Wideband X-band microstrip Butler Matrix,” *Progress in Electromagnetics Research*, PIER 74, pp. 131-140, 2007.

120. J. S. Neron and G. Y. Delisle, “Microstrip EHF Butler Matrix design and realization,” *ETRI Journal*, vol. 27, no. 6, pp. 788-797, Dec. 2005.
121. M. Traii, M. Nedil, A. Gharsallah, and T. A. Denidni, “A novel wideband Butler matrix using multi-layer technology,” *Microwaves Optical Technology Letters*, vol. 51, no. 3, pp. 659–663, Mar. 2009.
122. G. I. Kiani, K. L. Ford, L. G. Olsson, K. P. Esselle, and C. J. Panagamuwa, “Switchable frequency selective surface for reconfigurable electromagnetic architecture of buildings,” *IEEE Transactions on Antennas Propagation*, vol. 58, no. 2, pp. 581–584, Feb. 2010.
123. C. H. Tseng, C. J. Chen, and T. H. Chu, “A low-cost 60-GHz switched-beam patch antenna array with butler matrix network,” *IEEE Antennas Wireless Propagation Letters*, vol. 7, pp. 432-435, 2008.
124. A. M. Martir, I. M. Fernandez, and A. O. Monux, “Wideband Slot-Coupled Butler Matrix,” *IEEE Microwaves and wireless Components Letters*, vol. 24, no. 12, Dec. 2014.
125. P. Chen, W. Hong, Z. Kuai, and J. Xu, “A double layer substrate integrated waveguide Blass matrix for beamforming applications,” *IEEE Microwaves and Wireless Components Letters*, vol. 19, no. 6, pp. 374-376, June 2009.
126. S. Mosca, F. Bilotti, A. Toscano, and L. Vegni, “A novel design method for Blass matrix beam-forming networks,” *IEEE Transactions on Antennas and Propagation*, vol. 50, no. 2, pp. 225-232, Feb. 2002.
127. V. Z. Gradeja, *Bio-inspired optimization algorithms for smart antennas*, PhD thesis, University of Edinburgh, June 2011.
128. J. H. Winters, “Smart antenna techniques and their application to wireless ad hoc networks,” *IEEE Wireless Communications*, vol. 13, no. 4, pp. 77-83, Aug. 2006.
129. L. C. Godara, “Applications of antenna arrays to mobile communications. II. beam-forming and direction-of-arrival considerations,” *Proceedings of IEEE*, vol. 85, no. 8, pp. 1195-1245, Aug. 1997.
130. I. Stevanovic, et al., “Integral equation modeling of waveguide-fed planar antennas,” *IEEE Antennas and Propagation Magazine*, vol. 51, no. 6, pp. 82-92, Dec. 2009.
131. D. J. Bisharat, S. Liao, and Q. Xue, “Circularly polarized planar aperture antenna for millimeter-wave applications,” *IEEE Transactions on Antennas and Propagation*, vol. 63, no.12, pp. 5316-5324, Oct. 2015.

132. L. Hanzo, J. S. Blog, and S. Ni, “Intelligent antenna arrays and beamforming,” *3G, HSPA and FDD versus TDD Networking: Smart Antennas and Adaptive Modulation,* 2nd ed., John Wiley & Sons, Ltd, Hoboken, (Feb. 2008).

133. J. Liu, N. Li, and K. Xie, “Application of chaos mind evolutionary algorithm in antenna arrays synthesis,” *Journal of Computers,* vol. 5, no. 5, pp. 717-724, May 2010.

134. J. Liu, N. Li, Y. Yang, and K. Xie, “Synthesis of antenna arrays shaped-beam using mind evolutionary algorithm,” *IEEE First International Workshop on Education Technology and Computer,* China, vol. 2, pp. 481-485, March 2009.

135. C. Wan, Y. Han, W. Sheng, X. Ma, and R. Zhang, “Pattern synthesis with constrained excitations for transceiving arrays,” *IET Microwaves, Antennas & Propagation,* vol. 9, no. 9, pp. 964-974, 2015.

136. B. Fuchs, “Synthesis of sparse arrays with focused or shaped beampattern via sequential convex optimizations,” *IEEE Transactions on Antennas and Propagation,* vol. 60, no. 7, pp. 3499-3503, July 2012.

137. A. E. Hajj, K. Y. Kabalan, and M. A. Husseini, “Generalized Chebyshev arrays,” *Radio Science,* vol. 40, no. 3010, pp. 1-8, June 2005.

138. G. T. F. D. Abreu and R. Kohno, “A modified Dolph-Chebyshev approach for the synthesis of low sidelobe beampatterns with adjustable beamwidths,” *IEEE Transactions on Antennas and Propagation,* vol. 51, no. 10, pp. 3014-3017, Oct. 2003.

139. S. R. Zinka and J. P. Kim, “On the generalization of Taylor and Bayliss n-bar array distributions,” *IEEE Transactions on Antennas and Propagation,* vol. 60, no. 2, pp. 1152-1157, Feb. 2012.

140. A. Recioui and H. Bentarzi, “Null steering of Dolph-Chebychev arrays using Taguchi method,” *International Arab Journal of Information Technology,* vol. 10, no. 2, pp. 120-125, March 2013.

141. R. C. Hansen, “Array pattern control and synthesis,” *Proceedings of the IEEE,* vol. 80, no. 1, pp. 141-151, Jan. 1992.

142. M. J. Mismar, T. H. Ismail, and D. I. A. A. Nadi, “Analytical array polynomial method for linear antenna arrays with phase-only control,” *International Journal of Electronics and Communications,* vol. 61, pp. 485-492, 2007.

143. M. V. Subbarao, N. S. Khasim, J. Thati, and M. H. H. Sastry, “Tapering of antenna array for efficient radiation pattern,” *e-Journal of Science & Technology,* vol. 8, no. 2, pp. 37-42, 2013.

144. A. Smida, et al., “Phased arrays in communication system based on Taguchi-neural networks,” *International Journal of Communication Systems*, vol. 27, no. 12, pp. 4449-4466, Dec. 2014.

145. A. Buffi, P. Nepa, and G. Manara, “Design criteria for near-field-focussed planar arrays,” *IEEE Transactions on Antennas and Propagation*, vol. 54, no. 1, pp. 40-50, Feb. 2012.

146. D. Vakula and N. V. S. N. Sarma, “Fault diagnosis of planar antenna arrays using neural networks,” *Progress in Electromagnetic Research M*, vol. 6, pp. 35-46, 2009.

147. G. Oliveri, L. Manica, and A. Massa, “ADS-based guidelines for thinned planar arrays,” *IEEE Transactions on Antennas and Propagation*, vol. 58, no. 6, pp. 1935-1948, June 2010.

148. F. Liu, J. Wang, C. Sun, and R. Du, “Spatial differencing method for DOA estimation under the coexistence of both uncorrelated and coherent signals,” *IEEE Transactions on Antennas and Propagation*, vol. 60, no. 4, pp. 2052-2062, April 2012.

149. A. Khabbazibasmenj and S. A. Vorobyov, “Robust adaptive beamforming for general-rank signal model with positive semi-definite constraint via POTDC,” *IEEE Transactions on Signal Processing*, vol. 61, no. 23, pp. 6103-6117, Dec. 2013.

150. A. Naceur, B. Merahi, and T. A. Abdelmalik, “A combined DMI-RLS algorithm in adaptive processing antenna system,” *Arabian Journal for Science and Engineering*, vol. 39, no. 10, pp. 7109-7116, Oct. 2014.

151. J. Foutz, A. Spanias, S. Bellofiore, and C. A. Balanis, “Adaptive Eigen-projection beamforming algorithms for 1-D and 2-D antenna arrays,” *Antennas and Wireless Propagation Letters* vol. 2, pp. 62-65, July 2003.

152. S. A. Vorobyov, “Principles of minimum variance robust adaptive beamforming design,” *Signal Processing*, vol. 93, no. 12, pp. 3264-3277, Dec. 2013.